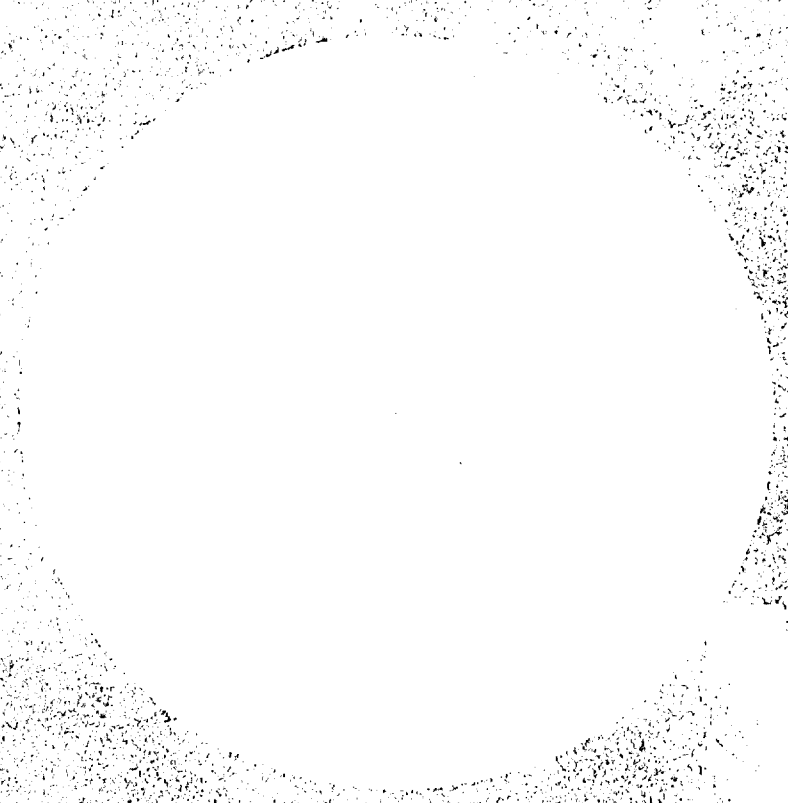


11

AD-A279 832

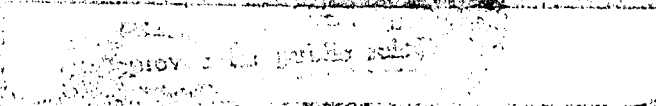
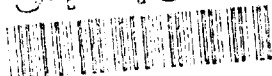


Best Available Copy



Best Available Copy

94-16077



1994 APR

**Best
Available
Copy**

In this *1994 NRL Review*, we present highlights of the unclassified research and development programs for fiscal year 1993. This book fulfills a dual purpose: it provides an exchange of information among scientists, engineers, scholars, and managers; it is also used in recruiting science and engineering professionals. As you read this *1994 NRL Review*, you will become even more aware that the Naval Research Laboratory is a dynamic team working together to promote the programs, progress, and innovations that will continue to foster discoveries, inventiveness, and scientific advances for the Navy of the future.

Cover: Dr. Isabella Karle of the Laboratory for the Structure of Matter received the Dower Award and Prize for Achievement in Science on April 7, 1994, in Philadelphia, Pennsylvania. This Award was established in 1990 by a bequest from Philadelphia chemical manufacturer Henry Dower to the Franklin Institute. The award honors international achievement in the physical and life sciences that significantly advances human knowledge and welfare. The Franklin Institute was organized in Philadelphia in 1824 as a memorial to Benjamin Franklin and as a means of promoting experiment and training in the sciences and technology. A biographical overview of Dr. Karle's professional career at NRL appears on page 9.

Contents

5 Mission

6 Preface

CAPT Paul G. Gaffney II, USN, Commanding Officer
Dr. Timothy Coffey, Director of Research

8 NRL's New Commanding Officer

CAPT Richard M. Cassidy, USN

9 A Career That Matters

Bower Award Recognizes Pioneering Contributions of Dr. Isabella Karle
David K. van Keuren

Accession For	
NTIS CRA&I	<input checked="" type="checkbox"/>
DTIC TAB	<input checked="" type="checkbox"/>
Unannounced	<input type="checkbox"/>
Justification	
By	
Distribution /	
Availability Codes	
Dist	Avail and/or Special
A-1	

19 The Naval Research Laboratory

- 21 NRL—Our Heritage
- 25 NRL Today
- 41 NRL in the Future
- 45 Highlights of NRL Research in 1993
- 52 Meet the Researchers
- 55 Color Presentation

59 Featured Research at NRL

- 61 Diamond Surface Chemistry
Pehr E. Pehrsson, John N. Russell, Jr., Brian D. Thoms,
James E. Butler, Michael Marchywka, and Jeffrey M. Calvert
- 73 Computational Materials Science
Larry L. Boyer, Michael J. Mehl, Dimitrios A. Papaconstantopoulos,
Warren E. Pickett, and David J. Singh
- 83 Self-assembled Molecular Templates: Microtubule-based Controlled
Release for Biofouling Control and Medical Applications
Ronald R. Price, Alan S. Rudolph, Jonathan V. Selinger, and Joel M. Schnur
- 91 Monitoring Whales and Earthquakes by Using SOSUS
Clyde E. Nishimura

103 Acoustics

- 105 High-Resolution Underwater Acoustic Imaging
Behzad Kamgar-Parsi
- 108 Cylindrical Wavenumber Calibration Array
Little D. Luker and Arnie L. Van Buren
- 111 Direct Measurement of Edge Diffraction from Acoustic
Panels of Decoupling Materials
Jean C. Piquette

THIS QUANTITY LIMITED 1

- 114 Structural Acoustics of Nearly Periodic Structures
Douglas M. Photiadis
 - 118 Acoustic Reverberation at Selected Sites in the
Mid-Atlantic Ridge Region
Jerald W. Caruthers, J. Robert Fricke, and Ralph A. Stephen
 - 122 Overcoming Chaos
Michael D. Collins and William A. Kuperman
-

125 Chemical/Biochemical Research

- 127 Fiber-Optic Sensor for Detection of Trace Levels
of Mercury in Water
*Kenneth J. Ewing, Ishwar D. Aggarwal, Gregory M. Nau,
and Thomas Bilodeau*
 - 130 Observing the Growth of Protein Crystals
John H. Konnert, Peter D'Antonio, and Keith B. Ward
 - 132 Global Warming Potential of Potential CFC Replacements
Nancy L. Garland, Herbert H. Nelson, and Laura J. Medhurst
-

135 Electronics and Electromagnetics

- 137 Multispectral Infrared Visualization and Processing
for Dim Target Detection
Dean A. Scribner, Michael P. Satyshur, and Melvin R. Kruer
 - 139 Flying Radar Target (FLYRT) Testing and Final Demonstration
Christopher S. Bovais, Ciaran J. Murphy, and Peggy L. Toot
 - 141 The Microwave Monolithic Integrated Circuit/Electronic
Warfare Receiver
Leo W. Lemley
 - 144 The Ionospheric Focussed Heating (IFH) Experiment
Paul A. Bernhardt
 - 146 Control of Interface Properties of GaSb/InAs Superlattices
*Robert J. Wagner, Brian R. Bennett, Benjamin V. Shanabrook,
John L. Davis, James R. Waterman, and Mark E. Twigg*
-

151 Energetic Particles, Plasmas, and Beams

- 153 Missile Hit-Points on the DDG-53
Dale A. Zolnick and Harold L. Toothman
- 154 Capillary Optics for X-ray Lithography
Charles M. Dozier, Michael I. Bell, and Dan A. Newman
- 156 Ultra Intense Laser Physics Research at NRL
Phillip A. Sprangle, Antonio C. Ting, Eric H. Esarey, and Jacob Grun
- 159 HRTS Ultraviolet Observations of a Solar Active Region
Kenneth P. Dere, Clarence M. Korendyke, and Guenter E. Brueckner
- 162 LIDAR Backscatter from a Rocket Plume
G. Charmaine Gilbreath, Amey R. Peltzer, and Anne E. Clement

165 Information Technology and Communication

- 167 Secure Information Through Replicated Architecture (SINTRA)
Database System
Judith N. Froscher and John P. McDermott
- 168 Embedded Training Methods for Command and Control Systems
Gene E. Layman
- 171 Historical Perspective on the NAVSTAR Global
Positioning System
Ronald L. Beard

175 Materials Science and Technology

- 177 Simulation and Visualization of Ultrasonic Waves in
Solids by Using Parallel Processing
*Richard S. Schechter, Henry H. Chaskelis,
Richard B. Mignogna, and P.P. Delsanto*
- 181 Ultimate Strength of Ultrafine Polycrystalline Materials
Chandra S. Pande and Robert A. Masumura
- 182 Element-Specific Magnetometry
Yves U. Idzerda and Gary A. Prinz
- 184 Origins of Magnetic Anisotropy in Magneto-optical
Storage Materials
William T. Elam, Vincent G. Harris, and Norman C. Koon

187 Numerical Simulating, Computing, and Modeling

- 189 Reactive Flows in Ram Accelerators
Chiping Li, Kazhikathra Kailasanath, Elaine S. Oran, and Jay P. Boris
- 190 Numerical Ocean Models
NRL Global Modeling Team

197 Ocean and Atmospheric Science and Technology

- 199 Sea Surface Temperature Retrievals from Satellite
Douglas A. May
- 200 Events Leading to the 1991-92 El Niño
John C. Kindle and Patricia A. Phoebus
- 203 Field Tests of the DOLPHIN—A Remotely Operated
Survey Vehicle
Maria T. Kalcic and Edit J. Kaminsky
- 206 Impacts of Weather Model Forecasts on Tactical
Environmental Decision Aids
Gary G. Love and John Cook

211 Optical Science

- 213 High-Frequency Approximations to Physical Optics
William B. Gordon
- 215 Broadband Thermal Optical Limiter
Brian L. Justus, Alan L. Huston, and Anthony J. Campillo

- 217 High-Speed, Low-Loss Transmission Line on
Silicon Membrane
Michael Y. Frankel
- 220 Paramagnetic Resonance and Optical Studies of GaN
*William E. Carlos, Evan R. Glaser, Thomas A. Kennedy,
and Jaime A. Freitas, Jr.*
- 222 Interferometric "Seeing" Measurements on Mt. Wilson:
Power Spectra and Outer Scales
David Mozurkewich and David F. Buscher
-

225 Space Research and Satellite Technology

- 227 Hubble Space Telescope Image Reconstruction on the
NRL Connection Machine
Paul L. Hertz and Michael L. Cobb
- 229 Impedance Model Study for the Common Pressure
Vessel Battery
*Daniel J. Shortt, William E. Baker, Jr., James C. Garner,
and George Barnard*
- 231 Advanced Release Technologies Program
William E. Purdy
- 233 Vibration Excitation Test of the LACE Satellite as
Observed by a Ground-based Laser Radar
Shalom Fisher, K.I. Schultz, and L.W. Taylor, Jr.
-

237 Awards and Recognition

- 239 Special Awards and Recognition
- 247 Individual Honors
- 259 Alan Berman Research Publication and Edison Patent Awards
- 264 Awards for *NRL Review* Articles
-

267 Professional Development

- 269 Programs for NRL Employees—*University education and scholarships,
continuing education, professional development, and other activities*
- 275 Programs for Non-NRL Employees—*Fellowships, exchange programs,
and cooperative employment*
-

279 General Information

- 281 Technical Output
- 282 Key Personnel
- 283 Organizational Charts
- 287 Contributions by Divisions, Laboratories, and Departments
- 290 Employment Opportunities for Entry-Level and Experienced Personnel
- 291 Location of NRL in the Capital Area
- 292 Subject Index
- 294 Author Index
- Inside back cover *NRL Review Staff*

To conduct a broadly based multidisciplinary program of research and advanced technological development directed at maritime applications of new and improved materials, technology, equipment, systems, and ocean, atmospheric, and space science and related technologies

The Naval Research Laboratory provides

- Primary in-house research for the physical, engineering, space, and environmental sciences
- Broadly based exploratory and advanced development programs in response to identified and anticipated N

Preface

Research for a Navy and a Nation

"The broad nature of NRL provides an interdependent grid of expertise that enables multidisciplinary solutions to Navy, Defense, and national challenges."



CAPT Paul G. Gaffney II, USN
Commanding Officer

When one enters through the main gate at the Naval Research Laboratory in Washington, DC, one is immediately reminded of the Laboratory's rich heritage. The bust of Thomas Edison greets each employee and visitor assuring all that the deliberate decision to create this great Laboratory involved the nation's most prestigious scientific, business, and Federal leaders. That these designers of NRL were so rigorous in their task has stood the Laboratory in good stead for over seven decades. The model they created in NRL, today serves as a benchmark for other Defense laboratories and development centers, which seek a quality workforce producing world-leading technology.

The broad nature of NRL provides an interdependent grid of expertise that enables multidisciplinary solutions to Navy, Defense, and national challenges. It is just this multidisciplinary advantage that pushes NRL into leadership positions in technologies addressing, for example, critical environmental quality (EQ) issues that our Navy and our world face.

Citing NRL's contemporary advances in EQ is but one example of the ability to apply technologies aimed at Navy needs to national needs, as well. Another example one should consider is NRL's contribution to advanced information networking so important to tactical Marine Corps and Navy operations and also part of the national imperative for an efficient Information Highway. NRL's use of new computer and materials technologies and novel integration techniques in spacecraft development blaze the way for renewed opportunities in the space industry. And, as this *Review* aptly portrays, decades long contributions from great scientists, like NRL's Dr. Isabella Karle, are directly influencing developments in the Navy and other parts of Government and industry.

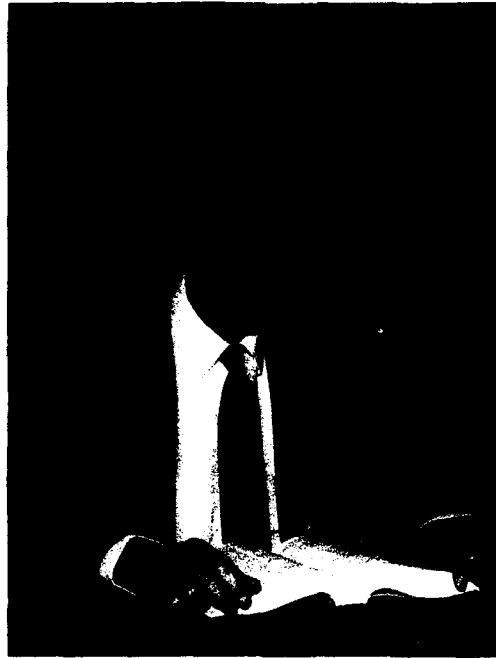
One of the best metrics to judge the utility of the Laboratory's work beyond its obvious and historic contribution to Navy and Marine Corps prowess is through direct partnerships with industry in joint licensing and/or Cooperative Research and Development Agreements. NRL is proud of and committed to its Navy leadership in technology transfer and dual use.

While NRL pursues the challenges of a Department of the Navy whose reach is truly global and whose foundation is technologically superior, we also intend to act responsibly and contribute to the national technological well being as America's corporate laboratory.

Predicting specific developments in science and technology in the coming decades is difficult and perhaps impossible. One can, however, predict that there will be continuing pressure on the scientific enterprise to contribute to the defense of the Nation as well as to contribute towards economic prosperity for the American people. This could be cast as a dilemma, but it need not be. When one performs the calculus of variations to determine the national investment strategy for science and technology, one must include among the many constraints the need to provide for the common defense and the need to contribute to the development of economic prosperity. History has taught us that both constraints must be honored.

The Naval Research Laboratory has played, and will continue to play, a special role in the area of defense. NRL has a responsibility to maintain a cadre of scientists and engineers whose principal job is to maintain the Nation in a state of scientific and technological readiness. In order to do this, NRL must remain current on important developments in science and technology at large, not just within NRL. This requirement demands that there be strong relationships between the Laboratory and the scientific and technology establishment. We have learned that one of the most effective ways to encourage such relationships is through sharing of facilities used to conduct research.

As I have said before, any science and technology organization, which today attempts to be an island unto itself, would soon be lost in the dust of the rapid advance in science and technology. Therefore, as NRL reevaluates its research infrastructure for the post cold war era, the sharing of facilities among academia,



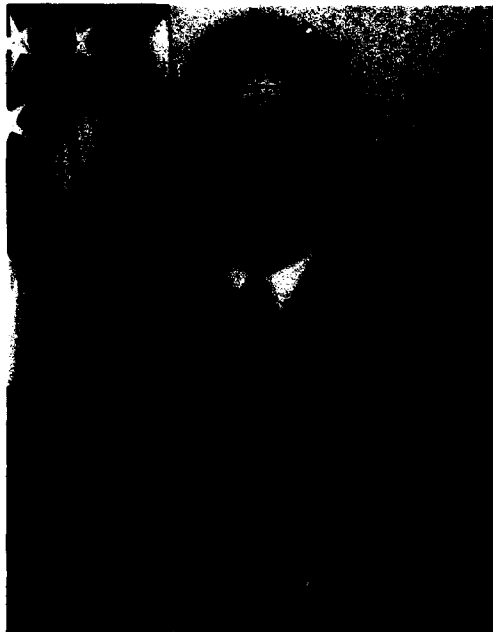
Dr. Timothy Coffey
Director of Research

"NRL has a responsibility to maintain a cadre of scientists and engineers whose principal job is to maintain the Nation in a state of scientific and technological readiness."

industry, and the Laboratory should be an explicit component of that reevaluation. This sharing should be consistent with the respective roles played by the Laboratory and its partners.

Recognition of our respective roles and of the need for partnerships and sharing of facilities, knowledge, and personnel will go far in contributing to a successful calculus of variations. It will be one of the most successful vehicles for fostering the dual-use concept, which has received so much discussion in recent years. NRL is prepared to play its role as a partner in the Nation's overall science and technology program, while at the same time, maintain focus on defense research issues.

NRL's New Commanding Officer



CAPT Richard M. Cassidy, USN

CAPT Richard M. Cassidy was previously assigned as Technical Director and Associate Program Manager in the AEGIS Program Office before coming to NRL.

Prior to assuming his major program manager duties, CAPT Cassidy served in an extensive number of combat systems engineering assignments in the AEGIS Program. He served as the AEGIS Combat System Engineering Manager (PMS 400B3) where he was responsible for the design, development, and lifetime support of *Ticonderoga* class cruiser and *Arleigh Burke* class destroyer combat systems. Prior to that he served as the AEGIS Combat Systems Operations Manager (PMS 400B5) and established the AEGIS FMS case with Japan as well as several battle group and advanced AAW programs. Other ashore assignments included: Director of AAW Special Programs in the Naval Sea Systems Command (SEA 06Y); DDG 51 Combat System Manager (PMS 400D5), where he was part of the original project team that designed the *Arleigh Burke* class;

instructor at the Engineering Duty Officer School; and System Engineer at the Joint Tactical Communications Office (TRI-TAC).

CAPT Cassidy's shipboard assignments included the USS *Stickell* (DD-888) and USS *Conyngham* (DDG-17). He became an Engineering Duty Officer in 1974.

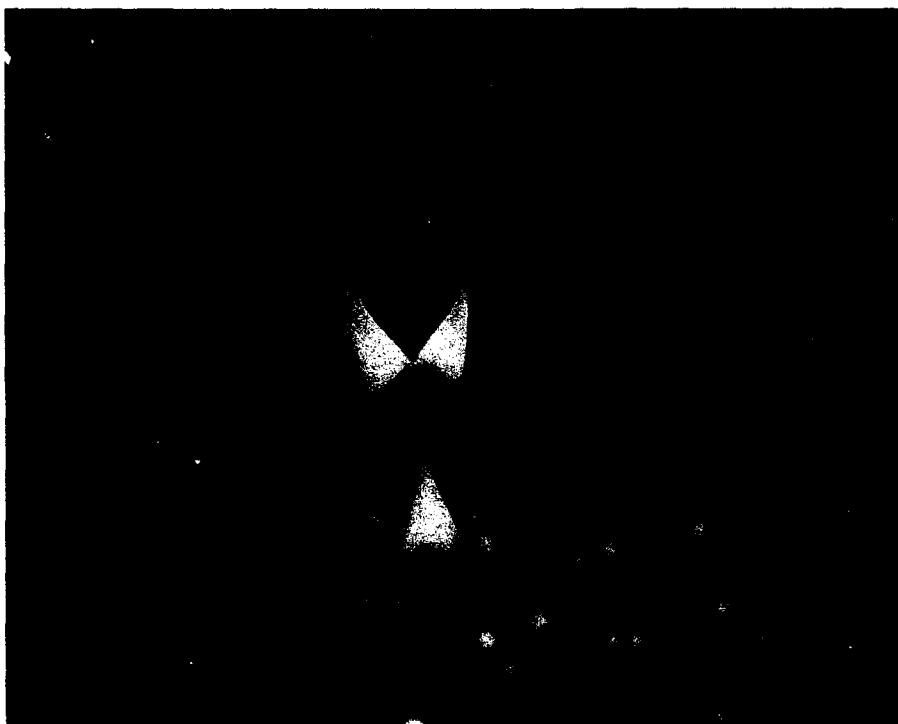
He is a 1970 graduate of the University of North Carolina where he received a B.A. in Economics. He also holds a Master of Science in Electrical Engineering from the Naval Postgraduate School and a Masters in Business Administration from Fairleigh Dickinson University. CAPT Cassidy was selected as the Navy's 1990 representative at the MIT Sloan School Program for Senior Executives.

CAPT Cassidy has been awarded the Defense Meritorious Service Medal, the Meritorious Service Medal (two awards), and the Navy Commendation Medal. He is married to the former Lois Bergman of Annandale, Virginia. The Cassidys reside in Annandale.

A Career That Matters*

Bower Award Recognizes Pioneering Contributions of Dr. Isabella Karle

David K. van Keuren
Historian



The presentation of the 1993 Bower Award and Prize for Achievement in Science to Isabella Karle marks the latest public recognition of this esteemed Naval Research Laboratory scientist's path-breaking achievements in crystallography and molecular chemistry. In receiving the award, Dr. Karle was cited by the Franklin Insti-

tute of Philadelphia for her "pioneering contributions in determining the three-dimensional structure of molecules, making use of both X-ray and electron diffraction, and in particular for her definitive introduction ... of the symbolic addition method to reveal molecular structure directly from X-ray studies" [1].

*With acknowledgement to Dr. Jerome Karle, "Structures That Matter," *Report of NRL Progress*, July 1973, pp. 86-89. Informational background for this article, unless otherwise noted, is provided by oral histories with Isabella and Jerome Karle on deposit in the NRL Historian's office.

The Award, presented as a memorial to Dr. Benjamin Franklin, honors outstanding achievement and innovation in the life and physical sciences and its application toward service in the public good. Dr. Isabella Karle is the fourth recipient of the prize and the first woman to receive it—clearly a fitting recognition of her half-century career in science and service to NRL, the United States Navy, and mankind in general.

EDUCATION AND EARLY INFLUENCES

Dr. Karle's ties to both science and the Navy date back to her high school days in Detroit, Michigan. Born Isabella Lugoski in 1921, she was introduced to chemistry while a student at Edwin Denby High School (named



Drs. Jerome and Isabella Karle with Professor Brockway (left) at the University of Michigan in 1945

after Warren G. Harding's Secretary of the Navy). Mrs. Deming, her chemistry instructor, was an inspiring teacher, passing along to students her knowledge and love of chemical science. The experiences and tastes acquired by Isabella in Deming's class have never left her. She decided to pursue chemistry in college and matriculated at what is now Wayne State University in January of 1938. The following fall, she transferred to the University of Michigan with a state scholarship conferred through competitive examination.

As one of a handful of women majoring in chemistry at Michigan, Isabella faced the daunting task of making her way in a heavily male-dominated classroom environment and profession. Nevertheless, through hard work and scholastic aptitude, she thrived at the university. Isabella took qualitative chemical analysis with Professor Robert Carney and subsequently served as his laboratory assistant. Later, she was a student in Lawrence Brockway's senior-level physical chemistry course and was invited to be his graduate student. Her future course was thereby set in more ways than one: she met her future husband, Jerome Karle, a first-year graduate student, at an adjoining bench in the class's laboratory section. The two were married in 1942.

Professor Brockway was a leader in the small circle of researchers who were using electron diffraction to study the molecular structure of simple organic molecules. Upon his arrival at Michigan from the California Institute of Technology in 1938, Brockway had built an electron diffraction apparatus to continue his studies in molecular structure. Isabella Karle, as one of his students, chose as her dissertation topic the electron diffraction analysis of gaseous state fluorine and hydrocarbon compounds. Both she and her husband

would later carry the expertise they acquired under Brockway to the Naval Research Laboratory.

FROM THE MANHATTAN PROJECT TO NRL

In 1943, the Karles were recruited to work for the Manhattan Project at the University of Chicago's Metallurgical Laboratory. There Isabella was assigned the responsibility of making plutonium chloride, as a step toward the production of plutonium for fission purposes. Having successfully completed their assigned research responsibilities, the Karles returned to Michigan in 1944. Jerome joined Brockway's staff under a research contract Brockway had with NRL's Chemistry Division, thus beginning his long connection with the Laboratory. Isabella, her Ph.D. now in hand, joined the University of Michigan's chemistry faculty as an instructor. In 1946, both were offered regular positions at the Naval Research Laboratory, where they joined Herbert Friedman's Electron Optics Section in the Optics Division.

REORGANIZATION OF NRL AFTER WORLD WAR II

The postwar years were a time of great expansion and change at NRL. The prewar Laboratory had served the Bureau of Engineering as essentially an applied job shop, with a limited research program squeezed out of bureau funds and the small annual Congressional appropriation [2]. The Naval Consulting Board's earlier idea of creating an industrial-style research and development (R&D) laboratory for the Navy had withered in the face of the post-World War I military draw-down and then the Great Depression [3]. Laboratory leaders in the 1944-1946 time frame, however, were intent

on holding on to recent wartime increases in personnel and funding. Furthermore, they hoped to add new scientific programs and to improve the quality of the research staff in the postwar era. From an emphasis on short-term war-related project work, they hoped to shift research emphases to long-term basic and applied investigations that would produce benefits for the Navy and Nation over the long haul [4].

With the organization of the Navy Bureau of Research and Inventions in 1944 and its successor the Office of Naval Research in 1946, new funding and administrative structures came into place that facilitated the organizational aims of NRL leadership. The high prestige of science after the war additionally assisted the goal of fashioning a strong Navy center for applied and basic research at NRL.

The postwar research program that resulted continued Laboratory research in such areas of strength as underwater sound, radar, metallurgy, and surface chemistry. To it were added new or much extended studies in areas such as upper atmospheric physics, atomic and radiation physics, solar physics and astronomy, radio astronomy, rocket research, and others [5]. The Karles' work in structural analysis through the use of electron diffraction was of interest to NRL scientific management and complemented the work of a growing corps of Laboratory researchers already investigating X-ray phenomena. Their expertise added an important and cutting edge scientific competency to the Laboratory's research portfolio.

GASEOUS ELECTRON DIFFRACTION WORK

Isabella's first task at the Laboratory was assembling and testing the new electron diffraction instrument



Dr. Karle carrying out experimental work on electron diffraction apparatus in 1949

designed by Jerome. Although NRL possessed a commercially made electron diffraction apparatus, it was limited to working with solid substances, and Jerome was interested in taking diffraction patterns from gases. The resulting instrument was far advanced over both the existing NRL machine and the instruments the Karles had used as graduate students at Michigan. Using state-of-the-art electronics and double lenses to focus the electron beam, the instrument provided a cleaner beam, a more precise diffraction photograph, and better data.

Isabella's next task was to get a quantitative measure of what was on the photographic plate. She accomplished this by using a microphotometer while rotating the concentric pattern about its center to average out the residual graininess that is present even in fine-grained photographic emulsions (which she had to choose carefully for their response to the

action of electrons). Before that time, measurements of scattering patterns were very qualitative.

Data yielded by scattering patterns, when put through a Fourier transform, results in a probability measurement of the occurrence of interatomic distances in the molecule. Jerome recognized that one implication of this was that the probability curve should not have any negative values in it: that is, the probability would be either 0 or a positive number. Based on this insight, Isabella carried out the experimental work and found out how to separate the atomic scattering from the molecular scattering so that the resulting curve—a representation of the probability of the occurrence of interatomic distances—was non-negative. From such a curve, she was able to determine not only the interatomic distances but also the vibrational and rotational motions in the gaseous molecules under study. The Karles simulta-

Drs. Jerome and Isabella Karle examine a model of batrachotoxinin A that they jointly determined in the 1960s



neously established a working relationship that has continued over their long career at NRL: Jerome acted as the theoretician, and Isabella was responsible for their joint work's experimental verification.

The Karles produced their first paper on the structure determination method in 1947 and followed it up with further publications in 1949 and 1950 [6-8]. This published record provided the basis by which other scientists were able to pick up on the Karles' method and use it in their own work.

X-RAY DIFFRACTION ANALYSIS

The non-negativity principle worked so well in electron diffraction structure determinations that Jerome and Herbert Hauptman, who had come to the Laboratory in 1947, quickly decided to attempt to apply it to the analysis of X-ray diffraction patterns derived from crystalline substances. They rapidly discovered that the available data were greatly overdetermined in respect to the numbers of unknowns. Consequently, they were able to construct an infinite set of inequalities that related intensities to each

other that in turn determined the phases. It had previously been believed that phase information was necessarily lost in the experiment. With both magnitude and phase information, the crystalline structure could then be deduced from the data.

The "direct method of phase determination" received its first airing at the meetings of the Crystallographic Society of America in 1949 and was subsequently published the next year in *Acta Crystallographica* [9]. Jerome Karle and Hauptman followed this up in 1953 with their paper on "The Probability Distribution of the Magnitude of a Structure Factor. I. The Centrosymmetric Crystal" [10]. The theoretical work for which they would eventually receive the Nobel Prize was now essentially done. However, it needed to be demonstrated experimentally to a generally skeptical scientific community. Jerome turned to Isabella Karle to accomplish this end.

Isabella quickly taught herself how to take X-ray diffraction photographs from a single crystal and started making scattering measurements. But this left her with the task of determining how to bridge the gap between the theory and the experiment. She

reminisces that "the theory in many of the formulas just assumed that there was an infinite amount of scattering data, which, of course, there never is, experimentally. There were many formulas. There were many intensities. Which ones [ought one] to begin with to try to determine their phases? That was a matter of trial and error and thought" [11].

Eventually, she determined a reasonable procedure with which to start a phase determination. Assignment of phases to three specially chosen reflections chooses an origin for the unit cell in a crystal, that is, the X, Y, and Z coordinates have to start off at 0 somewhere. By carefully selecting these reflections, she discovered that eventually they could evaluate the phases for many other reflections because the several types of formulas she was using augmented each other and gave information from more than one direction. This process allowed her to build up enough approximate phase information to put into a Fourier series, along with the related intensities, to get an electron density map.



Isabella Karle examines structure of jamine in 1964

Isabella made her first structure determination on p,p'-dimethoxybenzophenone in 1957 [12]. The final step in the solution required taking the data and computing a reliability factor between the determined structure and its measured analog. At that time, there was not a powerful-enough computer at NRL to do the necessary calculations. Consequently, she had to acquire time on IBM's large computer in New York City (displayed in a Avenue window) to make the necessary refinements. The cost was almost equivalent to an entire year's budget, but it worked: the calculated structure proved correct. Theory and experimental practice had been bridged.

THE SYMBOLIC ADDITION METHOD

However, Isabella soon realized that the method she used in determining the structure of p,p'-dimethoxybenzophenone was not going to work as well with other substances. For most structures, more than three initial phases were needed to proceed with a phase determination. It would be difficult, she concluded, to assign other phases a priori and carry on parallel phase determinations. But why not use unknown symbols? Once the idea occurred to her it wasn't long before she realized that she did not need to assign many unknowns—never more than five—before relationships started occurring between the symbols that were strong enough and, from a probability point of view, acceptable enough, to allow phase determinations to be made. This was the origin of the Symbolic Addition Method in phase determination, which eventually became the standard method of analysis in the field.

By the early 1960s, Isabella had become adept at using the new method for structure determinations of centro-



Dr. Karle and coworker Janet Estlin adjust Weissenberg (left) and precession cameras used in X-ray diffraction research during the late 1960s

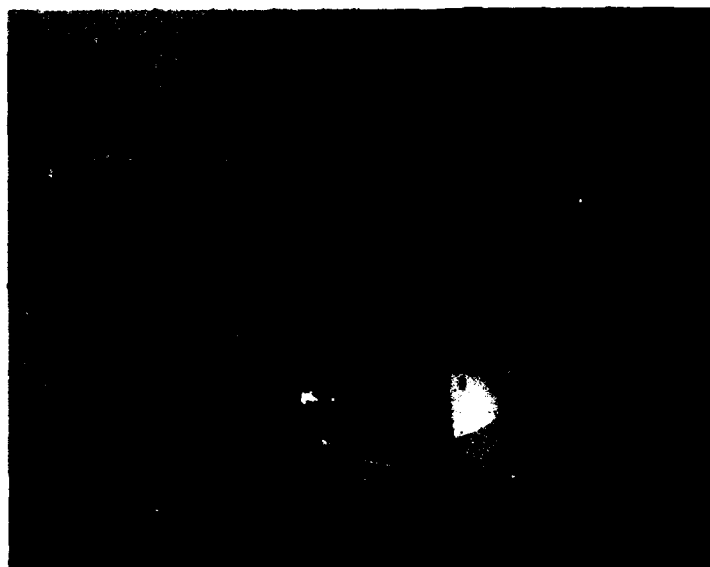
symmetric crystals (crystals with a center of symmetry). She first discussed the method in a paper on cyclohexaglycyl in 1963 and in another paper on jamine published shortly thereafter [13,14]. Symbolic Addition worked fine with centrosymmetric crystals. However, the case of non-centrosymmetric crystals, which included most of the organic substances researchers were interested in, presented extra difficulties.

The value of the phases in noncentrosymmetric crystals could vary from 0 to 2π , in contrast to centrosymmetric crystals in which phases have values only of 0 or π . This presented the problem of which values to assign to the symbols that remained unevaluated at the end of a phase determination. Isabella decided that the obvious solution was to assign just four values, 0, $\pi/2$, π , $-\pi/2$, to serve as a sufficiently close approximation. Usually one map, calculated from the several possible phase sets, would thereby

prove correct enough to demonstrate a piece of the structure, if not its entirety. Jerome then suggested using the piece that was known as a means for approximating the unknown parts of the structure. The tangent formula could then be applied to produce a better approximation. It was a stepwise development that eventually worked to solve the entire structure.

Isabella published her first noncentrosymmetric structure, that of arginine, in 1964 [15]. Numerous other structures followed in the next few years. In 1966, a landmark paper was published that summarized both the theory and the procedure [16]. Both the method and the large amount of NRL research that successfully applied it soon captured the attention of the scientific world. Other laboratories began to emulate the work at NRL, and, as the sophistication and speed of computers developed, many computer programs were written to facilitate the processes involved.

Isabella Karle stands in front of picture of Colombian poison dart frog and representation of toxin structure



COLLABORATIVE EFFORTS WITH NIH

NRL's success in mapping the structure of complicated organic substances quickly attracted the interest of other researchers. Dr. Bernhard Witkop of the National Institutes of Health (NIH) approached the Karles in 1968 with microgram amounts of the poison dart frog venom batrachotoxin A from the Colombian jungles. Dr. Witkop thought the venom might have medicinal applications and needed to know its chemical structure. The Karles were able to establish the structural formula of the toxin, thus initiating what would prove to be the first of many collaborations with Dr. Witkop and his colleagues at the Institute [17]. Many other collaborative efforts with organic chemists and biochemists followed.

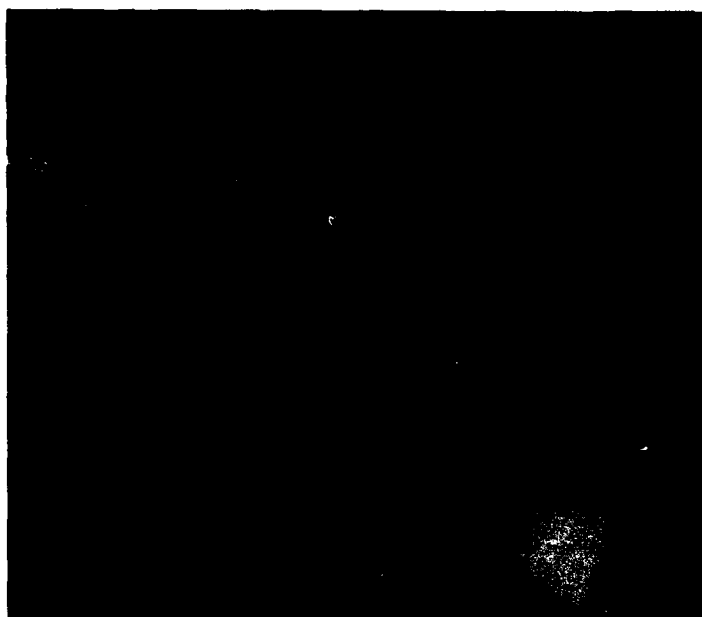
Isabella subsequently cooperated with Dr. Witkop on analyzing the structures of a number of derivatives of amino acids exposed to ultraviolet light. Other work in photochemistry (structural mapping of photoarrangement products) followed. More recently she has concentrated on under-

standing the structure of peptides, both on the molecular level and on the level of how the molecules are assembled together.

CURRENT RESEARCH

Dr. Karle's current research includes investigating how peptides associate to form ion channels in cell membranes, with the intent of understanding how ions are transported through the membranes. Other research involves peptidomimetics. The goal here is to better understand the structure of peptides before attempting to redesign them for more effective medical applications.

From the beginning of the Karles' work in electron diffraction at NRL in the later 1940s to the widespread acceptance and emulation of molecular structure determination by the direct method in the late 1960s, twenty years had passed. The striking and important research achievements of Isabella and Jerome Karle over this period of time and beyond amply justify the faith of NRL's wartime leadership in the potential rewards to the Navy and the Nation of long-term basic research.



The Bower Award announcement ceremony was held at the Washington Navy Yard on November 18, 1993. Dr. Karle is congratulated by (left to right) the Honorable Anita K. Jones, Director, Defense Research and Engineering; the Honorable John H. Dalton, Secretary of the Navy; Dr. Larry Tise, Executive Director, Franklin Memorial; and Dr. James L. Powell, President, Franklin Institute.

The Bower Award is yet another certification of the essential correctness of that vision. It is also a recognition of the finely tuned combination of intellectual acuity, experimental rigor and insight, and hard work that Isabella has brought to her work through the course of her scientific career. The applied results of this basic research are already benefiting the United States and humanity in innumerable ways.

REFERENCES

1. "The Bower Award and Prize in Science to Isabella L. Karle," Franklin Institute, Press Announcement, Nov. 8, 1993.
2. A.T. Drury, "A War History of the Naval Research Laboratory," 1946. On file at NRL Historian's office.
3. David K. van Keuren, "Science, Progressivism, and Military Preparedness: The Case of the Naval Research Laboratory, 1915-1923," *Technology & Culture*, October 1992, pp. 710-736.
4. Bruce Hevly, "Basic Research Within a Military Context: The Naval Research Laboratory and the Foundations of Extreme Ultraviolet and X-Ray Astronomy, 1923-1960," Johns Hopkins University Ph.D. dissertation, 1987.
5. Records on NRL's postwar reorganization are found in the records held by the NRL Historian's office and within NRL administrative records at the Federal Records Center, Suitland, Maryland. In particular, agenda records of the NRL Scientific Program Board, 1946-1949, NRL Historian's office, are useful in this regard.
6. Isabella and Jerome Karle, "An Objective Method for Studying Electron Diffraction by Gases," *Journal of Chemical Physics* 15, 764 (1947).
7. Isabella and Jerome Karle, "Internal Motion and Molecular Structure Studies by Electron

- Diffraction," *Journal of Chemical Physics* **17**, 1052 (1949).
8. Isabella and Jerome Karle, "Internal Motion and Molecular Structure Studies by Electron Diffraction. II. Interpretation and Method," *Journal of Chemical Physics* **18**, 957 (1950).
 9. Jerome Karle and Herbert Hauptman, "The Phases and Magnitudes of the Structure Factors," *Acta Crystallographica* **3**, 181 (1950).
 10. Jerome Karle and Herbert Hauptman, "The Probability Distribution of the Magnitude of a Structure Factor. I. The Centrosymmetric Crystal," *Acta Crystallographica* **6**, 131 (1953).
 11. Dr. Isabella Karle, Oral History, NRL Historian's office, p. 17.
 12. Isabella Karle, Jerome Karle, and Herbert Hauptman, "Crystal and Molecular Structure of p,p'-dimethoxybenzophenone by the Direct Probability Method," *Acta Crystallographica* **10**, 481 (1957).
 13. Isabella and Jerome Karle, "An Application of a New Phase Determination Procedure to the Structure of Cyclo(hexaglycyl) Hemihydrate," *Acta Crystallographica* **16**, 969 (1963).
 14. Isabella and Jerome Karle, "The Structure and Stereochemistry of Jamine $C_{21}H_{35}N_3$, by X-Ray Analysis," *Tetrahedron Letters* No. 29, 2065 (1963).
 15. Isabella and Jerome Karle, "An Application of the Symbolic Addition Method to the Structure of L-Arginine Dihydrate," *Acta Crystallographica* **17**, 835 (1964).
 16. Isabella and Jerome Karle, "The Symbolic Addition Procedure for Phase Determination for Centrosymmetric and Noncentrosymmetric Crystals," *Acta Crystallographica* **21**, 849 (1966).
 17. Isabella and Jerome Karle, "The Structural Formula and Crystal Structure of the O-p-Bromobenzoate Derivative of Batrachotoxinin A, $C_{31}H_{38}NO_6Br$, a Frog Venom and Steroidal Alkaloid," *Acta Crystallographica* **B25**, 428 (1969).



The Naval

Research
Laboratory

Best Available Copy

- 21 NRL—Our Heritage
- 25 NRL Today
- 41 NRL in the Future
- 45 Highlights of NRL Research in 1993
- 52 Meet the Researchers
- 55 Color Presentation

NRL—Our Heritage

Today, when government and science seem inextricably linked, when virtually no one questions the dependence of national defense on the excellence of national technical capabilities, it is noteworthy that in-house defense research is relatively new in our Nation's history. The Naval Research Laboratory (NRL), the first modern research institution created within the United States Navy, began operations in 1923.

Thomas Edison's Vision—The first step came in May 1915, a time when Americans were deeply worried about the great European war. Thomas Edison, when asked by a *New York Times* correspondent to comment on the conflict, argued that the Nation should look to science. "The Government," he proposed in a published interview, "should maintain a great research laboratory.... In this could be developed...all the technique of military and naval progression without any vast expense." Secretary of the Navy Josephus Daniels seized the opportunity created by Edison's public comments to enlist Edison's support. He agreed to serve as the head of a new body of civilian experts—the Naval Consulting Board—to advise the Navy on science and technology. The Board's most ambitious plan was the creation of a modern research facility for the Navy. Congress allocated \$1.5 million for the institution in 1916, but wartime delays and disagreements within the Naval Consulting Board postponed construction until 1920.

The Laboratory's two original divisions, Radio and Sound, pioneered in the fields of high-frequency radio and underwater sound propagation. They produced communications equipment, direction-finding devices, sonar sets, and, perhaps most significant of all, the first practical radar equipment built in this country. They also performed basic research, participating, for example, in the discovery and early

exploration of the ionosphere. Moreover, the Laboratory was able to work gradually toward its goal of becoming a broadly based research facility. By the beginning of World War II, five new divisions had been added: Physical Optics, Chemistry, Metallurgy, Mechanics and Electricity, and Internal Communications.

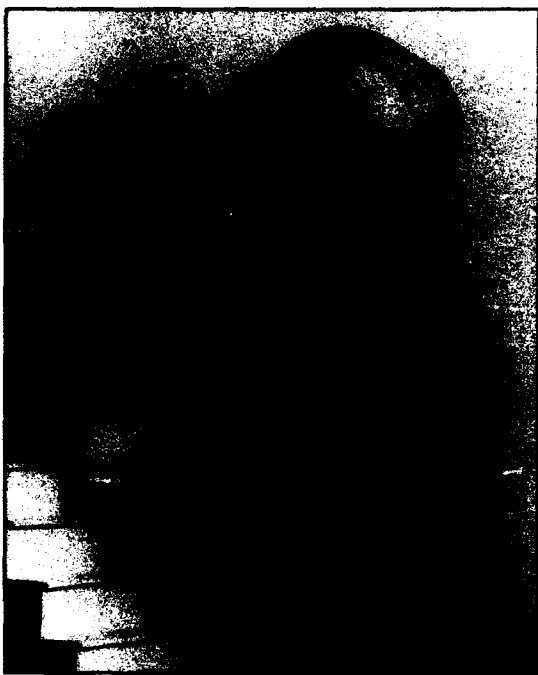
The War Years and Growth—Total employment at the Laboratory jumped from 396 in 1941 to 4400 in 1946, expenditures from \$1.7 million to \$13.7 million, the number of buildings from 23 to 67, and the number of projects from 200 to about 900. During WWII, scientific activities necessarily were concentrated almost entirely on applied research. New electronics equipment—radio, radar, sonar—was developed. Countermeasures were devised. New lubricants were produced, as were antifouling paints, luminous identification tapes, and a sea marker to help save survivors of disasters at sea. A thermal diffusion process was conceived and used to supply some of the ^{235}U isotope needed for one of the first atomic bombs. Also, many new devices that developed from booming wartime industry were type tested and then certified as reliable for the Fleet.

NRL Reorganizes for Peace—Because of the major scientific accomplishments of the war years, the United States emerged into the post-war era determined to consolidate its wartime gains in science and technology and to preserve the working relationship between its armed forces and the scientific community. While the Navy was establishing its Office of Naval Research (ONR) as a liaison with and supporter of basic applied scientific research, it was also encouraging NRL to broaden its scope and become, in effect, its corporate research laboratory. There was a transfer of NRL to the administrative oversight of ONR and a parallel

shift of the Laboratory's research emphasis to one of long-range basic and applied investigation in a broad range of the physical sciences.

However, rapid expansion during the war had left NRL improperly structured to address long-term Navy requirements. One major task—neither easily nor rapidly accomplished—was that of reshaping and coordinating research. This was achieved by transforming a group of largely autonomous scientific divisions into a unified institution with a clear mission and a fully coordinated research program. The first attempt at reorganization vested power in an executive committee composed of all the division superintendents. This committee was impracticably large, so in 1949 a civilian director of research was named and given full authority over the program. Positions for associate directors were added in 1954.

The Breadth of NRL—During the years since the war, the areas of study at the Laboratory have included basic research concerning the



Evelyn Longman-Batchelder sits before the Thomas Edison bust in clay form. She was the only sculptor ever to model Edison from life, visiting him at his Florida home for pictures and measurements. The bust was later installed and unveiled inside the main gate entrance at NRL in 1952.

Navy's environments of Earth, sea, sky, and space. Investigations have ranged widely from monitoring the Sun's behavior, to analyzing marine atmospheric conditions, to measuring parameters of the deep oceans. Detection and communication capabilities have benefited by research that has exploited new portions of the electromagnetic spectrum, extended ranges to outer space, and provided means of transferring information reliably and securely, even through massive jamming. Submarine habitability, lubricants, shipbuilding materials, fire fighting, and the study of sound in the sea, have also been steadfast concerns.

The Laboratory has pioneered naval research into space, from atmospheric probes with captured V-2 rockets, through direction of the Vanguard project—America's first satellite program—to involvement in such projects as the Navy's Global Positioning System. As part of the SDI program, the Low-Power Atmospheric Compensation Experiment (LACE) satellite was designed and built by NRL. Today, NRL is the Navy's lead laboratory in space systems research, fire research, tactical electronic warfare, microelectronic devices, and artificial intelligence. NRL has also evaluated new issues, such as the effects of intense radiation and various forms of shock and vibration on aircraft, ships, and satellites.

The consolidation of NRL and the Naval Oceanic and Atmospheric Laboratory, with centers at Bay St. Louis, Mississippi, and Monterey, California, has added new strengths to the Laboratory. NRL now serves as the lead Navy laboratory for research in ocean and atmospheric sciences with special strengths in physical oceanography, marine geosciences, ocean acoustics, marine meteorology, and remote oceanic and atmospheric sensing. The expanded Laboratory is focusing its research efforts on new Navy strategic interests and needs in the post-Cold War world. Although not abandoning its interests in blue water operations and research the Navy is also focusing on defending American interests in the world's littoral regions. NRL scientists and engineers are working to give the Navy the special knowledge and capabilities it needs to operate in these waters.

During the last year NRL researchers were responsible for important scientific and engineering advances in a number of areas. Scientists within the Laboratory's Marine Geophysics Division cooperated with academic scientists, Space and Naval Warfare Systems Command, and the U.S. Atlantic Fleet in using the Navy's integrated undersea surveillance system to detect and track whales and to detect seafloor seismic disturbances in the Atlantic Ocean. Named "Whales '93," the program seeks to use the acutely sensitive detection system for picking up the acoustic signals given off by whales and earthquakes. The program, even in its infancy, has yielded unprecedented information on both marine mammals and seismic activity in the Atlantic Ocean.

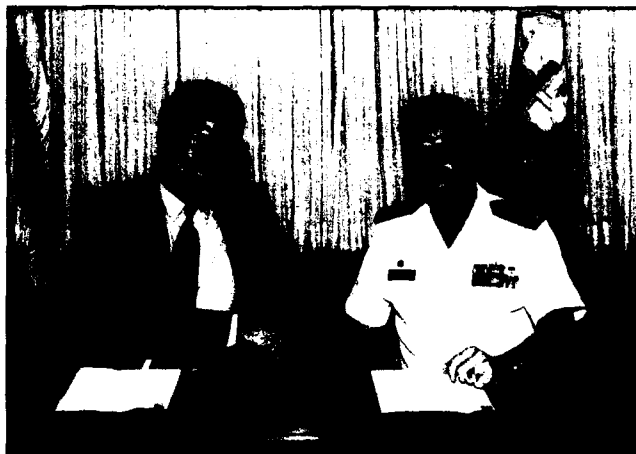
An underwater optical imaging system has been developed by Laboratory scientists that is capable of detecting and identifying submerged objects, at longer ranges than previously possible, in murky or turbid waters. Using a green laser pulse and a time-delayed camera shutter, the system is able to produce marked improvements in the image contrast of targets in turbid water. In another marine related research and development (R&D) advance, NRL chemists have tested an advanced fouling release coating for Navy ships. The hull coating permits the easy removal of organisms from ship hulls and is simultaneously safe for the ocean environment.

In other work, researchers at the Laboratory have designed and tested improved brackets for sonar transducers. The nonmetallic mounting brackets will provide improved reliability and reduced weight on submarines, as well as major cost savings to the Navy. A portable unit for dechlorinating shipboard seawater systems has been developed by the Laboratory's Marine Corrosion Facility in cooperation with the ARINC Research Corporation. The new unit will provide environmental compliance for the use of electrolytic chlorination needed to control marine biofouling in ship seawater cooling systems. NRL's Optical Sciences Division researchers have developed a signal processing technique for an open-loop, fiber-optic gyroscope. The new technique will provide the basis for a low-cost optical gyro system. Elsewhere in the Laboratory, scientists have designed and implemented a soft X-ray microscope that has recorded images of laser-produced plasmas at a wavelength of 130 Å with the highest spatial resolution ever achieved.

Two instruments developed by scientists at NRL to study atmospheric and solar science were launched as part of NASA's second Atmospheric Laboratory for Applications and Science (ATLAS) mission. The Solar Ultraviolet Spectral Irradiance Monitor (SUSIM) and the Millimeter-Wave Atmospheric Sounder (MAS) are studying the chemical and physical components of the Earth's middle atmosphere and the solar



The primary payload of instruments comprising the ATLAS-2 are shown on a spacelab pallet. The parabolic antenna belonging to the MAS instrument is in the box outlined. SUSIM is mounted on the rear right corner of the pallet. (photo courtesy of NASA)



Dr. William Kirwan, president of the University of Maryland, College Park, and CAPT Gaffney shake hands following the official signing of their CRADA to assist in transferring technology to companies in Maryland

energy injected into the atmosphere over the high northern latitudes. Preliminary measurements from the MAS have included complete, uniform readings of stratospheric temperature, water vapor, ozone profiles, and chlorine monoxide over about 75% of the Earth.

In other research, NRL geophysicists using a combination of satellite and radar imagery and airborne gravity and magnetic studies have found evidence of active volcanism and elevated heat flow beneath the West Antarctic Ice Sheet. Further studies and imagery suggest that other volcanic constructs are located elsewhere under the ice sheet. U.S. astronauts have also benefited from the results of NRL R&D. Astronauts on Space Shuttle flight STS-53 in December 1992 and STS-56 in April 1993 used the NRL-developed, hand-held Earth-oriented, real-time cooperative user-friendly location, targeting, and environmental system (HERCULES) to locate objects on Earth. The system allows astronauts to point a camera at a specific feature on Earth, record its image, and then determine the object's latitude and longitude.

NRL astronomers led a team of scientists that were the first to detect radio emissions from the bright supernova SN1993J in the nearby galaxy M81. This was the brightest and closest stellar explosion to occur in the northern sky in over 50 years. The team used the Very Large Array radio telescope to make their ob-

servations. Other NRL astronomers analyzed observations from NASA's Compton Gamma Ray Observatory to search for evidence of a black hole, which is thought might be near the center of the Milky Way galaxy. Early results show a high concentration of gamma rays emanating from a region around the center of the galaxy but, as yet, no variation in emissions that might indicate the presence of a black hole.

NRL was also active last year in transferring technology developed at the Laboratory to private industries for production and marketing. A cooperative research and development agreement (CRADA) was signed between NRL and the Virginia Center for Innovative Technology in Herndon, Virginia. Under the agreement the Laboratory and the Center will cooperate to transfer technology developed at NRL to companies in Virginia. In a similar agreement with the University of Maryland, NRL will cooperate with the University to transfer technology to Maryland companies. To date, NRL has signed 24 CRADAs and 20 patent license agreements. While the majority of CRADAs are with industrial firms, several are also with universities and nonprofit organizations. One of our licensees has formed a new company to manufacture and market an NRL-developed drug detection system. This company, located in southern California, employs 30 people, many of whom formerly worked in the defense industry.

NRL Today

ORGANIZATION AND ADMINISTRATION

The position of NRL within the Navy is that of a field command under the Chief of Naval Research.

Heading the Laboratory with joint responsibilities are the naval commanding officer, CAPT Paul G. Gaffney II, USN, and the civilian director of research, Dr. Timothy Coffey. Line authority passes from the commanding officer and the director of research to five associate directors of research, an associate director for strategic planning, and an associate director for business operations. Research is performed in the following areas:

- General Science and Technology
- Warfare Systems and Sensors Research
- Materials Science and Component Technology
- Ocean and Atmospheric Science and Technology
- Naval Center for Space Technology.

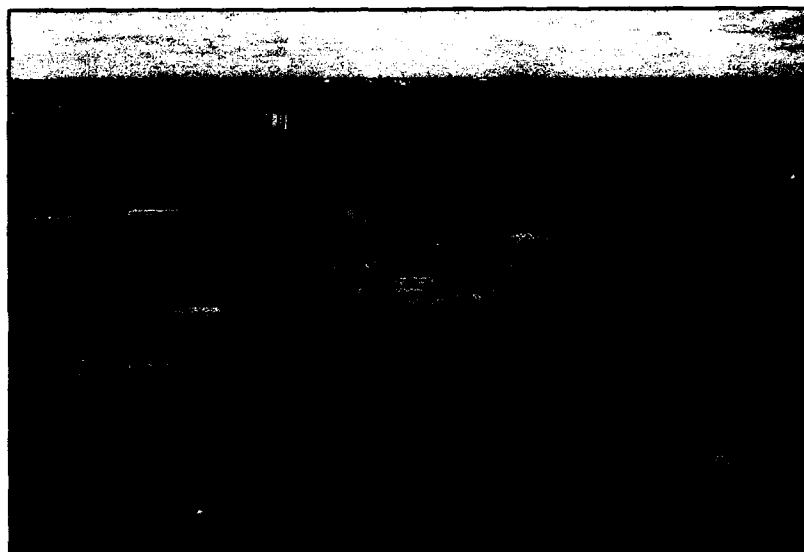
Further details of the Laboratory's organization that includes NRL-Stennis Space Center

(NRL-SSC) in Mississippi and NRL-Monterey (NRL-MRY) in California are given on the organizational chart appearing in the "General Information" section. NRL-SSC and NRL-MRY are the result of a merger with NRL and the Naval Oceanographic and Atmospheric Research Laboratory (NOARL) in 1992.

Through FY 93, NRL operated as a Defense Business Operating Fund (DBOF) activity. As a DBOF activity, all costs, including overhead, were charged to various research projects. Funding in FY 93 came from the Chief of Naval Research, the Naval Systems Commands, and other government agencies, such as the U.S. Air Force, Advanced Research Projects Agency, the Department of Energy, and the National Aeronautics and Space Administration as well as several nongovernment activities.

PERSONNEL DEVELOPMENT

At the end of FY 93, NRL employed 4079 personnel—42 officers, 74 enlisted, and 3963 civilians. In the research staff, there are 924



NRL headquarters in Washington as viewed from the east

employees with doctorate degrees, 493 with masters degrees, and 707 with bachelors degrees. The support staff assists the research staff by providing administrative, computer-aided designing, machining, fabrication, electronic construction, publication, personnel development, information retrieval, large main-frame computer support, and contracting and supply management services.

Opportunities for higher education and other professional training for NRL employees are available through several programs offered by the Employee Development Branch. These programs provide for graduate work leading to advanced degrees, advanced training, college course work, short courses, continuing education, and career counseling. Graduate students, in certain cases, may use their NRL research for thesis material.

For non-NRL employees, several post-doctoral research programs exist. There are also cooperative education agreements with several universities, summer and part-time employment programs, and various summer and interchange programs for college faculty members, professional consultants, and employees of other government agencies.

NRL has active chapters of Women in Science and Engineering, Sigma Xi, Toastmaster's International, Federally Employed Women, Inc., and the Federal Executive and Professional Association. Three computer clubs meet regularly—NRL Microcomputer User's Group, NeXT, and Sun NRL Users Groups. An amateur radio club, a drama group (the Showboat-ers), and several sports clubs are also active. NRL has a recreation club that provides basketball and softball leagues, swimming, saunas, whirlpool bath, gymnasium, and weight-room facilities. The recreation club also offers classes in martial arts, aerobics, swimming, and water walking.

A community outreach program at NRL provides tutoring for local students, science fair judging, participation in high school and college career day programs, an art and essay contest during Black History Month, student tours of NRL, and an annual holiday party for neighborhood children, with gifts donated by Laboratory employees. Through this program NRL has

active partnerships with four District of Columbia public schools.

NRL has an active, growing Credit Union with assets over \$155 million and a membership numbering over 18,900. Public transportation to NRL is provided by Metrobus.

For more information, see the *NRL Review* chapter entitled, "Programs for Professional Development."

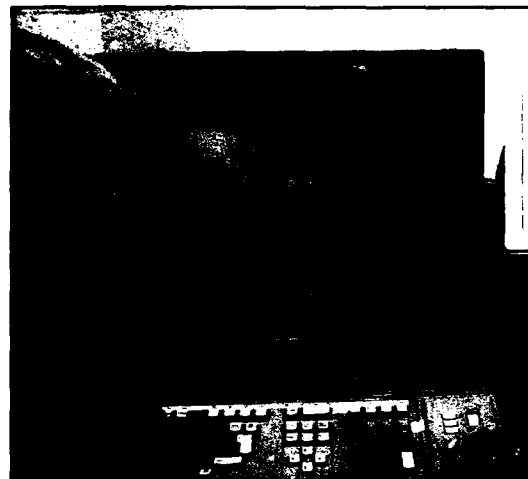
SCIENTIFIC FACILITIES

In addition to its Washington, DC campus of about 130 acres and 102 main buildings, NRL maintains 14 other research sites including a vessel for fire research and a Flight Support Detachment. The many diverse scientific and technological research and support facilities are described in the following paragraphs.

Research Facilities

- Radar

NRL has gained worldwide renown as the "birthplace of radar" and has maintained its reputation as a leading center for radar-related research and development for a half century.



The Radar Division has developed target signature programs that use surface modeling and graphics software and hardware to convert geometric shape data into a form suitable for electromagnetic scattering calculations. These programs also perform the electromagnetic calculations, sum the return from all ship components (e.g., hull, anchor, railing, vents), and display the geometric model and signature results.

An impressive array of facilities managed by NRL's Radar Division continues to contribute to this reputation. These include airborne and laboratory radar cross section measurement systems; two Ultrahigh-Resolution Inverse Synthetic Aperture Radars (ISAR), one for airborne installation and the other for shipboard installation; and a rooftop space-time adaptive array laboratory. Also, the division manages and maintains a radar display testbed, an IFF ground station, a digital signal processing facility, and a radar cross section prediction facility. A radar research and development activity is located at the Chesapeake Bay Detachment (CBD), Randle Cliffs, Maryland. It has separate facilities for specific types of systems that range from high-frequency, over-the-horizon systems to millimeter wave radars. The SENRAD radar testbed, a flexible and versatile system for demonstrating new developments in radar, and a point defense radar testbed are also located at CBD.

• Information Technology

The Information Technology Division (ITD) is at the forefront of DoD research and development in artificial intelligence, telecommunications, computer networking, human computer interaction, information security, parallel computation, and computer science.

The division maintains local area computer networks to support its research and hosts testbeds for advanced high performance fiber optic network research. The networks make available to local and remote users hundreds (more than 500 Macintoshes, PCs, and other workstations) of high performance computers. The ITD research networks are part of NRL's internal network and also connect via T1 lines to the regional SURAnet, to DISnet, and via ATM/SONET links to ATDnet, an experimental wide area network connecting a number of research organizations in the metropolitan area.

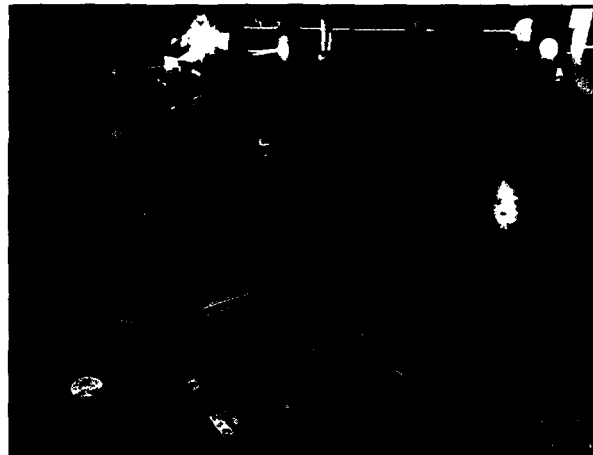
Major shared resources include the systems and networks available in the division's Center for Computational Science, including a 256 processor CM5, 16-k processor CM200 equipped with a 10-gigabyte data vault, dual

processor Cray Y-MP EL, 1.5-terabyte file server/archiver, and scientific visualization lab. The Center manages and operates the NRL local area network (NICEnet), which includes a new FDDI network. NICEnet provides external connections to networks worldwide.

The division facilities also include a Certification and Information Security Engineering Laboratory and an experimental facility with special displays, eye and gesture trackers, and speech I/O devices for research in human computer interaction.

• Optical Sciences

The Optical Sciences Division has a broad program of basic and applied research in optics and electro-optics. Areas of concentration in electro-optics include fiber optics, integrated optical devices, fiber-optic sensors, high-power diode lasers, and diode pumped solid-state lasers. Modern electro-optic sensors such as infrared focal plane arrays are developed by NRL as well as signal processors, digital processing, computer algorithms, and digitized background scene imagery to allow computer augmented sensor design for Naval applications.



Researchers from the Optical Sciences Division have developed a simple, ultrashort-pulse erbium all-fiber laser suitable for integration into fiber systems operating at 1.5 μm communications wavelength. The figure-eight laser (F8L) can be applied to high-speed optical communications, short-pulse optical sensors, and the optical probing of high-speed electrical circuits. Shown above is the actual F8L laser (note the quarter in the left foreground corner to reference for scale).

The division also maintains a capability to perform optical field measurements from ground-based, water-based, or air-based platforms at appropriate sites away from NRL. Facilities include:

Ultralow-Loss, Fiber-Optic Waveguides—NRL has developed record-setting ultrahigh transparency infrared waveguides. These fluoride glass materials offer the promise of long-distance communications without the need of signal amplification or repeaters.

Focal Plane Evaluation Facility—This facility has extensive capabilities to measure the optical and electrical characteristics of infrared focal plane arrays being developed for advanced Navy sensors.

IR Missile-Seeker Evaluation Facility—This facility performs open-loop measurements of the susceptibilities of infrared tracking sensors to optical countermeasures.

Large Optic, High-Precision Tracker—NRL has developed a tracker system with an 80-cm primary mirror for atmospheric transmission and target signature measurements. By using a quadrant detector, the servo system has demonstrated a 12-mrad tracking accuracy. An optical correlation tracker system tracks objects without a beacon.

High-Energy Pulsed Hydrogen Fluoride, Deuterium Fluoride Laser—NRL has constructed a pair of pulsed chemical lasers each capable of producing up to 30 J of laser energy at 2.7 to 3.2 μm and 3.8 to 4.5 μm in a 2-ms pulse. This facility is used to investigate a variety of research areas including stimulated Brillouin scattering, optical phase conjugation, pulsed laser amplification, propagation, and beam combining.

Fiber-Optics Sensors—The development and fabrication of fiber-optic sensor concepts, including acoustic, magnetic, and rate-of-rotation sensors, are conducted in several facilities within the Laboratory's Optical Sciences and Acoustics Divisions. Equipment includes facilities for evaluating optical fiber coatings, fiber splicers, an acoustic test cell, a three-axis magnetic sensor test cell, a rate table, and various computers for concept analysis.

Digital Processing Facility—This facility is used to collect, process, analyze, and manipu-

late infrared data and imagery from several sources.

Emittance Measurements Facility—NRL routinely performs measurements of directional hemispherical reflectance from 2 to 16 μm in the infrared by using a diffuse gold integrating sphere and a Fourier Transform Spectrophotometer (FTS). Sample temperatures can be varied from room temperature to 250°C and incidence angles from 0° to 60°.

Diode Pumped 2- μm Solid-State Lasers—Two micrometer lasers operate in an eye-safe region of the optical spectrum, an important issue for laser use in industry or in cases where eye damage to the public could be a safety and liability issue. Research at NRL in the 1980s had a major role in enabling room temperature flashlamp and diode pumped lasers. The lamp pumped lasers have found wide usage in laser surgery while diode pumped lasers appear leading candidates for eye-safe laser radars for aircraft as well as for laser sources to counter IR missile seekers.

• Electronic Warfare

The scope of research and development at NRL in the field of electronic warfare covers the entire electromagnetic spectrum, from basic technology research, component and subsystem development to system design and effectiveness



The Tactical Electronic Warfare's Scale Model Analysis Facility is a compact range established at NRL as a low cost method of measuring and analyzing the radar cross section of target platforms using submillimeter waves and accurate scale models of the target platforms and the environment

evaluation. Major emphasis is placed on providing the methods and means to counter enemy hostile actions in all battle phases, from the beginning—when enemy forces are mobilized for an attack—through the final engagement stages. For this purpose, NRL has constructed special research and development laboratories, anechoic chambers, and facilities for modeling and simulation. NRL has also added extensive new facilities where scientists can focus on the coordinated use of all organic defensive and offensive resources now present in the Fleet.

• Structure of Matter

The Laboratory investigates the atomic arrangements in materials to improve them or facilitate the development of new substances. Various diffraction methodologies are used to make these investigations. Subjects of interest include the structural and functional aspects of energy conversion, ion transport, device materials, and physiologically active substances such as drugs, antibiotics, and antiviral agents. Theoretical chemistry calculations are used to complement the structural research. A real-time graphics system aids in modeling and molecular dynamics studies.

• Chemistry

NRL has been a major center for chemical research in support of naval operational requirements since the late 1920s. The Chemistry Division continues its tradition with a broad spectrum of basic and applied research programs concerned with controlled energy release (fuels, fire, combustion, countermeasure decoys, explosives), surface chemistry (corrosion, adhesion, tribology, adsorbents, film growth/etch), advanced polymeric materials (high strength/low weight structures, drag reduction, damping, special function), and advanced detection techniques (environment, chemical/biological, surveillance). Facilities for research include a wide range of the modern photon electron, magnetic and ion-based spectroscopic/microscopic techniques for bulk and surface analysis; multiple facilities for materials synthesis and physical/chemical characterization; a

325-M³ (11,400 ft³) fire research chamber (Fire I), and a 475-ft ex-USS *Shadwell* (LSD-15) advanced fire research ship.

• Materials

NRL has capabilities for X-ray and electron diffraction analyses and for electron and Auger spectroscopy. Scanning, transmission, and combined scanning-transmission electron microscopes are used to study surface and/or internal microstructures. It has a secondary ion mass spectrometer for surface analysis that significantly extends the diagnostic capability of the technique. A high-resolution, reverse-geometry mass spectrometer is used to probe reactions between ions and molecules. The Laboratory has a fully equipped fatigue and fracture laboratory, a modern vacuum arc melting furnace for reactive metals, an ultrasonic gas atomization system for making metal powders, and hot isostatic press facilities. The Laboratory's cryogenic facilities include dilution refrigerators and superconducting magnetic sensors for measuring ultrasmall magnetic fields. Also available are two molecular beam epitaxy devices for growing thin films.

• Laboratory for Computational Physics and Fluid Dynamics

The Laboratory for Computational Physics and Fluid Dynamics (LCP&FD) is a participant in the DARPA Touchstone Scalable Parallel Processing Project. An Intel IPSC/860 Touchstone Gamma supercomputer provides the environment necessary to develop, debug, and benchmark parallel simulations. With multi-MFLOP processors as building blocks, the computer is configured as a hypercube and is a MIMD distributed memory machine. This 32-node machine is expected to attain a computational speed of several hundred MFLOPS. Access to the 518-node Touchstone Delta machine at Cal Tech and the new DoD HPCC resources is provided through high-bandwidth network communications.

Four IBM RS/6000 and two DEC AXP high-capacity workstation class compute server computers provide LCP&FD with medium- to

large-scale memory and computational power enabling the division to perform calculations, algorithm development, diagnostic, and evolution postprocessing for large simulations. A 64-million word Convex C210 currently provides LCP&FD with medium performance scalar and vector capability for jobs that require large amounts of memory.

A high-quality video studio has been created using digital recording techniques and provides the capability to create graphical representations of simulation data for analysis and presentation. Graphical workstations and servers including IRIS 4D, Sun Microsystems, and Macintosh are also available.

• Condensed Matter and Radiation Sciences

The Condensed Matter and Radiation Sciences Division is the primary Navy center studying the effects of radiation on material items including electronic equipment, satellites, etc., and the condensation of materials (thin films) on other objects through the use of charged-particle radiation. The division approaches these activities from both the theoretical and applied aspects, including application to environmental as well as military situations. The facilities for production and employment of



Shown here is the Condensed Matter and Radiation Sciences Division's computer-automated pulsed laser deposition system. This chamber is designed to deposit epitaxial multilayers and superlattices of multicomponent materials such as the high-temperature superconductors and other electronic ceramics.

photons, electrons, ions, and hypervelocity projectiles available to the division include:

High-Powered Microwave (HPM) Facility—

This facility is used to investigate the response of systems and components to pulsed high-power radiation. Effects, susceptibility, and survivability are the major research areas of interest. The large anechoic chamber (4.9 m × 4.9 m × 9.8 m long) can be used for frequencies ranging from 0.6 to 94 GHz.

*Laser Facilities—*The ultrafast lasers provide a broad range of capabilities by bringing together an extensive array of laser sources for the study of condensed matter interactions. Pulses of up to several joules are available from one system, while time resolutions down to 100 femtoseconds are produced by another. Synchronized, Q-switched oscillators are configured for pump-probe experiments. A range of optical, laser, and soft X-ray spectrometers are used to study nonlinear optical effects, time response, and laser-target interactions.

*Thin Film Preparation Facilities—*The division has several major capabilities for preparation of thin films of advanced materials, such as high-temperature superconductors and active dielectrics. These include ion-assisted evaporation (which produces dense, adherent films), various dc plasma sources (which can etch as well as deposit films), and pulsed laser deposition (for production of chemically complex films).

*X-ray Facility—*Laboratory X-ray sources, monochromators, detectors, and related equipment are available for X-ray energies from 0.7 to 25 keV and the dose rates up to 10^5 rads/s.

*Synchrotron Radiation Facility—*Intense, monochromatic X-ray photon beams, tunable from 10 eV to 12 keV, are available from the three beam lines developed by NRL at the National Synchrotron Light Source at the Brookhaven National Laboratory. Standard measurements include X-ray diffraction, absorption, reflectance, and photoelectron emission. Environmental target chambers can span a pressure range from 10^{-12} to 10^5 atmospheres and temperatures from 10 to 1500 K.

*60-MeV Electron Linear Accelerator (LINAC)—*The LINAC produces intense electron

beams that are used to study radiation effects on microelectronics and materials for DoD satellite and missile programs. It is also used to study radiation effects on the new, high-critical temperature superconductors.

Ion Implantation Facility—The facility consists of a 200-keV ion implanter with specialized ultrahigh vacuum chambers and associated in situ specimen analysis instrumentation. The facility is used to develop advanced surface treatments of materials to modify their properties and improve corrosion and wear resistance.

3-MeV Tandem Van de Graaff—This facility is used to study charged-particle radiation damage effects such as occur in space, to perform Rutherford backscattering spectroscopy and nuclear reaction analysis, to provide high-sensitivity composition depth profiles, and to perform MeV energy implants in materials.

Hypervelocity Impact Facilities—Three facilities are used for ballistics research at speeds exceeding 6 km/s with toxic and explosive targets while measuring projectile velocity, orientation, and dynamic projectile-target interaction.

• Plasma Physics

The Plasma Physics Division is the major center for in-house Navy and DoD plasma physics research. The division conducts a broad experimental and theoretical program in basic and applied research in plasma physics, which includes laboratory and space plasmas, pulsed-power sources, electric mass launchers, intense electron and ion beams, atomic physics, laser physics, and numerical simulations. The facilities include an extremely high-power laser, Pharos III, for the laboratory simulation of space plasmas and high-latitude nuclear explosion effects studies and the electric mass launcher laboratory to study railgun physics. The division has developed a variety of pulsed-power sources to generate electron and ion beams, powerful discharges, and various types of radiation. The largest of these pulsed-power sources, GAMBLE II, is used to study the production of megampere electron beams and for producing very hot, high-density plasmas. Other generators are used to produce particle beams that are injected into magnetic fields and/or cavities to



Plasma Physics Division's new facility, the Railgun Electric Launcher (a 1-m long railgun (front right)) is powered by a 0.5-MJ capacitor bank (rear). The railgun uses electric current to accelerate a projectile to very high velocities ($v > 2$ km/s). Applications include antiship missile defense, antitank weapons, long-range artillery, theater missile defense, and ultimately, space launch.

generate intense microwave pulses. A charged-particle-beam (CPB) propagation facility exists for testing advanced CPB propagation (both endo- and exoatmospheric) concepts. A 5-MW generator injects pulses of electron current into preheated ionization channels to study the effectiveness of propagation under various conditions.

• Electronics Science

In addition to specific equipment and facilities to support individual scientific and technology programs in electronics and electronic-materials growth and analysis, NRL operates the Nanoelectronics Processing Facility. The facility provides services to electronics programs throughout the Laboratory and to external organizations. This facility provides support for NRL programs that require microelectronics processing skills and equipment. The facility includes a nanowriter that can be used to fabricate nanoscale (80 Å) structures and, in general, supplies NRL programs with a range of items from discrete structures and devices to complete integrated circuits with very large scale integration (VLSI) complexity based on silicon metal oxide semiconductors (MOS) submicrometer technology.

• Bio/Molecular Science and Engineering

The Center for Bio/Molecular Science and Engineering conducts research and development using biotechnological approaches to solve problems for the Navy, the Department of Defense, and the nation at large. Problems currently being addressed include advanced material development (for electronic, biomedical, and structural applications), combat casualty care, environmental quality (including pollution cleanup and control), and biological warfare defense. The approach to these problems involves long-term research focused on the study of complex materials systems, coupled with integrated exploratory and advanced development programs. The staff of the center is an interdisciplinary team performing basic and applied research and development in areas that require expertise in bio and surface chemistry,



Scientists in the Electronics Science and Technology Division are developing high-temperature superconducting thin film devices. Here an applied superconductivity research team uses computer-aided techniques to measure and analyze the electrical properties of these devices.

biophysics, genetic engineering, cell biology, advanced organic synthesis, solid-state and theoretical physics, and electronics and materials engineering. In addition, the center has many collaborations throughout the Laboratory, at universities, and in industry to ensure that a broad base of the required expertise and critical evaluations are part of the research and development programs. Highlights of the program include the development of liposome-based blood substitutes, the manipulation of biologically derived structures on the nanometer scale, the development of ferroelectric liquid crystal systems with microsecond response times, discovery of an advanced resist system for high-speed, high-density integrated circuits, and the patterning of neuronal cells to form neural networks.

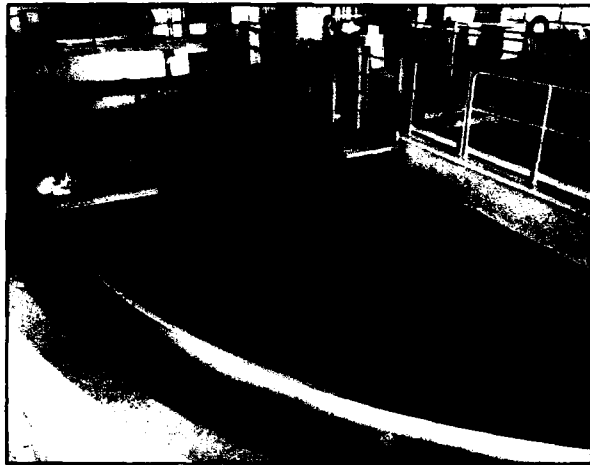
• Acoustics

NRL's facilities in support of acoustical investigations are located at the main Laboratory site; at Stennis Space Center in Bay St. Louis, Mississippi; and at the Underwater Sound Reference Detachment (USRD) in Orlando, Florida. At the main Laboratory site, there are three research tanks instrumented to study echo characteristics of targets and to develop devices. The most significant of the three is located in the NRL Laboratory for Structural Acoustics in Building 5, which includes a state-of-the-art acoustic pool for conducting scale-model scatter-

ing and radiation studies. Capabilities include near-field acoustic holography for studying complex 3-D sound fields near a target and the vibrations of the target itself. NRL has successfully produced the first near-field acoustical-scattered hologram in this facility. Among the benefits of the holographic capability is that near-field measurements can be projected to the far field, and target strengths can be obtained in any desired direction. In general, the pool complex permits model studies and demonstrations to be carried out at scales ranging from about 30:1 to several hundred to one. Projects involving modeling include, but are not limited to, target strength, radiation, signature reduction, classification, and structural acoustics. Advanced hull sensor technologies can be studied at any scale. There is also an underwater acoustic holography facility for research in acoustic fields and a water tunnel having a large blow-down channel with a 15-m test section used for acoustic and flow-induced vibration studies of towed line arrays and flexible cables.

The division also has several acoustic receiver array systems used to collect data for coherent signal processing. The primary system consists of a 64-element, towed, seismic-type receiver array with the associated tow cable, winch, and electrical components. The towed array component can be replaced with a 64-element, fixed bottomed array or 64-element vertical array. There are also two radio telemetered, buoyed, acoustic receiver array systems with 20-element arrays capable of being vertically or horizontally deployed. All receiver arrays are interfaced in o the At-sea Data Acquisition, Recording, and Real-time Processing System.

The division operates high-frequency (up to 600 kHz) acoustic measurement systems to obtain scattering, target strength, and propagation data using four large bottom-moored instrumentation towers and a high-speed, remotely operated vehicle. These data are used to simulate the performance of weapons and mine counter-measure sonars in shallow-water environments. The mid-frequency (30-1000 Hz) towed horizontal array system is used to understand the three dimensional characteristics of the acoustic ambient noise field; these measurements are



The Large Acoustic Tank is the core research capability for structural acoustics studies undertaken by the Acoustics Division. The steel cylindrical tank is 55 feet in diameter, 50 feet deep, and contains 800,000 gallons of deionized water. The entire tank is vibration and temperature isolated. This unique laboratory is also instrumented with precise measurement systems that includes large workspace in-water robotic scanners capable of generating Nearfield Acoustic Holography radiation and scattering databases.

used to develop tactics and advanced systems to exploit these characteristics. An acoustic simulation capability plus a dedicated laboratory based on multiple workstations that are linked to the NRL CM-5/200, Cray Y-MP EL, and national high-performance computer facilities provides benchmark simulations of acoustic performance based on high-resolution oceanographic and atmospheric environmental information.

• Remote Sensing

The Remote Sensing Division conducts a program of basic research, science, and applications to develop new concepts for sensors and imaging systems for objects and targets on the Earth and in the near-Earth environment, as well as in deep space. The research, both theoretical and experimental, leads to discovering and understanding the basic physical principles and mechanisms that give rise to the background environmental emissions and targets of interest and to absorption and emission mechanisms of the intervening medium. Accomplishing this research requires the development of sensor systems technology. The development effort includes active and passive sensor systems

used for the study and analysis of the physical characteristics of phenomena that evolve from naturally occurring background radiation, such as that caused by the Earth's atmosphere and oceans and man-made or induced phenomena, such as ship/submarine hydrodynamic effects. The research includes theory, laboratory, and field experiments leading to ground-based, airborne, or space systems for use in remote sensing, astrometry, astrophysics, surveillance, nonacoustic ASW, improved meteorological/oceanographic support systems for the operational Navy, and the environmental/global climate change initiatives. Special emphasis is given to developing space-based platforms and exploiting existing space systems.

• Oceanography

The Oceanography Division is the major center for in-house Navy research and development in oceanography. It is known nationally and internationally for its unique combination of theoretical, numerical, and experimental approaches to oceanographic problems. Theoretical research makes extensive use of the Maury Oceanographic Library (jointly operated by NRL-Stennis Space Center (NRL-SSC) and the



NRL-SSC's researchers tested two new acoustic measurement systems—the Digital Acquisition Buoy System (NDABS) and the Digital Acquisition Buoy System (ADABS)—on the USNS *Bartlett*, a research vessel operated by the Naval Oceanographic Office at Stennis Space Center. Both systems are used to measure ocean acoustic data. The difference between the systems is that NDABS uses fiber-optic cables for the telemetry data. Shown here are researchers from the Oceanography Division as they attach recorders to NDABS for field testing.

Naval Oceanographic Office), which is recognized as one of the best and most comprehensive oceanographic libraries in the world. The division numerically models the ocean and coastal areas of the world. This modeling is conducted on the Navy's and DoD's most powerful vector and parallel processing machines. To study the results of this intense modeling effort, the division operates a number of highly sophisticated graphic systems to visualize ocean and coastal dynamic processes. The seagoing experimental programs of the division are particularly well supported. Unique measurement systems include towed sensor and advanced microstructure profiler systems for studying micro- and fine-scale ocean structure. The division uses a number of self-contained, multi-channel in situ recording systems for acoustic and oceanographic measurements. The division deploys an integrated absorption cavity and optical profiler system for studying ocean optical characteristics. In the laboratory, the division operates an environmental scanning electron microscope for detailed studies of bio-corrosion in naval materials.

• Marine Geosciences

The Marine Geosciences Division is the major center for in-house Navy research and development in marine geology, geophysics, geo-acoustics, and geotechnology. It is also the Navy's lead activity for mapping, charting, and geodesy research and development. The division has acquired unique instrumentation suites for its studies of the seafloor and its subbottom. These include side-scan sonar systems; deep-towed, low-frequency acoustic reflection systems; parametric acoustic swath subbottom mapping systems; remotely operated vehicles; and electromagnetic mapping sensors. These systems allow studies ranging from sediment classification to mapping of inclusions and changes in the seafloor subbottom structure. The division deploys ocean bottom and subbottom seismometer systems for use in studies ranging from tectonic noise to studies of whale migration. Specialized seafloor probes allow measurement of the water pressure in sediment pores and acoustic compression and shear wave velocity and attenuation. Laboratory equipment includes a

transmission electron microscope with an environmental cell to carry out sediment-fabric and sediment-pollution adsorption studies. The Map Data Formatting Facility, a collection of computers and work stations with associated graphics manipulation software, is used to compress map information onto compact disk read-only memory for Navy and Marine Corps aircraft digital moving maps. The division also operates the NRL Magnetic Observatory at SSC. This facility includes two specially built wood buildings with minimal ferrous content and arrays of magnetometers that extend radially from the building. The Magnetic Observatory measures the ambient magnetic field, its changes, and other magnetic phenomena. The Observatory is part of a worldwide observing system. In addition to in-house laboratory work, the division incorporates the Chief of Naval Operations (CNO) sponsored Tactical Oceanographic Warfare Support Program Office, which develops high-resolution atmospheric, oceanographic and bathymetric instrumentation systems, and measurement techniques in support of CNO endorsed requirements.

• Marine Meteorology

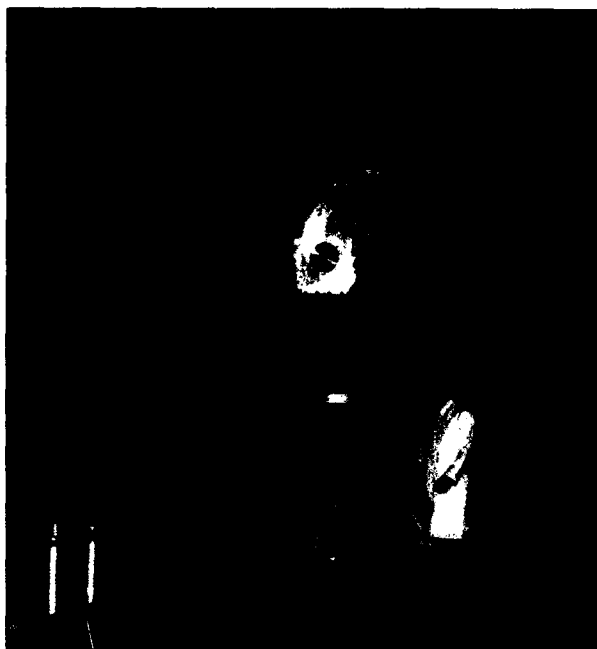
The Marine Meteorology Division is located in Monterey, California. NRL-Monterey (NRL-MRY) performs both basic and applied research in meteorology, in applications relevant to both central-site and shipboard meteorological analysis and forecasts. Located adjacent to the Fleet Numerical Oceanography Center (FNOC), the Navy's operational forecast center, NRL-MRY has developed both the global and regional forecast systems that are run at FNOC and that provide worldwide Navy forecasts. NRL-MRY is also the technical direction agent for TESS(3), a minicomputer-based environmental diagnosis/forecast system designed for shipboard use. Advanced technologies in use include satellite meteorology, advanced numerical techniques, and artificial intelligence.

• Space Science

NRL is the Navy's main laboratory for conducting basic research and development in the space sciences. The Space Science Division has



The Marine Meteorology Division's Computing Facility includes a data retrieval system and visualization laboratory. The facility retrieves data from the Fleet Numerical Meteorology and Oceanography Center daily and prepares data sets for various research projects. The graphics capability of the facility provides opportunities for satellite researchers to perform multichannel image manipulation tasks, and for numerical modelers to perform graphical model diagnoses. Also, the facility provides the developmental system hardware/software platform for the Tactical Environmental Support System project.



Researcher from the Spacecraft Engineering Department checks over the Deep Space Program Science Experiment spacecraft, called Clementine, before in-house testing begins at NRL's Payload Checkout Facility. Clementine was designed by NRL to carry the small, lightweight ultraviolet, visible, and infrared (IR) sensors. Clementine will achieve lunar orbit through a series of transfer loops and will spend approximately two months in two different lunar orbits. During this time, it will map the entire surface of the moon in visible and near-IR spectrums, before traveling on to fly by the near-Earth asteroid, Geographos.

a number of commitments for space experiments in the areas of upper atmospheric, solar, and astronomical research aboard NASA, DoD, and other space projects. Division scientists are involved in major research thrusts that include ultraviolet remote sensing of the upper atmosphere, studies of the solar atmosphere by using spectrographic techniques, and studies of astronomical radiation ranging from the ultraviolet through cosmic rays. This includes the mission operations and data analysis facilities for NRL's OSSE experiment on NASA's Compton Observatory. The division maintains facilities to design, construct, assemble, and calibrate space experiments. A network of VAX computers, super minicomputers, image processing hardware, a PDS microdensitometer, and Cray and Connection Machine accesses are used to analyze and interpret space data. The division also operates the BMDO Backgrounds Data Center, which is a repository and analysis center for experimental data pertaining to natural backgrounds.

• Space Technology

In its role as a center of excellence for space systems research, the Naval Center for Space Technology (NCST) designs, builds, ana-

lyzes, tests, and operates spacecraft, as well as identifies and conducts promising research to improve spacecraft and their support systems. NCST facilities that support this work include large and small anechoic radio frequency chambers, clean rooms, shock and vibration facilities, an acoustic reverberation chamber, large and small thermal/vacuum test chambers, control system interaction laboratory, satellite command and control ground stations, fuels test facility, and modal analysis test facilities. NCST has a facility for long-term testing of satellite clock time/frequency standards under thermal/vacuum conditions linked to the Naval Observatory; a 5-m optical bench laser laboratory; and a hologram research laboratory to conduct research in support of the development of space systems.

Research Support Facilities

• Technical Information Services

The Ruth H. Hooker Research Library and Technical Information Center contains more than one million items, including current journals. Its collections can be searched by computer-based catalogs. The Library also provides interlibrary loans, on-line literature



The Technical Information Division has just completed a new multiformat video editing suite. Built around a highly versatile video production switcher, the system combines video and audio switching with two channels of real-time digital effects and time code editing.

searches, access to CD-ROM databases, loans of microcomputer software and laptops, and a full range of reference services, including assistance in selecting and using microcomputer software. Library resources that include an online catalog, a number of CD-ROM databases, and INTERNET can be accessed from offices and laboratories through the InfoNet campus-wide information system.

Publication services include writing, editing, composition, phototypesetting, and publications consultation. The primary focus is on using computer-assisted publishing technology to produce scientific and technical information containing complex artwork, equations, and tabular material.

The research conducted at NRL requires a diversity of graphic support, such as technical and scientific illustrations, computer graphics, design services, photographic composites, calligraphy, display panels, sign making, and framing. A high-end workstation provides and delivers a new level of electronic airbrushing and photographic retouching.

Photographic services include high-speed motion picture, video, and still-camera coverage for data documentation both at NRL and in the field. A photographic laboratory offers custom processing and printing of black and white and color films. Photographic images can also be captured with state-of-the-art digital cameras and still video. Video services include producing video reports of scientific and technical pro-

grams. A video studio and editing facility with 3/4 in. and VHS editing equipment support video production.

The Electronic Imaging Center offers high-quality output from computer-generated files in PostScript, PICT, TIFF, and DICOMED DDC formats. The Imaginator film recorder produces high-resolution 35-mm slides, viewgraphs, and negatives. Photographic-quality color prints and viewgraphs are available from the Kodak XL7700. The Canon CLC500 scans color photographs to a Macintosh or PC disk. The Linotron Imagesetter produces gray-scale prints and transparencies at 1293 dpi.

• Center for Computational Science

The Center for Computational Science (CCS) conducts research and development to further the advancement of computing and communications systems to solve Navy problems. Promising technologies are transitioned to production systems. The CCS operates and maintains computer systems and networks that provide support for NRL, Navy, and DoD research. The CCS features two Connection Machines (massively parallel computer systems), a 16-k processor CM200 equipped with a 10-gigabyte data vault and a 256 processor CM5. These leading edge systems are being investigated and developed by the CCS. The CCS also provides a dual processor Cray Y-MP EL for production level support of vector computing.

The CCS supplies lab-wide data storage support with NRL's File Server/Archiver (FS/A) system. The FS/A provides 69 gigabytes of online storage and 1.5 terabytes of nearline storage featuring advanced robotics from Storage Technology in an automated tape cartridge system.

The CCS Visualization Lab functions as an information center, video production unit, and training center for the latest tools in scientific visualization. Using powerful workstations, researchers can turn the results of their computations into color prints, 35-mm slides, or video tapes. The Visualization Lab also provides assistance and training in workstation system administration.

The CCS facilities are accessed through NRL's local area network NICEnet, which includes a new local FDDI network. NICEnet provides external connections to network and computer systems worldwide. Dial-in modem access is also available.

FIELD STATIONS

NRL has acquired or made arrangements over the years to use a number of major sites and facilities for research. The largest facility is located at the Stennis Space Center (SSC) in Bay St. Louis, Mississippi. Others include a facility at the Naval Postgraduate School in Monterey, California, the Chesapeake Bay Detachment (CBD) in Maryland, and the Underwater Sound Reference Detachment (USRD) in Orlando, Florida. Additional sites are located in Maryland, Virginia, Alabama, and Florida.

• Flight Support Detachment (NRL FSD)

Located at the Patuxent River Naval Air Station in Lexington Park, Maryland, NRL FSD operates and maintains five uniquely modified P-3 Orion turboprop aircraft that are used as airborne research platforms. With the decommissioning of Oceanographic Development Squadron 8 (VXN-8) in September 1993, NRL FSD acquired not only two new P-3s but also two additional missions as well. Project Magnet measures and maps the Earth's magnetic



One of the P-3 Orion aircraft at NRL FSD. These aircraft are unique in that they serve as readily modifiable research platforms to meet a variety of research assignments.

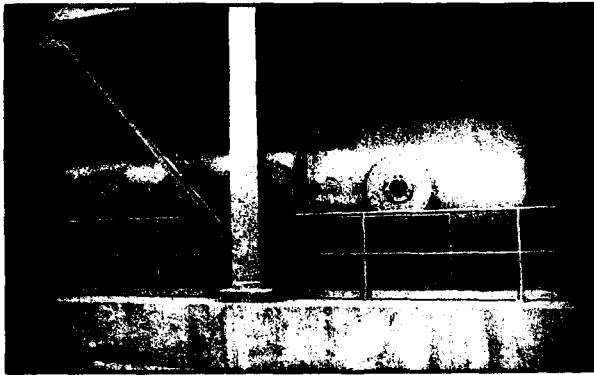
variation, while Project Birdseye conducts hydroacoustic research. NRL FSD's aircraft operate worldwide on extended deployment and annually log more than 2500 flight hours. These aircraft are the sole airborne platforms for numerous projects such as bathymetry, electronic countermeasures, gravity mapping, and radar development research. The detachment has a flawless safety record, having amassed more than 47,000 hours of accident-free flying over a 30-year period.

• Chesapeake Bay Detachment (CBD)

CBD occupies a 168-acre site near Chesapeake Beach, Maryland, and provides facilities and support services for research in radar, electronic warfare, optical devices, materials, communications, and fire research. Because of its location high above the Chesapeake Bay on the western shore, unique experiments can be performed in conjunction with the Tilghman Island site 16 km across the bay from CBD. Some of these experiments include low clutter and generally low background radar measurements. By using CBD's support vessels, experiments are performed that involve dispensing chaff over water and radar target characterizations of aircraft and ships. Basic research is also conducted in radar antenna properties, testing of radar remote sensing concepts, use of radar to sensor ocean waves, and laser propagation. CBD also hosts facilities of the Navy Technology Center for Safety and Survivability, which conducts fire research on simulated carrier, surface, and submarine platforms.

• Underwater Sound Reference Detachment (USRD)

Located at Orlando, Florida, USRD functions as a link in the traceability of underwater sound measurements to the National Institute of Standards and Technology and also performs R&D for sonar transducers and related acoustic materials. Its semitropical climate and clear, quiet lagoon (nearly circular and 11-m deep) is a distinct asset to its research and development on sonar transducers and underwater reference standards and to its improvement of techniques



USRD's newest acoustic measurement tank is capable of testing transducers or materials to 3000 psi at temperatures from 2° to 40°C

to calibrate, test, and evaluate underwater acoustic devices. USRD has two large, high-pressure tanks for simulating ocean depths to approximately 700 m and 2100 m. Smaller pressure tanks simulate depths to approximately 7000 m. A spring-fed lake, located in a remote area about 40 miles north of USRD (the Leesburg Facility), provides a natural tank for water depths to 52 m with an ambient noise level 10 dB below that for sea state zero; larger objects can be calibrated here. A conical shock tube (15-cm muzzle) simulates 60 lb of high explosive at a range of 20 ft for shock testing small sonar transducers. The detachment provides acoustic equipment and calibration services not only to hundreds of Navy activities and their contractors but also to private firms and universities not engaged in DoD contracts.

- Marine Corrosion Test Facility

Located on Fleming Key at Key West, Florida, this facility offers an ocean-air environment and clear, unpolluted, flowing seawater for studies of environmental effects on materials. Equipment is available for experiments involving weathering, general corrosion, fouling, and electrochemical phenomena, as well as coatings, cathodic protection devices, and other means to combat environmental degradation.

- Naval Research Laboratory-Stennis Space Center (NRL-SSC)

NRL-SSC, a tenant activity at NASA's Stennis Space Center (SSC) is located in the southwest corner of Mississippi about 50 miles northeast of New Orleans, Louisiana, and 20

miles from the Mississippi Gulf Coast. SSC encompasses over 200 square miles of land area including a perimeter *buffer* zone to insulate surrounding civilian communities from the noise of rocket engine testing by NASA. Other Navy tenants at SSC include the Commander, Naval Meteorology and Oceanography Command, and the Naval Oceanographic Office, who are major operational users of the oceanographic and atmospheric research and development performed by NRL. The Naval Oceanographic Office provides access for NRL researchers to one of the Navy's largest supercomputers. This unique concentration of operational and research oceanographers makes SSC the center of naval oceanography and the largest such grouping in the Western world.

NRL-SSC provides administrative and business operations support for NRL's Center for Environmental Acoustics, Remote Sensing Applications Branch, Oceanography Division, and Marine Geosciences Division. NRL-SSC occupies over 200,000 square feet of research, computation, laboratory, administrative, warehouse, and other facilities at SSC. Facilities include a number of large antennas to receive available oceanographic and meteorological satellite data, a Magnetic Observatory building constructed of nonferrous materials in an electromagnetically quiet area of SSC, a Pattern Analysis Laboratory, a Map Data Formatting Facility, a water-wave channel, and numerous laboratories for acoustic and oceanographic computation, instrumentation, analysis, and testing. Special areas are available for construction, staging, refurbishment, and storage of seagoing equipment.

- Marine Meteorology Division
Monterey, California (NRL-MRY)

Located in Monterey, California, as a tenant activity of the Naval Postgraduate School (NPS), this facility is collocated with the Fleet Numerical Meteorology and Oceanography Center (FNMOC) to support development and upgrades of numerical atmospheric forecast systems and related user products. NRL-MRY's mission has broadened considerably to include basic research and support to other customers. Collocation with FNMOC allows NRL-MRY access to the Navy's largest vector supercomputer mainframe and workstation resources. This access provides real time as well as archived global atmospheric and oceanographic databases for research on-site and at other NRL locations. Interfaces to the Defense Research and Engineering Network at FNMOC and Defense Simulation Internet at NPS have been established.

NRL-MRY's experience extends to prototype regional and shipboard atmospheric prediction systems. A third generation Navy system, the Tactical Environmental Support System (TESS(3)), developed for SPAWAR, is installed and has undergone various upgrades on-site to provide networking capabilities in line with the Copernicus architecture and remote workstation access. TESS(3) is functioning as an R&D testbed for new tactical/environmental decision aids (TDAs/EDAs), object oriented databases and Motif/X windows user interfaces. State-of-the-art graphics workstations (SGIs), network file servers (SUNs) and TAC 3 (HP) systems have been acquired for use by researchers. Environmental components of future systems are being developed within a system rooted in commercially available distributed database management software. This system, the Naval Environmental Operational Nowcasting System (NEONS), creates an environment that allows new products for weather and ocean forecasters

to be developed by blending satellite and conventional data. Both orbiting and geostationary data receivers are located at NRL-MRY.

- Other Sites

Some field sites have been chosen primarily because they provide favorable conditions to operate specific antennas and electronic subsystems and are close to NRL's main site. Maryland Point, south of NRL, operates two radio telescopes (25.6 and 26 m in diameter) for radio astronomy research. Pomonkey, a field site south of NRL, has a free-space antenna range to develop and test a variety of antennas. The antenna model measurement range in Brandywine, Maryland, has a 4.6-m diameter turntable in the center of a 305-m diameter ground plane for conducting measurements on scale-model shipboard and other antenna designs.

- Midway Research Center

The Midway Research Center (MRC), is located on a 158-acre site in Stafford County, Virginia. Located adjacent to the Quantico Marine Corps' Combat Development Command, the MRC has 10,000 ft² of operations and administration area and three precision 18.5-m diameter parabolic antennas housed in 100-ft radomes. The MRC, under the auspices of the Naval Center for Space Technology, provides NRL with state-of-the-art facilities dedicated solely to space-related applications in Naval communications, navigation, and basic research.

- Research Platforms

Mobile research platforms contribute greatly to NRL's research. These include five P-3 Orion turboprop aircraft and one ship, the ex-USS *Shadwell* (LSD-15) birthed in Mobile Bay, Alabama. The *Shadwell* is used for research on fire suppression techniques onboard ship.

NRL in the Future

To continue its growth and provide preeminent research for tomorrow's Navy, NRL must maintain and upgrade its scientific and technological facilities at the forefront. Its physical plant to house these facilities must also be adequate. NRL has embarked on a Corporate Facilities Investment Plan to renew its physical plant. This plan and future facility plans are described below.

THE CORPORATE FACILITIES INVESTMENT PLAN (CFIP)

The CFIP is a financial spending plan to provide modern research facilities at NRL by the year 2000. The plan calls for both Congressional and Laboratory investment and is updated and altered as changes occur in scientific emphasis and Congressional attitude. Over the past several years, Congressionally approved military construction (MILCON) funds were used to construct the new Electro-Optics Laboratory. Funds have also been approved for a small addition to NRL's Naval Center for Space Technology facilities, and funds have been requested for the construction of a new building for nanoscience research.

In the past years, NRL's overhead funds have been used to renovate laboratory and support areas in several existing buildings. Most noteworthy is the renovation of laboratory space for remote sensing and biomolecular science and engineering. The main facility for spacecraft fabrication and certification was upgraded to ensure structural soundness and enable more modern internal working areas.

• Radar

The Radar Division and the Naval Center for Space Technology have jointly established a new microwave test facility located in Building A-59. This compact range facility will allow test and evaluation of antennas and radar targets over a frequency range of 1 to 100 GHz. Presently, measurement equipment is being

upgraded. The indoor range and supporting laboratories occupy approximately 6000 ft² of space. Test objects up to 8-ft diameter can be accommodated. This facility obviates the need for an outdoor test range several thousand feet in length, achieving far-field radiation conditions from a large, prime focus, parabolic reflector.

• Optical Sciences

In mid FY 93, approximately 120 scientists and engineers from the Optical Sciences Division began occupancy of Building 216, the second phase of the Electro-Optics Research Laboratory (MILCON Project P-115). This facility is a 50,000-ft² addition to the existing Building 215. This move allows Buildings 12 and 30 to begin renovation under the NRL CFIP and replaces obsolete silica glass facilities with state-of-the-art facilities. It also allows the work in the areas of fiber optics, integrated optics, optical information processing, and infrared sensors to be pursued under one roof. Spaces are provided that were specially designed for modeling, testing, and checkout of sensors and components of optical systems in Buildings 215, 216, and/or the adjacent Building A-50.

• Long-Line Hydrophone Calibrator Facility

A major facility for the acoustic evaluation of towed arrays and other line arrays of hydrophones will be operational at the Underwater Sound Reference Detachment (USRD) in 1995. This facility will contain a 57-m long water-filled pipe that can be temperature and pressure controlled to simulate ocean environmental conditions. Piezoceramic projectors distributed in the pipe will ensonify an enclosed line array or module up to 48 m long with well-controlled sound fields that provide full through-the-beamformer calibration. The calibrator will be housed in a new building located at the USRD Leesburg Facility.

- Plasma Physics

A major 2-kJ KrF-laser facility will be established in the Plasma Physics Division by the end of FY 94. This facility is being initiated to provide intense radiation for studying inertial confinement fusion target heating at short wavelengths. A large-volume (2-m diameter by 5-m long) space chamber facility is operational to conduct space plasma physics research in the laboratory. A uniform axial magnetic field up to 1 kG and adjustable plasma density and temperature allow great flexibility to study laboratory simulation of space phenomena under controlled conditions.

- Electronics Science and Technology

Important division emphasis is focused on the continual upgrading of the Nanoelectronics Processing Facility and expanding activities in the nanoelectronics physics and vacuum electronics programs. Renovation of a new penthouse facility in Building 208 is planned for FY 94. This facility will consolidate and upgrade existing facilities for processing III-V semiconductor material devices in addition to serving the research needs of individual scientists within the division.

- Center for Bio/Molecular Science and Engineering

In January 1993 renovations began of Building 30 to accommodate the growing and diverse research programs of the Center for Bio/Molecular Science and Engineering. When completed, the center will have over 28,000 ft² of modern laboratory and office space. These facilities will include laboratories for biochemistry, organic synthesis, surface chemistry, and spectroscopy. Specialized facilities will include controlled-environment rooms, an advanced computer graphics laboratory, electron and scanning microprobe laboratories, and a sub-micron and nanostructure fabrication and characterization laboratory. Ample space is provided in which the center's interdisciplinary staff can meet and discuss joint projects. Renova-

tions are expected to be complete in the third quarter of FY 94.

- Ocean Acoustics Research Laboratory

NRL's Ocean Acoustics Research Laboratory (MILCON Project P-006), a 62,000-ft² building, will place 90% of NRL-SSC in one closely located area. This project will provide secure laboratory and computing facilities for research and development in underwater acoustics and in mapping, charting, and geodesy. Completion and occupancy should occur in FY 96.

- Vacuum Ultraviolet Space Instrument Test Facility

The Space Science Division recently completed a new solar instrument test facility in Building A-13. The new facility is designed to satisfy the rigorous contamination requirements of state-of-the-art solar spaceflight instruments. The facility has a 400-ft² Class 10 clean room specifically constructed to have low outgassing. The facility also houses the Solar Coronagraph Optical Test CHamber (SCOTCH). This completely dry-pumped, 550-ft³ vacuum chamber is maintained at synchrotron levels of cleanliness. Solar instrumentation up to 1 m in diameter and 5 m in length can be physically accommodated in the vacuum tank. The instrument optical performance tests are executed utilizing a variety of sources mounted on a 1-m diameter, 11-m long evacuated beamline. The chamber's ultimate pressure is 8×10^{-9} Torr; typical operating pressures with spaceflight instrumentation under test are $\sim 10^{-6}$ Torr. The facility also has a small thermal bake/vacuum test chamber utilized for vacuum conditioning and thermal testing of spaceflight components and subassemblies. Both the SCOTCH and the small test chamber are instrumented with temperature controlled quartz crystal monitors and residual gas analyzers for real-time, quantitative measurements of volatile contamination. The facility is currently used for the assembly and optical test of the Large Angle Spectrometric Coronagraph instrument for the European Space

Agency's Solar and Heliospheric Observatory spacecraft.

REHABILITATION OF SCIENTIFIC FACILITIES

Specialized facilities are being installed or upgraded in several of the research and support divisions.

• Flight Support Detachment

NRL's Flight Support Detachment (FSD) added two aircraft to its inventory in FY 94. Aircraft Bureau numbers 154587 and 158277 were previously assigned to Oceanographic Development Squadron 8 (VXN-8) prior to its decommissioning. Aircraft 154589 has completed its research modification and is awaiting final certification. Aircraft 149674 was upgraded with more powerful engines. Finally three of FSD aircraft will undergo navigation and communication upgrades starting in May 1994. These additions, modifications, and upgrades will ensure that NRL will have the finest airborne research capabilities well into the next century.

• Radar

The Radar Division has installed a computer aided engineering (CAE) facility to aid in digital system design. The system has full-color graphics workstations to provide capabilities for circuit design and simulation and printed circuit board layout. The facility has been used to design systems based on commercially available components as well as advanced systems incorporating VHSIC and gate array technologies. It has proven to be a valuable tool in evaluating new technologies for radar signal-processing requirements. The facility includes Sun workstations and IDAS software, which allows designs to be modeled and simulated at the system level. VHDL (VHSIC Hardware Description Language) software has been acquired for the workstations. This provides designers with an integrated toolset to model and simulate their designs from the system level down to the device level.

• Information Technology

The Information Technology Division continues to upgrade its local area network and research into high-performance network testbeds including ATM/SONET technology. The 256 processors with 32 Mb of memory in ARPA's CM5 operated at NRL will be replaced by newer, more capable SuperSparc processors with 128 Mb of memory per processor during the 1994 time frame. The need for additional facilities to supplement research in virtual environments and Global Grid demonstrations will lead to gradual development of a demonstration/VR and conference center in Building 34. An upgrade for the Human-Computer Interaction Laboratory will integrate and enhance its video and audio presentation and recording capabilities.

• Materials Science and Technology

Renovation is in progress for Building 3, which is made up of two of the original five buildings at NRL, to contain modern laboratories for studies of thin-film deposition and characterization, superconducting materials, magnetic materials, and other materials science projects. The new space will feature the most modern molecular beam epitaxy and other materials synthesis and processing equipment, an up-to-date fatigue and fracture laboratory and state-of-the-art diagnostic equipment including electron microscopes, spectrometers, and electron and X-ray diffraction equipment. The renovated building will also contain office and laboratory space for approximately 70 technical personnel.

• Plasma Physics

A state-of-the-art short-pulse (< 1 ps) high-intensity (> 1 TW) Table-Top Terawatt (T^3) laser has been procured for a variety of physics studies. The T^3 laser will be integrated into the Pharos III Nd-laser facility to boost its power into the 10 to 100 TW range. This will provide a facility to do fundamental physics experiments in intense laser-plasma interactions and intense laser-electron beam interactions.

A low-frequency (300 MHz to 10 GHz), high-power microwave facility, which uses a relativistic klystron concept, is being upgraded to produce multigigawatt coherent radiation pulses. A new laser facility is also planned. It will use a powerful KrF laser and a target chamber to conduct inertial confinement fusion research.

A new electric mass launcher facility has been established to investigate the evolution of the plasma armature in a high-velocity railgun. This facility is being upgraded to accelerate larger masses (~ 200 g) by using a 4-m long,

2.5-cm bore railgun powered by a 5-MJ capacitor bank.

- Electronics Science and Technology

In a move to further meet existing safety standards, potentially hazardous III-V semiconductor processes and associated chemicals will be moved to the new penthouse facility in Building 208. This facility employs a single-pass air-ventilation system to minimize hazards to personnel.

Highlights of NRL Research in 1993

Fiber Bragg Reflectors Fabricated In-line During Fiber Draw *Optical Sciences Division*

This work was motivated by the requirements of Smart Structure technology for dense, distributed sensing. It was recognized that these needs might best be met by arrays of Bragg reflectors placed along a few fibers, interrogated by the least possible instrumentation. Arrays of fiber Bragg gratings (FBGs) have been rapidly generated in a single-mode optical fiber as it was produced on the NRL silica draw tower. More than 450 grating elements were written in 1 hour at rates as high as three elements per second and in arrays sequenced in Bragg wavelength. The resultant array-bearing fiber did not suffer surface degradation and does not incorporate the numerous splices inherent in older techniques. This new technique uses the single-pulse method of grating writing developed at NRL to generate grating elements in the freshly drawn fiber soon after it emerges from the draw furnace and immediately before the protective coating is applied.

The Fiber-Optic Magnetic Array System (MARS) *Optical Sciences Division*

Fiber-optic sensors have been developed for detecting acoustic, magnetic, and electric fields; temperature and strain; and a variety of other parameters of Navy interest. These sensors have been incorporated into the fiber-optic Magnetic Array System (MARS). Development of this system culminated in the deployment of an underwater array of fiber-optic magnetometers off the coast of Norway in June 1993. This was the first demonstration of fiber-optic technology in undersea magnetic sensing. MARS will remain in operation for about 1 year, gathering data on the magnetic signatures of vessels and on fluctuations in Earth's magnetic field. The MARS program is a joint cooperative research and development effort between the United States and Norway to develop a fiber-optic undersea magnetic sensor system.

Single Molecule Recognition By Proximal Probes *Chemistry Division*

The development of the atomic force microscope makes it possible to measure forces as small as 10^{-11} Newtons between areas of contact as small as 100 nm^2 . This is equivalent to measuring the binding interaction between two hydrogen bonds. By using this measuring capability, a single-molecule sensor can be developed based on detecting molecules by directly measuring their molecular recognition interaction. The interaction force between an antigen and an antibody, each affixed to its own surface, was measured by changing the distance between the surfaces, the interaction force varying inversely with the number of sites on the antibody already occupied by an antigen. The development of sensors capable of single-molecule recognition will provide the Navy with a reliable technique to defend against chemical and biological agents.

**Structural Origins of Magnetic Anisotropy in
Amorphous TbFe Magnetic Thin Films**
Materials Science and Technology Division

Amorphous TbFe thin magnetic films have perpendicular magnetic anisotropy. Recent NRL experiments using extended X-ray absorption fine structure measurements show that the origin lies in the structural anisotropy developed in the films during growth. By using X-ray fine structure measurements, division scientists have obtained clear evidence for structural anisotropy in amorphous sputter-deposited TbFe films exhibiting perpendicular magnetic anisotropy. Modeling of the data suggests that perpendicular anisotropy in these films is associated with Fe-Fe and Tb-Tb pair correlations, which are greater in-plane, and Tb-Fe correlations, which are greater perpendicular to the film plane. Upon annealing at 300°C, the measured structural anisotropy disappears and the magnetic anisotropy decreases to a level consistent with magnetostrictive interaction between the film and the substrate.

Proximal-Probe-Based Fabrication of Semiconductor Nanostructure
Electronics Science and Technology Division

The potential for atomic-level manipulation of matter with the scanning tunneling microscope (STM) has spurred interest in the use of proximal probes as a nanofabrication tool. Controlled positioning of single adsorbate atoms on metallic surfaces has been accomplished. However, the ability to *manipulate* these atoms on a surface is difficult. This is particularly true for transferring a written pattern into a useable metallic or semiconductor structure. The problem is modifying very thin layers of materials, which by their very nature are not sufficiently robust to withstand the process of actual pattern transfer. A new method for fabricating semiconductor nanostructures addresses this problem. An STM is used to selectively grow a very thin oxide layer on a hydrogen-passivated Si(100) surface. The oxide serves as a robust mask for liquid etching that selectively etches only those portions of the surface not protected by the local oxide pattern.

Fiber-Optic Biosensor for Biological Warfare Detection
Center for Bio/Molecular Science and Engineering

A fiber-optic biosensor is being developed for biological warfare (BW) agents. This sensor uses antibodies and other biomolecules to recognize such agents rapidly and at extremely low concentration. The recognition molecules trap a complex that includes the BW agent and a fluorescent dye at the surface of an optical fiber. A signal is generated as the dye is excited by light traveling down the fiber. For on-site verification of the antibody-based tests, a scheme for using DNA technology for molecular recognition has been devised that uses the fiber-optic sensor as a readout device. A DNA-binding protein attaches the fluorescent DNA complex. Biological toxins were detected in river water and in clinical samples; rapid immunoassays for bacteria were developed; harmless bacteria released into the air were collected and detected; and the DNA-based assays, which can be used for verification of immunoassay screens, were developed.

Decadal Scale Effects of the 1982-83 El Niño *Oceanography Division*

Division scientists have uncovered evidence of present-day impact on the ocean circulation more than 11 years after the 1982-83 El Niño. They have done this by using a combination of satellite measurements of sea surface height, sea surface temperature (SST), and a high-resolution global ocean model. This El Niño spawned a Rossby wave along the coast of North America that lasted more than a decade and crossed the entire Pacific. During 1991-1992, it interacted with the Kuroshio Extension, an important heat-transporting current flowing eastward from Japan. This interaction routed a portion of the Kuroshio Extension's transport to a more northern path, causing the major warm anomaly seen in the satellite SST measurements. In 1992-1993, anomalies in sea surface height and temperature spanned the northern Pacific from Japan to Alaska. The remarkable sequence of events uncovered by this investigation indicate the surprisingly long-term oceanographic effects of the major 1982-83 El Niño.

Space Flight Tunable Passband Optical Filter *Space Science Division*

A tunable narrow passband optical filter has been space-flight-qualified for use on the first coronagraph capable of mapping the expansion velocity of the inner solar corona. The filter permits two-dimensional, monochromatic imagery and expansion velocity mapping of the solar emission line corona over a 1.5-deg field of view with high spatial resolution, spectral resolution, and efficiency. The design elements consist of a computer-controlled, tunable Fabry-Perot interferometer and a set of intermediate passband etalon filters. The nominal 0.07-nm wide Fabry-Perot passband is tunable to any wavelength over a 110-nm range with a precision of ± 0.0035 nm. Several technical difficulties were overcome: mount two interferometer plates securely enough to survive a 15-g launch without deforming their flatness by more than 0.5 nm; provide that absolute interplate spacing and parallel precision be maintained continuously to ± 0.15 nm; and accomplish experiment filter objectives with minimal mass (6 kg) and power (6 W). This filter will significantly increase the efficiency of future remote sensing spectroscopic instruments used to study the solar corona and the terrestrial upper atmosphere.

Multi-mission Advanced Tactical Terminal (MATT) and Man Portable Advanced Communications Terminal (MPACT) *Space Systems Development Department*

Division scientists have long been actively involved in developing satellite communications terminals for tactical intelligence reception. MATT and MPACT are development programs that support this involvement. In these programs the capability to receive, decrypt, process, and correlate information from various tactical links is assembled in modular, miniaturized packages. MPACT packages a combination of MATT modules and newly developed electronics into a briefcase weighing less than 30 pounds. MPACT will run on a laptop computer within the briefcase and will provide the user with ELINT and COMINT data. MATT and MPACT make real-time and near-real-time intelligence information available to a wide variety of military platforms that were previously excluded from such technologies because of size and weight constraints.

Extended Radar (Beyond the Horizon Capability)
Radar Division

The Navy needed the capability of detecting, with surface-based radar, low-flying cruise missiles at sufficient range to engage them with defensive weapons. In many situations involving surface-based radar, unfortunately, the utility of the sensor is limited by line-of-site constraints imposed by nature. Removing this constraint would increase the effectiveness of the sensor. Radar operating from an airborne platform has a greatly enhanced field of view, and tethered platforms supporting an entire radar system are used for border surveillance. These aerostats must be very large to provide the necessary payload capacity. Division scientists applied the aerostat approach only to the radar antenna. By using an elevated mirror, the distance to the horizon from a surface-based radar was increased three-fold. No significant modification to the system architecture or operation was required. This achievement provides a means for detecting low-flying cruise missiles with existing shipboard radars at ranges much greater than previously possible.

TESPEX Data Communication System
Information Technology Division

Previous acoustic data collection exercises involved two ships—one towing a hydrophone, the other an acoustic source. Data collection was hindered by noise from the vessel, analysis tools, and participating personnel; it was limited by space and cost constraints. Difficulties in obtaining the use of two or more ships prohibited extended periods of experimentation. To address these problems, a two-way data satellite communications network has been developed to relay acoustic data from a remote ocean buoy to a distant ship and to a shore station. This system allows remote control of the buoy's data collection equipment and shore monitoring of the status of the buoy's electronics. The network has been demonstrated successfully, delivering real-time data to a shore station for immediate analysis.

Navy Tactical Command System - Afloat (NTCS-A)
Reconstruction Module
Tactical Electronic Warfare Division

Reconstructing conditions that occurred at sea has previously been performed by manually collecting data and performing analyses. Modern Command and Control systems such as the NTCS-A are emerging. These systems contain powerful analytical capabilities that have the potential for both collecting data and conducting reconstruction analysis. Technical problems make it difficult to use these systems in a reconstruction mode. The Reconstruction Module is embedded in NTCS-A. It provides the capability to archive tactical event data processed within NTCS-A. This allows the replay or reconstruction of tactical events at sea on a quick-reaction basis for rapid on-scene analysis. The system can be used afloat or ashore for more post-event reconstruction and analysis by using additional data not available at the time of the event. Results of the analysis can be prepared by using the powerful presentation/briefing capability contained within the Reconstruction Module.

Development of an Acoustical Window for the BSY-1
Underwater Sound Reference Detachment

Many acoustic systems operate at frequencies in the near-ultrasonic range where acoustical transparency of the window becomes very important to system performance. The requirement that the window be rigid and impact resistant to protect electroacoustic components exacerbates the condition. No rigid, impact-resistant materials provide a sound speed low enough to be matched to sea water. However, an improved rigid, acoustical window for high-frequency underwater applications has been designed and tested. The window composite has the properties of a sound speed-density product that matches seawater perfectly and sound speed that is only about 20% greater than seawater. This composite gives very low insertion losses for a normally incident acoustic wave, and moderately low insertion losses at oblique angles. The new low-insertion loss, rigid, impact-resistant window can be used in the near-ultrasonic-frequency systems such as the BSY-1, BSY-2, and under-ice navigational sonar.

**Simulation of Flow Past Complex Geometries by Using
 a Parallel Implicit Incompressible Flow Solver**
Laboratory for Computational Physics and Fluid Dynamics

Problems of Navy interest represented by the incompressible Navier-Stokes equations include unsteady aerodynamic flows and turbulent separating flows over complex vehicles such as submarines. Recent innovations in microprocessor technology provide a variety of architectures for parallel computers that make it possible for these flow computations to be performed in a timely manner. For simulations of flows about complex geometries such as a fully appended submarine, an unobstructed grid approach offers the greatest flexibility with the fewest degrees of freedom. An incompressible flow solver based on unobstructed grids was developed for use with distributed memory parallel architectures and has been used for efficiently simulating flows over complex geometries. The performance of the parallel flow solver was also investigated.

**Development of a New Technique for Depositing
 Biocompatible Coatings on Surfaces**
Condensed Matter and Radiation Sciences Division

Calcium phosphate-based bioceramics have been used in medical and dental implant devices. However, because of their low tensile strength, they have not been used in orthopedic devices. This deficiency might be overcome by coating a high-strength metal with calcium hydroxylapatite. This is the primary mineral constituent of bones and teeth and one of the most biocompatible materials known. Current deposition methods for this phosphate are not entirely satisfactory. Division scientists have developed a pulsed laser deposition method for forming thin film coatings of hydroxyapatite on metal, ceramic, and polymer substrates. These are the most phase-pure coatings produced by any of the coating methods and offer significant benefits to the design of internal skeletal prostheses and other applications in which bonding to natural bone is desired.

Uniform Focal Distributions with the NIKE Laser Facility *Plasma Physics Division*

Laser fusion offers a means to study nuclear weapons physics, weapons effects, and, possibly, energy generation. One of the key requirements for laser fusion is obtaining sufficiently uniform and controlled laser focal profiles for symmetric pellet implosions. A beam-smoothing scheme to provide such uniform laser foci is being developed. KrF laser beams with highly uniform local profiles have been produced at the NIKE laser facility. The KrF laser was chosen for development because KrF has the short wavelength (248 nm) required for good laser-pellet coupling and characteristics that, in theory, would allow generation of highly uniform focal profiles. KrF inherently has the desired broad bandwidth and short wavelength. The uniform beams produced by the KrF laser may eventually allow studies of weapons effects using high-gain pellet implosions.

The RANDI-III Shallow-Water Ambient-Noise Model *Acoustics Division*

The emphasis in antisubmarine warfare has recently shifted from deep-water surveillance to shallow coastal-water tactical operations. Although the Navy has a credible sonar system performance-prediction capability for deep water, it does not have a corresponding capability for shallow water. The ambient noise calculation is one of the most important components of such a capability. A credible shallow-water ambient-noise prediction capability did not exist prior to the development of the RANDI-III (Research Ambient Noise Directionality - III) model. This model calculates the vertical and horizontal arrival structure of ambient noise in shallow water resulting from wind/seas and shipping. The model has been used successfully to predict unique characteristics of the ambient noise at several shallow-water locations.

Radio Discovery of Supernova SN1993J *Remote Sensing Division*

Supernovas are thought to play a basic role in the evolution of galaxies through the manufacture and distribution of many of the elements that determine the chemical makeup of galaxies. They are even suspected of being explosive triggers for the formation of stars and stellar systems. Very shortly after its discovery, division scientists were able to detect radio emissions from such an exploding star (SN1993J) in a nearby galaxy at a wavelength of 1.3 cm. This made it the shortest wavelength and earliest detection ever made for radio emission from a Type II supernova. The radio information adds significantly to our understanding of the nature of stellar explosions and the last stages of evolution of massive stars. Navy interest lies in maintaining and extending expertise in radio interferometric techniques, reference frame studies, and their application to Navy needs such as geolocation.

Tidal Atlas Software *Marine Geosciences Division*

To determine where tidal data were inadequate and to improve tidal prediction, division scientists developed and transitioned tidal atlas software for use in hydrographic survey operations. This software provides an integrated database of tides, bathymetry, and coastlines. The software can display tidal stations and tidal constituents for any user-specified area and can provide additional graphic displays. These displays can include tidal height, tidal zone, and co-tidal and co-range plots.

The software is useful for coastal modeling—providing tidal characteristics displays for model validation and input information for modeling applications. The software is completely menu-driven; users need no special commands. This software can quickly display worldwide tidal characteristics.

Variability of Coastal Atmospheric Refractivity (VOCAR)
Marine Meteorology Division

The VOCAR project consists of a theoretical, modeling, and field effort to understand, analyze, and predict complex coastal, mesoscale, and boundary layer atmospheric phenomena and structures that impact electromagnetic propagation and other tactically important variables. As part of the VOCAR program, a series of observations were made in the coastal zone during which NRL's mesoscale model produced daily forecasts over the VOCAR domain. An extensive set of model fields were archived for further analysis. These fields will be input to the Radio Physical Optics propagation model and compared with the propagation losses in the VOCAR region. Improvements are being tested to prevent nonrepresentative mesoscale errors in the boundary layer from contaminating the synoptic-scale analysis.

Space Surveillance Applications of Parallel Processing
Spacecraft Engineering Department

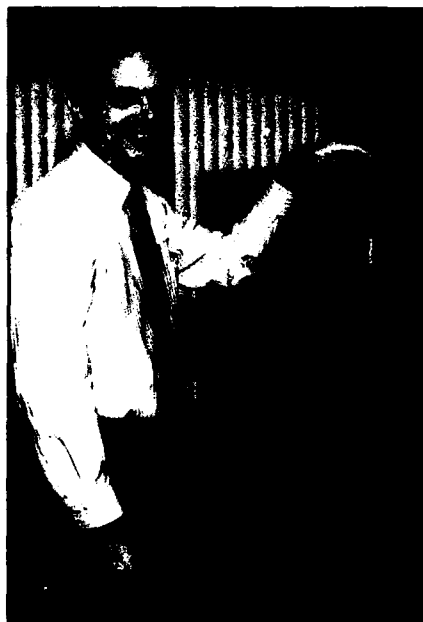
The development of the space station has increased awareness of potential dangers to spacecraft that can result from collisions with other spacecraft and debris. While the technology required to track and catalog objects in space down to ≥ 1 cm in size has been determined, the sensitivity of current radar tracking limits detections to ~ 30 cm and a current catalog of approximately 7,500 objects. With better computational facilities, the catalog could be increased to 25,000 objects. Equally important is the need to increase prediction accuracy. Analyzing threats to spacecraft and studying debris propagation is now possible with a new program (CM-COMBO) developed for a massively parallel processor computer (the Connection Machine). This program is capable of simultaneously comparing the miss distance between all objects in space.

Meet the Researchers

NRL is proud of its numerous researchers. Every year, we feature some of these people so that you may get to know them and, as a result, understand how their diverse scientific backgrounds come together to keep the Laboratory on the horizon of discovery.

Dr. Patricia A. Tatem, a research chemist and Project Technical Manager of the Navy Technology Center for Safety and Survivability, conducts and manages research and development of innovative damage-control hardware and software for insertion into current and future naval platforms.

"My career-long tenure at NRL has been both rewarding and satisfying. I feel that the greatest responsibility I have as an NRL scientist is to make a difference in the quality of life of a sailor. One of the most gratifying rewards that I have experienced has been seeing the results of my fire safety/damage control research make an impact on the fleet in the new construction and backfit programs of naval platforms. I know that these improvements have created a less hazardous environment for sailors to go about their daily duties."



Dr. Henry D. Dardy of the Information Technology Division is NRL's Chief Scientist for Computational Science. He leads the Center for Computational Science's (CCS) advanced research effort to rapidly prototype an all digital information infrastructure for voice, video, data, and imagery at the Laboratory. The effort is part of the National High Performance Computing and Communications Program within the DoD. The CCS team is working with various government agencies, academia, and industry to develop massively parallel processing hardware and software and to link these rich computational resources to researcher's facilities through ATM telecommunications technology end-to-end.

"NRL has a long and proud tradition of developing fundamental concepts that provide leading edge capabilities to researchers and in the long run find application in the real world. Our efforts are laying the foundation for an exciting information age. It combines the gifted talents and interactions of researchers at the Laboratory and across the country. Efforts like these place NRL in the forefront of discovery and innovation that can be of great importance for society in general."

Dr. Bhakta B. Rath is the Associate Director of Research of the Materials Science and Component Technology Directorate. In this position he has the responsibility for planning and the administration of basic and applied research in structure of matter, condensed matter physics, chemistry, electronics, materials science, plasma physics, computational physics, and bio/molecular science and technology.

"It is a distinct opportunity and challenge to be a member of a research team of one of the most prestigious laboratories of the world. NRL, throughout most of its history, has maintained strong emphasis on a broad spectrum of scientific and engineering disciplines, which provides a unique environment for world class researchers engaged in innovations to meet the current and future needs of the U.S. naval forces and the Nation."

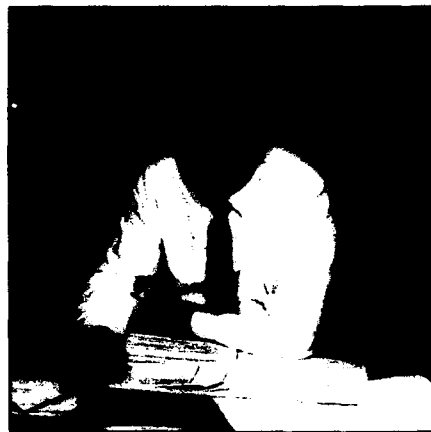


Dr. Judith L. Lean, research physicist in the Space Science Division, has developed models of the variations in the Sun's radiative energy output over times scales from days to centuries. Such models are utilized to study dramatic solar-induced changes in the outer layers of the Earth's atmosphere and ionosphere, as well as more subtle changes in the lower atmosphere and biosphere. She has participated in many national and international activities studying the Sun and its impact on climate change, the ozone layer, and the Earth's environment. Dr. Lean recently chaired a National Academy of Sciences Working Group on Solar Influences on Global Change.

"It is a delight to study the Sun at the very Laboratory that over forty years ago made the first rocket-borne observations of the solar ultraviolet spectrum and to work in a branch that over the decades has developed a world-renowned capability for interpretive and theoretical solar terrestrial physics. Particularly exciting is the prospect of utilizing this expertise to achieve a better understanding of solar variability for both the DoD and the national global change research program."

Mr. David K. Woodington, Director of the Research and Development Services Division, is responsible for all laboratory facilities and supporting infrastructure.

"The quality of NRL's facilities and supporting infrastructure is essential for state-of-the-art scientific research. I am extremely fortunate to be part of the NRL facilities family, which continues to provide these facilities. Clearly, the quality and dedication of the NRL personnel in my division are unmatched within the Navy. NRL provides an environment that fosters motivation for each of us to achieve excellence."



Dr. William B. Moseley is Superintendent of the Oceanography Division at NRL Stennis Space Center, Mississippi. The division conducts research and development on the physical, dynamical, biological, and chemical processes of the ocean and marine boundary layer. The oceanographic research is both theoretical and experimental in nature and is focused on understanding ocean hydro/thermodynamics, ocean circulation, ice dynamics, air-sea exchanges, ocean optics, small and microscale turbulence, bioluminescence, and microbially induced corrosion.

"Oceanography at NRL is an innovative, productive mix of scientists, engineers, and technicians working together to solve multidisciplinary problems in response to Navy needs, national/international interests, and scientific opportunities. Understanding the ocean environment is critical for the Navy because the ocean directly or indirectly affects every Navy platform, system, and operation."

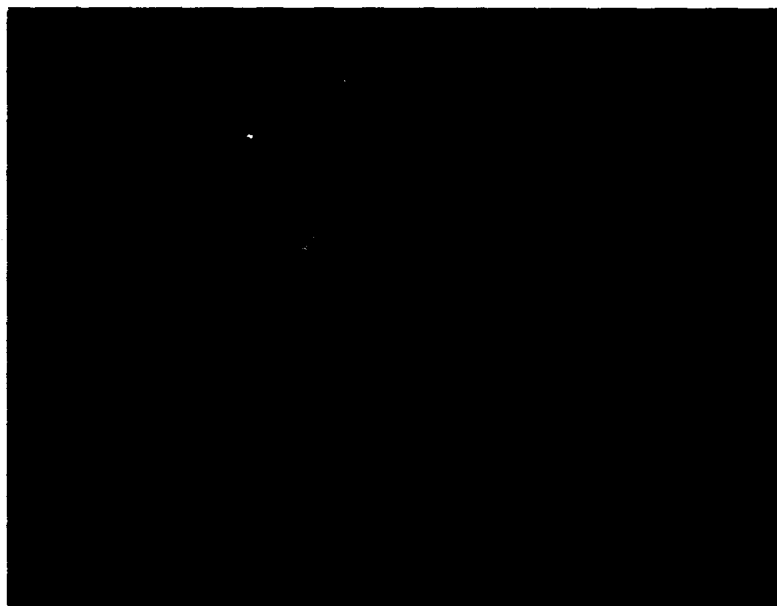


Dr. John B. Hovermale is Superintendent of the Marine Meteorology Division in Monterey, California. This newly established division emphasizes basic and applied research in analysis and prediction of atmospheric phenomena and is closely allied with NRL's studies in remote sensing and ocean sciences. Development of forecast guidance products from numerical weather forecasts and satellite information is also a major long-term thrust in the division. Dr. Hovermale's career has been devoted to these research areas for almost 30 years in university teaching, in the U.S. Weather Service, and for the Navy.

"I find it a pleasure and challenge being a new member of NRL, having admired its reputation throughout my career. I hope to help in expanding NRL's role in ocean and atmospheric sciences. We see our division as a primary player in developing global and coastal mesoscale prediction systems and in coupling these systems with ocean and upper atmosphere models developed elsewhere. Tri-service plans developed jointly within DoD define NRL as the principal model developer for all service requirements."

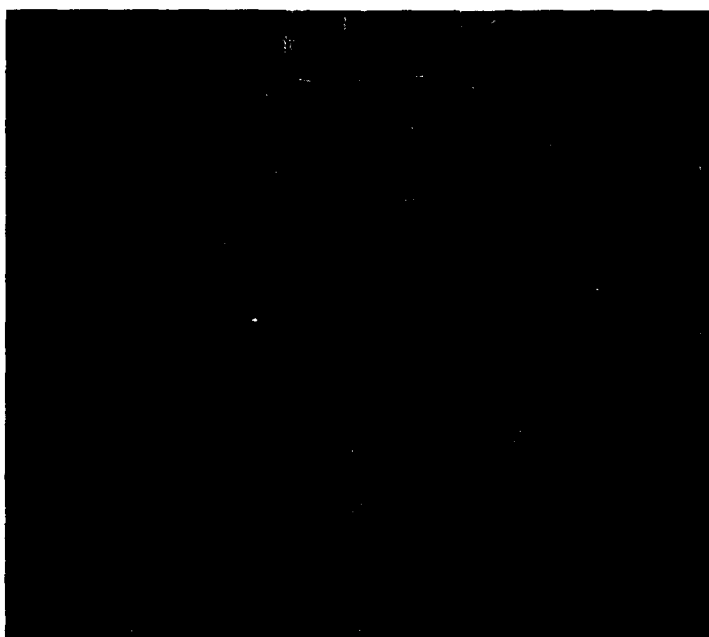
Color Presentation

For visual interest, we present some of NRL's latest scientific achievements.



New multispectral algorithms have been developed that significantly improve the ability to detect low contrast targets in background clutter. The algorithm performance depends on the band-to-band spectral correlation of the background clutter. The surface shown is a visual representation of a correlation matrix derived from background measurements recently gathered by NRL scientists at Wright-Patterson Air Force Base. The range of each dimension is approximately 3 to 14 microns and the red color represents regions of high correlation. The diagonal of the matrix, which has unity correlation, can be seen extending from the lower left to the upper right of the figure. (M.R. Surette, W.A. Shaffer, and J.V. Michalowicz, Code 5621)

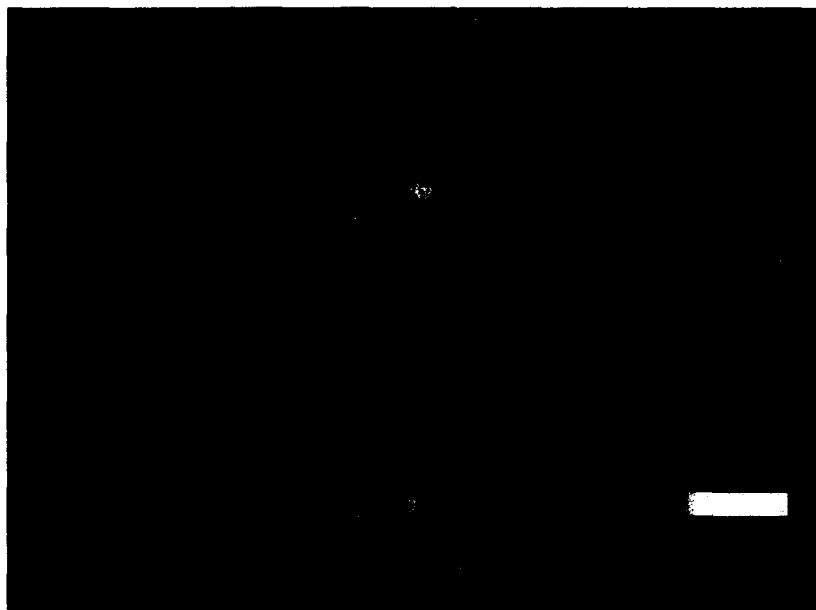
Satellite infrared (gray shade), passive microwave (color), and altimeter ice index data (white) are combined to delineate ice concentration, edge, and floes along the east Greenland coast. Infrared cloud contaminated pixels are substituted with passive microwave ice concentration data to provide both ice pack detail and full areal coverage. The passive microwave and altimeter data improve the integrated image by providing information about the Odden event (extending eastward from the ice pack), which is indiscernible in the infrared data. (D.A. May, Code 7240)





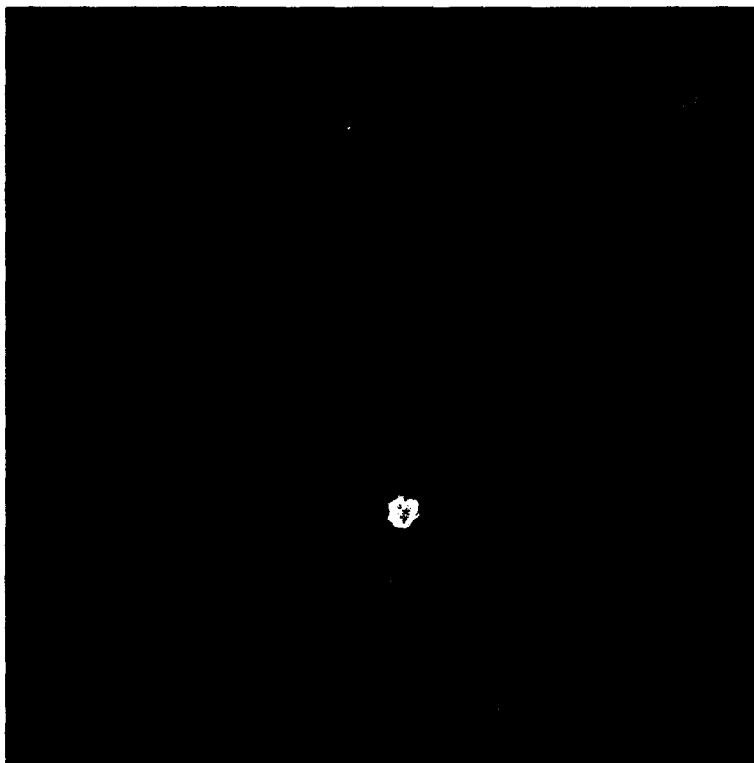
Geometry of a submarine model with 96 subdomains. (R. Ramamurti, Code 6410)

The Global Positioning System (GPS) provides the capability to accurately determine a user's position at any point on the ground, in the air, or on the sea. The ability to determine a user's position in three dimensions requires siting four GPS satellites simultaneously. This is not always guaranteed, and coverage outages occur. The maximum coverage gaps that occur over a one-week period are displayed as color-coded bins. Each bin represents a 40 by 40 km square. Over 320,000 bins were required to cover the surface of the Earth. (B.V. Sweeney and J.V. Michalowicz, Code 5621)

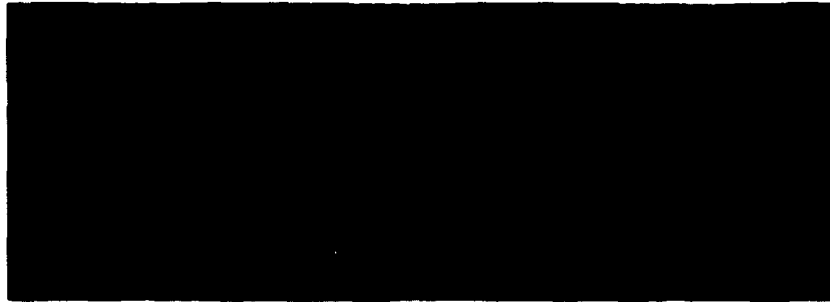




The Deep Space Program Science Experiment spacecraft, called Clementine, will spend two months mapping the moon before heading a flyby of the asteroid, Geographos, in August 1994. The Clementine interstage, which is jettisoned in a 350 by 172,000 km Earth orbit, will monitor radiation during its one-year lifespan. (P. Regeon, Code 8133)

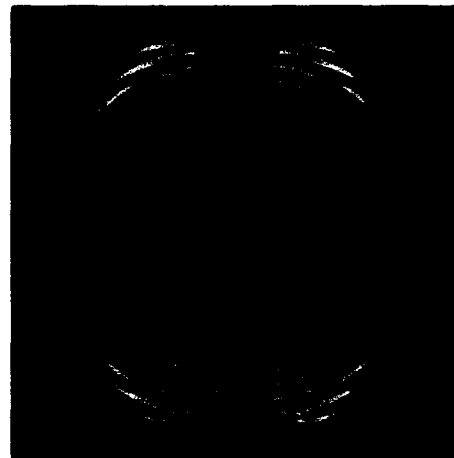


Artificial light emissions produced by a beam of high-power radio waves reflecting in the ionosphere. Each image of 100 by 100 km space is separated in time by one minute. The radio wave beam is focused by a large-scale density cavity in the bottom of the ionosphere. Eventually, the beam burns a hole through the ionosphere. (P.A. Bernhardt and J.D. Huba, Code 6794)



Sequential visualizations of the vorticity magnitude reveal the dynamics in a gas jet emerging from a square nozzle. The colors in these visualizations range from semitransparent blue to opaque red ($0.05\Omega_{\text{peak}} - 0.60\Omega_{\text{peak}}$). The figure depicts the large-scale vorticity dynamics controlling the jet development, characterized by vortex rings undergoing self-deformation, hairpin vortices originated by vortex induction and stretching in the initial shear layer, and, further downstream, a more disorganized flow regime characterized by tube-like vortices. (F.F. Grinstein, Code 6410)

Simulated field configuration of an antenna array using a cellular automaton model on the NRL Connection Machine. Dark colors indicate high-field strengths. The main lobe structure is clearly visible perpendicular to the line of the array. (J.B. Cole and S.K. Numrich, Code 5580; and R.A. Krutar and D.B. Creamer, Code 7120)



These figures depict the evolution of the three-dimensional ablative Rayleigh-Taylor instability on a laser-accelerated planar plastic target. The initial mass density perturbation (left) has been integrated in the direction of the incident laser before plotting. The integrated mass density perturbation after 4.7 ns of hydrodynamic evolution (right) shows the nonlinear coupling of modes with hemispherical bubbles dominating at late times. In both figures, dark blue to gray areas indicate regions of most mass, and yellow areas indicate regions with the least mass. (J.P. Dahlburg and J.H. Gardner, Code 6440; and D.E. Fyfe, Code 6410)

**FEATURED
RESEARCH
AT
NRL**

61 Diamond Surface Chemistry

*Lehr E. Pehrsson, John N. Russell, Jr., Brian D. Thomas,
James E. Butler, Michael Marchywka, and Jeffrey M. Culvert*

73 Computational Materials Science

*Larry L. Boyer, Michael J. Mehl, Dimitrios A. Papaconstantopoulos,
Warren E. Pickett, and David J. Singh*

**83 Self-assembled Molecular Templates: Microtubule-based Controlled
Release for Biofouling Control and Medical Applications**

Donald R. Price, Alan S. Rudolph, Jonathan V. Selinger, and Joel M. Smith

91 Monitoring Whales and Earthquakes by Using SOSUS

Clyde E. Nishimura

Diamond Surface Chemistry

Pehr E. Pehrsson, John N. Russell, Jr., Brian D. Thoms, and James E. Butler
Chemistry Division

Michael Marchywka
Space Science Division

Jeffrey M. Calvert
Center for Bio/Molecular Science and Engineering

DIAMOND CHEMICAL VAPOR DEPOSITION

Diamond possesses numerous physical and chemical properties that have technological, industrial, and scientific applications. It has the highest thermal conductivity and hardness of any material, high optical transmission, a large bandgap and high carrier mobilities, and the lowest friction coefficient (under select conditions) [1,2]. These properties make diamond of particular interest to the electronics community for use as a heat spreader for thermal management or as an active electronics device material [3].

The current interest in diamond surface chemistry reflects recent advances in diamond growth by chemical vapor deposition (CVD), under what were once thought to be thermodynamically impossible conditions. Figure 1 is a schematic diagram of the CVD process [4]. CVD deposits diamond from a gas-phase mixture of hydrogen (H_2), hydrocarbon (usually methane, CH_4), and sometimes an oxygen-containing species or halogen (O_2 , CO , Cl_2 , HCl). The gases in the growth chamber are activated by various methods including microwave or radio frequency plasmas, DC discharge, combustion flame, or even a hot metal filament. All of these techniques fragment the hydrocarbon molecules to form a "soup" of hot hydrocarbon molecules and fragments. Most importantly, they split the hydrogen molecules into atomic hydrogen. The resulting hydrocarbon

and atomic hydrogen species move through the reactor by diffusion and convection and impinge on the substrate. Adsorption, diffusion, reaction, and desorption of various species occur simultaneously on the substrate surface. Under a select set of conditions, diamond nucleates and

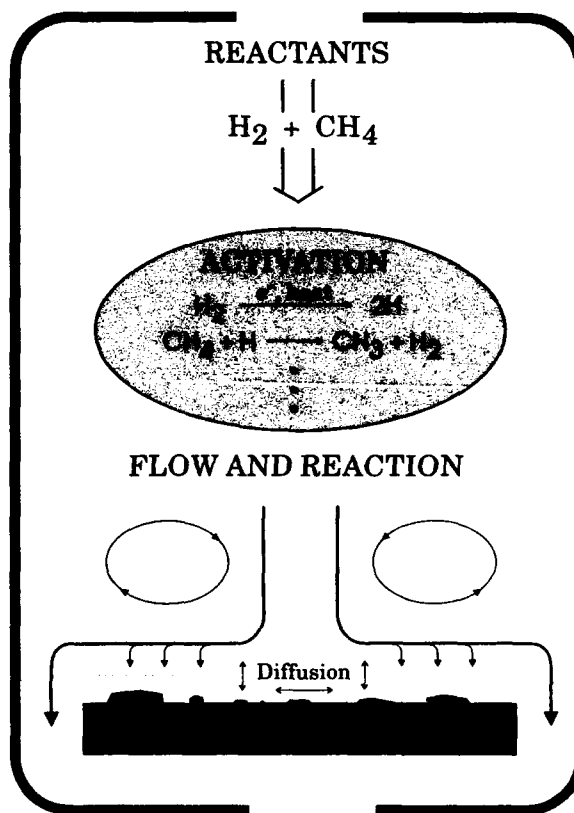


Fig. 1 — Schematic rendition of the CVD diamond deposition process. (Originally published in Ref. 4)

grows while the deposition of graphitic (or sp^2) carbon formation is suppressed.

Hydrogen and oxygen play multiple roles in CVD diamond growth, both in the gas phase and on the surface of the growing film [5]. The principal effects of atomic hydrogen on the diamond growth process are thought to include: control of the gas phase chemistry, stabilization of the sp^3 -hybridized surface carbon atoms, preferential reaction with sp^2 -hybridized carbon, and abstraction of adsorbed hydrogen to produce reactive surface sites for carbon incorporation. Gas-phase hydrogen atoms (H) can adsorb on the surface and fill vacant sites or abstract surface hydrogen to form volatile molecular hydrogen. The desorbing hydrogen creates vacant surface sites and radicals at which methyl radicals and other hydrocarbon species adsorb and which are ultimately incorporated into the growing diamond lattice. The competing adsorption, desorption, and abstraction processes create a dynamic balance that leaves some open surface sites for addition while not completely denuding the surface of adsorbates. Such denuded (unterminated) surfaces rapidly develop double bonds and nucleate undesirable sp^2 -bonded carbon. Adsorbed hydrogen stabilizes the diamond surface and explains why diamond grows under CVD conditions. Oxygen species likewise bond at vacant surface sites and create open sites by desorbing or abstracting other surface species. At elevated temperatures, oxygen etches both sp^2 carbon (graphite) and sp^3 carbon (diamond) surfaces.

The complex CVD process is controlled by the thermodynamics and kinetics of multiple competing deposition and etching surface reactions. Our objective is to understand and improve the CVD process by studying the structure and thermal stability of the bare diamond surface and surfaces terminated with hydrogen, oxygen, or hydrocarbons. We also must understand heat-induced desorption products and the interaction between gas phase species and diamond surfaces terminated with other species. This knowledge is essential for developing the diamond growth models and process controls required to optimize growth rates, morphology, quality, and the post-deposition surface manipu-

lation necessary to exploit diamond's superb materials properties.

THE DIAMOND SURFACE

The diamond surfaces studied at NRL include both single crystals and polycrystalline films. The single crystals are either natural stones, man-made in a high-temperature/high-pressure (HTHP) press, or CVD-grown homoepitaxial layers on natural or HTHP stones. The homoepitaxial layers are especially useful since many natural and HPHT diamonds are insulating and hence unsuitable for many electron-based analyses because of surface charging. Small amounts of boron or other dopants introduced into the feedgas make the CVD-grown layers electrically semiconducting.

Diamond surface chemistry presents unique challenges and pitfalls. Surface chemistry in general, and CVD growth in particular, can occur principally at steps, ledges, and other defects. Crystals cut off-axis have higher densities of defect and ledge structures, which can lead to variable or unrepresentative data for surface reactions on a particular crystallographic surface. Commercially available diamonds are only cut to within 2° of the low-index ((100), (110), and (111)) faces, limiting their utility for some studies. Useful experiments require knowledge of how closely the sample surface matches the low-index planes and how smooth those surfaces are, along with confirmation that the surface remains essentially unchanged and uncontaminated by sp^2 carbon or other species during various treatments. The diamond grit polishing often used to finish diamond surfaces hinders formation of scientifically useful diamond surfaces by creating large numbers of microscopically rough surface wear tracks and pits. Sputtering and vacuum annealing techniques used in the surface science of metal crystals cannot be used because they convert the diamond surface to graphite. However, recent scanning tunnelling microscope (STM) work [6] and our own low-energy electron diffraction (LEED) and STM results show that (100) and (110) diamond surfaces heated to 800°C in a microwave hydrogen plasma become

reproducibly smoother and well-ordered, with dramatically lower step and other defect densities. Such representative surfaces are proving highly useful for surface science and homoepitaxial growth studies.

SURFACE ANALYSIS

Most of our experiments are conducted in ultrahigh vacuum (UHV) chambers with base pressures of $1-5 \times 10^{-10}$ Torr (Fig. 2). Independent heating and cooling capabilities allow control of the diamond surface temperature. Diamond surfaces at various temperatures are dosed with molecular hydrogen (H_2), deuterium (D_2 , an isotope of hydrogen), or oxygen (O_2) by backfilling the chamber. During some experiments, a tungsten filament heated to $>1800^\circ\text{C}$ excites H_2 or D_2 and dissociates a fraction of it to highly reactive atomic hydrogen (H) or deuterium (D). A hot (1150°C) iridium (Ir) filament excites molecular oxygen to more reactive vibrational and electronic states, and may convert some fraction to highly reactive atomic oxygen (O). The flux of atomic species to the diamond surface is unknown, so the doses listed are the total flux of the molecular species in Langmuirs ($1 \text{ L} = 10^{-6}$ Torr s).

We use a variety of electron-based, optical, and mass spectrometric techniques to interrogate the interactions between gas-phase species and diamond surfaces. Vibrational spectroscopies provide chemical bond information about adsorbates and surface structure. In high-resolution electron energy loss spectroscopy (HREELS), monochromatic low-energy electrons are scattered from the surface of interest and lose measurable amounts of energy through excitation of surface adsorbate and lattice vibrations. The specific amount of energy lost to these vibrations identifies the surface chemical species; the number of electrons losing that amount of energy reveals the surface coverage of that species. We obtain similar information with IR photons by multiple internal-reflection infrared spectroscopy (MIRIRS).

Auger electron and X-ray photoelectron spectroscopies (AES and XPS) provide compositional and chemical identification of the diamond surface (i.e., whether it is sp^2 or sp^3



Fig. 2 — A view into the UHV chamber used for HREELS and other analysis of diamond surfaces. The small square in the center of the shot is a piece of polycrystalline diamond film. The light comes from a heater in back of the sample. (Photo courtesy J. McNally)

bonded carbon and whether it is contaminated with other species), and give the type and extent of non-hydrogen surface termination. Secondary electron emission (SEE) and electron loss spectroscopy (ELS) also confirm whether the surface is diamond or contains sp^2 carbon contamination. LEED measures the degree of surface order. Low-energy electrons scattered from a surface that consists of a regular array of atoms undergo constructive and destructive interference, which are observed as spots on a phosphor screen. The spot patterns are characteristic of the surface structure. The sharpness and contrast of the spots increase with respect to the background as the surface order improves. A differentially pumped, random flux-shielded, quadrupole mass spectrometer measures desorption products vs surface temperature in temperature programmed desorption (TPD) experiments. The adsorbate surface coverage after various treatments is obtained by integrating the area under the desorption curve. The combination of chemical species-specific probes

(HREELS, AES, XPS, TPD) and techniques sensitive to surface structure (LEED, STM) provides a detailed picture of the diamond surface and adsorbates.

HYDROGEN CHEMISTRY ON DIAMOND SURFACES

The stretch and bend vibrational frequencies observed with HREELS reveal the C-H and C-C bonding on hydrogenated diamond surfaces. The C-H stretching frequency at $2800\text{--}3000\text{ cm}^{-1}$ increases in the order $\text{CH}_3 < \text{CH}_2 < \text{CH}$, and also increases for hydrogen bonded to single, double, and triple-bonded carbons. HREELS shows that molecular hydrogen does not react with nude, room-temperature, polycrystalline diamond surfaces composed primarily of (111) facets. However, *atomic* hydrogen adsorbs on the surface in the monohydride state (CH , not CH_2 or CH_3) with C-H bonds normal to the surface and the surface carbon in the sp^3 , single-bonded configuration. Upon heating the diamond to $T > 900^\circ\text{C}$, the H desorbs from the surface, as evidenced by the disappearance of the C-H vibrational stretch and bend features. TPD shows that the hydrogen desorbs exclusively as H_2 . Hydrogen abstraction rates are determined by using HREELS to monitor the disappearance (appearance) of the C-H (C-D) stretch after successive doses with excited deuterium (D), a hydrogen isotope with a different stretching frequency (Fig. 3). These results indicate that hydrogen adsorption on a diamond surface at 80°C occurs 20 times more efficiently than abstraction, higher than in analogous gas phase reactions. Current attempts to model CVD diamond surface reactions use numbers derived from gas phase reactions, and thus can be improved. The adsorption and abstraction rates are unchanged on diamond at 600°C . The independence of the rates on surface temperature indicates that the incident hydrogen atoms are not in thermal equilibrium with the surface during these reactions. Consequently, the reaction mechanism for hydrogen abstraction is best described as the direct collision of an H atom with a diamond site, which results in either adsorption or removal of a surface hydrogen.

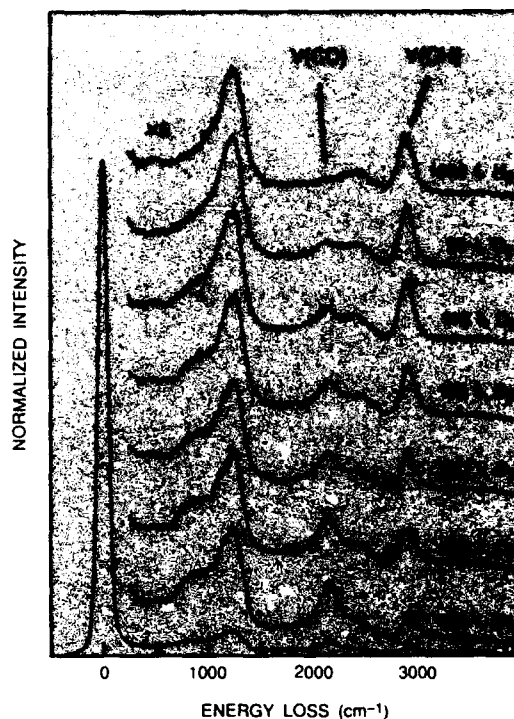


Fig. 3 — A series of HREELS spectra showing the gradual replacement of the C-H stretch and bend modes by those of C-D as the sample is dosed with excited deuterium

Diamond (100) surfaces can also be denuded by annealing in vacuum or reterminated by dosing with hydrogen or oxygen. Surfaces stripped of surface-terminating groups sometimes eliminate the energetically unfavorable "dangling bonds" by rearranging the surface atoms to form new bond configurations, often accompanied by changes in the bond angles and atom positions near the surface. There are several proposed configurations for the hydrogen-saturated C(100) surface. Figure 4 is a schematic rendition of possible structures for hydrogenated (100) diamond. Our HREELS and LEED data indicate that hydrogenated C(100) has a monohydride dimer structure with every surface carbon atom bonded to one hydrogen atom and three other C atoms. The (100) diamond surface exposed to hydrogen atoms exhibits a two-domain, 2×1 LEED pattern (Fig. 5(a)), which is consistent with this structure. A surface with dihydride carbon atoms has a square 1×1 LEED pattern. In addition,

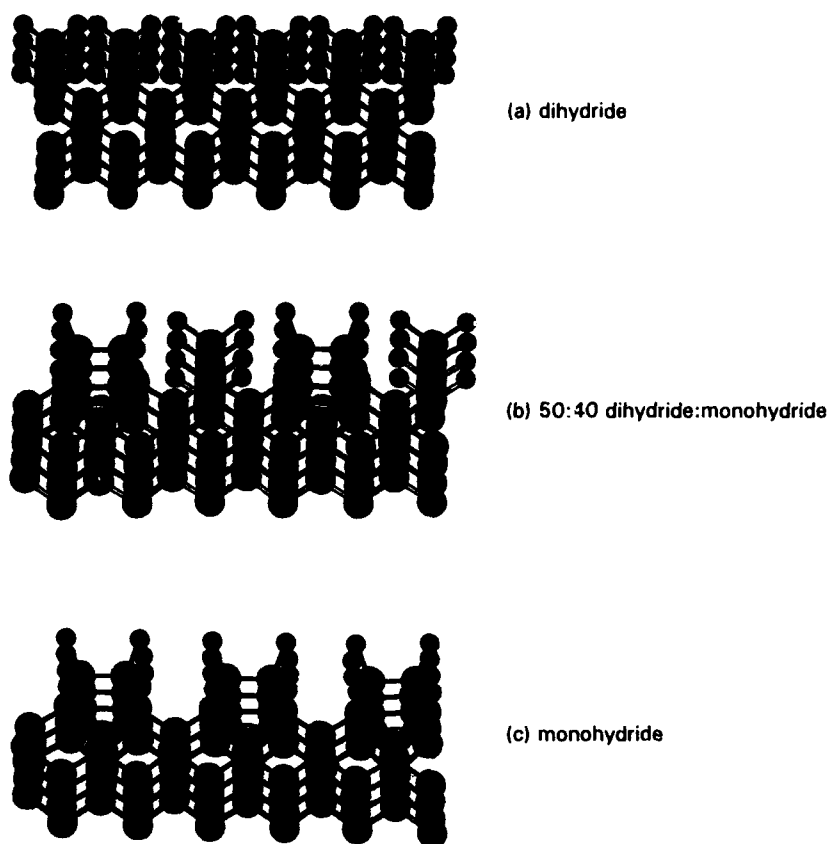


Fig. 4 — Three possible structures for the hydrogenated diamond (100) surface; (b) and (c) relax the severe steric constraints of (a). (Originally published in Ref. 5)

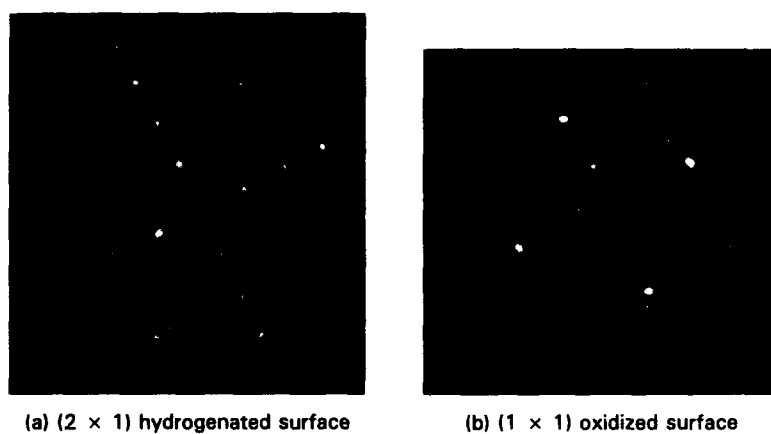


Fig. 5 — Low-energy electron diffraction (LEED) patterns on (100) diamond

the HREELS stretching vibrational frequency indicates that there are CH groups on the surface, but no CH₂ groups. The 2×1 LEED pattern persists even after the sample is heated to almost 1100°C, but the accompanying loss of the HREELS C-H stretching vibration confirms the desorption of most of the surface hydrogen. The appearance of several new vibrational peaks suggests changes in the surface carbon-carbon bonding, consistent with a pi-bonded dimer reconstruction at adjacent open sites. ELS, SEE, and AES all confirm the partial conversion of the surface to sp² carbon under these conditions. This reconstruction is not desirable during CVD because it is the first step toward graphite growth, which degrades the quality of the deposited diamond.

The LEED patterns from hydrogenated (110) faces also sharpen and brighten in a hydrogen plasma, indicating a smoother, more well-ordered surface. The background H₂ partial pressure impedes TPD measurement of hydrogen desorption from the diamond surface. For these studies, diamonds are exposed to D atoms created with the hot tungsten filament. TPD shows that neither molecular hydrogen nor deuterium react with bare diamond (110) surfaces at room temperature, but that atomic hydrogen and deuterium do chemisorb. Conversely, a deuterated surface heated to 1027°C evolves molecular deuterium (D₂). We expect adsorption and desorption to be reversible processes. Therefore the adsorption of H(D) atoms and the desorption of H₂ (D₂) molecules indicates that molecular hydrogen requires additional energy (i.e., there is an activation barrier) to react with the bare surfaces.

Figure 6 shows D₂ thermal desorption spectra from a C(110) surface that was exposed to D₂/D at room temperature. The surface coverage derived from the desorption spectra saturates at exposures of ~200 L. Molecular deuterium desorbs between 227°C and 1027°C, yielding an asymmetric desorption peak with a coverage-independent maximum at 892°C. The peak shape and invariant maximum temperature are characteristic of desorption kinetics which are first order in (directly proportional to) the adsorbate atomic D concentration. Recombinative desorption rates usually depend on the

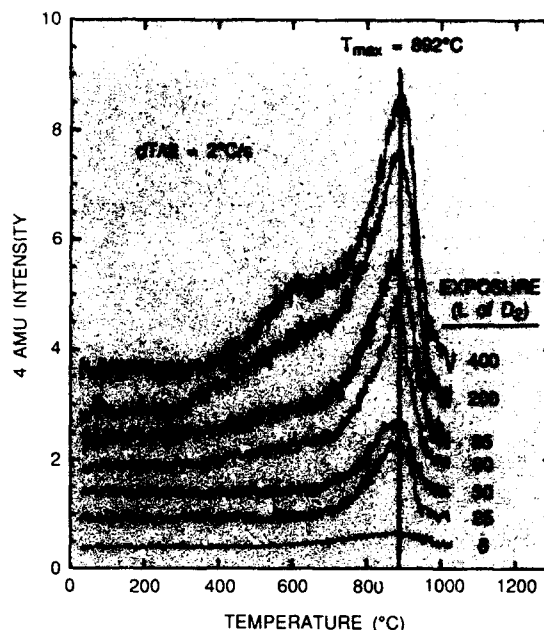


Fig. 6 — Temperature-programmed desorption spectra from a hydrogenated diamond (110) surface exposed to excited deuterium at 27°C

probability of collision between two adsorbate atoms, which is proportional to the square of the surface species concentration. The apparent first-order recombinative desorption kinetics for D₂ desorption implies that the rate-limiting step for the overall kinetics is not molecular desorption, but another step in the sequence of events preceding desorption. The actual rate-limiting step could be generation of a reactive site, the mobility of surface species, or another event directly proportional to surface hydrogen concentration.

OXYGEN CHEMISTRY ON DIAMOND SURFACES

Oxygen also adsorbs on the diamond surface, terminating surface sites and influencing the surface rearrangement and availability of sites for hydrocarbon addition. The dominant C-O surface species varies with the specific diamond face and reaction temperature. TPD shows that oxygen desorbs from the diamond surface as either CO or CO₂, so the desorbing oxygen removes carbon atoms and etches the diamond surface. Desorption of different O-containing surface groups requires cleavage of

different numbers of C-O bonds, which influences the oxygen desorption temperature and the relative oxidative stability of each face. Polycrystalline diamond films composed primarily of (111) facets and dosed with atomic oxygen develop a HREELS feature at 1000-1080 cm^{-1} . This is consistent with oxygen in an ether (bridge-bonding) configuration spanning two surface carbon atoms. The HREELS feature corresponding to ether-bonded oxygen disappears after an oxidized (111) sample is heated in vacuum to desorb the surface oxygen. Most of the oxygen desorbs at lower temperatures ($T < 750^\circ\text{C}$) than hydrogen ($T > 950^\circ\text{C}$) and so lowers the temperature needed to form vacant surface sites for the addition of hydrocarbon species to the diamond lattice. Oxygen also reacts with surface hydrogen and removes it from the diamond surface at 450°C .

Exposure of the hydrogenated (100) diamond surface to excited oxygen converts the LEED pattern from a sharp 2-domain 2×1 to a 1×1 pattern (Fig. 5(b)). This is consistent with cleavage of the carbon dimer bonds present on the hydrogenated surface. HREELS spectra from oxidized (100) surfaces have a feature at 1720 to 1800 cm^{-1} , corresponding to oxygen atoms double-bonded to single carbon atoms (a carbonyl or ketone).

Neither UHV annealing to desorb surface hydrogen nor oxidation with excited oxygen alters the LEED pattern on (110) diamond, so that surface probably does not reconstruct. The HREELS spectra show both carbonyl and ether-bonded oxygen. TPD and AES reveal that the bare (110) diamond surface at 0°C becomes oxygen-saturated when exposed to 600 to 1200 L of oxygen excited with an Ir filament. The broad CO and CO_2 TPD desorption features from the oxidized surface have maximum desorption rates at $\sim 597^\circ\text{C}$ and 527°C , respectively. The CO desorption intensity is an order of magnitude higher than for CO_2 , indicating that most of the oxygen leaves the surface as CO. The CO and CO_2 desorption peak maxima and temperature range are independent of the oxygen surface coverage, suggesting that CO and CO_2 desorption also follow first-order kinetics. The desorption activation energy for the majority of CO and CO_2 species on the

surface is estimated at 55 and 51 kcal/mole, respectively. If the oxygen-covered surface is annealed to desorb part of the oxygen monolayer, cooled, and then reheated to 1027°C , the final CO thermal desorption curve continues where the preheated desorption curve ends. This indicates that oxygen adsorbs in a distribution of sites on the surface and that the sites are inaccessible to each other by diffusion of the surface oxygen.

POST-DEPOSITION APPLICATIONS OF DIAMOND SURFACE CHEMISTRY

Implantation and Electrochemical Etch

Diamonds are usually cleaned with boiling acids or an oxygen plasma to remove non-diamond carbon and metal contaminants prior to use in device fabrication. Both treatments oxidize diamond to similar levels and alter its electrical characteristics. High-temperature annealing and/or hydrogen plasmas eliminate the surface oxygen and restore surface conductivity and other electrical characteristics. Thus, surface termination and reconstruction are critical to the characteristics and reproducibility of diamond-based devices.

Under some conditions, the diamond surface oxidizes to even higher levels than observed with acids or oxygen plasmas. The surface of a diamond immersed in a distilled water bath between two electrodes with a 50 to 300 V potential applied between them oxidizes to a higher degree than in plasma or acid baths alone, although the diamond itself does not appear to etch. However, regions of the diamond damaged by ion implantation not only oxidize but are electrochemically etched. High-energy ion implantation creates subsurface damage in the region of the crystal lattice where the ions come to rest, leaving a relatively undamaged outer layer. Selective removal of the subcutaneous damage layer with the electrochemical etch undercuts the relatively undamaged top layer to produce a very thin sheet of high-quality diamond [7]. Figure 7 shows a 50-nm-thick diamond sheet curling up from an implanted and partially etched polycrystalline diamond film.



Fig. 7 — Scanning electron micrograph of a thin (50-nm) sheet of diamond lifting off of a polycrystalline film implanted with 170 eV carbon ions and partially electrochemically etched in distilled water. Magnification is 100 \times .

The relatively undamaged top surface of implanted crystals provides a template for further diamond growth. Implanted single crystals subjected to CVD growth prior to electrochemical etching develop a homoepitaxial diamond layer on the top surface, i.e., the lattice of the CVD-diamond layer is a continuation of the crystal lattice of the substrate. The high quality of the diamond film is confirmed by Raman spectroscopy, the flat growth surface, and regular 90° crystalline fractures on stressed films. CVD growths thicken and stiffen the liftoff layer so that it does not curl. The resulting "tiles" can be placed on a surface and arranged into a mosaic. Further CVD growth on the diamond tiles could create a sheet of virtually "single-crystal" diamond over large areas and irregular surfaces. We have produced a metal-insulator-semiconductor (MIS) capacitor from homoepitaxial diamond grown on the liftoff layer and then coated with SiO₂ and appropriate metal patterns. An array of such devices would constitute a charge-coupled device (CCD) and could function as an uncooled, back-illuminated UV imager that is insensitive to visible light.

Surface Functionalization and Electroless Metallization

The diamond surface can be chemically manipulated to facilitate metallization and attachment of other technologically useful thin films for microelectronic device fabrication, sensors, etc. Attaching adherent metal coatings to diamond by using traditional evaporation or sputtering approaches usually requires pre-sputtering of the diamond surface before metallization, or annealing to 900°C to form an intermediate carbide layer. Both techniques are problematic for many applications and can have a deleterious effect on desired interfacial electrical characteristics because of surface graphitization or dopant diffusion. These problems are eliminated with a new NRL process in which a metal-binding self-assembled (SA) organosilane film chemisorbs onto a diamond surface previously oxidized by one of the techniques discussed earlier [8]. The SA films can be patterned by either direct exposure to UV radiation or by photoresist masking techniques. Immersion of the patterned SA film surface into an aqueous palladium catalyst solution results in selective attachment of the catalyst to the patterned SA film. When the substrate is then placed in an electroless plating bath, metal selectively deposits in an additive fashion onto the catalyzed region of the surface (Fig. 8). The resulting patterned metal films adhere to the diamond without sputtering or annealing.

SUMMARY

Diamond has great potential in a diverse array of technological applications. These include passive and active electronics, as well as numerous other tribological, optical, and coatings applications. However, the current knowledge of diamond surface chemistry is inadequate for full exploitation of this potential. We are pursuing increased understanding of diamond surface chemistry to improve the CVD process and post-deposition manipulation of the surface chemistry for metallization and other applications. We obtain such chemical knowledge by preparing representative diamond surfaces and monitoring their interactions with a variety of

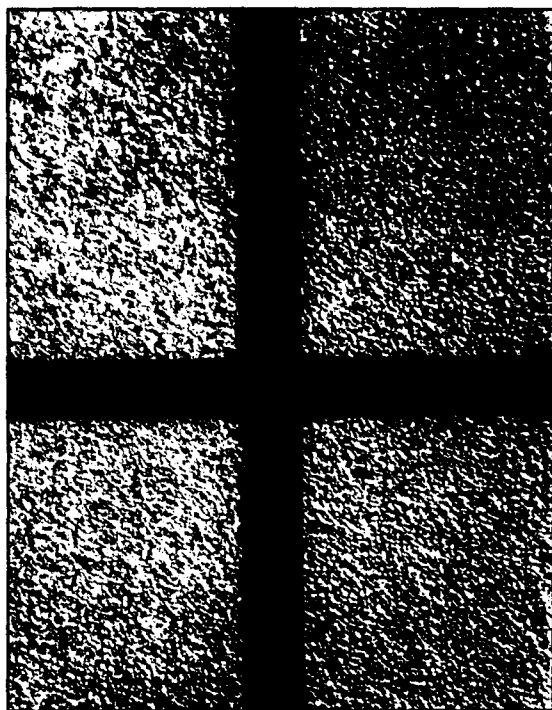


Fig. 8 — Optical micrograph of a polycrystalline diamond film after functionalization, patterning and metallization with 100 nm of Ni. The Ni-coated regions are light colored; the unmetallized diamond film is dark. Magnification is 50 \times .

gases under different pressure and temperature conditions, and by developing and implementing new processes for diamond surface modification. The resulting chemical insight aids in the development of superior diamond growth processes and surface manipulation techniques of use to the Navy, as well as the industrial and scientific communities.

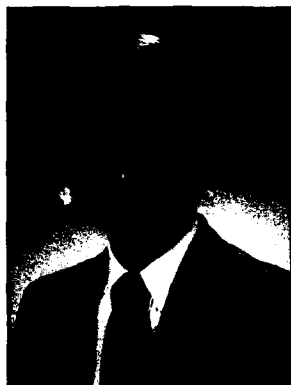
ACKNOWLEDGMENTS

The authors gratefully recognize the many contributions of Daniel Vestyck, Michael Owens, Robert Mackey, Steven Potochnik, Charles Dulcey, Martin Peckerar, and Mu-San Chen; support from Office of Naval Research and Advanced Research Projects Agency; and the assistance of Norton Diamond Films and General Electric.

REFERENCES

1. J.E. Field, *The Properties of Diamond* (Academic Press, N.Y., 1979).
2. R.F. Davis, Z. Sitar, B.E. Williams, H.S. Kong, H.J. Kim, J.W. Palmour, J.A. Edmond, J. Ryu, J.T. Glass, and C.H. Carter, Jr., "Critical Evaluation of the Status of the Areas for Future Research Regarding the Wide Band Gap Semiconductors Diamond, Gallium Nitride and Silicon Carbide," *Mat. Sci. Eng.* **B1**, 77 (1988).
3. G.S. Gildenblatt, S.A. Grot, and A. Badzian, "The Electrical Properties and Device Applications of Homoepitaxial and Polycrystalline Diamond Films," *Proc. IEEE* **79**(5), 647 (1991).
4. P.E. Pehrsson, F.G. Celii, and J.E. Butler, "Chemical Mechanisms of Diamond CVD," in *Diamond Films and Coatings*, R.F. Davis, ed. (Noyes Publications, Park Ridge, N.J., 1993).
5. J.E. Butler and R.L. Woodin, "Thin Film Diamond Growth Mechanisms," *Phil. Trans. R. Soc. Lond. A* **342**, 209 (1993).
6. K.V. Ravi and D. Yaniv, "Atomic Force Microscopy of the (100) Surface of Flame Synthesized Diamond," Paper 523, 183rd Mtg. of the Electrochemical Society, Honolulu, Hawaii, May 16-21, 1993.
7. M. Marchywka, P.E. Pehrsson, S.C. Binari, and D. Moses, "Electrochemical Patterning of Amorphous Carbon on Diamond," *J. Electrochem. Soc.* **140**(2), L19 (1993).
8. J.M. Calvert, P.E. Pehrsson, C.S. Dulcey, and M.C. Peckerar, "Selective Metallization of CVD Diamond Films," *Mat. Res. Soc. Symp. Proc.* **260**, 905 (1992).

THE AUTHORS



Pehr E. Pehrsson received a B.S. degree in chemistry from the College of William and Mary in 1978, and a Ph.D. in physical chemistry from the Catholic University of America in 1985. His dissertation topics included ion implantation of polymers and Auger line-shape analysis of transition metal carbides. He was an NRC/NRL Postdoctoral Fellow in the Electronics

Science and Technology Division of the Naval Research Laboratory from 1985-1987, where he investigated laser-induced chemical vapor deposition and surface modification of SiC. Dr. Pehrsson joined the Chemistry Division at NRL in 1987; his work involves the surface science of high-temperature chemistry, including carbon oxidation and the nucleation and growth of diamond by chemical vapor deposition. In addition, he is active in functionalization of diamond surfaces and selective chemical vapor deposition of metals.



John N. Russell, Jr. received degrees in chemistry from Dickinson College (B.S. degree, 1981) and The University of Pittsburgh, (Ph.D., 1987). His dissertation topics included the surface chemistry of organic molecules on single-crystal metal surfaces and the adsorption/desorption kinetics of hydrogen on nickel. He was a Postdoctoral Fellow at the Corporate

Research Science Laboratories of the Exxon Research and Engineering Company from 1987 to 1989. At Exxon, his research encompassed laser-induced-desorption studies of surface diffusion and time-resolved nonlinear spectroscopy measurements of surface reaction kinetics. Dr. Russell joined NRL in 1989; his research involves studies of diamond surface structure and chemistry, and the fundamental mechanisms of chemical vapor deposition processes. Dr. Russell is a member of the American Chemical Society, the American Physical Society, and the American Vacuum Society.



Brian D. Thoms received degrees in physics from the University of Illinois at Urbana-Champaign (B.S., 1983) and Cornell University (M.S., 1986, Ph.D., 1991). His thesis research involved studies of the interactions of hydrogen and hydrocarbons with silicon surfaces. Dr. Thoms has been at NRL as a National Research Council postdoctoral research

associate since 1991. At NRL, he has used electron-based spectroscopic techniques to investigate the influence of hydrogen atoms on the structure and bonding of diamond surfaces. Specific problems he has addressed include the measurement of adsorption and abstraction rates on polycrystalline diamond surfaces, the structure of bare and hydrogen-terminated C(100), and the scattering mechanism of low-energy electrons from diamond surfaces.



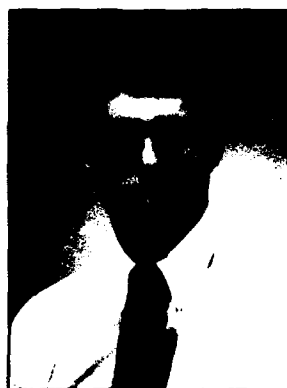
James E. Butler received a B.S. degree in chemical physics from the Massachusetts Institute of Technology in 1966, and a Ph.D. in chemical physics from the University of Chicago in 1972. He was a postdoctoral fellow at the National Institutes of Health from 1972 to 1974, and a research fellow at the James Franck Institute at the University of Chicago from

1974 to 1975. Dr. Butler joined NRL in 1975, where he is currently the head of the Gas/Surface Dynamics section of the Chemistry Division. In that capacity he has coordinated and managed NRL's diamond CVD program. His current interests include chemical processes occurring in the growth and etching of solid-gas interfaces, spectroscopy and structure of transient surface and gaseous species, excited states of molecules, and collision and reaction kinetic processes in gas phase and on surfaces important to various chemical vapor deposition processes. He is a member of the American Physical Society, Optical Society of America, Coblenz Society, Sigma Xi, Chemical Society of Japan, and Materials Research Society.



Michael Marchywka earned the BSEE degree from the University of Michigan in May, 1984 and the MSEE degree in 1985. He worked on instrumentation for magnetic recording research at Kodak Research Laboratories before coming to NRL in 1988. At NRL, he has worked on various phases of UV and vacuum UV detection and instrumentation. This work has

included the measurement of silicon detector properties, design of laboratory test equipment, and development of processing techniques for fabricating UV detectors based on semiconducting diamond. Three patent applications have resulted from his recent work. Mr. Marchywka is a member of Tau Beta Pi, the national engineering honor fraternity.



Jeffrey M. Calvert received a B.A. degree in chemistry from Colgate University in 1977, and a Ph.D. in inorganic chemistry from the University of North Carolina-Chapel Hill in 1982. Since 1982, he has been a research scientist at the Naval Research Laboratory in Washington, DC. In his current position in the Center for Bio/Molecular Science and Engi-

neering, Dr. Calvert is responsible for both basic research and applied development programs in molecular engineering and advanced lithography. Dr. Calvert has published more than 50 papers in scientific journals, of which about 30 are related to self-assembled materials and lithography; he also has 12 published and pending patents. Dr. Calvert is a member of SPIE, the American Chemical Society, and the Electrochemical Society.

Computational Materials Science

Larry L. Boyer, Michael J. Mehl, Dimitrios A. Papaconstantopoulos,
Warren E. Pickett, and David J. Singh
Condensed Matter and Radiation Sciences Division

INTRODUCTION

As we advance toward the 21st century, our nation's technological and industrial base has become increasingly dependent on advanced materials. Nowhere is this more evident than in modern Navy systems. Along with the increasing importance of new high-performance materials, there has been a growing demand for computer-based modeling of materials, both in an effort to predict new materials and to gain an understanding of the basic mechanisms underlying useful properties. A variety of theoretical tools are used for this purpose in the Complex Systems Theory Branch. These range from approximate methods to precise, density-functional (DF), electronic structure-based techniques. The approximate methods are used for very complex materials, but they are limited, both in terms of precision and the variety of properties that can be calculated. The DF electronic structure-based techniques yield the highest precision and can be used to calculate a wide variety of properties while using only the composition and perhaps the structure of the material as input.

Theoretical predictions of new materials can be made by computing the relative stability of collections of atoms in various crystallographic arrangements and compositions. Such calculations are performed from first-principles calculations by using DF techniques, without resorting to experimental input. The DF theory proposed in the mid 1960s by Hohenberg, Kohn, and Sham [1] shows that the total energy is a universal functional of the electron charge density for any system of electrons in the external potential of the atomic nuclei. The DF theory

was also formulated in terms of solutions of a set of coupled one-electron Schrodinger-like equations, thus reducing the problem of a large number of mutually interacting electrons in a solid to a coupled set of one-electron problems. The DF theory became a practical computational scheme when Kohn and Sham proposed the local density approximation (LDA), which treats the exchange and correlation energy as that of a uniform electron gas. These theoretical developments, coupled with the rapid increase of computer power, have led to remarkable advances in computational materials science.

EXPLORING WITH LARGE LATTICE STRAINS

There are many examples of first-principles calculations of the energy E of a solid for *small* variations in crystal structure—to determine, for example, phonon modes and elastic constants. However, there are relatively few examples of total energy calculations for crystal distortions large enough to transform between two widely differing structures, transformations that necessarily involve large lattice strains, i.e., strains beyond the elastic limit. We describe a method of exploring for low-energy structures along paths in strain space that transform a lattice into itself, and illustrate the method with specific results for silicon.

A crystal lattice is specified by the set of all vectors given by the linear combination of three primitive vectors with integer coefficients. For any lattice there are many choices for the three primitive vectors. For example, silicon has the diamond structure, which has a face-centered cubic (fcc) primitive lattice. Two choices for

the primitive vectors are given, in units of half the lattice constant, by the columns of the matrices

$$A = \begin{pmatrix} 1 & 1 & 0 \\ 1 & 0 & 1 \\ 0 & 1 & 1 \end{pmatrix} \quad \text{and} \quad B = \begin{pmatrix} 1 & 1 & -1 \\ 1 & 0 & 0 \\ 0 & 1 & 1 \end{pmatrix}$$

A is the conventional choice. The matrix $S = B A^{-1}$ transforms A to B, leaving the lattice invariant. S is nonsymmetrical and therefore cannot be produced by a torque-free stress. However, it can be symmetrized by multiplying by its transpose (S^T), taking the square root of the diagonalized product and transforming back to the original coordinate system. This gives the so-called magic strain transformation [2] $S_m = U[U^T S^T S U]^{1/2} U^T$, where U is the matrix of the eigenvectors of $S^T S$. The transformed lattice $S_m A$ is the same as $B = S A$, apart from the rotation R, where $R S A = S_m A$, or $R = S_m S^{-1}$.

A NEW STRUCTURE FOR SILICON

Let S_m to be the end point of a continuous transformation. For our example (A and B given above), the lattice stretches by 78% along the (0.85, -0.16, -0.50) direction, 0% along (1, -1, 2) and -44% along (0.34, 0.90, 0.28), as given by the eigenvalues and eigenvectors of S_m . The transformation can be produced by compressing the lattice along the latter direction, allowing the remaining crystal structure parameters to relax to minimum energy. For the diamond structure, which has two atoms per primitive cell, this includes a relative displacement of the two sublattices. Figure 1 shows the energy curve that results when using the Stillinger-Weber (SW) model [3] for silicon if the additional lattice strains are confined to stretching (or contracting) along the other two orthogonal directions. Two features to notice are: (a) The maximum energy corresponds roughly to the thermal energy available at the melting temperature. This feature is present in similar calculations for all other solids treated thus far (rare gas solids, aluminum, iridium, and NaCl). This could explain a well-known trend that correlates large elastic constants with high

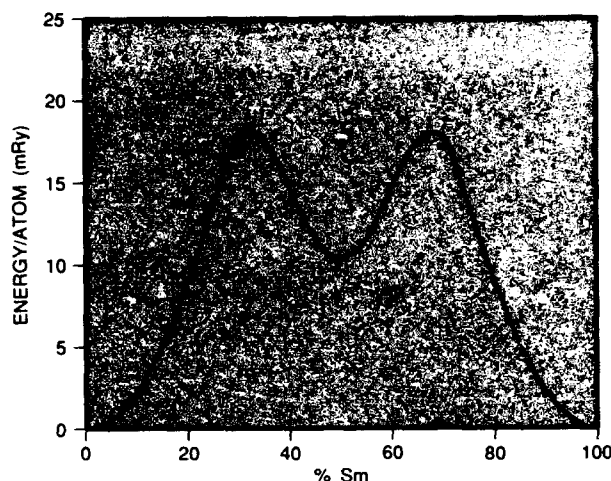


Fig. 1 — Energy per atom, for the Stillinger-Weber model, as a function of the percent of the transformation S_m completed. The central minimum denotes a metastable structure.

melting temperatures, since the curvature at 0 and S_m is given by the elastic constants. (b) The minimum at the midpoint between 0 and S_m indicates the presence of a nearby stable structure. We call it bct5 because it has a body centered tetragonal lattice with each atom at the approximate center of a pyramid with corners occupied by 5 near neighbors. The energy of SW silicon, when fully relaxed in the bct5 structure, is 7 mRy/atom above the diamond structure.

The stability of the SW-bct5 structure has been examined with lattice dynamics, elastic constant calculations, and molecular dynamics simulations [4]. All studies showed the structure to be quite stable. For example, molecular dynamics simulations place the melting temperature near that of cubic silicon. When the bct5 structure is computed by using first principles methods, its energy is 16 mRy/atom above the diamond structure—more than a factor of two larger than that given by the SW model. Thus, we do not expect bct5 silicon to be as stable as indicated by the SW model, which has been verified by comparing the elastic constants computed by both methods [4]. However, both models are indeed elastically stable and have stable long-wave optic modes. A short-wave (zone boundary) instability would lower the energy without disturbing, to lowest order, the underlying lattice, aside from cell doubling

along the direction of the unstable wave vector. Such distortions would further stabilize the bct5 structure against returning to the cubic (diamond) form.

ELECTRONIC STRUCTURE OF bct5 SILICON

The electronic properties of the bct5 phase have been determined by first-principles methods. This phase is a metallic one, in contrast to the semiconducting diamond-structure phase but like the known high-pressure β -tin form. A charge density contour map (Fig. 2) compares the bonding of these three forms of silicon. High-density regions (red) between atoms denote covalent bonding. Thus, we find that the bct5 structure is an intermediate phase between the lowest energy diamond lattice (coordination 4, all covalent bonds) and the high-pressure β -tin lattice (coordination 6, all metallic bonds), both in terms of geometry (coordination 5) and electronic behavior (both metallic and covalent bonding). Because of the partial covalency in the bct5 structure, it is less metallic than in the β -tin form.

BETTER EMPIRICAL MODELS

Large lattice strain calculations may be very useful in developing better empirical interatomic force models. The interatomic potentials currently used in simulations are often constructed

Table 1 — Energy and Volume Comparison

	E-E ₀ (mRy)		V/V ₀	
	SW	FP	SW	FP
bct5	7	16	.91	.86
β -tin	15	16	.86	.77

without much consideration for whether or not they give correct energies for large distortions. As a result, potentials are likely to be unreliable for describing properties such as the structure of the liquid state and deformations under pressure. Table 1 compares the energies (per atom) and volumes, relative to the values for cubic silicon (E₀ and V₀) calculated with the SW model and by first principles (FP). The SW potential for silicon was constructed to give reasonable liquid state properties. Even so, it gives approximately five near neighbors in the liquid; in reality, there are on average a little more than six. This discrepancy could be related to the fact that the SW potential overstabilizes the bct5 structure.

PREDICTION OF MAGNETISM IN CoH

Significant advances in computational techniques and computer power allow theorists to survey a large number of materials for desired properties much faster than experimentalists can perform the measurements. One example is our discovery of magnetism [5] in CoH, which occurred independently from experimental work

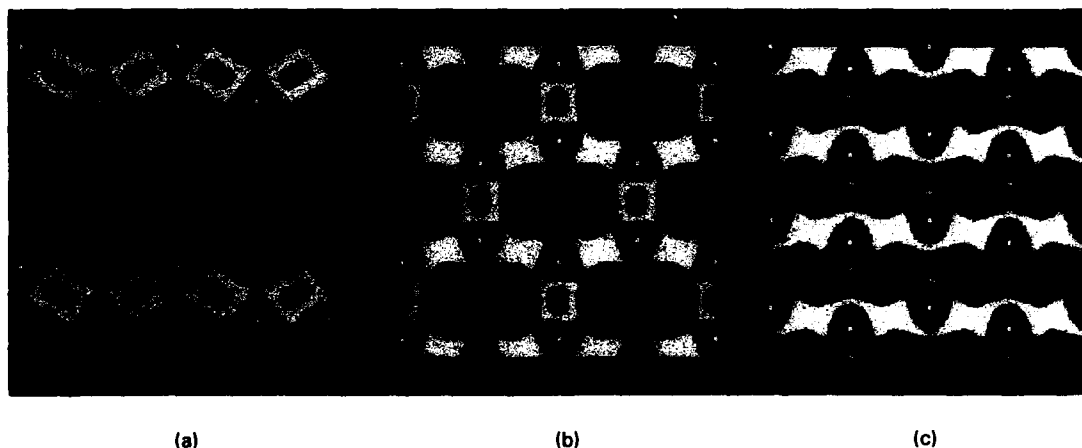


Fig. 2 — Valence charge density contour plot (red, high density; blue, low density) for the (110) planes of the three structures of silicon: diamond (a), bct5 (b), and β -tin (c)

performed at about the same time [6]. By using lattice parameters predicted by total energy calculations, we computed the band structure for all transition-metal monohydrides in the fcc rock salt structure. The results of these calculations were used to evaluate the Stoner criterion for ferromagnetism, i.e., $N(E_F)I > 1$. $N(E_F)$ is the electronic density of states at the Fermi level, E_F , and I is a magnetic interaction strength.

Figure 3 shows our results for the 3d, 4d, and 5d classes of metal hydrides. This figure shows that CoH easily exceeds the Stoner criterion with a value of approximately 2. FeH comes close to the Stoner limit with a value of 0.91, while the rest of the 3d as well as the 4d and 5d monohydrides have values well below 1.0. The calculations reveal an unexpected "symmetry" in that the peak in magnetic tendency is found at 10 valence electrons for all the three transition metal series. This also correlates with the pure metals, where Ni, the only stable fcc structure monatomic magnetic material, also has 10 valence electrons.

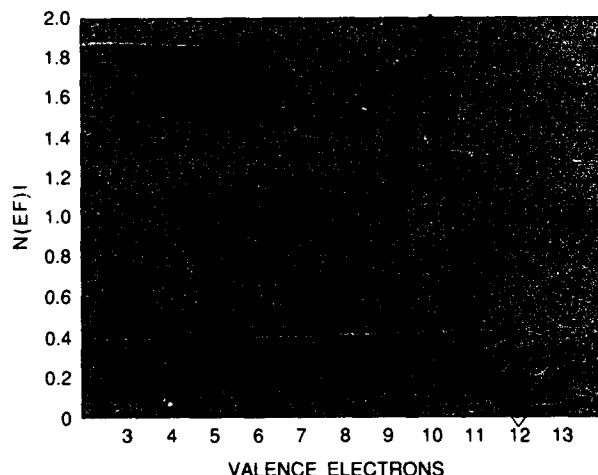


Fig. 3 — The Stoner factor $N(E_F)I$ plotted as a function of valence electrons for all transition metal monohydrides. A maximum of about 2 is reached for CoH, which was predicted to be a new magnetic material.

Mössbauer studies on CoH_x and FeH_x were reported at the same conference [6] where we presented our calculations [5]. The experimental findings identified an fcc CoH γ phase and an hcp FeH phase for $x \leq 0.9$ in which both exhibited ferromagnetism. Because our results

of Fig. 3 correspond to the stoichiometric limit $x = 1$, we extended our calculations of CoH_x for $x = 0.9$ by using the coherent potential approximation. We found that disorder lowers the value of $N(E_F)I$ to the value 1.7, which is still well above the Stoner limit. In FeH, a value $N(E_F)I$ close to but below the Stoner criterion is found consistent with the fact that magnetic fcc FeH is unknown in nature. However, the proximity to the Stoner criterion suggests the possibility of magnetism in related structures—exactly what is found for hcp FeH.

BEATING THE N^3 PROBLEM

The main limitation on the applicability of standard DF methods arises from the fact that the computational requirements increase rapidly with the complexity of the material in question. A useful measure of the complexity of a solid is the number of atoms N in a primitive unit cell, molecule, or cluster. Most elemental solids have $N = 1$ or 2. The high-temperature superconductor, $\text{YBa}_2\text{Cu}_3\text{O}_7$, which has been studied extensively at NRL, has $N = 13$, while buckminsterfullerene C_{60} has $N = 60$. Conventional DF algorithms have computational requirements proportional to N^3 (denoted $O(N^3)$), so that each doubling of N results in an eight-fold increase in computer time. Although methods suitable for treating 100 or more atoms of certain types exist, this $O(N^3)$ scaling has restricted calculations for transition element containing materials to less than 40 atoms per cell. However, recent work in NRL's Complex Systems Theory Branch has led to new real-space algorithms [7] that bypass the previously dominant N^3 steps and extend the range to 100 or more atoms with no restriction on the type of material. The ability to perform calculations for materials containing transition elements is particularly significant to the Navy because of the need for improved magnets, ferroelectrics, superconductors, and refractory and structural materials, all of which generally contain these elements. The first application of these new algorithms was to elucidate the properties of a prototypical member, $\text{Cs}(15\text{-crown-5})_2$, of a novel class of solids called electrides. In this material, the Cs atom acts as if it were a transition metal because of

the highly unusual chemical interaction between the crown ether molecules (15-crown-5 \equiv $C_{10}O_5H_{20}$) and the Cs outer core electrons.

ELECTRIDES: ELECTRONS AS ANIONS

Electrides are unusual solids formed from alkali metal atoms encapsulated by crown ether or cryptand molecules. These materials have crystal structures containing large empty spaces. A prototypical example, $Cs(15\text{-crown-5})_2$, can be described as a distorted CsCl-type lattice having a Cs atom surrounded by two crown ether molecules on the "Cs" site and an empty space at the "Cl" site. The description of the chemical cohesion in the electrides is even more unusual. The encapsulated alkali metal atoms (Cs plus two crown ethers) are regarded as the positive ions in an ionically bonded crystal with single electrons, localized in the empty site, acting as the balancing negative ions [8]. This view, although indirectly supported by some experiments, has been challenged and was the subject of considerable controversy. However, because of the complexity of the electride crystals, this question could not be resolved either theoretically or experimentally until the development of the large-scale electronic structure algorithms discussed above. With these and a few hours of supercomputer time, Singh and co-workers [9] calculated the electronic structure of $Cs(15\text{-crown-5})_2$.

Figure 4 is a schematic energy level diagram. The electronic states are divided into two well-separated groups:

- occupied bonding molecular orbitals associated with the cohesion of the crown ethers and their interaction with the complexed alkali atom; and
- the corresponding antibonding and non-bonding orbitals, which are unoccupied.

There is one additional band, containing exactly one electron per unit cell, in the gap between the bonding and antibonding manifolds. The character of the states comprising this band determines the nature of the electrides, i.e., conventional molecular solids or novel ionic

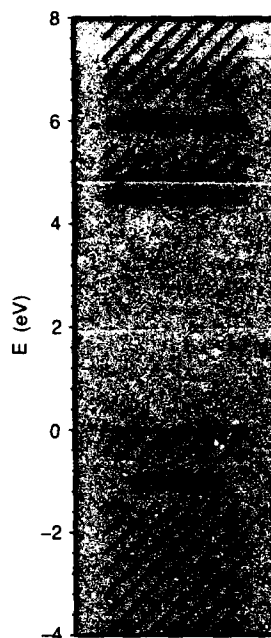


Fig. 4 — Schematic representation of the electronic energy bands of $Cs(15\text{-crown-5})_2$. The narrow band near the top of the gap contains the electride state.

materials. Figure 5 is an isosurface (3D-contour) plot that shows the charge density associated with this state. The charge is strongly localized in the "empty" sites, has maxima at their centers, and does indeed show that these electrons play the role of negative ions in the electrides! The electrides are the only known materials with this property.

Several related, interesting, and potentially useful features of the electrides emerge from this calculation. Among these is the fact that, because of the location of the interstitial electrons in the electrides, they should be very weakly bound to the solid. This means that electride crystals are anticipated to have record low work functions (important in thermionic and field emission). Furthermore, because of the proximity of these materials to correlation-induced metal-insulator transitions, unusual doping dependencies of their physical properties are expected. When the electrides are successfully doped, these variations can be measured and their utility assessed. Independent of this, because of the presence of only one partially occupied band, doped electrides are likely to be very useful as model systems for studying correlation-induced metal-insulator transitions. This is an important but at present poorly understood subject.

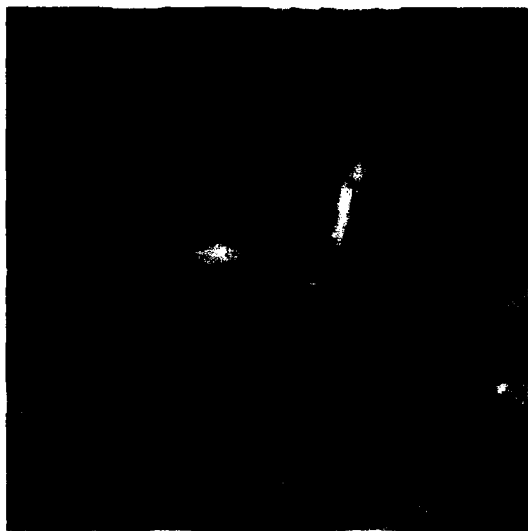


Fig. 5 — The charge density of the electrified state represented by an isosurface (constant density) plot. The positions of the atoms are denoted by colored spheres (Cs, green; C, red; O, blue; H, yellow).

TOWARD COMPLEX MATERIALS SYSTEMS

Historically, computational materials science has been divided into the study of macroscopic systems, by using continuum theory and the experimentally observed elastic properties of materials, and first-principles methods, which are restricted to the study of small clusters or periodic lattices with only a few atoms in the unit cell. The gap between these regimes has decreased with the development of first-principles calculations that break the N^3 barrier. These calculations allow systems containing hundreds of atoms to be studied by using modern computers. Unfortunately, no matter how efficient first-principles methods become, it is doubtful that they will soon be able to handle clusters or unit cells containing thousands of atoms. Computations on these large systems are necessary for a detailed atomistic understanding of the creation and motion of structural defects such as vacancies, interstitial atoms, dislocations, grain boundaries, anti-phase boundaries, and twinning (all of which are important for determining the strength and ductility of materials), as well as the general problem of alloy formation.

NRL's Complex System Theory branch is actively pursuing ways to bridge the gap between the atomistic first-principles and macroscopic continuum calculations. New methods are being tested that have the property that they reproduce the result of the accurate first-principles calculations when applied to small systems, yet can handle large numbers of atoms in a reasonable amount of computer time. Although we are not yet able to handle the motion of systems with thousands of atoms at room temperature, we are developing techniques that will be able to handle such systems in the very near future.

This research uses the results of first-principles calculations to fit a tight-binding Hamiltonian [10]. The tight-binding Hamiltonian provides a simple method to reproduce the quantum mechanics of the first-principles calculations without the necessity of performing a full-scale self-consistent calculation [11]. Because the method can be formulated in terms of interactions only between atoms that are close together, the computational effort no longer scales as $O(N^3)$, but rather as $O(N^2)$ or even $O(N)$, depending on the algorithms used.

DIAMOND GROWTH AND SURFACES

We have implemented a tight-binding total energy functional, with parameters fit to first-principles density-functional calculations of carbon clusters and hydrocarbon molecules. This functional is capable of exploring situations that are much too difficult even for our extended first-principles methods discussed above. This method is simple enough that in its first application [12] it was applied to all three high-index surfaces of diamond [(111), (100), (110)], for both the clean case and for varying levels of hydrogen coverage. In cases where first-principles studies exist, it reproduces the known results. The tight-binding method has provided new predictions of surface stabilities and reconstructions. The method readily provides the frequencies of hydrogen vibrations that can be compared directly with experimental data to demonstrate correspondence, or lack of it, between the predicted structure and the one obtained in the laboratory.

This tight-binding method has been applied to a situation that is both topical and demonstrates its potential. Spurred by work in NRL's interdivisional accelerated research initiative "Diamond Film Growth: Mechanisms," this method was applied to simulate the dynamic relaxation of atoms at and near a step on the (111) diamond surface. Figure 6 illustrates both the initial configuration, with carbon atoms tetrahedrally bonded, and the fully relaxed structure. It is predicted that, at low temperature, the atomic layer above the step essentially graphitizes, except that bonds at the step ledge are not broken. At high temperature, where the hydrogen that is normally present is desorbed, it is likely that the entire layer above the step will defoliate as a flake of graphite. If, however, hydrogen is reintroduced before the step ledge bonds are broken, tetrahedral bonding reasserts itself, and the diamond structure around the step is restored. Similar bond-breaking and rebonding processes are expected to be involved in the growth of diamond from hydrocarbon molecules.



Fig. 6 — Structures of the ideal (top) and fully relaxed (bottom) step on the (111) diamond surface. Colors represent the relative energies of the atoms: blue is low energy, as in bulk diamond or in graphite; red denotes a very high, unfavorable energy associated with dangling bonds; and yellow and green denote intermediate energies.

DEFECTS IN METALS

To further demonstrate the power of the tight-binding method, we studied the formation of a vacancy in silver. The calculation starts with a supercell of 128 atoms (Fig. 7). A silver atom is removed from the supercell, forming a vacancy site, and the atoms near the vacancy are allowed to relax. The tight-binding method is then used to determine the energy required to form this vacancy. Although this process takes several hours of computer time on a workstation, a first-principles calculation of the same properties would consume several weeks of supercomputer time. Our calculations show that the energy required to form a vacancy in silver is 1.2 electron volts (eV), in good agreement with the experimental value of 1.05 eV [13].

Further development of the tight-binding method will allow us to directly determine the dynamical matrix of a quantum mechanical system, allowing a complete description of the motion of atoms in a solid and thermodynamic properties. Coupled with calculations on large

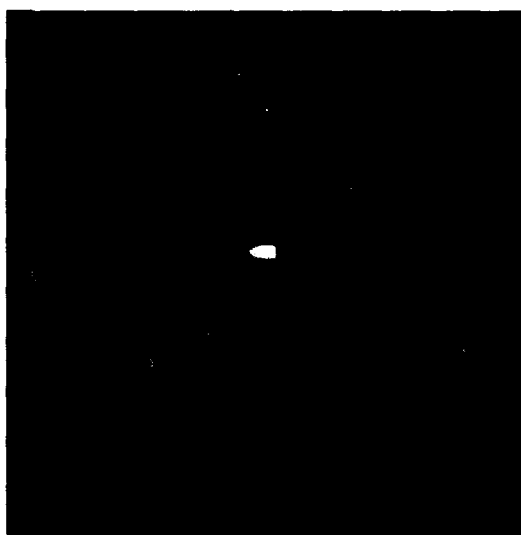


Fig. 7 — Vacancy in a supercell of silver atoms. The spheres represent the atoms. Relaxation of the atoms around the vacancy can occur. The tight-binding method has been used to study properties of the vacancy in supercells of more than 100 atoms.

systems containing thousands of atoms, we will begin to be able to bridge the gulf between first-principles calculations and the macroscopic world.

REFERENCES

1. P. Hohenberg and W. Kohn, "Inhomogeneous Electron Gas," *Phys. Rev.* **136**, B864 (1964); W. Kohn and L. Sham, "Self-Consistent Equations Including Exchange and Correlation Effects," *Phys. Rev.* **140**, A1133 (1965).
2. L.L. Boyer, "Magic Strains in Face Centered and Body Centered Cubic Lattices," *Acta Cryst.* **A45**, FC29 (1989); B.W. Van de Waal, "A General Procedure to Derive Magic Strain Tensors," *Acta Cryst.* **A46**, FC17 (1990).
3. F.Q.H. Stillinger and T.A. Weber, "Computer Simulation of Local Order in Condensed Phases of Silicon," *Phys. Rev. B* **31**, 5262 (1985).
4. L.L. Boyer, E. Kaxiras, J.L. Feldman, J.Q. Broughton, and M.J. Mehl, "New Low-Energy Crystal Structure for Silicon," *Phys. Rev. Lett.* **67**, 715 (1991); **67**, 1477 (1991).
5. D.A. Papaconstantopoulos, "Magnetism in Transition Metal Hydrides," *Europhys. Lett.* **15**, 621 (1991); D.A. Papaconstantopoulos, J.P. Skroch, and G.D. Drew, "Calculation of the Total Energy, Electron Phonon Interaction and Stoner Parameter in the 5d-Transition Metal Hydrides," *Proc. Int. Symp. on Metal-Hydrogen Systems: Fundamentals and Applications*, F.D. Manchester, ed. (Elsevier Sequoia, 1991) pp. 401-410.
6. G. Schneider, M. Baier, R. Wordel, F.E. Wagner, V.E. Antonov, E.G. Ponyatovsky, Y. Kopilovskii, and Makarov, "Mössbauer Study of Hydrides and Deuterides of Iron and Cobalt," *Proc. Int. Symp. on Metal-Hydrogen Systems: Fundamentals and Applications*, F.D. Manchester, ed. (Elsevier Sequoia, 1991) pp. 333-342.
7. D.J. Singh, H. Krakauer, C. Haas, and A.Y. Liu, "The Projector Basis Technique and Car-Parrinello Scaling in Mixed Basis, LAPW and Extended LAPW Electronic Structure Methods," *Phys. Rev. B* **46**, 13065 (1992); D.J. Singh, *Planewaves, Pseudopotentials and the LAPW Method*, (Kluwer, Boston, 1994).
8. J.L. Dye, "Electrides: Ionic Salts with Electrons as the Anions," *Science* **247**, 663 (1990).
9. D.J. Singh, H. Krakauer, C. Haas, and W.E. Pickett, "Theoretical Determination that Electrons Are the Anions in Electrides: $\text{Cs}^+(15\text{-crown-5})_2\text{e}^-$," *Nature* **365**, 39 (1993).
10. J.C. Slater and G.F. Koster, "Simple LCAO Method for the Periodic Potential Problem," *Phys. Rev.* **94**, 1498 (1954); D.A. Papaconstantopoulos, *Handbook of the Band Structure of Elemental Solids* (Plenum Press, New York, 1986).
11. M.M. Sigalas and D.A. Papaconstantopoulos, "Transferable Total-Energy Parametrizations for Metals: Applications to Elastic-Constant Determination," *Phys. Rev. B* (in press).
12. B.N. Davidson and W.E. Pickett, "Tight-Binding Study of Hydrogen on the (111), (100) and (110) Diamond Surfaces," *Phys. Rev. B* (in press).
13. K. Mosig, J. Wolff, J.E. Kluin, and Th. Hehenkamp, "Investigation of the Equilibrium Concentration of Lattice Vacancies in Silver and Dilute Silver-Tin Alloys with a Differential Dilatometer," *J. Phys.: Condens. Matter* **4**, 1447 (1992).

THE AUTHORS



Larry L. Boyer graduated from Doane College in Crete, Nebraska, in 1965 with a B.A. degree and majors in mathematics and physics. He received an M.S. and a Ph.D. in physics from the University of Nebraska in 1968 and 1970, respectively. His postdoctoral research between 1970 and 1973, at the University of Nebraska and Princeton University,

was in deriving simple models for interactions in complex ionic materials — $\text{Gd}_2(\text{MoO}_4)_3$, a ferroelectric material and apatite, which is the main constituent mineral of bones and teeth. He joined NRL in September 1973 to do theoretical and experimental work on complex interactions in simple ionic materials and multiphonon infrared absorption in alkali halides. He has made major contributions in developing techniques for band-structure calculations, applying and developing simplified models for the electronic structure and dynamics of ionic materials, and in relating results of lattice dynamics to phase transitions. He won the NRL-Sigma Xi Pure Science Award in 1988 for work in condensed matter theory developing *ab initio* electronic structure models and applying them to calculate equations of state and lattice instabilities of ionically bonded solids.



Michael J. Mehl graduated from the University of Kansas in 1973. He received his M.S. and Ph.D. degrees from Indiana University in 1975 and 1980, respectively. From 1979 to 1981 Dr. Mehl was a Postdoctoral Fellow at Rutgers University, working with Prof. David Langreth. He held a similar position at the University of Maryland from 1981 to 1983, work-

ing with Prof. Ted Einstein. Dr. Mehl came to NRL in 1983 as a contractor, working for Sachs-Freeman Associates. He joined the Condensed Matter Theory Branch as a full-time employee in 1986. In 1991-1992 he was a participant in the Advanced Graduate Research Program, studying at the Institut Romand de Recherche Numerique en Physique Materiaux in Lausanne, Switzerland. Since coming to the Laboratory, Dr. Mehl has worked on a wide variety of problems in condensed matter physics, including ionic systems, phase transitions, and the electronic and mechanical properties of intermetallic alloys. He is currently working on methods for doing large-scale simulations of metals based on first-principles electronic structure calculations.



Dimitrios A. Papaconstantopoulos was born in Athens, Greece, and graduated from the University of Athens with a B.S. degree in physics in 1961. He received a Ph.D. in theoretical solid state physics from the University of London, England in 1966. He was a professor of physics at George Mason University from 1967 to 1977 and chairman of the physics

department from 1974 to 1977. He worked at NRL as a consultant from 1970 to 1977 and as a government employee from 1977 until the present. He is currently head of the Complex Systems Theory Branch. His areas of expertise include band structure calculations, superconductivity, and theory of alloys. He has authored approximately 150 journal papers and 2 books and has given more than 200 presentations at professional meetings. He has won three Alan Berman Research Publication awards and the 1990 Sigma Xi Pure Science Award. He has been a Fellow of the American Physical Society since 1981.



Warren E. Pickett received his Ph.D. in theoretical solid state physics from State University of New York/ Stony Brook in 1975. Since 1979 he has been a condensed matter theorist at the Naval Research Laboratory, studying semiconductors, metals and superconductivity, and indulging an avid interest in new materials with novel properties.

He has spent sabbatical

years at Daresbury Laboratory, England (1983-4) and at Cambridge University, England (1990-1). He received the Scientific Achievement Award from the Washington Academy of Sciences in 1985, and in 1989 was elected Fellow of the American Physical Society. At NRL he has been the recipient of the E. O. Hulbert Award (1990) and the Sigma Xi Technical Achievement Award in Pure Science (1993). In 1992 he was named NRL Senior Scientist for Condensed Matter Theory.



David J. Singh graduated from the University of Ottawa with a B.Sc. (summa cum laude) in physics in 1980. He continued his education at the University of Ottawa, obtaining a Ph.D. degree in physics in 1985. He was a Post-Doctoral Fellow at the College of William and Mary. Dr. Singh joined NRL as a National Research Council Post-Doctoral Fellow in

1983, becoming a staff member in 1990. His research at NRL has focused on the electronic structure of complex solids with particular emphasis on first-principles approaches. He has authored more than 80 scientific papers as well as a book on the LAPW method for electronic structure calculations.

Self-assembled Molecular Templates: Microtubule-based Controlled Release for Biofouling Control and Medical Applications

Ronald R. Price, Alan S. Rudolph, Jonathan V. Selinger, and Joel M. Schnur
Center for Bio/Molecular Science and Engineering

INTRODUCTION

The area of self-assembled ultrafine particulate-based composites (nano composites) has been a major thrust in advanced material development in NRL's Center for Bio/Molecular Science and Engineering. We have focussed on the application of biologically derived, self-assembled cylindrical microstructures to form advanced composite materials for controlled-release applications. These microstructures, called tubules, have many applications in the material sciences. An exciting use of these materials is as "microvials" for long-term release applications.

Over the past several years there has been a great deal of interest among scientists in the area of "nano" technology and materials self-assembly. A particularly interesting approach is to use bottom-up molecular-level engineering to produce new materials with improved physical properties. Nature uses this approach to form simple mineral crystals as well as large complex living systems. Initial progress in understanding the basic rules governing self-assembly has provided advances in scientific disciplines ranging from molecular biology to materials science.

Research conducted at the Center for Bio/Molecular Science and Engineering has led to the discovery that modified phospholipid molecules (1,2-bis(10,12 tricosadinyoyl)-sn-glycero-3-phosphocholine ($DC_{8,9}PC$)) form tubular microstructures (Fig. 1). While exploring the physical characteristics of this lipid, Yager and Schoen [1] found that $DC_{8,9}PC$ formed novel, small microcylinders, which they called tubules. These microscale lipid cylinders

self-assemble either by thermal cycling or through crystallization in a mixed solvent system. The resulting submicron-scale structures typically are cylinders with diameters of 0.5 microns and lengths from tens to hundreds of microns. Further investigation has shown the structures to be formed from lipid ribbons that are wound in helical fashion around the central axis of the structure. The resulting structure can best be described as approximating a paper drinking straw. Recently, human bile has been found to form self-assembled microtubules very similar to those observed from man-made lipids. Further exploration into the nature of this lipid has resulted in the formation of phospholipid



Fig. 1 — Negative stained TEM image of lipid microtubules with diameters averaging 0.4 μm

filaments and helices. Recently a theoretical mathematical model based on chiral molecular packing has been proposed [2] to explain the phenomenon.

An important use of both the lipid microtubules and the resulting metallic microcylinders (Fig. 2) is in the area of microentrapment and controlled release. Microencapsulation and controlled release has been a subject of interest since the 1950s. Self-assembly of novel structures and their adaptation to the field of controlled release may open a new range of opportunities for tailoring the delivery of active materials in a wide range of applications over long time frames. In contrast to many existing systems where release can vary from minutes to a few months, microtubules are capable of controlling delivery of agents over much longer time periods, e.g., from months to years.



Fig. 2 — SEM image of copper-coated microtubules at a magnification of 6,000 \times

ENTRAPMENT AND RELEASE FROM HOLLOW MICROCYLINDERS

The concept of entrapment and release from cylinders was first patented in 1977. This patent described the use of a large-diameter hollow glass cylinder to retain a fragrance or pheromone that is released at a zero order rate until depleted. The patent described release periods of a few hours. An improvement was the capping of one end to allow material to be retained and released over a slightly longer period of time. Glass macrocylinders are also used to entrap and retain blood samples. Blood is

entrapped by capillary action in glass capillary tubes where the blood is retained for analysis. The use of these large-scale glass or plastic hollow tubes was restricted, because no means had been devised to retain volatile materials in such a large cavity. The requirement to trap the contents by sealing the ends or by providing a barrier did not offer a significant improvement in release times. In addition, because these cylinders were so large in scale, they could not be used to build a composite system, nor could they be easily dispersed within a coating. They were simply a convenient form in which to trap volatile materials that would then evaporate into the air. Independently at NRL, microtubules were used to entrap and retain liposomes. When characterizing metallic microcylinders by transmission electron microscopy, it was necessary to encapsulate them into an epoxy matrix to form thin cross sections of the metallic walls. It was noted that the epoxy had been able to infiltrate the center core of the microstructures and polymerize. When these same epoxy composites were subjected to ion etching, it was also noted that the epoxy core was intact.

At about this same time, a sample of copper antifouling paint from the USS *Forrestal* was sent to our laboratory for analysis. The sample was examined by scanning electron microscopy and energy-dispersive X-ray microanalysis. This revealed that the coating was loaded with bacteria living in a polymeric sponge formed by the resins in the paint after the copper antifoulant and rosin leaching agent were prematurely released from the coating. It seemed reasonable to expect that hollow cylinders with ultrasmall diameters, such as the lipid tubules discovered at NRL, could have applicability for controlled-release applications, including antifouling.

To demonstrate the viability of this concept, we initially chose to study tetracycline as a proof of principle. It was not known if the tetracycline could be encapsulated in or subsequently released from the microcylinders. A series of experiments was devised in which tetracycline was mixed into an epoxy monomer carrier and entrapped in the microtubules, and the same experiment was conducted with an epoxy polymeric material. The idea was that the epoxy saturated with the tetracycline

entrapped in the metallic microcylinders would work in a manner similar to blood in a glass capillary tube. In a proof of principle experiment, tetracycline was found to release from an epoxy coating over time, compared to the control that simply was an epoxy polymer film saturated with tetracycline (Fig. 3) [3]. Other experiments varied the epoxy from a water-miscible form (Quietol) to an EPON epoxy that was not water-soluble. Figure 4 illustrates the

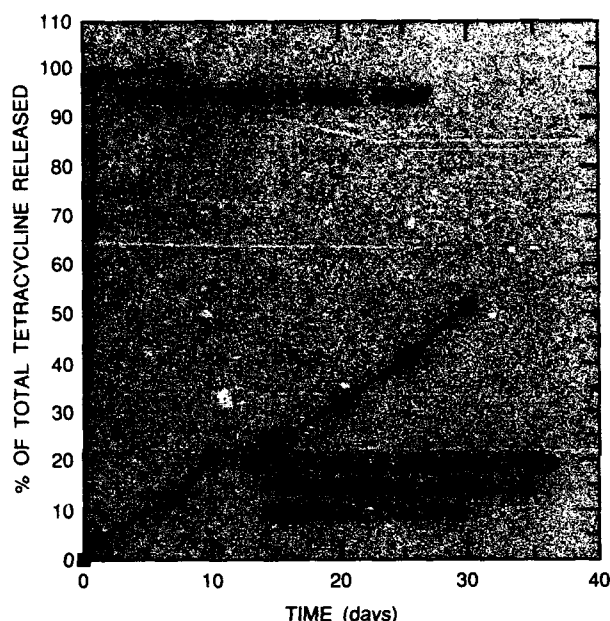


Fig. 3 — Release of tetracycline from epoxy coating, both free associated and encapsulated

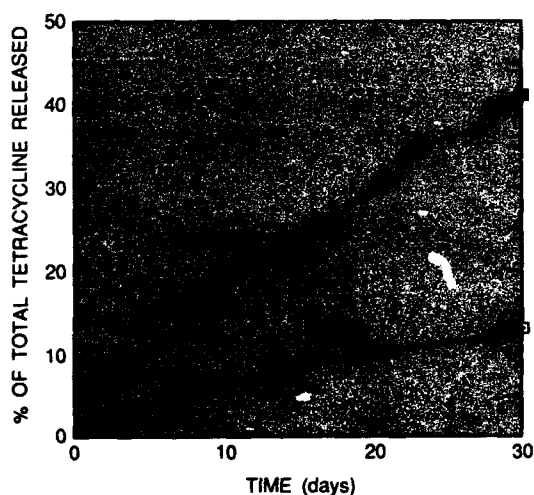


Fig. 4 — Release profile of tetracycline from a water-miscible Quietol carrier and from a nonwater-miscible EPON 812 carrier

differing release profiles for each of these resins, providing an initial insight that, in fact, the microcylinders might show promise as a controlled-release system.

To understand the release phenomenon and the variables that govern release, a mathematical model has been developed. Critical variables include the inner diameter of the cylinders, the length of the cylinders, and the initial concentration of the encapsulant. Further factors could be the solubility of the encapsulant in the exterior environment, the molecular weight of the encapsulant, and the type of polymeric carrier (if any) used to retain liquid or particulate materials in the central core of the cylinder. For the case of a metal-coated lipid tubule with solid, impermeable walls, the encapsulant is capable only of diffusing from the open ends of the cylinder. This diffusion process is easily described by the effective one-dimensional diffusion equation

$$\frac{\partial c(x,t)}{\partial t} = D \frac{\partial^2 c(x,t)}{\partial x^2},$$

where $c(x,t)$ is the concentration of the encapsulant at position x and time t , and D is the effective one-dimensional diffusion constant. The boundary conditions for a cylinder of length L with open ends are $c(0,t) = c(L,t) = 0$. If the encapsulant is uniformly distributed inside the cylinder at the beginning of the release process, the initial condition is $c(x,0) = c_0$. The solution of the differential equation is then

$$c(x,t) = \sum_{n=0}^{\infty} \frac{4c_0}{(2n+1)\pi} \times \exp \left[\frac{(2n+1)^2 \pi^2 D t}{L^2} \right] \sin \left[\frac{(2n+1)\pi x}{L} \right],$$

which gives the concentration profile as a function of both position within the core and time. Integrating this expression over x gives the total concentration of encapsulant with the tubule,

$$c_{tot}(t) = \sum_{n=0}^{\infty} \frac{8c_0 L}{(2n+1)^2 \pi^2} \exp \left[\frac{(2n+1)^2 \pi^2 D t}{L^2} \right].$$

Two limiting cases of these expressions should be pointed out. For short times, the total concentration of encapsulant drops off rapidly as a square root law,

$$c_{\text{tot}}(t) \approx c_0 \left(1 - 2 \sqrt{Dt/\pi}\right).$$

In contrast, for long times the total concentration decays as a single exponential,

$$c_{\text{tot}}(t) \approx \frac{8c_0L}{\pi^2} \exp \left[-\frac{\pi^2 Dt}{L^2} \right],$$

with the exponential decay time $L^2/\pi^2 D$. This long-term behavior is the significant regime for controlled-release applications.

This model leads to the following important conclusions. First, the release time for any molecules encapsulated inside tubules scales as the tubule length squared. Thus a high aspect ratio is an important parameter for determining the time scale of the release process. Second, the release scales inversely with the effective one-dimensional diffusion constant D . This effective diffusion constant describes the effects of the inner diameter of the cylinder and the polymeric carrier that may be incorporated inside the cylinder. In particular, if a polymeric carrier is inside the tubule, the encapsulant molecules must diffuse through a tortuous network of pores to escape from the cylinder. The effective diffusion constant can then be related to the volume fraction of this porous medium. Detailed comparisons between the predictions of the model and experimental measurements are currently underway.

Preliminary results show reasonable agreement between theory and experimental results, with typical release times of 900 hours, provided a second exponential decay process having a typical decay time of 3 hours is added. This second decay process can be attributed to the release of molecules adsorbed onto the exterior of the cylinder. The model clearly shows that the controlled release from hollow cylinders would be very attractive for *long-term* release applications.

CONTROLLED-RELEASE ANTIFOULING COATINGS

Legislative action has banned the use of tin antifouling coatings on vessels of less than 25 meters and completely banned the sale and use of organotin-based paints in many states. The U.S. Navy has adopted a policy to remain with copper-based antifouling coatings until either a totally nontoxic alternative can be found or a paint developed with biodegradable antifoulants that does not cause environmental harm. Current technology is adapted to either the use of organotin co-polymeric coatings or the delivery of copper as the primary toxicant. Therefore a new and novel coating would be needed to entrap and deliver a range of antifoulants that may not be compatible with polymeric paint coatings. Most of the current microencapsulant systems are not well-suited for very long periods of controlled delivery; in addition, they often are not compatible with the solvents used in polymeric paints.

One aspect of the antifouling coatings research funded by the Office of Naval Research has centered on the development of paints that use natural products or their analogs to control marine fouling [4]. Natural compounds extracted from a number of marine animals and plants have proven effective in repelling marine fouling in short-term screening tests (Fig 5). Figure 6 shows a set of test rods that have analogs of natural products simply added to the paint base. Figure 7 is an identical set of rods except that the analog is encapsulated in microtubules. It can easily be seen that the simple addition of active compounds to a coating is not sufficient to obtain satisfactory results. Figure 8 shows a pair of steel test rods that had been suspended in Coconut Harbor, Hawaii, for a 7-month period. Here again it is evident that the microencapsulated material appears to repel settlement, while the associated free material fouled.

Natural products are active against a large number of marine species, not only for repelling barnacles but also for providing antimicrobial activity. Analog compounds have demonstrated a very narrow spectrum of activity against marine barnacle larva, and require either an



Fig. 5 — Extract of a sea pansy that has been microencapsulated in copper microtubules and added to a PVC coating vs a G-10 epoxy control rod (exposed at Beaufort, North Carolina)

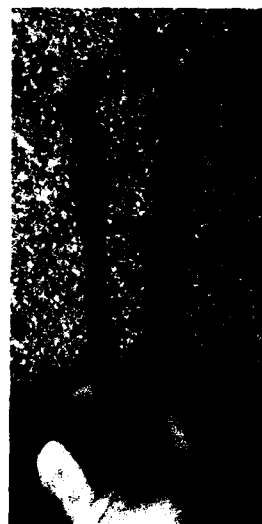


Fig. 6 — Set of three test rods removed at 2-week intervals from Pearl Harbor, Hawaii, containing a natural product analog known to repel settlement of barnacle larva



Fig. 7 — Set of three rods (identical to Fig. 6), except that analog agent is microencapsulated in tubules

Fig. 8 — Long-term (7-month) set of rods removed from waters at Coconut Harbor, Hawaii; cleaner rod has microencapsulated agent



algicide or antimicrobial to offer the same broad spectrum activity. One compound of interest is Khellin, a natural product derived from the seeds of the *Ami visnaga* tree. Khellin is active at a concentration of 0.22 $\mu\text{g/ml}$ and acts as a narcoleptic agent for barnacle larva. Cybrid larva exposed to Khellin are observed to recover and exhibit enhanced ability to settle and metamorphose following return to a nontreated seawater environment. Thus this compound appears to be a nontoxic repellent for barnacle larva. Other compounds that are insect pheromones are also capable of repelling larva. Ablative coatings containing zinc oxide as the ablative pigment were loaded with three of the analog compounds. In one treatment, a biocide C-9211 (an isothiazolone) was added as an antimicrobial. The results of short-term screening assays performed at the University of Hawaii and at Duke University Marine Laboratories indicated that these agents could protect hull surfaces much like the F-121 and ABC-3 copper-based coatings used as controls.

CONTROLLED RELEASE OF PROTEINS FROM LIPID MICROCYLINDERS

Controlled delivery systems based on lipid microcylinders can also be used in biological systems for the release of proteins. Many types of cells express biological response modifiers such as growth factors and cytokines. Such proteins regulate cell reproduction and differentiation and are active in both homeostasis and pathological growth of cell populations.

Growth factors and cytokines are important in the regeneration of soft tissue following injury. Many growth factors (such as TGF-Beta) have very short lifetimes at the wound site. Microencapsulation and controlled release of these compounds from lipid microcylinders may prove beneficial in accelerating wound healing. Initial efforts have centered on issues of toxicity and in-vitro release of TGF-Beta.

Profiles of the release of ^{125}I labeled TGF-Beta from microcylinders have been measured. TGF-Beta is a relatively hydrophobic protein that releases at a slow initial rate of 5-10 ng/day, with a sustained 1-ng/day release rate. This profile is consistent, independent of initial

concentration. Proteins do associate with lipid membranes at a rate dependent on the "hydrophobicity" of the protein. In this case, the desorption of the protein from the surface of the microcylinder is an additional factor in modeling their release from microcylinders.

Interaction of the lipid microcylinders with T-cells and macrophages isolated from peripheral human blood has been studied. Because both T-cells and macrophages are important mediators of the immune response during wound healing, this study was conducted to elucidate any adverse reactions by the cells to the polymerizable lipids used to form the microtubules. Macrophages have been observed to adhere and stretch along the axis of the microcylinders, with no evidence that they are phagocytized [5]. The inclusion of ganglioside GM_1 in the bilayer walls of the cylinders has been demonstrated to reduce the degree of adhesion.

Current studies are being conducted to elucidate the functional response of macrophages to the lipid cylinders. Hydrogel/lipid microcylinder composites have been implanted in healthy mice and used in rat full-thickness skin wound models.

SUMMARY AND CONCLUSIONS

Many issues must be resolved before the full potential of this approach can be realized. Variables controlling release rates must be fully elucidated. Issues of cost, toxicity, and efficacy need to be addressed before commercial development.

The lipid itself is expensive to produce, and problems may be created during pilot plant scale up. Recent improvements in the synthesis of these lipids from lower cost precursors such as soybean phosphatidylcholine, and the ability to recycle lipids from metallic microtubules may provide a means of lowering the costs. These same issues will affect the commercial applications of lipid microcylinders in medicine.

The ability to use natural products in anti-fouling paints also is not certain. Issues such as providing broad-spectrum biofouling control without persistent biocides, the ability to retain activity in the environment over prolonged (5-year) service cycles, and the ability to produce

the metallic microcylinders at a commercially viable price is uncertain, although alternatives may be available. If cost and suitable production issues can be successfully addressed, this approach seems to be quite attractive.

There are a number of other applications for long-term release in, for example, agriculture, antifungals, and bioremediation. Our studies have made it clear that ultrasmall cylinders provide an excellent approach to obtain such long-term release.

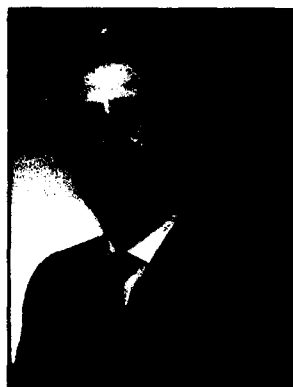
ACKNOWLEDGMENTS

The authors acknowledge Dr. Barry Spargo for his input on medical applications for controlled release. In addition we acknowledge the support for this project from the Office of Naval Research and the Advanced Research Projects Agency.

REFERENCES

1. P. Yager and P.E. Schoen, "Formation of Tubules by a Polymerizable Surfactant," *Mol. Cryst. Liq. Cryst.* **106**, 371 (1984).
2. J.V. Selinger and J.M. Schnur, "Theory of Chiral Lipid Tubules," *Phys. Rev. Lett.* **71**, 4091 (1993).
3. J.M. Schnur, R. Price, and A.S. Rudolph, "Biologically Engineered Microstructures: Controlled Release Applications," *J. Controlled Release*, in press.
4. R.R. Price, M. Patchan, A. Clare, D. Rittschof, and J. Bonaventura, "Performance Enhancement of Natural Antifouling Compounds and Their Analogs Through Microencapsulation and Controlled Release," *Biofouling* **6**, 207 (1992).
5. A.S. Rudolph, G. Stilwell, R.O. Cliff, B. Kahn, B.J. Spargo, F. Rollwagen, R.L. Monroy, "Biocompatibility of Lipid Microcylinders: Effect on Cell Growth and Antigen Presentation in Culture," *Biomaterials* **13**, 1085 (1992).

THE AUTHORS



Ronald Price has been a research biologist with the Center for Bio/Molecular Science and Engineering since 1986. A graduate in biology from California State Polytechnic University in Pomona, California, he has been employed as a chemist at Wynn Oil Company, a territory manager with Carl Zeiss, Inc., in electron optics sales, and has managed the electron

microscopy facility for the Departments of Anatomy and Pathology at Wright State University in Dayton, Ohio, prior to coming to NRL. He is currently a member of the editorial board of the *Journal of Microencapsulation* and a member of Sigma Xi and the International Biodeterioration Society and the International Society of Microencapsulation, where he was appointed to the steering committee. He has published in the areas of phospholipids, controlled release and natural products antifouling, and is an inventor or co-inventor on several patents at NRL. He has presented his work extensively in international biofouling forums. His current research interests include microencapsulation and controlled release, the characterization of artificial lipid membranes, and biotransformations.



Alan S. Rudolph received his bachelor's degree in biology at the University of Michigan in 1981 and his doctoral degree in zoology in 1985 from the University of California at Davis. He joined the Naval Research Laboratory as a National Research Council postdoctoral fellow in 1986. Dr. Rudolph has authored more than 60 publications and 6 patents in the molec-

ular basis for the stabilization of biological systems during environmental stress and in biological controlled-release systems. He is currently a group leader in the Center for Bio/Molecular Science and Engineering and manages research programs in blood substitute and wound repair.



Jonathan V. Selinger studied physics at Harvard University, receiving his A.B. degree in 1983, A.M. in 1985, and Ph.D. in 1989. He then did postdoctoral work in Los Angeles, with a joint appointment at the UCLA Department of Physics and the Caltech Department of Chemical Engineering. In 1992 he came to the Center for Bio/Molecular Science

and Engineering at NRL. Dr. Selinger's research focuses on the theory of complex fluids, an interdisciplinary field that spans physics, chemistry, and chemical engineering. He has developed theories for phase transitions, correlation functions, and pattern formation in polymers, liquid crystals, Langmuir monolayers, and self-assembled microstructures. In related work on the theory of disordered solids, he has modeled the statistical mechanics of random magnetic systems and metallic glasses.



Joel M. Schnur received an A.B. in chemistry from Rutgers University in 1966 and M.S. and Ph.D. degrees in physical chemistry from Georgetown University in 1969 and 1971, respectively. After several postdoctoral fellowships, Dr. Schnur joined the Optical Sciences Division of the Naval Research Laboratory in 1973. For the next 10 years he pur-

sued research in advanced spectroscopies applied to the study of complex organic materials. In 1983, he was awarded a Professor Associé at the Université of Paris VI. In 1984 he returned to NRL where he is now Director of the Center for Bio/Molecular Science and Engineering. Dr. Schnur's research has led to more than 100 publications and 20 patents.

Monitoring Whales and Earthquakes by Using SOSUS

Clyde E. Nishimura
Marine Geosciences Division

INTRODUCTION

In the years immediately following World War II, investigators pioneering the use of hydrophones in the nascent field of underwater acoustics detected numerous unknown signals. They hypothesized these signals to be originating from cetaceans (e.g., whales) or oceanic earthquakes. Because the applied mission of this research was detecting and tracking submarines, these sounds were simply cataloged and then basically forgotten by the Navy—leaving behind a trail of colorful names for these signals such as the A-Train, Jeze monster, commas, and barnyard chorus, to name a few. And so for several decades, the oceans reverberated with the mysterious sounds of whales vocalizing in relative anonymity.

This all changed in November 1992, as the Space and Naval Warfare Systems Command (SPAWAR) and the Commander Undersea Surveillance Atlantic (CUSL) jointly initiated Whales'93, an innovative dual-use scientific program that used existing Department of Defense (DoD) assets to pursue fundamental environmental research. With the use of the U.S. Navy's Integrated Undersea Surveillance System network of underwater hydrophone sensors in the Atlantic (IUSS), the Whales'93 program sought to

- catalog the acoustic signals from large marine cetaceans to determine their poorly known spatial and temporal distributions in their deep-water environment, and
- detect and locate T-phase radiation centers from oceanic earthquakes to obtain a picture of low-magnitude seismicity.

The Marine Geosciences Division of NRL has been a major participant in this program from its inception, assisting in the initial planning and implementation of Whales'93. We also worked directly with active Navy fleet personnel, primarily at CUSL and the Naval Ocean Processing Facility (NOPF) at Dam Neck, Virginia, as well as with researchers from Cornell University. This short article briefly describes the background of the Whales'93 program and the various acoustic signals from whales and earthquakes.

SOSUS AND SOFAR

Based on experience gained during the first and second world wars, the United States realized that antisubmarine warfare represented a mission of high importance. Its priority grew during the Cold War to one of critical proportions with the buildup of a sizable Soviet submarine fleet. To counter this threat, in the mid-1950s the U.S. Navy developed the Sound Surveillance System, better known as SOSUS, which used passive underwater acoustics to detect and track submarines over ocean-wide expanses. Eventually this system expanded to become IUSS, a cohesive network of both fixed and mobile assets for acoustic monitoring of the oceans.

Because IUSS is an operational component of the U.S. Navy, security restrictions are still imposed. Hence, details of SOSUS are not provided in this brief article, instead they are left to the imagination of aficionados of Tom Clancy novels. What can be stated is that SOSUS consists of a series of fixed (i.e., ocean-bottom-mounted) hydrophones. Received acoustic signals are transmitted back to

land-based processing centers via underwater communication cables where time-series data from the individual hydrophone elements are summed according to preselected bearings of arrival at the arrays. This is the well-known technique known as beam-forming. The beam-formed acoustic data, which are directional in coverage, are subsequently transformed into a lofargram (low-frequency acquisition and ranging), which is subsequently plotted, displayed, and then scrutinized by highly trained Naval Ocean Technician Analysts (OTAs). The exact frequency range of the system is classified, but it is sufficient to say that it is optimal for long-range detection of acoustic emissions (e.g., propeller noise) from submarines and ships; it is also ideal for studying large cetaceans and oceanic earthquakes.

The ability to detect low-frequency signals from submarines, whales, and oceanic earthquakes at long distances is due in part to the existence of the sound fixing and ranging (SOFAR) channel in much of the world's oceans. This low-velocity zone is created by changes in the temperature and pressure of seawater at depth; it results in trapping of horizontally propagating acoustic waves. The focusing of this energy within the SOFAR channel is highly analogous to that of an optical lens. Because the attenuation of low-frequency energy in the oceans is extremely small, acoustic signals are diminished only by geometric spreading.

WHY WHALES?

Past cetacean research has primarily been conducted by using observations made in coastal areas or by studying captured animals. The expense of performing long-term observations by either plane or ship in the deep-water regions of the oceans is prohibitive. The logistical problems of attempting to capture and hold large marine animals, such as the 150-ton blue whale, for study, speaks for itself. Hence, passive acoustic monitoring of the vocalizations of cetaceans in their deep-water environment represents a highly attractive research option. But why should the U.S. Navy be conducting such research?

The answer to this question is simple. The Navy is in a unique position; it can contribute an invaluable resource for performing fundamental environmental research while still maintaining IUSS operational capabilities. Use of the existing SOSUS arrays, whose construction could not have been realistically financed by purely academic funding, therefore represents an effective dual use of DoD assets. In these times of growing environmental concern, it is clear that the national security of the United States not only involves military objectives but also includes protection of the world's environment. IUSS dual use therefore represents a sound course of action.

Besides the knowledge that they are being responsible denizens of the oceans, the Navy also directly benefits from such studies. The analysis of the vocalization from cetaceans is a challenging problem that involves the study of broadband, short-time-duration transient signals. These types of problems appear to be critical for monitoring diesel submarines in a littoral environment. Furthermore, monitoring 50 simultaneously vocalizing whales is a task that demands efficiency and high analytical skills. The knowledge gained during Whales'93 is being translated back into IUSS operational procedures. Finally, it is not presumptuous to think that the study of cetaceans, who have been evolving their acoustic processors for millions of years, may lead to a better understanding of underwater acoustics.

DATA

As part of the Whales'93 program, NRL installed a 16-channel data acquisition system at NOPF Dam Neck; this system is a clone of the system installed by the National Ocean and Atmospheric Administration at a similar Naval Facility at Whidbey Island, Washington. This personal computer-based system continuously records a mixture of raw hydrophone and beam-formed data received on the SOSUS fixed hydrophone arrays in the western Atlantic. To make the volume of data being collected manageable, an upper frequency limit of 200 Hz (anti-aliasing filter) has been imposed during data acquisition. The time-series data are

recorded on 8-mm digital tapes that are subsequently processed at the newly opened Dual Use Analysis Center located at NRL.

Transient signals from mysticetes (baleen whales) are easier to interpret by applying time-frequency transformations; the most commonly used and simplest to implement technique is the short-time FFT spectrogram. The basic function of time-frequency methods is the generation of an image in which time is one axis and frequency the other. The respective amplitude of the signal is displayed by using some color-coded scheme or by varying gray-level intensities. Like all time-frequency methods, there is an inherent trade-off between time and frequency space. For instance, increasing the length of the FFT increases the frequency resolution at the expense of lower time resolution. Bilinear time-frequency methodology, such the Wigner-Ville distribution, are also being used. This is not presented in this article because most people are more familiar with spectrogram analyses.

Another basic method for displaying acoustic data is simply a time-amplitude (i.e., time-series) plot; seismograms and electrocardiograms are examples of this type of diagram. Although the frequency content of the signal is not explicitly computed, it can be inferred by visually inspecting the number of zero crossings that occur within a specified time band; greater zero crossings mean higher frequencies. Simple time-series plot are extremely useful for displaying the timing of transient pulses and for displaying complex short-duration waveforms that are not easily interpretable when using spectrograms.

SIGNALS FROM WHALES

To date, numerous acoustic signals from primarily four different mysticetes (blue, finback, humpback, and minke whales) have been recorded at NOPF, Dam Neck. These species identifications were made by Dr. Christopher Clark of Cornell University and are based on comparisons of the recorded acoustic signals with previously reported visual/acoustic observations reported in the scientific literature [1-5]. For the humpback and finback whales, our confidence in the matching of the signals with

the species is extremely high. For the blue and minke whales, the published literature is rather sparse, and hence our confidence is somewhat lower. It should be noted that a component of the Whales'93 program was to obtain, by overflights of USN P-3 aircraft, visual and acoustic confirmation of the species identification with the acoustics received by SOSUS. Unfortunately, this aspect of the program was not implemented because of logistical problems.

Finback (*Balaenoptera physalus*)

The finback whale is the second largest of the mysticetes, measuring up to 24 m in length, with a mass of more than 7×10^4 kg (80 tons). The signals from this sleek baleen whale have been relatively well studied in the past [2], although its migratory pattern, like that of the other species mentioned in this article, is poorly known. The study of finbacks is also of some provincial interest; Dr. Alan Berman, former Director of Research at NRL, once published a paper in the *Journal of Underwater Acoustics* describing signals recorded on Navy hydrophones from a suspected cetacean species. Unfortunately, like many early investigators, he did not know at that time that those signals were from a finback whale.

The low-frequency acoustic signals from finback whales are characterized by downswept frequency pulses of approximately 1-s duration, 25 to 18 Hz spectral content, an interpulse spacing of 7 to 30 s, and a source level of up to 186 dB re μ pascal at 1 m. A single finback vocalization bout is usually characterized by a relatively constant repetition rate (Fig. 1) with the pattern broken up by discrete rests (e.g. animal is breathing at the surface); the number of pulses between these rests varies considerably. In many instances, several vocalizing finback whales were being recorded on a single beam, which resulted in saturation of the 20 Hz centered band. This type of signal is the infamous "Jeze monster."

A common finback vocalization is the production of doublet pulses spaced 1 to 2 s apart. Additionally, finback signals sometimes contain the odd harmonics of the fundamental pulse frequency; Fig. 2 shows a doublet sequence

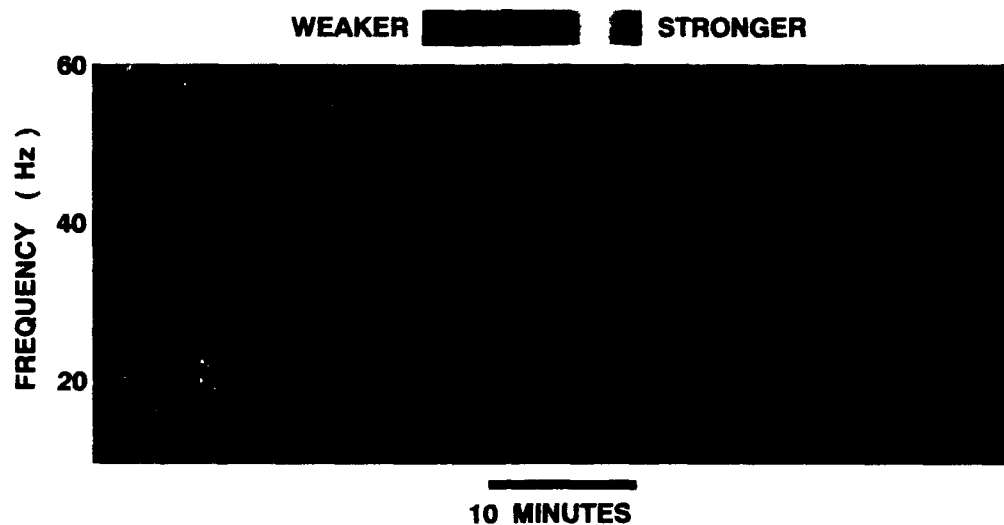


Fig. 1 — Compressed time spectrogram showing the pulse pattern from at least two finback whales. The individual pulses appear as the thin vertical lines centered on 22 Hz. Some of the signal rests represent times when the animal is at the ocean surface breathing.

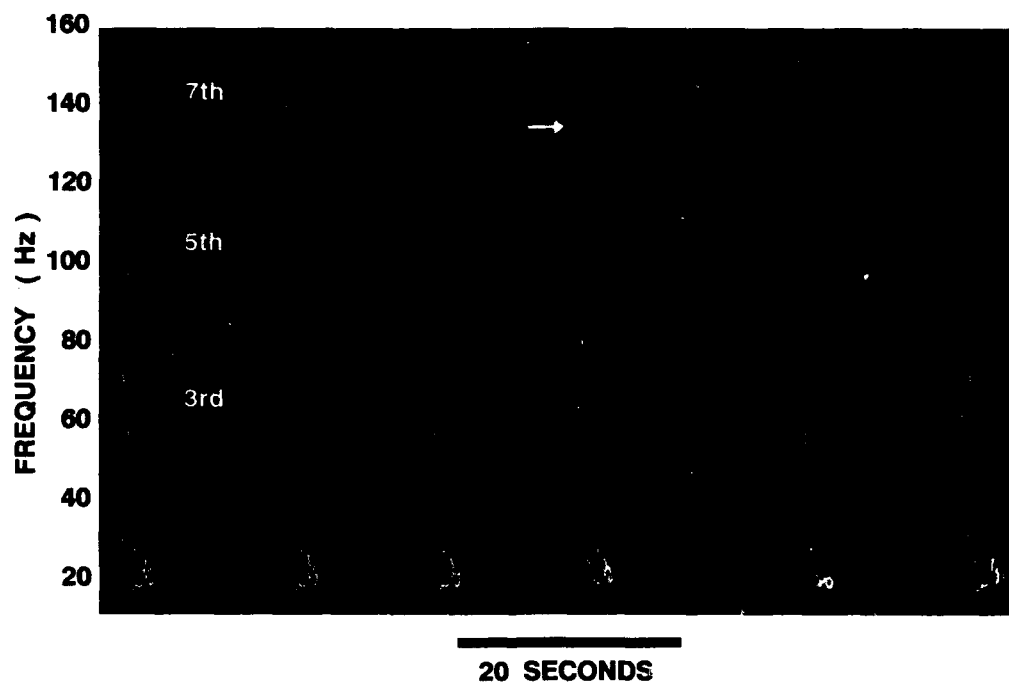


Fig. 2 — Detailed spectrogram showing the fundamental and odd harmonics of a finback vocalization, which is also characterized by the presence of doublet pulses. The third, and sometimes fourth, pulses are most likely multipath arrivals. The arrow points out a signal that is not the true seventh harmonic of the fundamental frequency pulse.

with harmonics. The harmonics are smaller in amplitude than the fundamental frequency component and are only recorded when the animal is close to the receiving array. The presence of only odd harmonics is representative of vibrations within a closed-ended pipe and may be indicative of the mechanism that the finback uses to produce these low-frequency pulses.

Humpback (*Megaptera novaeangliae*)

The humpback whale is clearly the Pavoratti of the mysticetes—they produce long complex sequences of sounds of high tonal quality with a frequency content spanning three orders of magnitude. These sequences, known as songs, are composed of units, phrases, and themes, with the individual songs lasting up to several hours [3]. New Zealand acousticians dubbed these mysterious signals the barnyard chorus, which attests to their range and complexity. Most people are familiar with the haunting melodious song of the humpback whale; it has been popularized by musicians such as Paul Winter and Judy Collins and featured in movies such as *Star Trek IV*. The humpback song is believed to be produced only by the males of this species (i.e., George not Gracie) as an integral part of their mating ritual, which occurs during the winter months in the northern and southern hemispheres.

The spectrogram shown in Fig. 3 displays the low-frequency components (i.e., grunts, groans, and moans) of one of these humpback songs. The repetitive nature of the song is clearly apparent by a simple visual comparison of one sequence to the next, as are subtle variations; this is very representative of the humpback song. When speeded up by a factor of 16, audio playbacks of these sequences resemble bird calls. Unfortunately, much of the humpback vocalization occurs at higher frequencies than the 200 Hz upper limit of our recordings, which limits our ability to fully interpret these songs. To help overcome this problem, we have installed a new UNIX-based data acquisition system at NOPF Dam Neck that is capable of recording full-frequency bandwidth data from all individual hydrophones and beams from a single array. This system will allow us to

gather more information on the humpbacks and will also enable us to perform close-in tracking of the whales.

Minke (*Balaenoptera acutorostrata*)

The minke whale is the second smallest of the mysticetes, measuring approximately 11 m in length, with a mass of a mere 9×10^3 kg (10 tons). The most common vocalization consists of a sequence of more than 100 pulses with a repetition rate of 3 to 5 pulses per second. The individual pulses have a duration of about 100 ms and a center frequency of usually ~ 120 Hz. These signals are audible to human hearing. During the course of this program, Navy OTAs at times were serenaded by nearly continuous vocalization from several minke whales that were being broadcast live by a teenager's boom-box at NOPF Dam Neck. The pulse sequence of the minke whale is well known to the OTAs and is the "A-Train" in the lexicon of the IUSS community.

The initial results of Whales'93 indicate that the basic pulse trains from minke whales are highly repeatable within the context of a single vocalization bout, which can last for several hours. In Fig. 4, a compressed time spectrogram shows a series of minke whale vocalizations that appear as vertical bands in the image. Because the time-integration (FFT length) is much longer than the interpulse spacing, sidebanding about the center frequency of the pulses is generated, resulting in a smearing of the signal across frequency space. Although the apparently extreme frequency content of the minke sequence is partially an artifact, the timing of the sequences is not.

The pulse trains from the minke whales occasionally come in pairs; two such paired sequences are shown by the brackets in Fig. 4. Closer inspection of these types of paired sequences shows that the first pulse train is characterized by an increase in the repetition rate, while the second of the pair is characterized by a complementary decrease. There is also a possibility that there may have been a higher frequency component to these types of sequences that was above the digitizing limits of the data acquisition system.

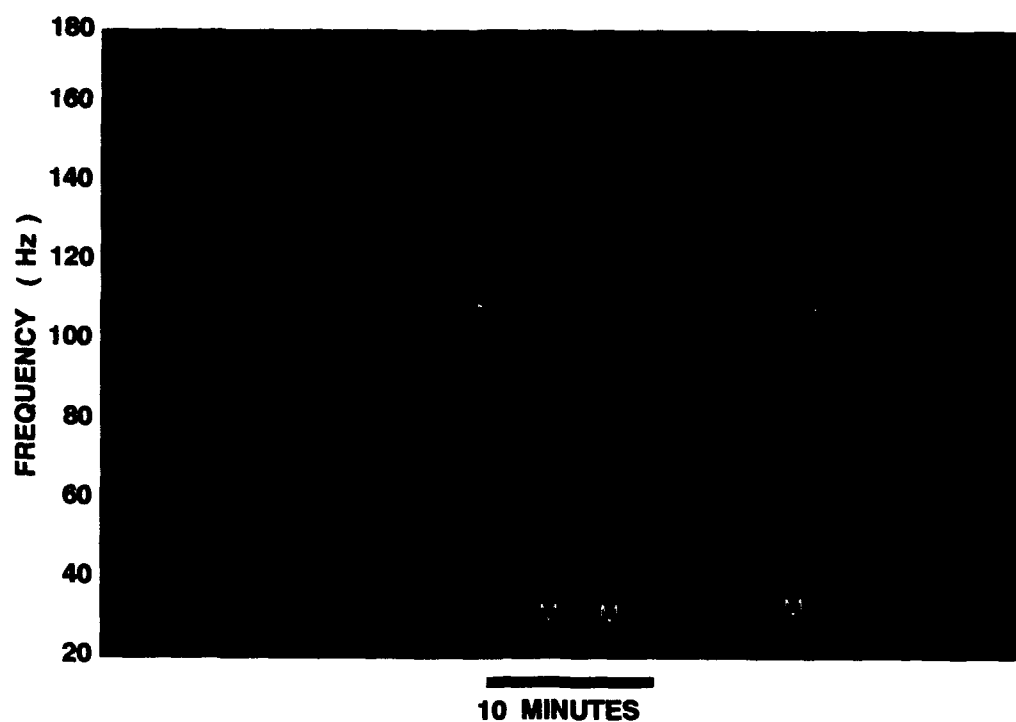


Fig. 3 — Spectrogram displaying four consecutive low-frequency phrases of a humpback song. The individual phrases are similar in nature although subtle differences are also apparent. The Ms indicate some of the vocalizations from a minke whale.

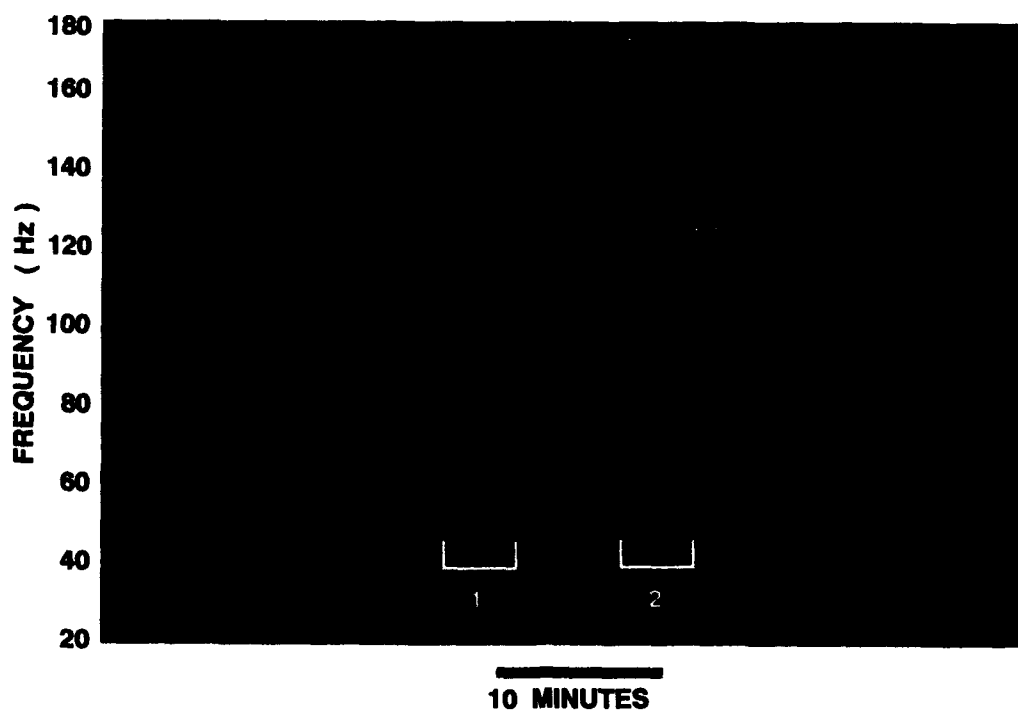


Fig. 4 — Compressed time spectrogram showing a series of paired vocalization sequences from a minke whale. These signals appear as vertical bands whose apparent frequency range is distorted as the result of side-banding.

What is enlightening is that the timing of the pulses from one paired sequence to the next can be extremely similar. For instance, Fig. 5 plots the time-series of two increasing repetition rate pulse trains that occurred 10 min apart. It is clearly evident that the timing of the pulses is identical except for a slight mismatch at the beginning of the sequences. This type of timing capability seems to be intrinsic to the minke (as well as the finback and blue) whales; it strongly suggests that these vocalizations are not random. The requirement for having such an exact biological clock is unknown, although it is hoped that further investigations will lead to a greater insight into the cause and reasons.

Additional types of minke pulse sequences were also observed during Whales'93; preliminary analyses indicate at least three other dominant subclasses. For instance, another fairly typical minke sequence is characterized by the onset of a series of rapid pulses. Approximately half-way through the sequence, the repetition rate abruptly slows down, with an associated change in the individual pulse signature (Fig. 6). Once again, the purpose behind why the animal chooses to vocalize in such a

manner is unknown. In the near future we will attempt to correlate other environmental parameters (e.g., water depth, weather conditions, sea surface temperature, etc.) with the occurrence of the various vocalizations in an attempt to shed some light on this curious behavior.

Blue (*Balaenoptera musculus*)

The blue whale is the largest animal ever to inhabit this planet, with an overall length of 27 m and a mass of 1.3×10^5 kg (150 tons). They are also somewhat mysterious animals who apparently spend much of their time underwater and, as this program has illustrated, in the deep-water regions of the Atlantic. The blue whale produces low-frequency sounds characterized by the presence of a long monochromatic tone followed by a downswep FM component whose total duration is on the order of 20-30 s (Fig. 7). This long-duration signal, which can have a source level of up to 190 dB re μ pascal at 1 m, is one of the most energetic biological sound sources in the oceans. Finally, unlike the finback, the second harmonic is sometimes observed.

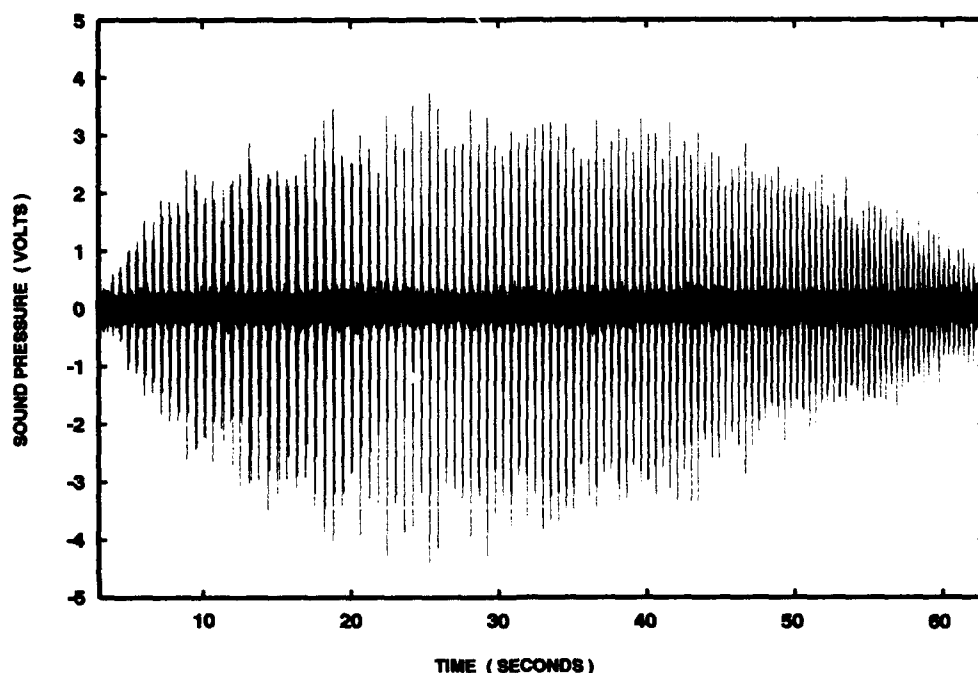


Fig. 5 — Time series plot displaying two sets of pulses (black and red lines) from a minke. These two sequences are separated in time by 10 min and are the first pulse trains bracketed in Fig. 4. The near-reproducibility of the timing of the pulse trains is remarkable.

Time Per Scanline = 5 s



Fig. 6 — Time series plot showing a sudden change in the repetition rate and pulse signature of a minke whale vocalization. Time is continuous from left to right, and from the top to the bottom scanline. Note the complexity of the pulses after this sudden change, which occurs with the last pulse on the upper line.

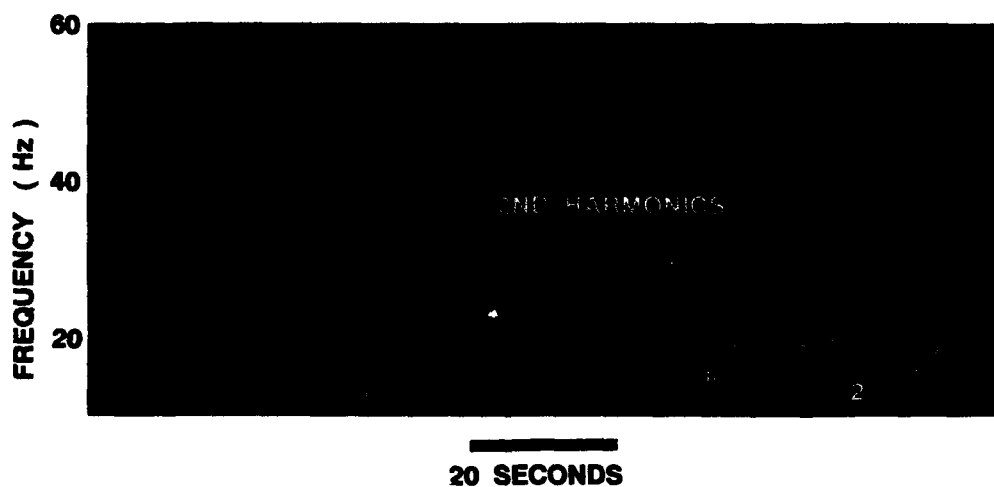


Fig. 7 — High time resolution spectrogram of the signal from a blue whale. The low-frequency vocalization is usually characterized by a tonal followed by a downswept FM component (1). The duration of the FM downswept component can be relatively short (2). Faint signals from the finback whale are also present (F).

A fairly amusing highlight of the Whales'93 program centers on the signal from the blue whale. The shape of the blue whale vocalization as displayed in a lofargram apparently resembled a "comma" in the fertile minds of the OTAs, hence, this name was given for such a signal. Aware that the "commas" had some biological origin, the Navy decided that the true source was snapping shrimp, an animal *several* orders of magnitude smaller than the blue whale. Perhaps driven by this minor embarrassment or more likely, by 23 years of successfully hunting submarines, LT George Gagnon of NOPF Dam Neck tracked an individual blue whale for 43 days over a distance measuring 3200 km. Ol Blue, as this whale was nicknamed, vocalized at a rate of one "comma" every 74 s for most of those 43 days. This constant repetition rate gave Gagnon confidence that he was reacquiring Ol Blue after long gaps of nonvocalization.

SIGNALS FROM EARTHQUAKES

In 1940, Daniel Lineham reported on the observation of a new unreported seismic signal. This signal originated from earthquakes along the western Antilles that were recorded on seismographs of the Weston Observatory near Boston. Since these signals arrived after the primary (*P*, or compressional) and the secondary (*S*, or shear) waves that travel through the solid earth, he aptly named his new discovery the Tertiary or T-phase. The origin of the T-phase remained a mystery until the late 1940s when Ivan Tolstoy and Maurice Ewing of Columbia University realized that the T-phase represented seismic signals from earthquakes in which the propagating path was primarily through the oceans [6]; this proposal was a natural extension of their pioneering work in underwater acoustics. Further work by Tolstoy, Ewing, and Frank Press eventually convinced an initially skeptical seismological community unfamiliar with underwater acoustic propagation.

It has been known since the 1950s that a single underwater hydrophone detects at least 10 times more earthquakes than a comparably situated landbased seismometer. Hence, the utility of T-phase research is in determining the tempo-

ral and spatial distribution of low-magnitude earthquakes in an oceanic region. This improvement in detection threshold is critical when monitoring for the onset of active volcanism along the Mid-Atlantic Ridge. Terrestrial analogs show that earthquakes associated with volcanic activity are characterized by the occurrence of large numbers of low-magnitude events and the general absence of large-magnitude earthquakes.

Long-range-propagating T-phases are characterized by the presence of broadband signals with a frequency content usually below 25 Hz. This low-frequency content is a function of the attenuation of higher frequencies by propagation through the solid earth and by bottom-interacting acoustic propagation near the radiation center where this seismic energy is converted to underwater acoustic energy. Occasionally, shallow focused earthquakes that occur in an optimal geological setting will excite T-phases with frequency contents over 100 Hz (Fig. 8). The duration of the T-phase can at times be used to estimate the earthquake source magnitude, with durations of several minutes fairly common.

SUMMARY

The various signals that were presented in this article are but a small portion of those observed during Whales'93. They do illustrate, however, the diverse nature of the low-frequency sounds of the humpback, minke, blue, and finback whales. And as another migration season begins, we are left with numerous questions. Do the vocalizations change from year to year? Are there differences in the vocalizations from varying areas of the Atlantic? What function do these sounds serve? To help resolve these issues, NRI is currently installing additional recording systems at other Naval Facilities in the Atlantic. This will greatly increase our knowledge base and will hopefully provide some insight for solving these questions.

Finally, the Whales'93 program unequivocally demonstrated that the concept of dual usage of DoD assets for environmental research can be successfully implemented and achieved. Utilization of hardware such as the SOSUS

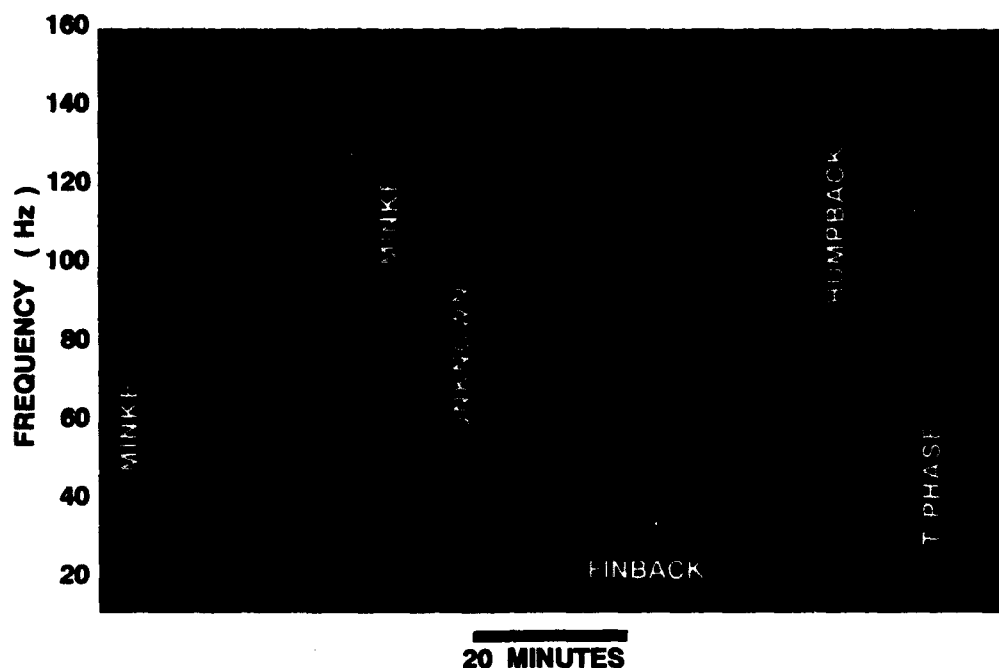


Fig. 8 — Compressed time spectrogram showing numerous T-phases from underwater earthquakes. Numerous signals from finback, humpbacks, minkes, as well as an unknown source, are also prevalent.

arrays was obviously a critical factor in this success. But what cannot be understated is the *scientific* contribution by the small cadre of IUSS personnel who provided invaluable guidance and assistance to outside investigators. Those of us who were fortunate enough to participate in the Whales'93 program look forward to another whale migration season, and eagerly await the return of Ol Blue.

ACKNOWLEDGMENTS

I especially thank Dr. Chris Clark, LCDR-SEL G. Gagnon, LCDR Lysa Olsen, Dr. Dennis Conlon, and CDR Dale Liechty for their support and immeasurable help throughout this program. CAPT John Parrish (retired) and CAPT Kirk Evans provided the visionary guidance that led to Whales'93. Special appreciation is given to all the dedicated Naval personnel of IUSS.

REFERENCES

1. C.W. Clark, "Acoustic Behavior of Mysticete Whales," in *Sensory Abilities of Cetaceans*, J. Thomas and R. Kastelein, eds. (Plenum Press, New York, 1990), pp. 571-583.
2. W.A. Watkins, P. Tyack, and K.E. Moore, "The 20-Hz Signals of Finback Whales (*Balaenoptera physalus*)," *J. Acoust. Soc. Am.* **82**, 1901 (1987).
3. R.S. Payne and S. McVay, "Songs of Humpback Whales," *Science* **173**, 585 (1971).
4. H.E. Winn and P.J. Perkins, "Distributions and Sounds of the Minke Whale, With a Review of Mysticete Sounds," *Cetology* **19**, 1 (1976).
5. P.L. Edds, "Vocalization of the Blue Whale, *Balaenoptera musculus*, in the St. Lawrence River," *J. Mamm.* **63**, 345 (1982).
6. I. Tolstoy, and M. Ewing, "The T-phase of Shallow-focus Earthquakes," *Bull. Seism. Soc. Am.* **40**, 25 (1950).

THE AUTHOR



Clyde E. Nishimura received degrees in geophysics from the University of Hawaii at Manoa (B.S. 1978) and Brown University (Ph.D. 1986) where he did research on plate tectonics and solid-earth seismology. After postdoctoral work at Brown, he came to NRL in 1988 as an NRC postdoctoral fellow where he concentrated on multi-beam bathymetric and side-

scan sonar imaging techniques as well as micro-earthquake studies. In 1990, he returned to the University of Hawaii as an assistant geophysicist in the School of Ocean and Earth Science and Technology where he was in charge of data processing for the SeaMARC II operations. He returned to NRL's Marine Physics Branch as a permanent employee in 1991 where he has conducted research on seafloor mapping techniques, T-phases, and cetacean acoustics. Dr. Nishimura is a member of Sigma Xi and the American Geophysical Union.

ACOUSTICS

- 105 **High-Resolution Underwater Acoustic Imaging**
Behzad Kamgar-Bursi
- 108 **Cylindrical Wavenumber Calibration Array**
Little D. Luker and Arnie L. Van Buren
- 111 **Direct Measurement of Edge Diffraction from Acoustic Panels of Decoupling Materials**
Jean C. Piquette
- 114 **Structural Acoustics of Nearly Periodic Structures**
Douglas M. Photiadis
- 118 **Acoustic Reverberation at Selected Sites in the Mid-Atlantic Ridge Region**
Jerald W. Caruthers, J. Robert Fricke, and Ralph A. Stephen
- 122 **Overcoming Chaos**
Michael D. Collins and William A. Kuperman

High-Resolution Underwater Acoustic Imaging

B. Kamgar-Parsi
Information Technology Division

The capability to image underwater objects with high resolution, such that small features of about 1 cm can be resolved, is important in many Navy and commercial applications. These applications include identifying objects, manipulating valves, and inspecting pipes for cracks or barnacle build up. Cameras and lasers have high resolution but fail at centimeter ranges in turbid water—a common condition in coastal waters or in waters disturbed by people.

Acoustic signals, however, propagate in turbid water with little degradation, thus sonars are the only real alternative for imaging in such conditions. In joint efforts, University of Washington Applied Physics Laboratory, Naval Explosive Ordnance Disposal Technology Center (NEODTC), and NRL have developed and tested underwater systems for three-dimensional (3-D) imaging from distances of several meters. The systems use a lens to focus incoming sound waves, thereby eliminating the beamforming electronics used in traditional forward-looking sonars. Hence, they are relatively compact and light. The lens technology is not new [1], but recent advances in desktop computing and visualization now make it possible to process and display the large amount of data in real time. We describe two of the prototypes and present examples of images reconstructed from data taken from stationary and moving platforms.

The Acoustic Eye: An innovative sensor that operates in a manner analogous to the human eye is the acoustic eye, it consists of a thin, hemispherical shell and a retina containing small ceramic transducers [2]. A specially chosen fluid focuses incoming acoustic waves onto the retina. The current fluid maintains focus over a 15°C temperature range. The transmission time delay gives target range; the location of the retinal element receiving the acoustic return gives bearing and elevation. This prototype is a 300 kHz sonar whose retina contains an 8×16 array of transducers. Each

transducer forms a conical beam with 1.5° resolution between the -3 dB points. The small number of transducers is due to sensor technology limitations. Efforts are underway to replace piezoelectric ceramic transducers with new transducer technologies that will populate a retina with more elements that have narrower beam patterns.

This system has a resolution of 25 cm at a range of 10 m; thus, a single scan produces a sparse sample that cannot resolve centimeter-size features. To obtain a higher resolution image, overlapping samples are needed. Hence, we mount the eye on a platform and slowly pass it over an object while it pings and acquires data. Typically, one ping-cycle of the eye is 1 s long. In a tow tank experiment, we passed the eye over a vehicle called Pluto (Fig. 1) along four different directions. Figure 2 shows the images obtained from the four single passes, as well as the passes combined.

The Acoustic Lens: In this imaging sonar, beam-forming is done with a bi-concave solid lens made of crystal polystyrene [3]. The lens is lighter than the acoustic eye, and maintains focus over a wider temperature range. The drawback is the off-axis aberration, which is nonexistent in the eye. At the focal point is a single 3 MHz transducer with a 0.15° conical beam. Although resolution increases by increasing the frequency, range becomes more limited because of greater sound attenuation. To obtain an image, the system mechanically scans and interrogates the object at regular intervals (typically 0.5 cm) from left to right and from top to bottom. This scanning strategy requires a few hours to produce an image, but it

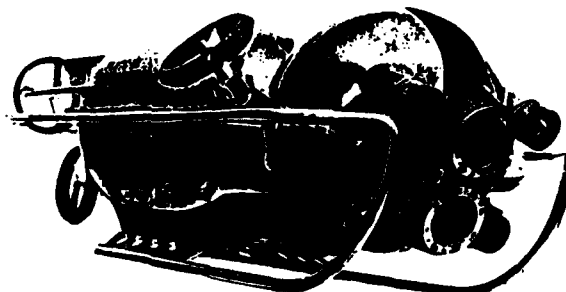
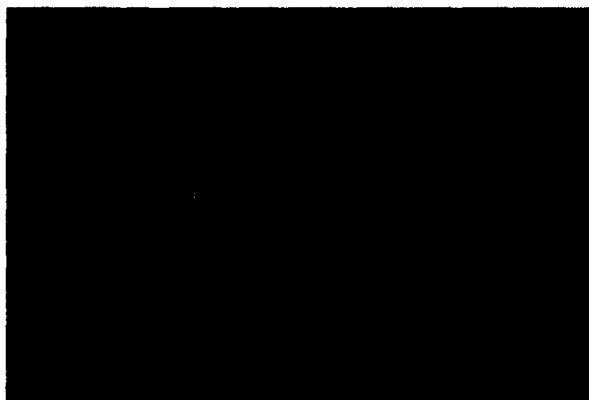


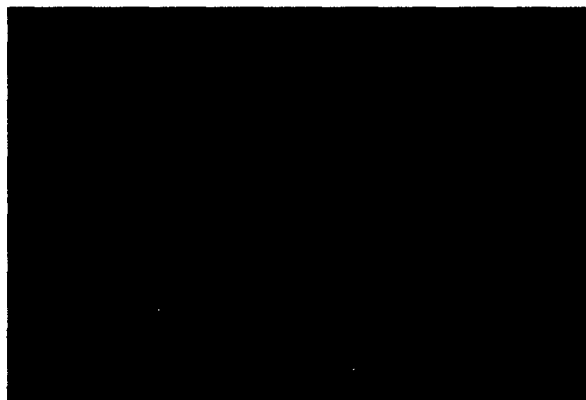
Fig. 1 — Pluto, a 1.6-m-long remotely operated vehicle



(a) Four different single passes



(b) The four passes combined without registration



(c) The four passes combined after registration; note that even such details as the valve on the side and the strobe lights and cameras in the head begin to emerge as bumps in the right locations. Also note that sensor resolution is about half the size of Pluto's head.

Fig. 2 — Volume rendered reconstructions of Pluto from data taken by the acoustic eye mounted on a moving platform. The closest viewing distance was 8 m. Images are rotated to correspond to the same pose as in Fig. 1.

mimics an ideal lens with a large focal plane populated with some 100×100 transducers, obviously with no aberration and no cross talk among the elements. To speed up image acquisition, mechanical scanning must be replaced by a focal plane populated with many transducers. However, this will result in significant off-axis image distortions. Techniques for reducing aberrations through compound lens design, as in sophisticated cameras, together with innovative scanning strategies are under investigation.

Experiment were conducted in a test tank, where objects with small bolt patterns and ribs, similar to those shown in Fig. 3, were imaged from a distance of about 2 m under various levels of turbidity. Results show that the images are not degraded by the mud and silt commonly found in shallow water. Some degradation occurs at high levels of suspended sand. Figure 4 is a typical image produced by the acoustic lens.

Scene Reconstruction: Data acquired by the sensors are the acoustic backscatter energy from within volume elements, or range bins, shaped like a sliced cone. The range bins vary in size and are irregularly positioned in space. To reconstruct the scene, we represent the space with a regular grid of small cubic volume elements, or voxels, and estimate the backscatter from each voxel. A high voxel value indicates



Fig. 3 — Photograph of an object used in underwater imaging tests

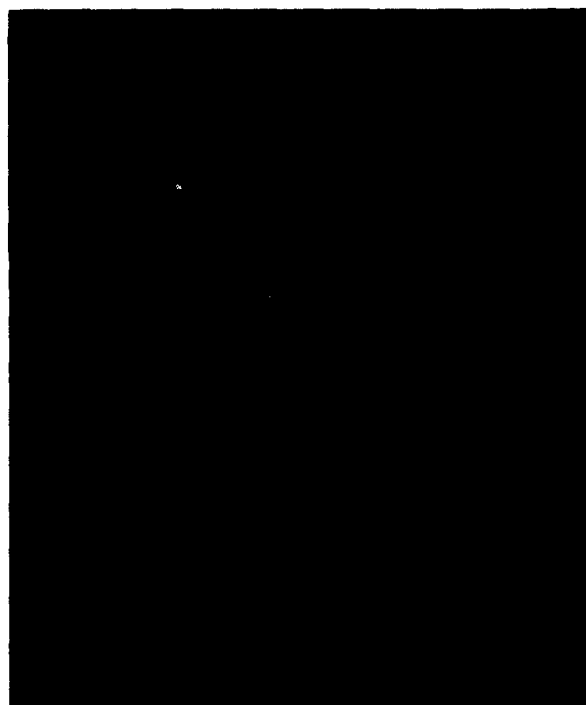


Fig. 4 — Reconstruction of the object shown in Fig. 3 from data taken by the acoustic lens on a stationary platform. View direction was normal to the plane of the bolt pattern. The isolated spot to the right is a bolt head (not visible in the photograph) on the side of the cylinder. The noisy appearance of the flat plain incline is due to the unfavorable look angle resulting in weak backscatter and, therefore, less certain surface detection.

the presence of a surface. This is done in two stages. First, since each range bin intersects several voxels its backscatter must be distributed among them. Second, a voxel is often ensounded by several beams, resulting in different estimates that must be combined to yield a single value. Algorithms for distributing returns involve modeling the beam patterns and computing range bin intersections with voxels. This is conceptually straightforward, but it can be computationally intensive. Algorithms for combining estimates are nontrivial because we have to deal with occlusions, partial illuminations, and differences in angle of incidence.

Having obtained a 3-D grey level image, we must find a way to see the object of interest through the fog of ambient noise. How best to enhance and visualize the object is also a topic of ongoing investigation. When data are high resolution and relatively clean, we first apply a

surface detection algorithm to identify the surface voxels; we then tile the surface with voxel-sized polygons, which performs a sub-voxel interpolation; finally, we render the surface. Figure 4 is generated through this process [3]. Note that various details, such as the bolt pattern and the small circular feature, can be clearly seen. In cases where the resolution is not sufficiently high and the image is further blurred by sensor motion, surface detection often fails to produce the best possible image. Therefore, we filter the scene and use volume rendering to visualize the object. Pluto's images are generated by this technique [2].

Image resolution may be further enhanced by combining several different images of the same scene. But images must first be registered. Figure 2(b), for example, is the result of combining the four passes over Pluto by using only the recorded navigational data. We have developed algorithms, based on moment matching, that perform image registration with enough accuracy to significantly enhance the resolution. Figure 2(c) is the result of registering and combining the four passes. These registration techniques need to be further developed; in practical situations the imaging system, held by a diver or mounted on a small vehicle, is subject to uncontrolled motions. Image registration for motion compensation may become indispensable in obtaining sharp, high-resolution images.

The underwater acoustic images taken from stationary and moving platforms show the remarkable degree of detail that can be currently obtained. Improvements in transducer technology, lens design, and scanning techniques, together with further algorithm developments for processing and visualizing the backscatter data, are expected to produce even higher resolution 3-D images while reducing image acquisition time.

Acknowledgments: The imaging system prototypes were designed and fabricated by Ed Belcher of University of Washington, Don Folds of ARINC Research Corp., and Bruce Johnson and Debra Scroggins of NEODTC. Larry Rosenblum and Behrooz Kamgar-Parsi of

NRL have helped with visualization and algorithm development.

[Sponsored by ONR]

References

1. D.L. Folds, "Status of Ultrasonic Lens Development," in *Underwater Acoustics and Signal Processing*, Proc. NATO Advanced Study Institute, Copenhagen, Aug. 1980, (D. Reidel Publishing, Boston, 1981), pp. 263-279.
2. L.J. Rosenblum and B. Kamgar-Parsi, "3D Reconstruction of Small Underwater Objects Using High-resolution Sonar Data," Proc. IEEE AUV '92 Conf., Washington, DC, June 1992, pp. 228-235.
3. B. Johnson, D. Scroggins, D. Folds, B. Kamgar-Parsi, and E. Belcher, "3D Acoustic Imaging with a Thin Lens," Proc. Oceans '93, Victoria, BC, Oct. 1993, to appear. ■

Cylindrical Wavenumber Calibration Array

L.D. Luker and A.L. Van Buren
Underwater Sound Reference Detachment

There has been considerable interest in recent years in the acoustic effects of the turbulent boundary layer (TBL) produced by the motion of a vehicle in water. The Navy has specific concerns about interference by the pressure field in the TBL with the proper operation of transducers used in towed sonar arrays. The "flow noise" produced by the TBL is generally characterized by pressure fluctuations that are transported in the flow direction at a speed somewhat less than the free-stream velocity. Since these fluctuations are transported at speeds less than the sound speed in water, they have nonacoustic wavenumbers (i.e., wavenumbers higher than acoustic wavenumbers at the same frequency in water) and are, therefore, evanescent.

To gain better understanding of the effects of flow noise, it would be useful to be able to calibrate the response of a sonar array as a function of the wavenumber of the excitation for frequencies of interest. This could be achieved if a device existed that could generate a pressure field consisting of essentially a single non-acoustic-wavenumber component. The structure being analyzed could then be placed in the pressure field and its behavior monitored for different wavenumbers. NRL has constructed and evaluated a prototype Cylindrical Wavenumber Calibrator (CWC) to generate nonacoustic-wavenumber pressure fields in the water within the calibrator (Fig. 5). It can therefore be used to simulate the effects of flow noise on a towed array placed in the water.

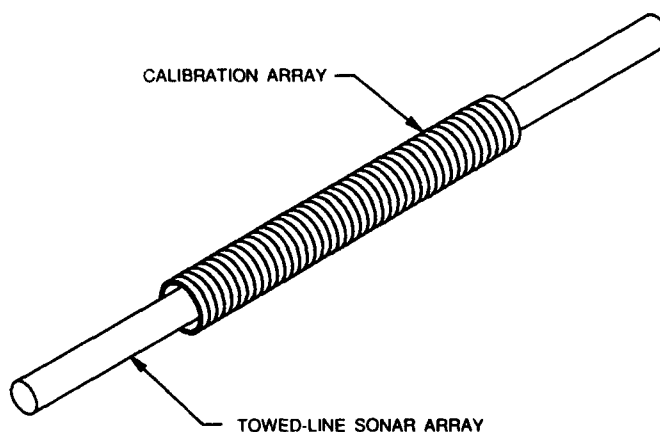
Prototype CWC: The prototype CWC was constructed by using a piezoelectric polyvinylidene fluoride (PVDF) tube for the active elements. PVDF is a fluorocarbon polymer that can be treated to produce a relatively strong piezoelectric effect. The CWC consists of (from the inside to the outside, see Fig. 6): a urethane coating; an inner (ground) electrode; a PVDF tube; and the outer electrodes. This arrangement resulted in a CWC with 40 active bands that could be controlled with independent electrical drives to each band. The prototype has a length of 25 cm and an inner diameter of 3 cm. PVDF was chosen as the active material partially because it allowed the construction of a CWC with relatively flexible walls. Theoretical analysis showed that a CWC with flexible walls could

produce nonacoustic pressure fields within the CWC with more uniformity in the radial direction (i.e., less dependence on the radial position) than a CWC with stiffer walls [1].

Determination of the Band Drives: Operation of the CWC requires the determination of appropriate sets of electrical band drives that will produce acceptable nonacoustic-wavenumber fields within the CWC. The method used is to first determine the electroacoustic transfer matrix for the system, and then use the inverse transfer matrix to calculate a set of drives that will produce a desired pressure field [2]. The desired field is specified in two regions. The first region is a "window" in the central portion of the CWC where a pressure field of uniform amplitude and the desired nonacoustic wavenumber is specified. The second region is the remainder of the inside of the CWC where a zero-amplitude field is specified. A transfer matrix can be determined either by measurements or by using a mathematical model of the CWC. Both methods have been explored and the results used to create nonacoustic-wavenumber pressure fields within the prototype. A mathematical model is also used to compute the predicted pressure inside the CWC by using a computed set of band drives.

Results: The prototype has been used to produce pressure fields with various nonacoustic wavenumbers at different frequencies. Figure 7 shows an example of the pressure field within the CWC. Here a 71-m/s evanescent pressure

Fig. 5. — Calibration of a towed-line sonar array using a CWC array to generate nonacoustic-wavenumber pressure fields within the CWC



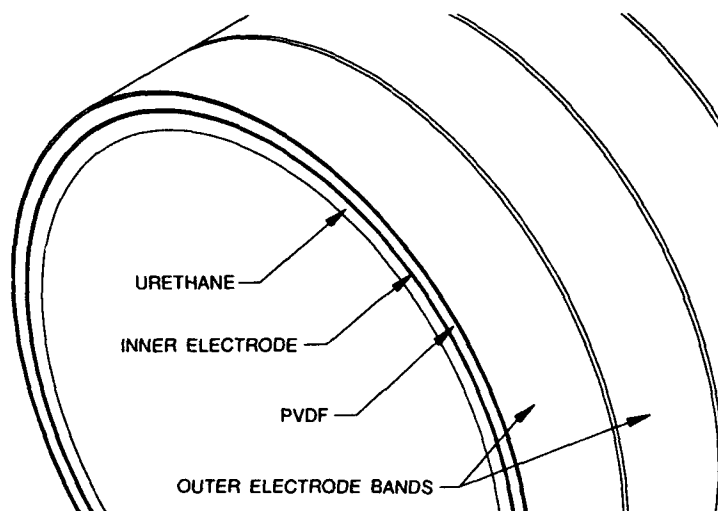


Fig. 6 — Construction details of the prototype PVDF CWC

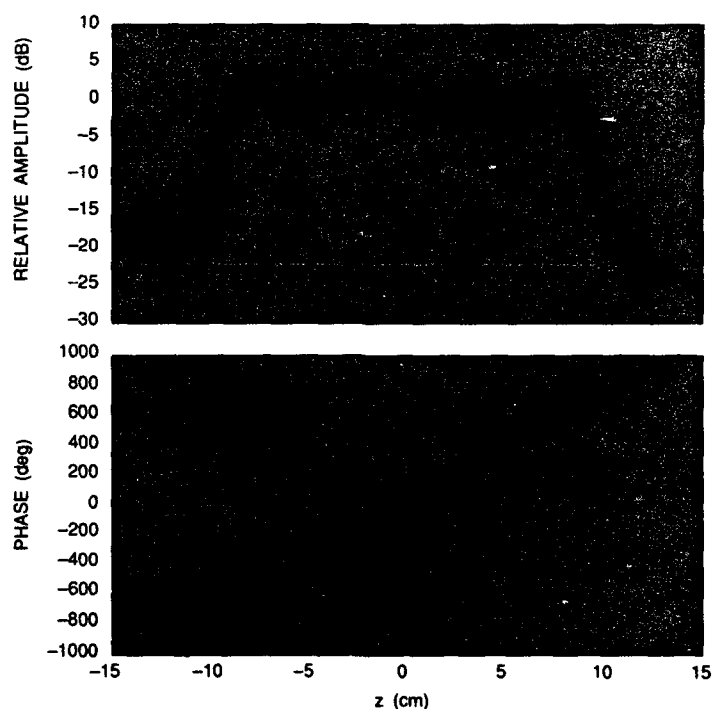


Fig. 7 — Pressures within the CWC for a 71-m/s evanescent pressure field at 1600 Hz with drives computed by using the measured transfer matrix and a window running from -8.9 to $+8.9$ cm. Predicted amplitude and phase are shown by thick lines; thin line at 0 dB indicates window extent; shaded dots indicate actual pressures measured along the centerline of the CWC

field was created at 1600 Hz with drives computed by using the measured transfer matrix and a window running from -8.9 to $+8.9$ cm. The upper graph plots the amplitude; the lower graph plots the phase in degrees. The predicted amplitude and phase are shown with the thick lines. The thin line at 0 dB indicates the window extent. The shaded dots indicate the actual pressures measured along the centerline of the CWC. The theoretical and experimental results obtained with the prototype show that relatively uniform nonacoustic-wavenumber pressure fields can be created within the CWC.

[Sponsored by ONR]

References

1. L.D. Luker, "Investigation of a Cylindrical Nonacoustic Wavenumber Calibration Array," NRL Memorandum Report 7385 (1993).
2. L.D. Luker, J.F. Zalesak, C.K. Brown, and R.E. Scott, Jr., "Automated Digital Benchtop Calibration System for Hydrophone Arrays," *J. Acoust. Soc. Am.* **73**, 1212 (1983). ■

Direct Measurement of Edge Diffraction from Acoustic Panels of Decoupling Materials

J.C. Piquette

Underwater Sound Reference Detachment

Decoupling materials are used extensively in underwater applications. An example is the acoustical isolation of a hull-mounted detector from the interfering influence of sound radiated by hull vibrations. Decoupling materials are typically characterized by very low sound speeds relative to the sound speed of water (and can even have a sound speed less than one half that of air). Such very low sound speeds can make it impossible to separate by gating the wave directly transmitted through a sample

panel from the wave diffracted around the sample edge, despite the greater geometric path length travelled by the diffracted wave. Hence, it is often impossible to avoid edge-diffraction contamination of measurements obtained to evaluate sample performance. Heretofore, the absolute level of this contamination has been unknown, and its level could only be roughly inferred by approximate methods.

Experimental Difficulties: Direct measurements of edge diffraction arising in panel tests of decoupling materials have not been reported previously because of the great difficulties that arise in attempting to obtain such measurements. Decoupling materials are often described as "pressure-release" materials, i.e., materials that exhibit a zero-pressure condition over their boundary surfaces. This condition theoretically would not permit sound to be directly transmitted. Materials that approximately exhibit the pressure-release property are typically rather soft (and can deform when submerged). When increased intrinsic rigidity is engineered into these materials to prevent deformation under hydrostatic pressure, the resulting material invariably loses some of its pressure-release property. A transmitted wave of significant amplitude will then pass through the material. Only the measurement of the amplitude of this directly transmitted wave is generally desired in a panel test of a decoupling material; the edge-diffraction contribution represents a contamination of the desired measurement. On the other hand, any attempt to directly measure the edge-diffracted wave is also frustrated by the virtually simultaneous presence of the transmitted wave. In this case, the transmitted wave must be viewed as a contamination.

The difficulty in directly observing the edge-diffracted wave was overcome by fabricating a special "airbox" sample. This sample is literally a "box of air," fabricated with thin polycarbonate walls. (Polycarbonate is a relatively rigid material that nonetheless exhibits a reasonably good impedance match with water, thus providing little disturbance of the desired acoustic field.) The wave directly transmitted

through a layer of air of the desired thickness (with water on either side) is theoretically expected to have an amplitude typically 60 dB below that of the interrogating wave. Hence, direct observation of the edge-diffraction component is much more straightforward when using the airbox than it would be when using a sample fabricated from a typical pressure-release material.

Measurement Setup: Special rigging apparatus was designed and fabricated to permit acoustic measurements to be obtained from the airbox (Fig. 8). This special rigging also permits acoustic measurements to be carried out on small samples, as well as on large samples, of decoupling materials. The rigging design allows the samples to be submerged in a lake test facility in a horizontal orientation. This reduces the sample deformation that would occur if the

samples were submerged in the standard vertical orientation.

It is important to note that the acoustical sources used in the measurements were driven in the transient-suppressed mode [1]. This was found to be necessary because, despite the rather large rigging, the use of ordinary gated-sine drives was found to produce measured waveforms that failed to reach steady state prior to the reception of rigging reflections.

Experimental Measurements: Figure 9 shows edgewave levels for the 1 to 21 kHz frequency interval. (The dB units of the vertical axis are referenced to the incident-wave amplitude at the sample surface located closest to the acoustic source.) The acoustic source is either an F56 or an F43 [2], a standard sound source used in panel tests conducted at the Underwater Sound Reference Detachment. The dashed-line

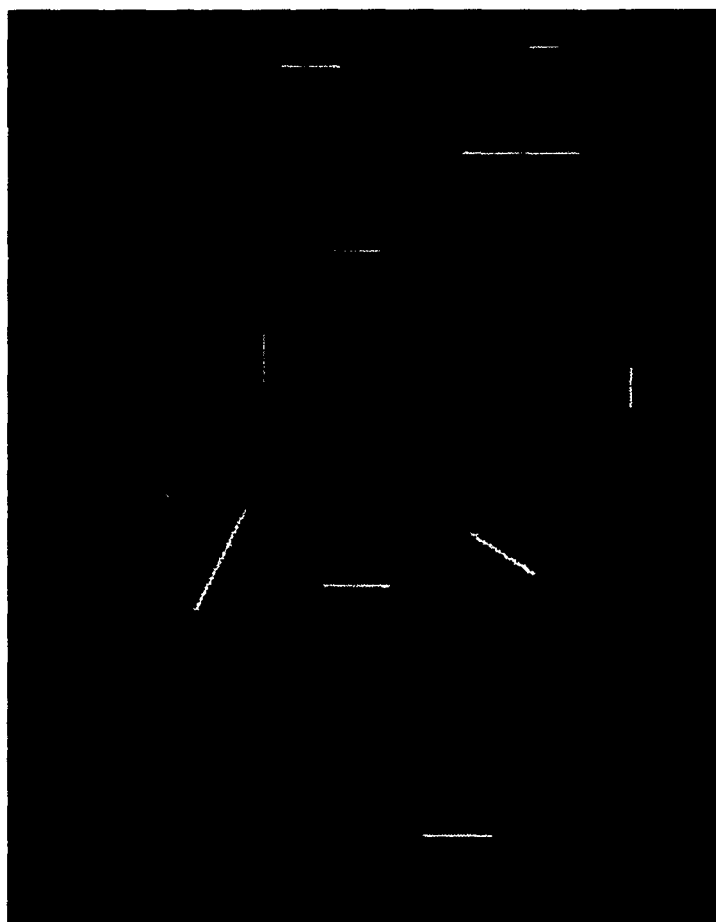


Fig. 8 — Airbox sample and special test rig, depicted in the horizontal orientation. Outside dimensions of the main rigging frame are 244 × 244 cm.

curve represents results obtained with the hydrophone located at a 5-cm offset behind the airbox; the solid-line curve represents results for a 20-cm offset. As expected, the edgewave level is of generally greater amplitude for the greater hydrophone offset.

To demonstrate the validity of the measurements presented in Fig. 9, additional measure-

ments on samples fabricated from a commercially available closed-cell foam material were made. This material, MicrocellTM, is manufactured by Sentinel Products of Hyannis, Massachusetts. Figure 10 shows insertion-loss levels for both a large ($229 \times 229 \times 2.54$ cm) Microcell sample (dashed line) and for a small ($76.2 \times 76.2 \times 2.54$ cm) Microcell sample

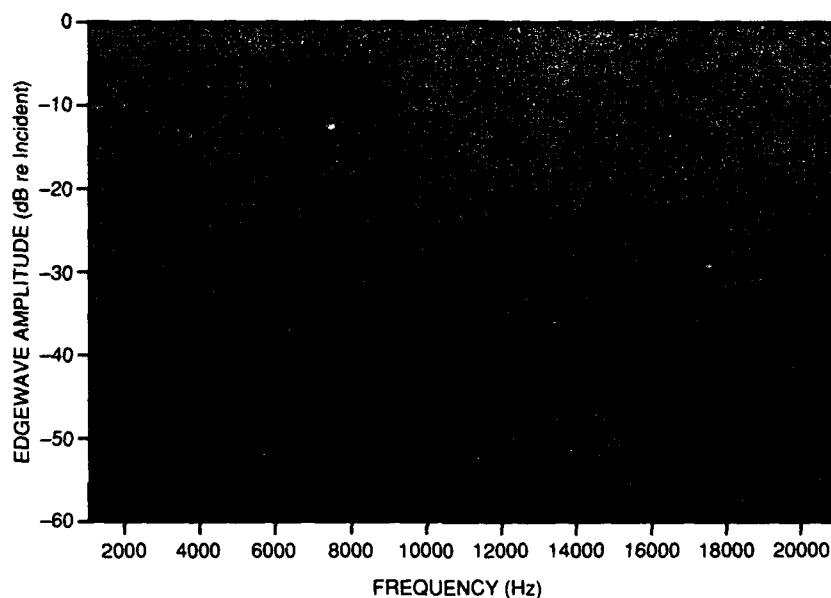


Fig. 9 — Edge diffraction levels as measured from the airbox sample

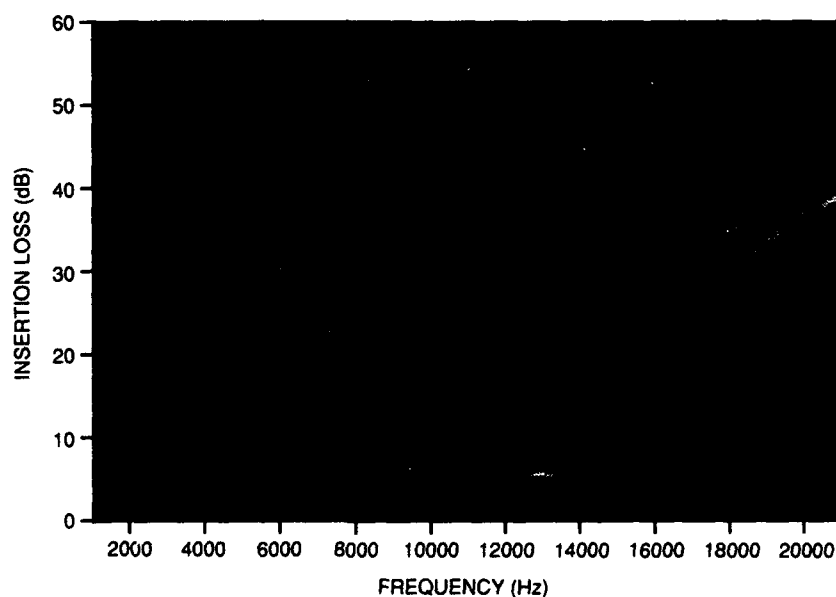


Fig. 10 — Insertion loss for a large (dashed line) and small (solid line) sample of Microcell compared with a "synthetic" insertion loss deduced by summing the complex large-sample measurements and airbox measurements (dot-dashed line)

(solid line). (Insertion loss is defined to be the amplitude in dB of the waveform measured in the transmission region of a test sample. The dB units are referenced to the amplitude of the interrogating wave when the sample is absent.) The solid- and dashed-line curves differ primarily because an edge-diffracted wave is present in the small-sample measurement but is absent in the large-sample measurement. (The edge-diffracted wave in the large-sample measurement, as well as rigging and facility surface and bottom echoes in all the measurements, are avoided by judicious placement of the data-acquisition gate.)

The dot-dashed curve of Fig. 10 represents the results of calculating a "synthetic" insertion loss for the small Microcell sample by combining airbox measurements with large-sample measurements. By summing the complex amplitudes of these two measurements, the two wavefields that are simultaneously present in a small-sample measurement are simulated. These two wavefields are the directly transmitted wave (this is all that is present in the large-sample measurement), and the edge-diffracted wave (this is all that is present in the airbox measurement). The reasonably close agreement of the solid and dot-dashed curves of Fig. 10 shows the validity of using the airbox to directly observe the edge-diffraction component that arises in panel tests of decoupling materials. The differences between the solid- and dashed-line curves of Fig. 10 illustrate the magnitudes of the errors that can occur in attempting to characterize the insertion loss of a decoupling material by carrying out tests on a relatively small sample. Such small samples are generally required to accommodate panel tests in facilities capable of simulating environmental conditions of temperature and pressure at great ocean depths.

[Sponsored by ONR]

References

1. J.C. Piquette, "Electroacoustic Transducer Transient Suppression," *1993 NRL Review*, pp. 97-99.
2. I.D. Groves, "High Pressure Piezoelectric Ceramic Transducer," NRL Memorandum Report 6895 (Feb. 1969). ■

Structural Acoustics of Nearly Periodic Structures

D.M. Photiadis
Acoustics Division

Introduction: Interesting phenomena have been observed in the acoustic behavior of thin elastic structures with nearly periodic arrays of discontinuities. The framed hull of a submarine is one such structure, and its acoustic behavior has great significance for Navy antisubmarine warfare (ASW) and silencing programs. This article describes some recently discovered phenomena—acoustic scattering from flexural Bloch or Floquet waves and Anderson localization of structure-borne vibration.

The Role of Surface Waves in the Acoustic Signature: Surface vibration of an elastic structure generates acoustic waves in a surrounding fluid through the outward displacement of the structure. Various surface vibrational modes are known to manifest themselves distinctly in the acoustic cross-section because of enhanced coupling to plane waves when phase matching occurs: An increased signal is detected when the trace wave speed $c/\sin(\theta)$ of an incoming (outgoing) acoustic plane wave at angle θ relative to the surface normal matches the phase wave speed of a surface mode. This characteristic signature can be observed only for supersonic surface waves, those with phase speeds greater than the sound speed of the ambient fluid. The far field pattern resulting from such surface wave coupling as a function of frequency and angle is very simple for a non-dispersive wave. It is merely an enhanced cross-section at a fixed angle. However, for a dispersive wave it can trace out a complex locus in frequency-angle space. The dispersion relations

of the vibrational modes are thus of primary importance in developing an understanding of the acoustic signatures of elastic structures.

Elastic Modes of Uniform Thin Shells:

Vibrational energy propagates along a uniform thin plate or cylindrical shell in three distinct modes for frequencies such that the wavelengths of the elastic waves are greater than about twice the thickness of the shell. Two of the modes involve primarily in-plane motion, the quasi-longitudinal and quasi-shear waves. The third mode, the quasiflexural wave, consists primarily of out-of-plane motion. Typically, the same vibrational modes exist when immersed in a fluid, albeit somewhat slowed and damped by the fluid. In the frequency band of primary interest here, the midfrequency range, the membrane waves are supersonic while the flexural wave is subsonic. Hence, while the flexural wave is naturally well coupled to acoustic waves because its motion is primarily outward and into the fluid, it shows no distinctive features in the cross section because its phase speed is subsonic. Only the fast membrane waves, whose coupling to the fluid is generally somewhat weak because the motion is mostly in-plane, show any characteristic features in the cross-section of a uniform thin plate or cylindrical shell.

Effects of Periodic Discontinuities on the Dispersion Relations: The presence of an array of discontinuities with periodicity a on a structure can strongly modify the dispersion relations of the surface waves because of multiple scattering effects. The natural waves of the system will now be Floquet or Bloch wave packets of the form $\psi_k(x) = \exp(ikx)U(x)$. The periodic function $U(x)$ gives the mode shape in a single bay of the system, and the complex exponential gives a slow phase variation from bay to bay. To a great extent the "Bloch" wavenumber k may be treated as the usual wavenumber of traveling waves: One may interpret ω/k as the phase speed and $\partial\omega/\partial k$ as the group speed of the wave packet.

Scattering From Flexural Bloch Waves: The dispersion relations for the Bloch wave-

number k are quite different from the dispersion relations for the free waves. When compared to the dispersion curves of a corresponding free wave, the dispersion curves for the Bloch wave are repeatedly folded and develop gaps at the edges of the Brillouin zones, $k = \pm n\pi/a$. The most dramatic impact of this phenomena is the appearance of a new sequence of high-frequency, supersonic branches of each free wave of the uniform system, including the previously subsonic flexural wave. This enables the flexural wave to phase match to an acoustic plane wave and generate a characteristic signature in the acoustic cross-section. Figure 11 shows the measured backscattering cross-section from otherwise identical ribbed and unribbed cylindrical shells as a function of frequency and angle. The appearance of strong new features resulting from the ribs is striking. Overlaid on the figure are theoretical dispersion curves for the flexural Bloch wavenumber. The impressive qualitative agreement between experiment and theory provides strong evidence that phase matching to flexural Bloch waves can be a dominant scattering mechanism of thin shells/plates with periodic discontinuities in the midfrequency range [1].

Anderson Localization of Flexural Vibration: Irregularity can not only destroy the long-range coherence of the surface waves but also can give rise to localized vibration, as opposed to the traveling wave solutions discussed above. This phenomena is called Anderson localization. The critical parameters that determine the amount of the localization are the width B of the bands for which Bloch solutions exist and the frequency shift W that arises as a result of a deviation from periodicity. Sizable localization effects can occur if the frequency shifts W are larger than the allowed bandwidths B . As vibration tries to propagate, it becomes very likely that a region of the system is encountered for which no traveling wave solutions exist.

Consider the propagation of each azimuthal mode n independently for an axisymmetric system. The small mode number helical flexural waves can be localized. However, as a result of the adjoining fluid as well as practical limitations on the sizes of the frames, the bandwidths

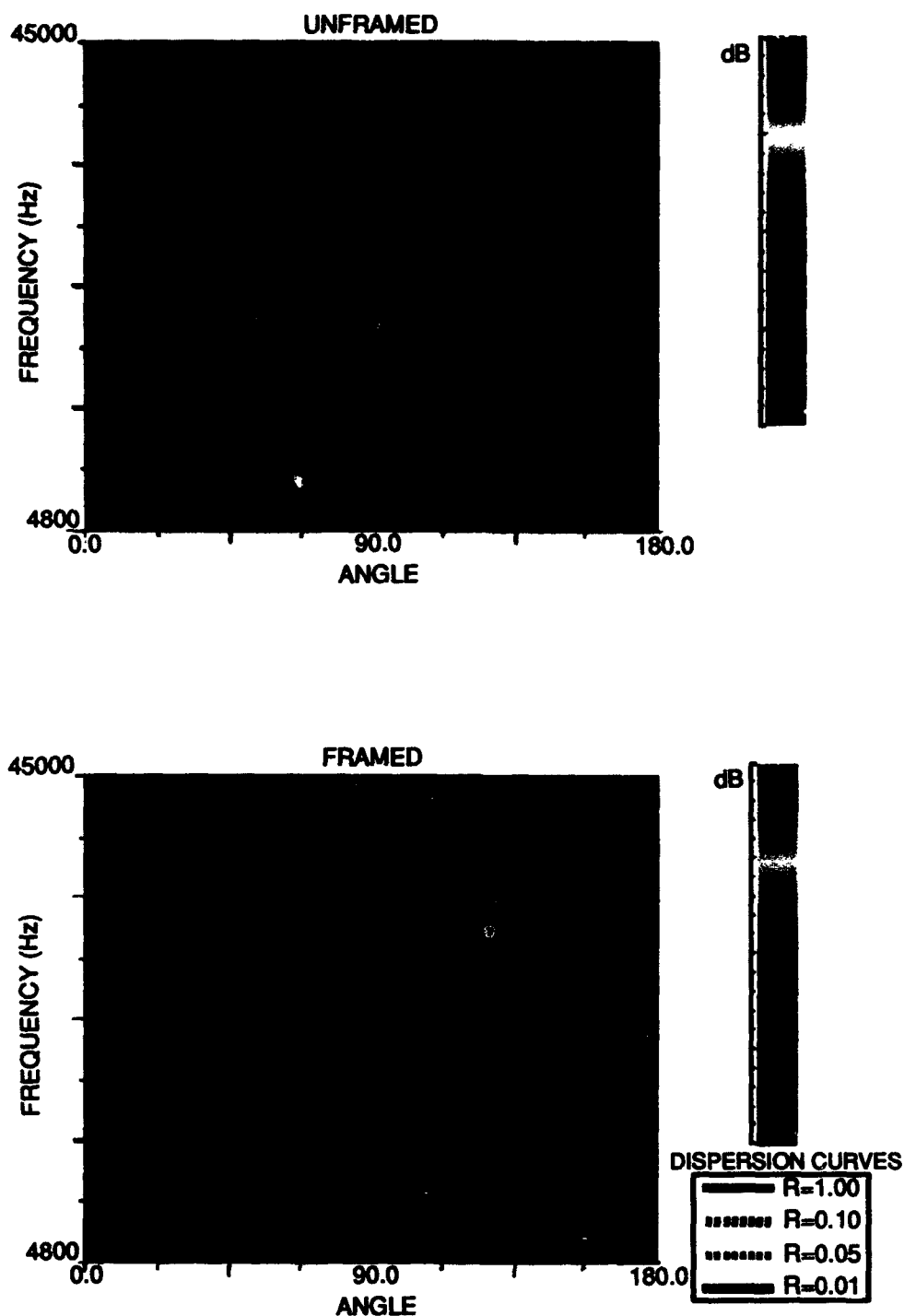


Fig. 11 — Backscattering cross-section from framed and unframed shells. Overlaid on the figure are dispersion curves for an infinite periodically ribbed shell. The parameter R to which the dispersion curves are fairly sensitive controls the rotational strength of the soldered connection of the ribs to the shell.

of the system cannot become small. Therefore dramatic effects do not arise from small amounts of irregularity. As the mode number n or pitch of the helical flexural wave increases, the bandwidths of the system narrow considerably and strong localization effects can result from even a small amount of irregularity. Figure 12 shows numerical simulation results that illustrate this phenomena for the $n = 15$ helical flexural mode. In the simulation, one additional feature, a transmission resonance in which the frames become transparent, has been included.

Conclusion: The acoustics of near-periodic structures involve many interesting phenomena.

Some recent discoveries at NRL, the importance of flexural Bloch waves in the acoustic cross section, and the localization of vibrational energy by irregularity have been described. It is believed that the discovery of these effects will have a major impact on our understanding of the acoustics of submarine structures.

[Sponsored by ONR]

Reference

1. D. Photiadis, J. Bucaro, and B. Houston, "Scattering from Flexural Waves on a Ribbed Cylindrical Shell," *J. Acoust. Soc. Am.*, in review, 1993. ■

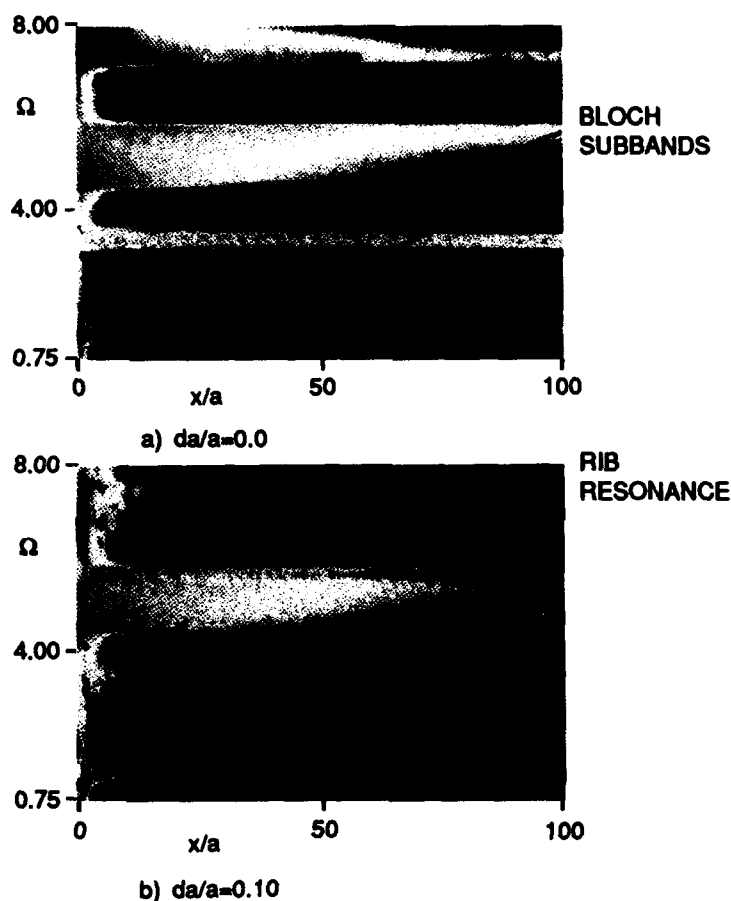


Fig. 12 — Localization of the $n = 15$ flexural mode of a ribbed cylindrical shell. The color mosaics show the response of a regularly (a) and irregularly (b) ribbed cylindrical shell to a source near $x = 0$. The vertical axis is frequency scaled to the ring frequency of the shell and the horizontal axis is position.

Acoustic Reverberation at Selected Sites in the Mid-Atlantic Ridge Region

J.W. Caruthers
Acoustics Division

J.R. Fricke
Massachusetts Institute of Technology

R.A. Stephen
Woods Hole Oceanographic Institution

Sound scattering from rough surfaces is a very complex phenomenon. Although it has been studied extensively, full understanding of a three-dimensional scattering function is still lacking. In 1989 the Office of Naval Research (ONR) established the Acoustic Reverberation Special Research Program (ARSRP) to improve this understanding for scattering from the sea surface and the seafloor.

As a part of the ARSRP bottom-scattering effort, researchers from NRL, several universities, and oceanographic institutions have pursued experimental and theoretical studies of acoustic reverberation in a region of the Mid-Atlantic Ridge (MAR) near 46°W, 26°N, called the ONR Atlantic Natural Laboratory. Extensive, high-quality, bottom reverberation data were collected in two cruises to the area: ARSRP'91 (also called the Acoustic Reconnaissance Cruise) in the summer of 1991, and ARSRP'93 in the summer of 1993. In these experiments, both distant and short-range reverberation data were taken at frequencies around 230 Hz. The RV *Cory Chouest* worked alone in ARSRP'91. In ARSRP'93, the *Cory* worked with Wood Hole's RV *Knorr* and the NATO/SACLANT ship RV *Alliance*. Here we discuss the character of the short-range (7-18 km) reverberation data collected by the *Cory* near a sedimented pond, designated Site A by the ARSRP.

Geomorphology: To support analyses of the acoustic data, two geological and geophysical (G&G) cruises were also conducted in the Atlantic Natural Laboratory. Figure 13 shows the geomorphology in a portion of the survey

area (65 × 50 nmi) at 200-m resolution. Three distinct morphological provinces are in this area. The morphology in the vicinity of Site A is typical of "outside corner" crust [1]. This crust is formed at a mid-ocean ridge segment adjacent to a passive transform fault. The relief is subdued and is dominated by orthogonal, steeply dipping normal faults that face toward the valleys and are aligned parallel and perpendicular to the ridge. The rock type is primarily basalt. This structure persists through most of the southern half and the northernmost quarter of Fig. 13. Regions C, C', and C'' are typical of "inside corner" crust that formed at a ridge adjacent to an active transform fault. The relief is dominated by fault scarps with variable orientation, but primarily oblique to the ridge axis. The exposed-rock types are more plutonic than volcanic, representative of deeper crustal levels in "normal" crust. Between the inside and outside corners is a flat sedimented valley (labelled V), running WNW to ESE, about 4400 m deep. Broad-scale features in the acoustics data are caused by the orthogonal ridges and fault scarps where they protrude into the insonifying beam. It is not yet clear, however, whether the fine-scale reverberation is different for inside and outside corners, but the sedimented valleys appear to produce weaker scatter. The insert of Fig. 13 shows three ping positions (44, 76, and 77) and ship headings for reference in later discussions of the scattering at Site A.

Figure 14 shows the one-way transmission loss to the region of interest on the seafloor. The source, a 10-element vertical line array, was steered 9 degrees down from horizontal to insonify the seafloor at ranges from 7 to 18 km. This downward steering ensures a reduction of the energy reflected from the sea surface, and greatly simplifies the transmission-loss character on the bottom. The waveform of the transmitted signal was a linear FM about 55 Hz wide centered at 230 Hz.

Reverberation: The scattering diagrams of Fig. 15 clearly show the effects of the ridges at Site A. Each of the lines in the three displays is the time evolution of the reverberation intensity along a beam at the angle given on the vertical

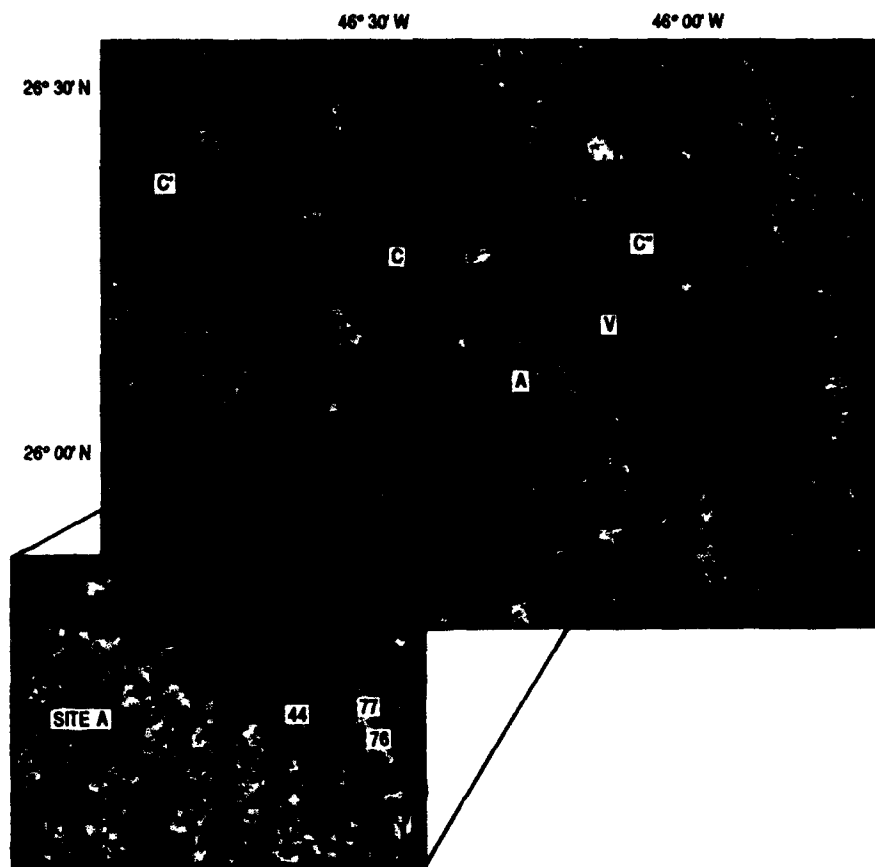


Fig. 13 — Geomorphology for a 3000-nm² region of near the MAR as it would appear if lit by a rising Sun. Insert shows Site A and ping positions discussed.

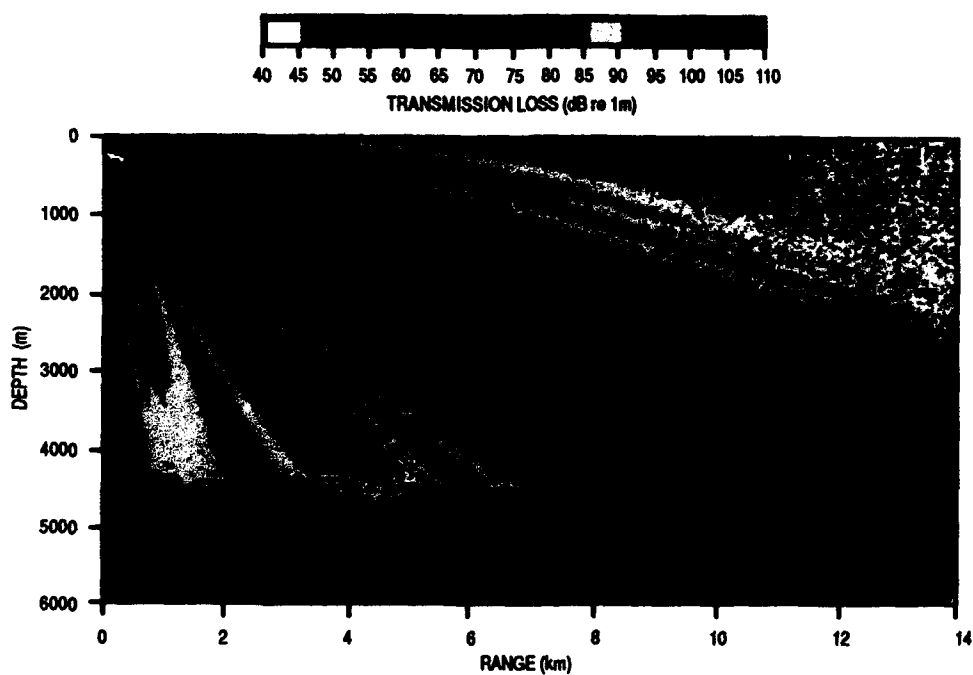


Fig. 14 — Transmission loss predicted by UMPE for 9-degree downward steering of source array into Site A

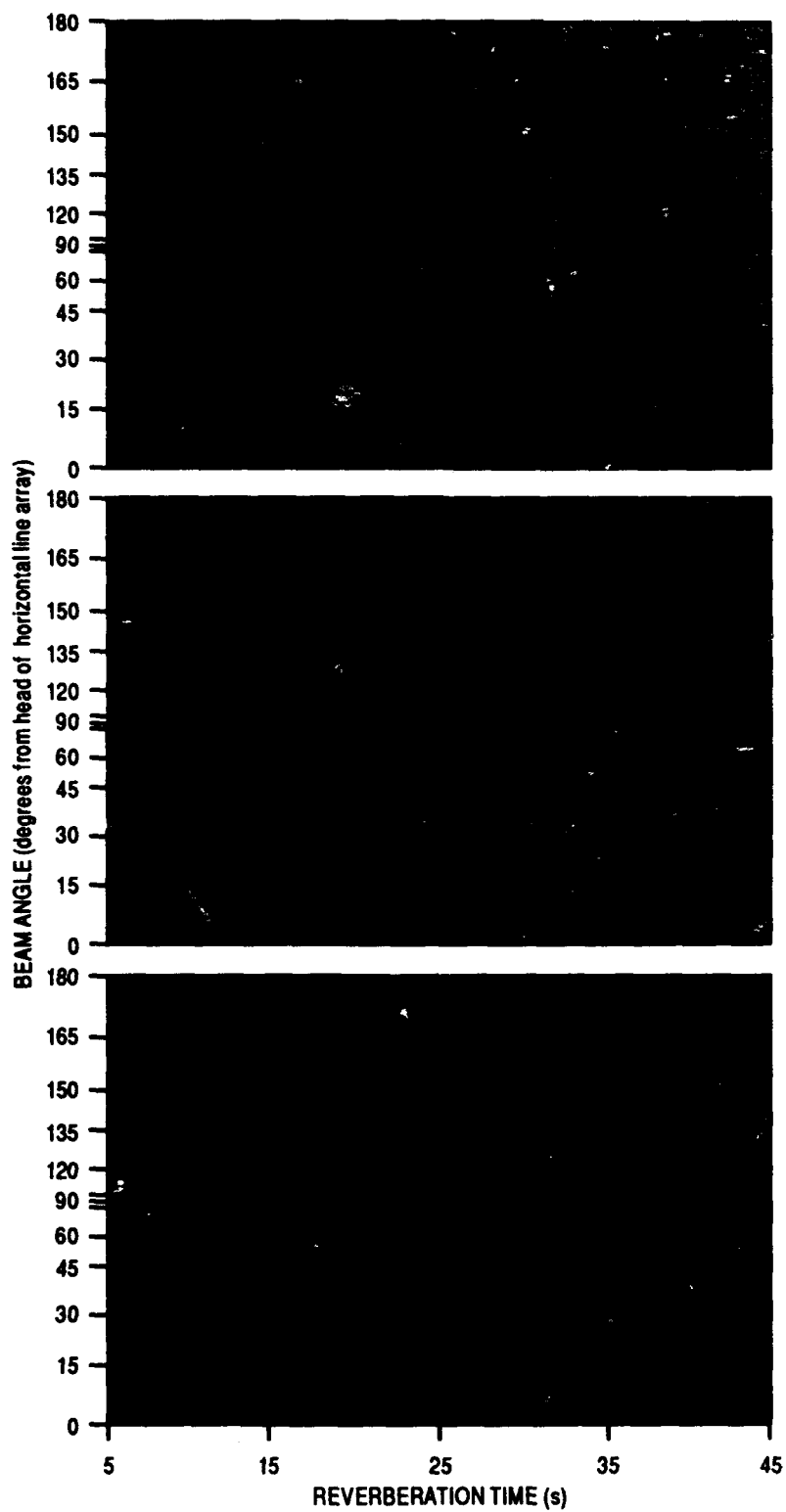


Fig. 15 — Reverberation evolution for pings 44, 76, and 77. Scattering at Site A seen in region from 15 to 30 seconds and 5 to 90 degrees.

scale as measured from the head of the horizontal receiving array (track of the ship). (Reverberation intensity is the matched filtered output in each beam, expressed in dB.) For all three pings the ship is at about the same position, forming a small triangle about 1.3 km on a side, so the times of echoes from individual points along the ridges are about the same. In the diagrams, reverberation from the ridges occurs at about 15 to 30 s. For pings 76 and 77 the shapes should also be about the same since the receiving array has the same orientation. The heading of the receiving array for ping 44 was different from the heading for pings 76 and 77, so the angular positions and orientations of the ridges appear differently in its scatter diagram.

A detailed analysis of these scattering patterns shows that they are consistent with these expectations. One should be aware, however, that because the receiver is a horizontal line array, there is a left/right ambiguity; that is, one cannot tell from which side of the array the

echoes are coming. For the track for ping 44, Site A is in the right forward half of the angles around the array (i.e., 5° to 90°); the ambiguous region is to the left at equivalent angles. Site A is in the left forward half of the array for pings 76 and 77; the ambiguous region is to the right of the array. The ambiguous regions for ping 44 and for the set 76 and 77 are, therefore, not the same and some uncorrelated scattering can be expected. Detailed analysis shows, however, that the dominant scatter for all three pings is coming from Site A, and the ambiguous sides are contributing very little scatter in these cases.

The Bistatic Scattering Strength Model:

The bistatic scattering strength model (BISSM) [2,3], which predicts reverberation by using fine-scale morphology such as is available for the ARSRP experiments, was run for several pings at Site A. Figure 16 shows the results for ping 77. BISSM-predicted reverberation is

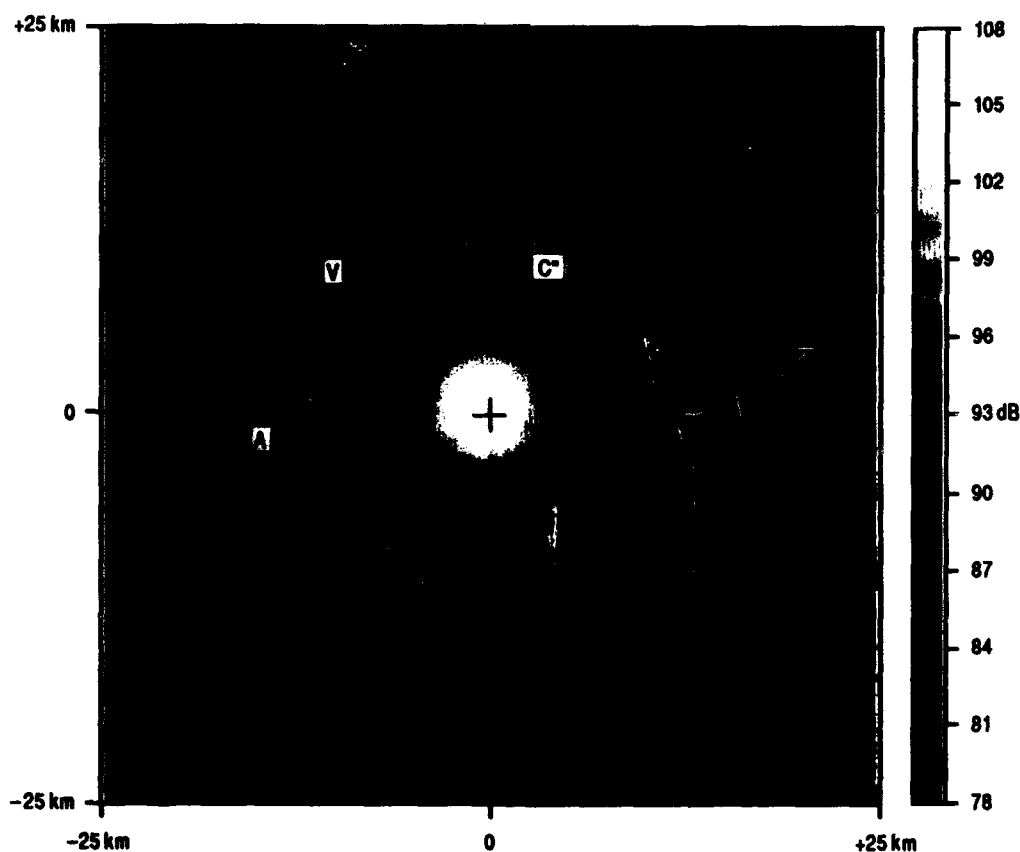


Fig. 16 — Reverberation levels (for each 200×200 m patch) predicted by BISSM and mapped onto the seafloor

mapped onto the seafloor at its origination points. Bright yellow represents regions of the seafloor that are "lit up" by the acoustic energy. The bright spot in the center is directly under the ship at ping 77, and the circular patterns are indicative of the directionality of the acoustic energy for the vertical line array source steered down at 9 degrees. The bright region to the NNE is the side of a seamount (C') of the inside corner character (C-type); just beyond is the dark shadow on its far side. Directly under the ship and to the NW/ESE is a flat, sedimented area (V-type) of low backscatter. A little further around counter-clockwise, to the West and WSW, is a series of ridges showing bright faces on their forward slopes followed by dark shadows on their far slopes. These are the ridges at Site A. The darkness all around the diagram beyond the illuminated area is where the acoustic rays bend upward from the bottom and leave the rest of the bottom in a shadow zone. Also, when the data displayed in Fig. 16 are mapped into beam/time diagrams (like Fig. 15), there is a strong match between predicted and measured scatter. Quantitatively, BISSM has been validated in these cases by the adjustment of an empirical coefficient to a value of 17 dB (generally accepted by the ARSRP).

Summary: Seafloor morphology is clearly a controlling factor in the broad-scale scattering observed in a rugged region like the Mid-Atlantic Ridge. Strong contrast was found between scattering from deeply sedimented areas and from rugged, exposed-rock ridges. Less pronounced differences were found between exposed-rock regions of known geological differences, e.g., inside vs outside corner. Prominent features were found to be repeatable for pings from nearby positions and between cruises, suggesting that variations in the transmission loss is not the cause for the features observed. It is suggested here that the dominant effects being observed are the effects of the modulation of the grazing angle dependence of scattering by the variation of the slopes of the scattering surfaces. It is likely that the degree and form of surficial roughness (i.e., fine-scale morphology or texture) is also a factor in defining the character of the echoes.

Acknowledgments: We recognize the contributions of the following scientists: Dr. Moshen Badiey, Program Manager, ARSRP, Dr. Brian Tucholke, collecting, analyzing, and providing the geomorphological information used here, Dr. Kevin Smith for UMPE (University of Miami Parabolic Equation) calculations used in Fig. 14, and Dr. Jorge Novarini and Mr. E.J. Yoerger for assistance in the development of BISSM.

[Sponsored by ONR]

References

1. J.W. Caruthers and J.C. Novarini, "Modeling Bistatic Bottom Scattering Strength Including a Forward Scattering Lobe," *IEEE J. Oceanic Eng.* **18**, 100 (1993).
2. J.W. Caruthers and E.J. Yoerger, "ARSRP Reconnaissance Results and BISSM Modeling of Direct Path Scatter, in *Ocean Reverberation*, eds. D.D. Ellis, J.R. Preston, and H.G. Urban (Kluwer Academic Publishers, Dordrecht, The Netherlands, 1993) pp. 203-208.
3. J.A. Karson and H.J.B. Dick, "Tectonics of Ridge-Transform Intersections at the Kane Fracture Zone," *Marine Geophys. Res.* **6**, 51 (1983). ■

Overcoming Chaos

M.D. Collins and W.A. Kuperman
Acoustics Division

Chaos has long been considered an insurmountable limiting factor in nonlinear scientific computation. Because chaotic initial value problems are extremely sensitive to initial conditions and numerical truncation errors, there is a limit to how far solutions can be integrated forward in time. For example, it is very difficult to extend weather forecasts beyond about 10 days into the future [1]. This article describes an approach for overcoming chaos for a class of nonlinear dynamics problems. The

results provide a glimmer of hope that well-posed techniques will eventually be developed for solving sophisticated nonlinear problems such as weather forecasting.

Ray Chaos: In the limit of high frequency, many wave propagation problems may be solved with ray tracing techniques. Although wave equations are linear for many applications, the differential equations that describe ray paths are almost always nonlinear. If the wave medium is heterogeneous, chaotic solutions to the ray equations may exist. For example, ray chaos can arise in ocean acoustics problems [2], which involve variations in the speed of sound that are strong with depth and weak with the horizontal coordinates. Since nonlinear boundary value problems require iterative solutions, the ray equations are usually solved by providing initial conditions and integrating along the ray path.

An eigenray is a ray path that connects two specified end points. Eigenray problems are usually solved with the shooting method, which involves iterating for the correct initial conditions. When chaos exists, the shooting method is ill-posed for eigenray problems involving widely separated end points. Since eigenrays are often used to perform ocean acoustic tomography, it was feared that experimental configurations would be seriously limited by ray chaos, especially the ocean basin and global-scale experiments that are being conducted to monitor global warming [3].

Nonlinear Iteration: We have found that iteration methods for the nonlinear boundary value problem are well-posed. The nonlinear differential equations of ray theory are therefore somewhat analogous to stiff linear differential equations, which are ill-posed as initial value problems but well-posed as boundary value problems. The results shown in Fig. 17 are for an eigenray problem involving a two-dimensional acoustic medium in which the speed of sound varies sinusoidally in both directions. Blue corresponds to the minimum sound speed of 1470 m/s. Red corresponds to the maximum sound speed of 1530 m/s. The bold curve repre-

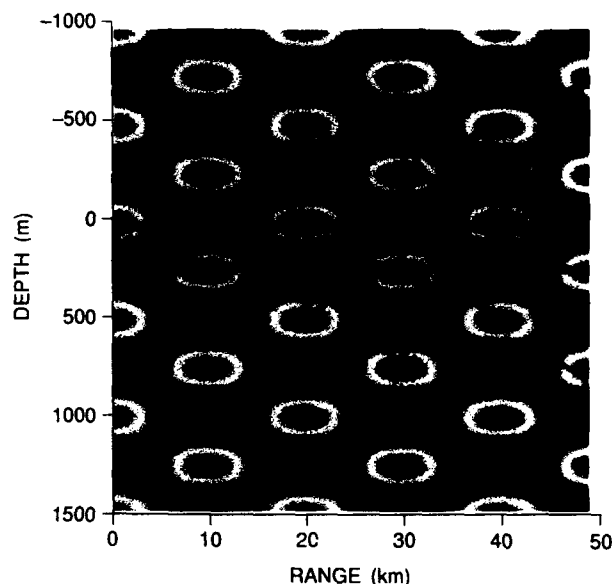


Fig. 17 — An eigenray and launched arrays in a doubly periodic medium

sents an eigenray obtained with an iteration method. The fine curves represent ray paths obtained with the shooting method. The launch angles of these rays, which diverge from the eigenray in opposite directions, differ by one billionth of a degree. To obtain accurate results, it was necessary to use high-precision numerics for the ill-posed shooting method but not for the well-posed iteration method. The iteration method was tested for end points separated by as much as 1000 km in this doubly periodic medium and performed well for each case.

[Sponsored by ONR]

References

1. E.N. Lorenz, "The Predictability of a Flow Which Possesses Many Scales of Motion," *Tellus* **23**, 289 (1969).
2. K.B. Smith, M.G. Brown, and F.D. Tappert, "Ray Chaos in Underwater Acoustics," *J. Acoust. Soc. Am.* **91**, 1939 (1992).
3. A.B. Baggeroer and W. Munk, "The Heard Island Feasibility Test," *Physics Today* **45**(9), 22 (1992). ■

**CHEMICAL/
BIOCHEMICAL
RESEARCH**

- 127 Fiber-Optic Sensor for Detection of Trace Levels
of Mercury in Water

*Kenneth J. Ewing, Ashwar D. Aggarwal, Gregory M. Nau,
and Thomas Boudreau*

- 130 Observing the Growth of Protein Crystals

John H. Koone, Peter D'Antonio, and Keith B. Ward

- 132 Global Warming Potential of Potential CFC Replacements

Nancy L. Gurland, Herbert H. Nelson, and Laura J. McElroy

Fiber-Optic Sensor for Detection of Trace Levels of Mercury in Water

K.J. Ewing and I.D. Aggarwal
Optical Sciences Division

G.M. Nau and T. Bilodeau
University Research Foundation

Introduction: The U.S. Navy is concerned with the amount of environmentally hazardous materials produced by operational ships, most of which are subsequently discharged into the ocean. To decrease the amount of environmentally hazardous materials being discharged into the ocean, the Navy has implemented the environmentally sound ship program. The goal of this program is to develop remediation and monitoring systems for Navy vessels that will significantly reduce or eliminate the discharge of environmentally hazardous materials into the ocean. Onboard sensors are needed to monitor the concentrations of heavy metals (such as mercury, lead, and silver) in the remediation process effluent streams. The U.S. Army Environmental Center and the Department of Energy are also developing sensors to detect and measure heavy metals in soil and groundwater by using the cone penetrometer system. Toxic heavy metals such as mercury, lead, chromium, and arsenic are commonly found contaminants at industrial waste sites, land fills, and abandoned industrial facilities. To clean up sites contaminated with these toxic metals, the location of the metals, either in the solid form or in the groundwater must be determined. Additionally, sensors are needed for monitoring metal ion concentrations in sewage plant effluents and mine water run-off. In all cases, the sensors must be sensitive, selective, monitor in real time and in situ, and be cost effective. Because of their small size and low cost, fiber-optic chemical sensors are uniquely suited [1] for in-situ, real-time monitoring of water, air, and soil for toxic materials.

Heavy Metal Detection: Our approach to detecting heavy metals in water involves immobilizing a metal-specific colorimetric reagent into a stable polymeric matrix. When the re-

agent/polymer film encounters metal ions in solution, the color of the film changes. By monitoring the color of the film with a fiber-optic spectrometer, the concentration of metal in water can be determined. One polymer used for immobilizing the reagent is nafion. Nafion consists of a trifluoroethylene backbone with pendent side chains of perfluorinated vinyl ethers terminated with sulfonic acid groups. The reagent used for detecting mercury in this work is phenylazoformic acid 2-phenylhydrazide, compound with 1,5-diphenylcarbazine, PAPDC. This reagent contains one mole of 1,5-diphenylcarbazine to one mole of 1,5-diphenylcarbazine. 1,5-diphenylcarbazine is used in colorimetric determinations of the metal ions Cr(VI), Au(III), Cu(II), Hg(II); 1,5-diphenylcarbazine is chiefly used for colorimetric determination of Cr(III) and Hg(II). PAPDC is immobilized into the nafion film by soaking the nafion in a 0.1-M solution of PAPDC in ethanol for 24 hours. After this time, the film is ready for mounting in the fiber-optic flow cell.

Fiber-Optic Sensor System: Optical Setup. The optical setup used to monitor the change in absorptivity of metal-specific films is diagrammed in Fig. 1. The spectrometer system, consisting of a white light source and spectrometer, was purchased from Ocean Optics (Dunedin, Florida). The spectrometer, with dimensions $15 \times 4 \times 6$ cm, consists of a diffraction grating (1200 lines/mm) imaged onto a 1024-element array of silicon charge-coupled device (CCD) detectors. The NRL system uses a 500- μ m optical fiber to carry light down to a flow cell and a 50- μ m optical fiber to carry light from the flow cell to the spectrometer. Alternatively, a small white light source (0.1-W tungsten/halogen micro-flashlight bulb) can be used as the light source, in this case only a 50- μ m optical fiber is required to carry light back to the spectrometer.

Flow Cell. The flow cell design is also shown in Fig. 1. The light from an optical fiber, or micro light bulb, is collimated by using a graded index (GRIN) lens. A polymer film that contains the immobilized metal-specific colorimetric reagent is held tightly across the face of the GRIN lens. The collimated light

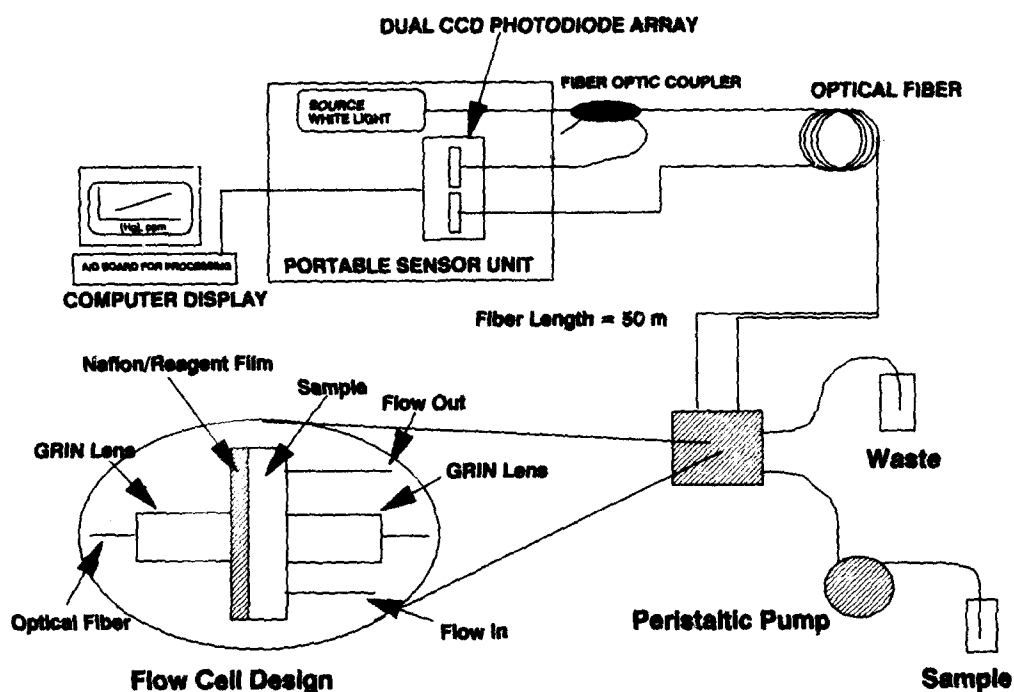


Fig. 1 — Block diagram of fiber-optic heavy-metal sensor system; details of the flow cell design are also shown

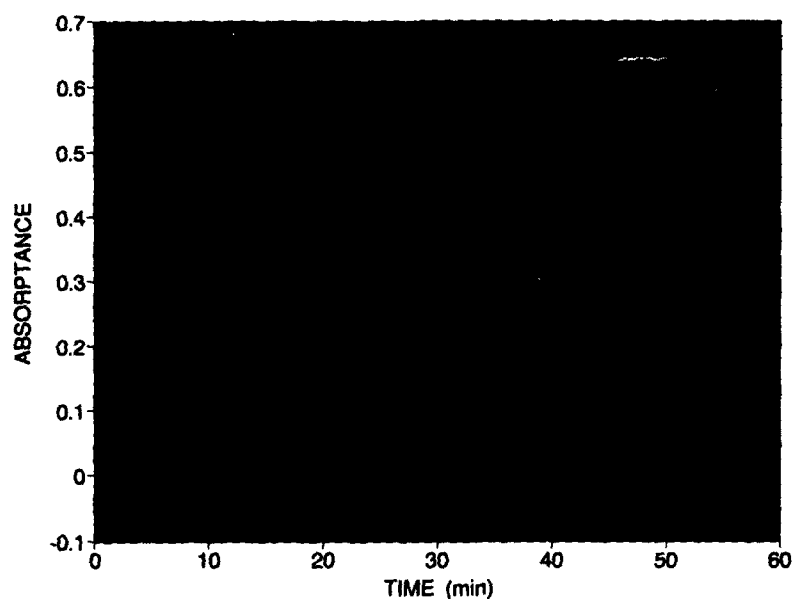
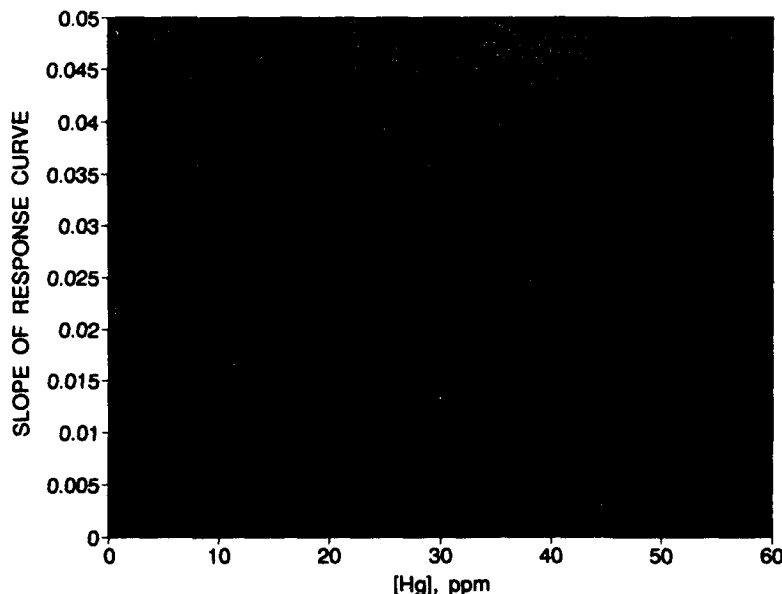


Fig. 2 — Sensor response curve for different concentrations of mercury in water at a pH of 6.5. Results for different concentrations of mercury were obtained by first stopping the pump, moving the inlet tube from one mercury solution to another, then starting the pump.

Fig. 3 — Plot of the slope of the response curve vs the mercury concentration. Regression analysis of the data gave a correlation coefficient of 0.996, the equation for the fitted line is: Slope of Response Curve = $9 \times 10^{-4}[\text{Hg}]$, ppm - 4.3×10^{-4} .



passes through the reagent/polymer film, then passes through the sample chamber containing the solution and is collected by a second GRIN lens. A 50- μm optical fiber (50-m length) is attached to the collection GRIN lens by using an SMA connector and carries light to the spectrometer. The solution is injected into the cell by using a peristaltic pump, flows over the reagent/polymer matrix, and is collected in a waste container.

Sensor Response to Mercury in Water:

Figure 2 shows the response of the PAPDC/naftion film to part-per-million levels of mercury in water at a pH of 6.5. In this experiment, the change in absorptivity of the PAPDC/naftion film was monitored as the mercury solution was continuously pumped through the absorption cell. It is evident from this figure that as the mercury concentration increases, the slope of the response curve (the rate of change in the absorptivity with respect to time) increases. A plot of the slope of the response curve vs the mercury concentration produces a linear working curve (Fig. 3). The line in this figure was calculated from the data via linear regression; a correlation coefficient of 0.996 indicates excellent linearity of the data. By using a larger sample chamber and injecting a fixed volume of mercury solution into the sensor, as little as 14

parts-per-billion of mercury in water can be detected.

Future Work: Although the response of this sensor has been determined for mercury in water, the precise mechanism of the reagent immobilization and its effect on the reactivity of the reagent are unknown. By determining how the immobilization matrix affects the reactivity of immobilized reagents, new, highly specific reagent polymer films can be prepared. Our current work focuses on how the acidity or basicity, degree of crosslinking, etc., of a polymer may affect the reaction kinetics of a given reagent in a polymeric matrix. The goal of this work is to determine what properties of the matrix control reagent reactivity and, subsequently, the specificity of the reagent/polymer film to a given metal ion. Results of this work will be used to design and prepare metal-specific sensors for determining other heavy metals such as lead, chromium, and silver in water.

[Sponsored by ONR and the U.S. Army Environmental Center]

Reference

1. O.S. Wolfbeis, ed., *Fiber Optic Chemical Sensors and Biosensors*, Vols. 1 and 2 (CRC Press, Boston, 1991). ■

Observing the Growth of Protein Crystals

J.H. Konnert, P. D'Antonio, and K.B. Ward
Laboratory for the Structure of Matter

Introduction: The relationship between the molecular structure of macromolecules, as obtained by crystal structure analyses, and their biological function has been widely recognized and has ushered in the new field of structural biology. The goal of a crystal structure analysis is to determine the three-dimensional (3-D) arrangement of the thousands of atoms from which the biologically active macromolecule is composed. The environments and relative positions of the biologically active regions of the molecule can then be related to their functions in living organisms. The structure is obtained by mathematically analyzing the diffraction pattern obtained by directing an X-ray beam at a single, highly ordered crystal. Quite often, the crystal structure determination is hampered by the difficulty of growing crystals that are large and well-ordered enough to produce high-quality diffraction patterns. The emerging science of scanning probe microscopy holds promise in elucidating mechanisms that inhibit crystal growth, and, thus, in indicating techniques for obtaining crystals of higher quality. We have studied lysozyme, an enzyme that breaks down the cell walls of bacteria, with the Atomic Force

Microscope (AFM). The dynamic growth and dissolution of lysozyme crystals from their mother liquor has been observed at the molecular level. Although the molecular structure of this material has already been accurately determined by X-ray diffraction, the enzyme is readily available and provides an ideal material with which to develop techniques applicable to other macromolecules.

The Atomic Force Microscope: The AFM traces the surface of a material with a very small stylus (a tip radius of approximately 40 Å for the experiments reported here) while exerting an extremely small force (less than a nano-Newton of vertical force for the results reported here). The topological data are recorded and then analyzed and displayed in various ways. Figure 4 illustrates a lysozyme crystal being scanned. The stylus is fixed to the underside of the tip of the triangular, flexible, 0.2-mm-long cantilever. A laser beam is reflected from the tip of the cantilever, and the deflection of this beam is monitored as the sample is scanned under the tip. The sample is translated vertically with a feedback circuit that maintains a constant cantilever deflection (and constant, small force on the sample).

Growth Steps, Spiral Dislocations, and Molecules: In 1990, Durbin and Feher first demonstrated that the surfaces of growing protein molecules could be observed with the

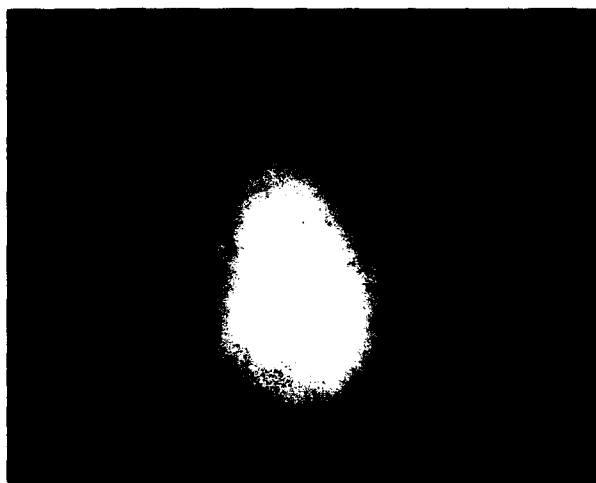


Fig. 4 — Top view of lysozyme crystal in stabilizing solution with AFM cantilever tip in position

AFM [1]. The observation that the scanning tip does not completely scramble the ordered addition of molecules to the surface was, for many, an unexpected and pleasant surprise. We have been able to duplicate their observations and directly monitor growth steps, ledges, and spiral dislocations. Additionally, we have used image processing algorithms developed at NRL to obtain, for the first time anywhere, images of the lysozyme crystal faces with molecular resolution [2].

Figure 5 displays growth steps, in conjunction with a spiral dislocation, on the (110) face of lysozyme. In most but not all regions, the observed ledges are 56 Å in height. This indicates that this crystal face is growing in layers that are predominantly two molecules thick. The spiral dislocation is itself a defect in the crystal. The molecules in the dislocation will tend to be misoriented relative to those molecules in other portions of the crystal according to the pitch of the screw. All misorientations such as this will degrade the quality of the X-ray pattern and make the determination of molecular structure more difficult. On the other hand, a few spiral dislocations may be necessary for the crystals to grow at a speed sufficient to attain a useful size in a reasonable length of time. The crystals appear to grow primarily by adding molecules to the edges of the growth steps. Here the molecular pairs being added have two surfaces to bond to, rather than the single surface that would be available if they attached in the middle of a layer. The numbers and types of defects observed on the surfaces of crystals are being correlated with the quality of their diffraction patterns.

Figure 6 displays the (110) face of lysozyme at molecular resolution. The most striking features of the image are the observed crystallographic periodicities of 112 Å horizontally and 39 Å vertically. Each such 2-D unit cell would expose the surface of four molecules if the surface structure is similar to the internal structure. Another feature that recurs is the nearly centered periodic array of minima. As mentioned, the crystal grows by adding layers that are predominantly two molecules thick. Related to this, if the surface structure is the same as planes of molecules present within the



Fig. 5 — Processed image of a spiral dislocation

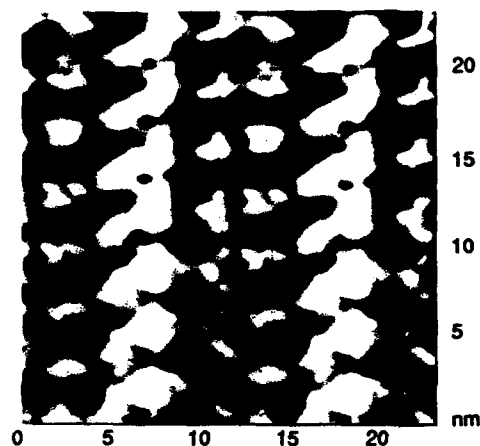


Fig. 6 — Processed image showing high-resolution details on the (110) surface; crystallographic periodicities of 112 Å horizontally and 39 Å vertically are apparent

crystal, two distinctly different surfaces could be exposed. Analyses of images such as that shown in Fig. 6 have allowed us to choose between those alternatives and determine the probable arrangement of atoms at the (110) surface.

Conclusions: This survey of some of the types of quantitative information concerning the surfaces of lysozyme crystals that can be obtained with an AFM indicates that it may be a very useful tool for studying the mechanisms of crystal growth. In favorable instances, the tip perturbs the surface to such a sufficiently small extent that there is a real possibility for observing not only individual molecules, but also their

shapes. At one step lower in resolution, it will be interesting to investigate the fine details of defects such as screw dislocations. Do the dislocations occur continuously as one progresses around the screw? What is the nature of growth and dissolution within pits where many crystal surfaces are exposed? Much interesting work remains to be done in applying these techniques.

[Sponsored by ONR and NASA]

References

1. S.D. Durbin and W.E. Carlson, "Lysozme Crystal Growth Studied by Atomic Force Microscopy," *J. Cryst. Growth* **122**, 71 (1992).
2. J.H. Konnert, P. D'Antonio, and K.B. Ward, "The Observation of Growth Steps, Spiral Dislocations, and Molecular Packing on the Surface of Lysozme Crystals with the Atomic Force Microscope," *Acta Cryst. D*, in press. ■

Global Warming Potential of Potential CFC Replacements

N.L. Garland and H.H. Nelson
Chemistry Division

L.J. Medhurst
*NRL/NRC Postdoctoral
Research Associate*

The Montreal Protocol and subsequent amendments to the U.S. Clean Air Act mandate an end to the production of chlorofluorocarbon (CFC) refrigerants by 1995 because of their role in the depletion of stratospheric ozone. This has prompted an intense search for non-ozone-depleting substitutes for use in refrigerators and air-conditioning plants. In recent years, fluorine-substituted alkanes, hydrofluorocarbons (HFCs), have been investigated as promising alternate refrigerants. Unlike CFCs and another class of proposed substitutes, hydrochlorofluorocarbons (HCFCs), HFCs do not contain chlorine or bromine atoms, which are participants in the catalytic cycles responsible for ozone destruction

in the stratosphere. In addition, the hydrogen atoms present in HFCs allow them to react with tropospheric oxidants such as the OH radical, limiting their residence time in the atmosphere. The HFCs are, however, extremely effective greenhouse gases. Their many C-F bonds lead to strong infrared (IR) absorption in regions of the spectrum where the natural atmosphere is transparent. The resulting absorption and re-radiation of IR wavelengths traps heat in the lower atmosphere.

The Navy is the largest user of CFC-114 as a refrigerant; it is used in the air-conditioning plants on 25 different classes of Navy ships. Several HFCs exhibit physical and refrigeration properties that make them ideal candidates for backfit substitution in these air-conditioning plants. Before a final choice can be made, however, the atmospheric impact, particularly the Global Warming Potential (GWP), of these compounds must be assessed.

Experimental Measurements: Simply put, the Global Warming Potential of a species is determined by the lifetime in the atmosphere of the species, primarily determined by its temperature-dependent reaction rate with atmospheric hydroxyl radicals, and the ability of the species to absorb infrared radiation in the 7 to 13 μm atmospheric window [1]. We have measured these properties for the four potential replacements for CFC-114 shown in Fig. 7: FC-236ea ($\text{CF}_3\text{CHFCHF}_2$), FC-236cb ($\text{CF}_3\text{CF}_2\text{CH}_2\text{F}$), FC-236fa ($\text{CF}_3\text{CH}_2\text{CF}_3$), and E-134 ($\text{CHF}_2\text{OCHF}_2$).

OH reaction rate constants are measured by using laser pump-and-probe techniques. The experiments are carried out in a temperature-controlled cell that can be varied over the range 250 to 320 K, temperatures appropriate to the troposphere. OH radicals are produced by excimer laser photolysis of HNO_3 . Their subsequent decay because of reaction with the HFC of interest is monitored by exciting fluorescence with a second, excimer-pumped dye laser. Table 1 lists the reaction rate constants that are obtained. The HFCs have long tropospheric lifetimes, and these lifetimes have been shown to be insensitive to spatial variations and seasonal cycles [2]. A good estimate of their lifetimes can be obtained by scaling the known

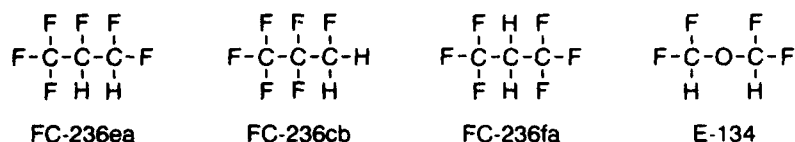


Fig. 7 — Structure of four possible replacements for CFC-114; abstractable hydrogen atoms are highlighted in color

Table 1 — Measured OH Reaction Rate Constants and Infrared Absorption Strengths and Calculated Atmospheric Lifetimes of Four Potential CFC-114 Replacements

HFC	OH Reaction Rate Constant ($10^{-13} \text{ cm}^3 \text{ s}^{-1}$)	Relative IR Absorption	Atmospheric Lifetime (years)
FC-236ea	$(2.0 \pm 0.9) \exp[-(2.0 \pm 0.3)/\text{RT}]$	9	1.5
FC-236cb	$(2.6 \pm 1.6) \exp[-(2.2 \pm 0.4)/\text{RT}]$	10	1.6
FC-236fa	$(0.2 \pm 0.1) \exp[-(1.8 \pm 0.3)/\text{RT}]$	62	2.2
E-134	$(5.4 \pm 3.5) \exp[-(3.1 \pm 0.4)/\text{RT}]$	24	2.3

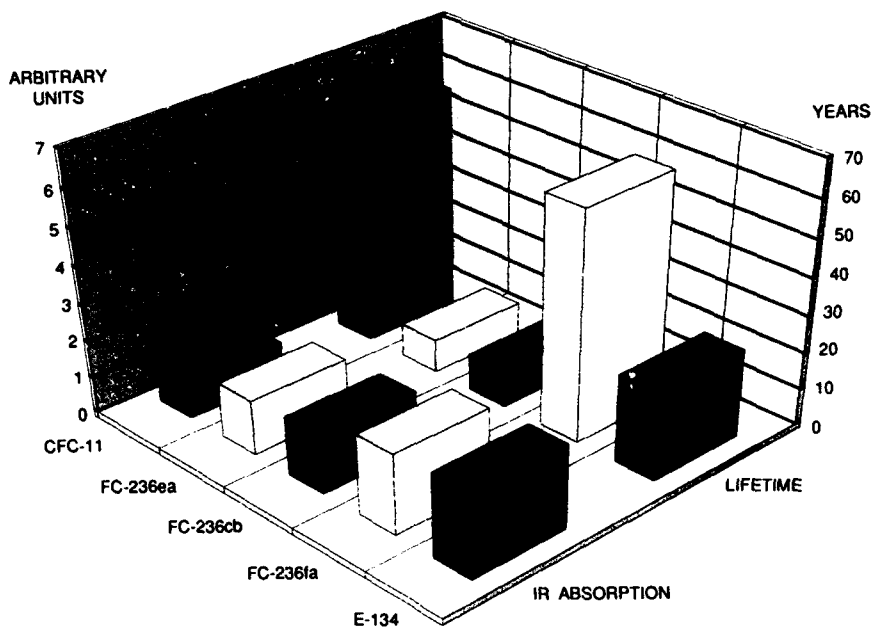


Fig. 8 — Graphical depiction of the results of our measurements of relative absorption strength in the 7 to 13 μm region. Shown are atmospheric lifetimes of four proposed replacements for CFC-114 and values for the reference compound CFC-11. For both parameters, larger values lead to higher Global Warming Potential.

atmospheric lifetime of methyl chloroform by the ratio of the OH reaction rate constants. Table 1 also lists lifetimes calculated by using this method. Infrared absorption strengths in the region 7 to 13 μm are measured by using a 21-m pathlength gas cell in a Fourier transform infrared spectrometer. Compounds of interest are diluted to 10 to 50 ppm in air and flowed through the cell. The absorption is reported relative to CFC-11 whose GWP is defined as 1.0.

Conclusions: Figure 8 shows the results of our measurements along with the values for the reference compound CFC-11. For both properties plotted (atmospheric lifetime and IR absorption in the 7 to 13 μm window), larger values indicate higher Global Warming Potential. Although FC-236ea and FC-236cb have a slightly higher absorption strength than CFC-11, they have much shorter atmospheric lifetimes and thus pose little threat as greenhouse gases. The other two compounds under consideration as replacements for CFC-114, FC-236fa and E134,

have even larger IR absorption strengths and long atmospheric lifetimes. Therefore, both of these compounds have significant Global Warming Potential. Fortuitously, FC-236ea, besides having a very low GWP, has almost identical refrigeration properties to CFC-114. It is therefore an ideal candidate for replacement purposes.
[Sponsored by ONR]

References

1. R.G. Gann et al., "Preliminary Screening Procedures and Criteria for Replacements for Halons 1211 and 1301," National Institute of Standards and Technology Technical Note 1278, Washington, D.C., 1990.
2. M.C. Prather, "Vol. II, Appendix: AFEOS Report," of *Scientific Assessment of Stratospheric Ozone: 1989*, World Meteorological Organization, Global Ozone Research and Monitoring Project, Report No. 20, Washington, D.C., 1990. ■

**ELECTRONICS
AND
ELECTROMAGNETICS**

- 137 **Multispectral Infrared Visualization and Processing
for Dim Target Detection**
Dean A. Scribner, Michael P. Satychur, and Melvin R. Kru
- 139 **Flying Radar Target (FLYRT) Testing and Final Demonstration**
Christopher S. Bovais, Ciaran J. Murphy, and Peggy L. To
- 141 **The Microwave Monolithic Integrated Circuit/Electronic
Warfare Receiver**
Leo W. Lemley
- 144 **The Ionospheric Focussed Heating (IFHD) Experiment**
Paul A. Bernhardt
- 146 **Control of Interface Properties of GaSb/InAs Superlattices**
*Robert J. Wagner, Brian R. Bennett, Benjamin V. Shanabrook,
John L. Davis, James R. Waterman, and Mark E. Wig*

Multispectral Infrared Visualization and Processing for Dim Target Detection

D.A. Scribner, M.P. Satyshur, and M.R. Kruer
Optical Sciences Division

An emerging Navy role in local theater-level conflicts is to be first on the scene and to provide surveillance of the littoral battlefield (shoreline to about 200 nm inland) as part of a multiservice task force. As evidenced in many television news clips of the Gulf War, infrared sensors provide a day-night capability for viewing military targets. In many scenarios, an ability to provide long-range detection with low false alarm rates has been demonstrated. In this new scenario, Navy targets of interest are located in a more cluttered background than in previous open-ocean and open-air scenarios. Robust infrared detection requires additional information to discriminate targets from the background. Tri-service research efforts are attempting to develop a multispectral infrared (IR) technology to gain the desired new capability.

Previous implementations of multispectral IR have typically addressed special applications involving the detection of unique spectral phenomena such as plumes, or the rejection of unwanted solar glints or flares. In these applications, improved performance is typically achieved by using spectral ratios or by using two spectral bands that are very closely correlated except for the anomalous plume, glint, flare, etc., and then performing a locally normalized difference between images in the two colors. A more general approach to exploiting the full multidimensional color space for detecting dim targets in clutter is to develop signal processing that uses a color vision approach similar to that of biological systems.

Composite IR Color Images: Composite IR color images are generated from previously recorded multispectral data and computer visualization is performed to analyze the general phenomenon (including color constancy). Although most existing infrared imagery is not adequate for multispectral processing because of

misregistration, improper spectral bands, and high noise levels, one fairly old set of ERIM (Environmental Research Institute of Michigan) data is quite useful. The image selected is a 640×1200 pixel airborne scene with well-registered 8-bit data in three wavelength bands—LWIR (long-wavelength IR) (9.0 to $11.6 \mu\text{m}$), MWIR (medium-wavelength IR) (4.5 to $5.5 \mu\text{m}$), and SWIR (short-wavelength IR) (2.0 to $2.6 \mu\text{m}$). The visualization strategy is to construct a composite color image by normalizing and scaling each IR band to correspond to the red, green, and blue bands of a visible display system. The resulting images constructed with this algorithm are displayed on a standard color monitor and are easily analyzed by the human eye-brain cognitive system.

Figure 1 is an example of a composite IR color image obtained from this process along with an image for each of the three individual bands. Each image is a 320×200 image of the Port Hueneme, California, background into which a 4×6 grid of artificial aircraft shapes has been inserted. The "colors" of the inserted target aircraft cannot be arbitrarily assigned; they are highly dependent on spectral phenomenology factors such as surface emissivity, surface temperature, and atmospheric transmission. To approximate realistic targets, color values are obtained from different man-made objects within the scene, such as the top of a fuel storage tank or the deck of a Navy ship. Figure 1 illustrates that the embedded targets are more easily seen by the eye in the multispectral representation than in single-band representations where the targets disappear because of zero-contrast between the aircraft and background.

Spatio-Spectral Filtering: To make a quantitative comparison of spatio-spectral discrimination (composite color processing) vs single-band discrimination (spatial-only processing), matched filters are derived and applied to detect targets embedded in the background imagery. The single-band filters (2-D spatial-only), are derived in the conventional manner by using the smoothed power spectrum of the background and the target shape (specifically that of the aircraft shown in Fig. 1). The color

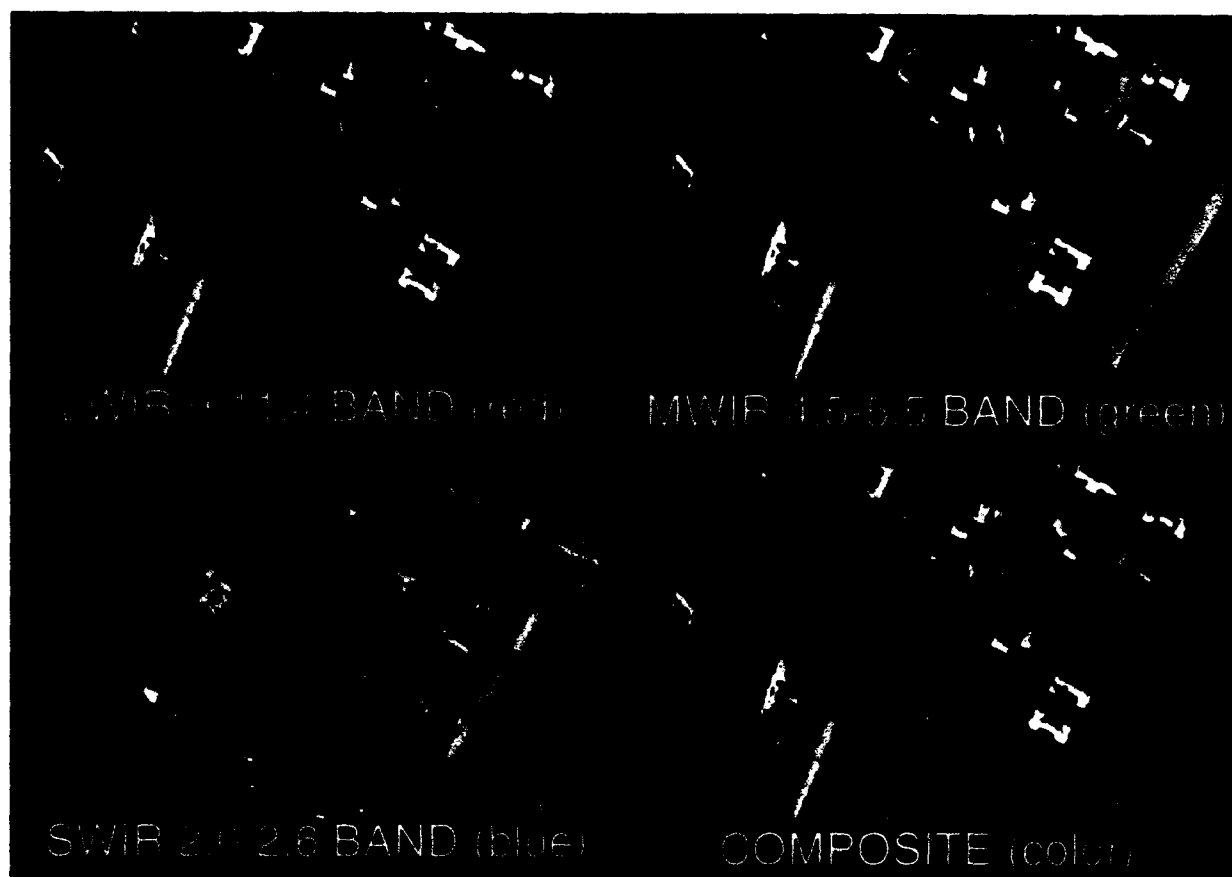


Fig. 1 — Multiband infrared of Port Hueneme, CA. The three infrared bands are combined by forming a composite "rgb" color image. The imagery contains a 4×6 grid of artificially inserted aircraft.

filter (3-D spatio-spectral) is derived by considering the target and the background as a 3-D space with the third dimension being the spectral values at each pixel.

A rigorous analysis of target detection is usually based on receiver-operator curves (ROC), in which detections and false alarms are compiled based on varying levels of threshold settings. To compare color vs spatial processing, Fig. 2 shows ROC curves corresponding to thresholding of the outputs of the matched filters applied the images seen in Fig. 1 containing inserted targets. The various points along each ROC curve correspond to different threshold settings. Data are shown for spatial-spectral processing of the composite color image (solid curve), spatial processing of the LWIR image (dashed curve), spatial processing of the MWIR image (dotted curve), and spatial processing of the SWIR image (dot-dash curve). If it is desired to have the number of missed detections

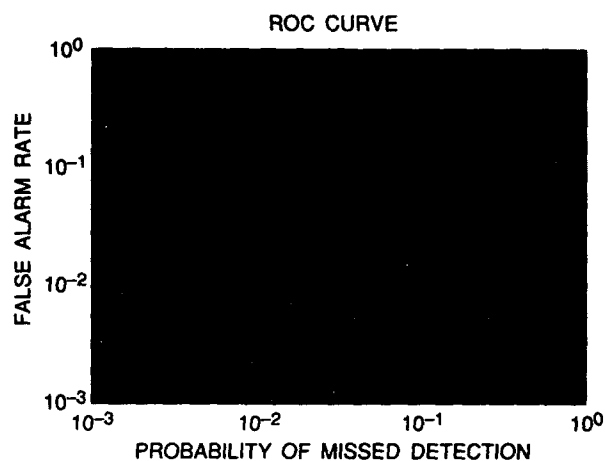


Fig. 2 — False Alarm Rates vs Probability of Missed Detections for artificial targets embedded in the Port Hueneme data

equal to the number of false alarms, then this corresponds to a line drawn from the lower left corner to the upper right corner of the ROC

curve figures. For equal values of missed detections and false alarms, the composite spatio-spectral filter yields a factor of 5 to 20 improvement over the single-band, spatial-only processing.

Similar improvements in target detection have been demonstrated by using other images and target colors. Significantly greater improvements are observed by using spectral bands that are optimized for the particular targets and backgrounds of interest. Spectral bands for optimal detection depend on target signature, backgrounds, solar conditions, and other variables and are yet to be determined for practical problems. Measurements to determine subclutter detection limits must be performed with color IR sensors having good spatial registration, proper spectral bands, and low noise.

[Sponsored by ONR] ■

Flying Radar Target (FLYRT) — Testing and Final Demonstration

C.S. Bovais, C.J. Murphy, and P.L. Toot
Tactical Electronic Warfare Division

The Flying Radar Target (FLYRT) Advanced Technology Demonstration (ATD) was a three-year effort to develop and demonstrate an active electronic RF distraction decoy compatible with the shipboard Mk 36 decoy launching system (DLS). This highly successful program combined diverse technologies to meet exacting systems requirements for a distraction decoy. The stowed FLYRT was boosted as a ballistic round from the launcher by a solid-fuel rocket motor and transformed into an autonomous, electric-powered flying decoy.

The FLYRT electronic payload and air vehicle were developed and tested concurrently, then integrated for an at-sea final demonstration. The decoy payload performance and effectiveness were verified in over-the-water captive carry testing in which Naval ships were defended by the decoy against advanced threat simulators. Land-based flight tests confirmed the vehicle's performance and navigation capabilities. During these tests, a complete teleme-

try suite replaced the payload and provided data for thorough analysis of the test results. The performance of the integrated decoy was demonstrated during an at-sea system test on NRL's Chesapeake Bay Detachment test range. An overview of the key technology developments, air vehicle and payload testing, system integration, and final demonstration are presented.

Key Technologies: The vehicle design was limited in velocity to fly at ship-like speeds. Compatibility with the unmodified barrel of the Mk 36 DLS restricts vehicle size. Key technology areas critical to the success of the FLYRT decoy included the development of a low launch acceleration solid-fuel rocket motor; a three-axis fiber-optic gyro (FOG); mechanisms for wing, tail, and antenna deployment; a highly efficient brushless dc electric motor and speed controller; and a vehicle configuration optimized to achieve the required antenna isolation.

Payload Testing: The vehicle and payload were developed concurrently and thoroughly tested independently prior to full system integration. The compact design of the active electronic RF payload allows integration into the limited volume of the FLYRT vehicle. To meet this constraint, the payload uses both solid-state and optical signal processing technology. Initial brassboard prototypes were tested in the laboratory with RF measurement equipment and threat simulators. The results of this testing were used to refine and finalize the payload design. It was then necessary to test the payload in a tactical situation to prove the decoy concept. Captive carry testing was conducted over the water in a realistic defense scenario where the payload, installed in a FLYRT airframe, was suspended from a helicopter (Fig. 3). Several Navy ships were used in the testing as protected assets, and the performance of the payload was fine-tuned to optimize effectiveness.

Vehicle Testing: The FLYRT airframe and its components underwent extensive testing prior to land-based launches and flight testing. As a result of these tests, aerodynamic, electric propulsion, and autopilot performance, mechanism operation, and airframe structural integrity

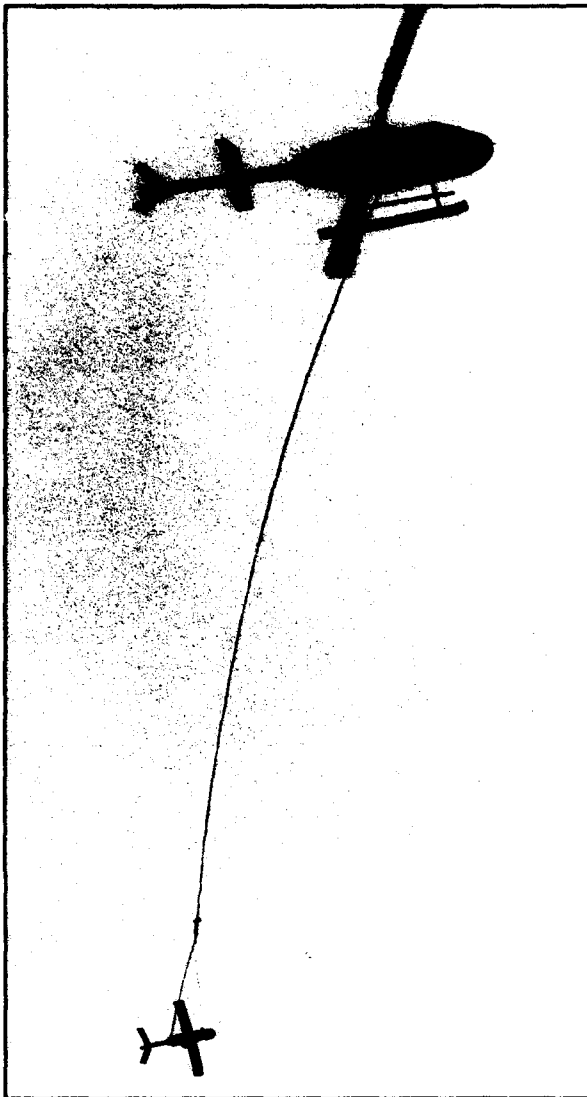


Fig. 4 — FLYRT vehicle in flight

◀ Fig. 3 — Captive carry testing



Fig. 5 — FLYRT
launch from NRL's
LCM-8

were preflight qualified. The first eight live fire tests were conducted to verify rocket motor performance. For these tests, the rocket motor was attached to an instrumented, ballasted tube to simulate the FLYRT airframe. Ten land-based launches of the FLYRT airframe were conducted, based on a step-by-step systems build up to the final vehicle (Fig. 4). This testing method allowed individual system evaluation by limiting the number of unknown variables.

Conclusion: The FLYRT decoy capability was demonstrated on 9 September 1993 during an at-sea test in which Navy ships were defended by the decoy against advanced threat simulators (Fig. 5). The extensive testing of the vehicle and payload prior to system integration proved vital to the success of the final demonstration.

Acknowledgments: The FLYRT airframe and payload were developed in-house by the Off-Board Countermeasures Branch, Tactical Electronic Warfare Division, with support from the Optical Techniques Branch, Optical Sciences Division. The solid-fuel rocket motor was developed by Thiokol Corporation, Elkton Division.

[Sponsored by ONR] ■

The Microwave Monolithic Integrated Circuit/Electronic Warfare Receiver

L.W. Lemley

Tactical Electronic Warfare Division

With the proliferation of microwave monolithic integrated circuits (MMIC) through the Defense Advanced Research Projects Agency (DARPA), it became possible to design and build an electronic warfare (EW) receiver with MMIC chips. The Electronic Warfare Support Measures (ESM) Branch of the Tactical Electronic Warfare Division (TEWD) undertook to design and build such an MMIC/EW receiver. Current technology results in EW radio frequency (RF) receivers that are too large (3,944 cubic centimeters), too heavy (6,124 grams),

require too much power (86 watts), and cost too much (\$120,000).

MMIC Technology: In the 1970s, DARPA initiated the gallium arsenide (GaAs) program that made microwave monolithic integrated circuits possible. GaAs, as a basic material, had a high carrier/hole mobility characteristic that removed the out-of-frequency barrier of commonly used solid-state materials and permitted high-frequency operation. It took nearly 20 years to assemble the necessary tools, experts, technicians, and industrial capabilities to begin producing useful MMICs. The MMIC chips produced were oriented toward utility in the circuits and systems that were most extensively used, expendables for example. Commercial applications, with their attendant use in the millions of chips and low-cost amortization, profoundly influenced production and circuits. Ease of development and production, in turn, has influenced MMIC availability. Once a device is demonstrated, it is copied and prolifically produced by everyone in the MMIC business. Thus, many choices of low-noise amplifiers (LNAs), mixers, and switches are available. The more difficult, less in-demand circuits, such as narrowband filters and broadband voltage-controlled oscillators (VCOs) are less available. Many of these circuits are needed in electronic warfare applications.

Proof of Concept: The Phase I MMIC/EW receiver was designed to demonstrate that a broadband EW receiver could be fabricated with MMIC technology. The MMIC devices were chosen from those available throughout the United States. Many of the devices were just coming out of Joint Venture development. The EW receiver architecture chosen was the most challenging design—a double conversion, broadband, 0.5 to 18.0 GHz, superheterodyne receiver. Simpler architectures could easily have been dismissed as trivial demonstrations. The Phase I MMIC/EW receiver was fabricated to be comparable with current conventional EW superheterodyne receivers. The MMIC/EW receiver has the same or better operating characteristics as current conventional EW superheterodyne receivers (Fig. 6 and Table 1). A



Fig. 6 — Conventional EW receiver, Phase I MMIC/EW receiver, Phase II MMIC/EW receiver

Table 1 — Conventional and MMIC/EW Receiver Characteristics

Characteristic	Conventional	Phase I MMIC	Phase II MMIC
RF range (GHz)	0.5 - 18.0	0.5 - 18.0	0.5 - 18.0
Tune step (kHz)	10	1000	1000
Tune speed (ms)	5	40	40
Noise figure (dB)	12	13	14
Dynamic range (dB)	55	55	60
Image rejection (dB)	70	60	60
IF bandwidth (MHz)	50	40	75
Size (cm × cm × cm)	29 × 17 × 8	20 × 15 × 4	11 × 8 × 1
Weight (grams)	6124	907	138
Power (watts)	86	44	25
Cost (\$)	120,000	60,000	10,000

unique feature of this and subsequent MMIC/EW receivers is the multiple intermediate frequencies (IFs) that are used to avoid images and spurs. Different IFs are switched, depending on the tuned radio frequency (RF). Another unique feature is a power management capability that supplies power only to those circuits in the receiver that are needed to operate at the instantaneous tuned RF. All other circuits are unpowered, thereby reducing the power demand of the MMIC/EW receiver.

Phase II MMIC/EW Receiver: The encouraging success of the Phase I MMIC/EW receiver provided the design and impetus for a Phase II MMIC/EW receiver. In Phase II, MMIC chips were custom built for the EW receiver application by NRL's Electronics Science and Technology Division. Specifically, wideband, high-dynamic-range MMIC mixers were designed and fabricated. In addition, a wideband LNA was modified by Texas Instruments, Incorporated, for the Phase II MMIC/

EW receiver. These and other improvements have resulted in a Phase II MMIC/EW receiver that is an order of magnitude smaller in size, weight, power, and cost, than the Phase I receiver (Fig. 7). The Phase II receiver retains the operating characteristics of the Phase I and current conventional receivers (Table 1). This receiver is a triple conversion superheterodyne architecture with a 160 MHz output. A first local oscillator (LO) synthesizer, having 1.0 MHz resolution, is contained within the receiver package. An input is provided to operate the Phase II receivers coherently, rather than by individually synthesized tuning. Any number of Phase II receivers can be tuned together coherently for multiple-receiver applications.

Control and Display: The MMIC/EW receivers would normally be integrated into a system. They are controlled through an RS-485 bus with capability for multiple individual receiver control. However, each receiver can be controlled through the RS-485 from any personal computer (PC), laptop, notebook, or smaller. The control is accomplished through application-specific integrated circuits (ASICs) that were custom built at DARPA's MOSIS (Metal Oxide Semiconductor Implementation System) Facility. In addition, the same laptop PC can be used to

display the MMIC/EW receiver output through a digitizer card in its expansion slot. Complete control is accomplished through the laptop PC software. This permits unprecedented control and display of the MMIC/EW receiver without additional control/display hardware.

Receiver-on-a-Chip: Although MMIC chips have their limitations, it is now possible to consider a monolithic receiver-on-a-chip. The MMIC chips used in the EW receivers to date are single-circuit chips. The MMIC program is beginning to think about multi-circuit chips. It would be difficult to put together a monolithic chip with all of the circuits represented in the Phase II MMIC/EW receiver. Perhaps it is not even wise to have all of that capability on one chip. In many cases, only certain aspects of that capability are used or wanted. The yield of larger MMIC chips decreases with size. However, with some compromises in performance, it is now possible to envision an MMIC/EW receiver-on-a-chip. The fewer number of MMIC chips results in even lower cost and higher EW receiver availability.

Acknowledgments: The MMIC/EW Receiver is funded by OCNr under PE 0602740N and the National Security Agency's Tactical

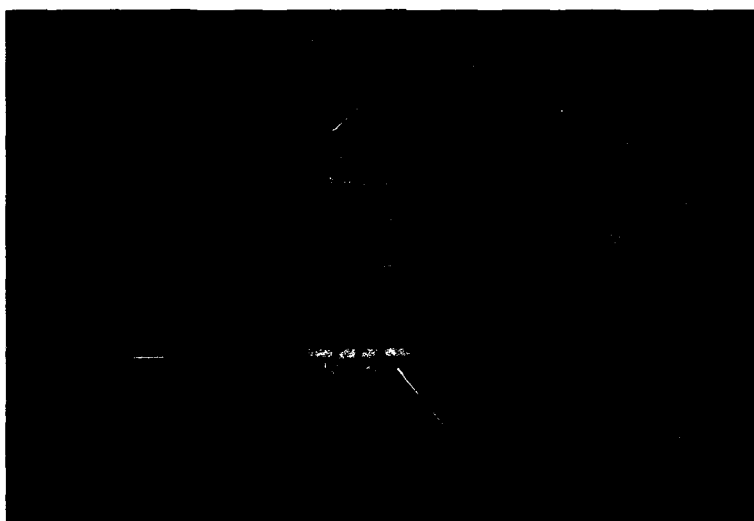


Fig. 7 — Phase II MMIC/EW receiver components (for size comparison, conventional paper staple)

SIGINT Technology Program. Dr. Stanley Gontarek, OUSD (AT), and Dr. John A. Montgomery, TEWD superintendent, provided significant encouragement in pursuing the MMIC/EW receiver. Drs. Denis Webb and Kenneth Slager, NRL/ESTD, helped in the development of custom MMIC mixers. William Caplan and Philip Griffith, Kaman Sciences, provided fabrication support for the MMIC/EW receivers.

[Sponsored by ONR/NSA]

References

1. E. Cohen, ed., "MMIC from the Department of Defense Perspective," *IEEE Trans. Microwave Theory Tech.* **38**(9), 1171 (1990).
2. L.W. Lemley, "MMIC/EW RF Receiver (Monolithic Microwave Integrated Circuit/Electronic Warfare)," NRL Memorandum Report 5720-93-7190, May 13, 1993. ■

The Ionospheric Focussed Heating (IFH) Experiment

P.A. Bernhardt
Plasma Physics Division

For purposes of communications and understanding the physics of the upper atmosphere, NRL has been conducting experiments involving ionospheric modification. Artificial disturbances in the ionosphere can be produced by high-power radio waves and chemical releases. A new technique has been developed in the Plasma Physics Division to greatly enhance the power density of electromagnetic waves from ground-based transmitters. This technique, called ionospheric focussed heating (IFH), extends the electric field strengths of radio waves in the ionosphere beyond all previous levels. IFH uses a chemical release from a rocket or satellite to produce a large lens in the ionosphere. A powerful beam of electromagnetic waves from a ground-based transmitter is made even more powerful by the focussing action of this lens.

The Artificial Lens: A large-scale lens is made in the ionospheric plasma by releasing a chemical that attaches electrons. The chemical that NRL has been using in their ionospheric hole-making experiments is halon (CF_3Br), which is commonly used for extinguishing electrical fires. Releasing this chemical into the ionosphere yields a cloud of negative bromine ions in place of the ambient electrons in the ionosphere. The electron attachment is rapid; a 30-km-diameter hole is produced with a 30-kg release. For high-frequency electromagnetic waves, the refractive index inside the ionospheric electron-hole is larger than that in the surrounding electron gas. Consequently, the hole acts like a convergent lens to produce a focal region above the chemical release point. Numerical simulations of this artificial lens show a factor of 100 increase in radio wave intensity.

Experimental Test: The first test of IFH occurred on 30 May 1992. The Ionospheric Focussed Heating (IFH) rocket was launched from the north coast of Puerto Rico during a joint NASA/NRL rocket campaign. The sounding rocket carried an instrument and chemical payload along a trajectory that crossed the intersection of the beams from the 430 MHz incoherent scatter radar (ISR) and the 5.1 MHz high-power radio-wave facility, both located near Arecibo, Puerto Rico. Figure 8 illustrates the relative geometry of the rocket trajectory, high-frequency (HF) radio beam, ISR beam, and chemical release. The release of 30 kg of CF_3Br into the F-region ionosphere at 285-km altitude produced a plasma hole that acted like a convergent lens to focus the HF transmissions. The release occurred 196.3 s after launch. The equivalent radiated power inside the radio beam was raised from 60 MW to more than 6 GW from the focussing through artificial lens.

Plasma wave receivers and electric field detectors constructed by the Charged Particle Physics Branch were under the nosecone of the IFH rocket. After the nosecone was ejected, booms were deployed to measure the disturbance produced by the focussed HF waves. Figure 9 illustrates the spectra of waves in the 0 to 5.5 kHz frequency range (top) and the corresponding electrostatic turbulence downshifted

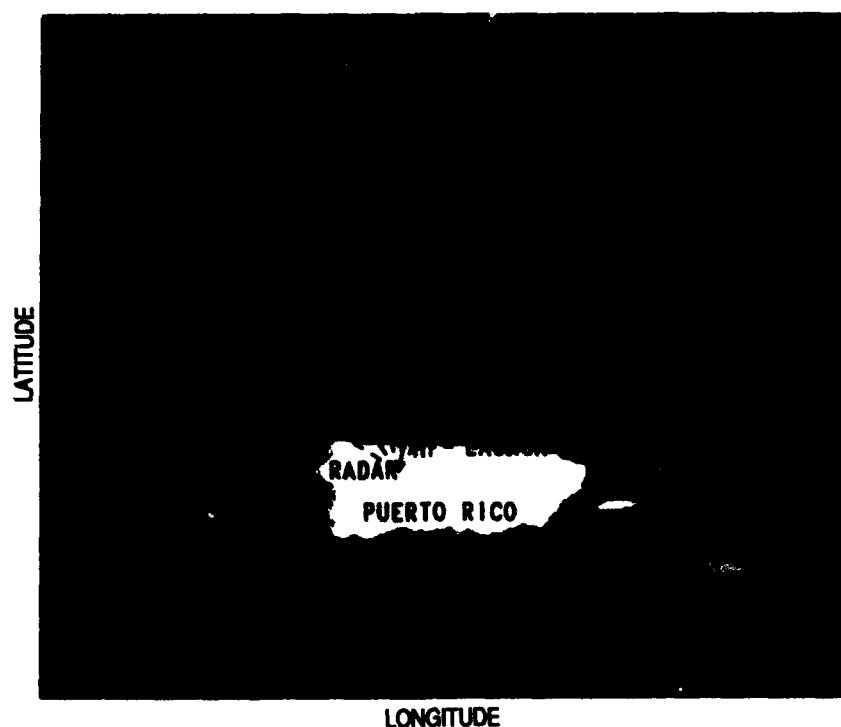


Fig. 8 — Ground projection of the IFH rocket trajectory relative to the island of Puerto Rico. The location of the 5.1 MHz HF transmitter and the 430 MHz UHF radar are also indicated. The CF_3Br release occurred along the trajectory slightly to the east of the HF beam.

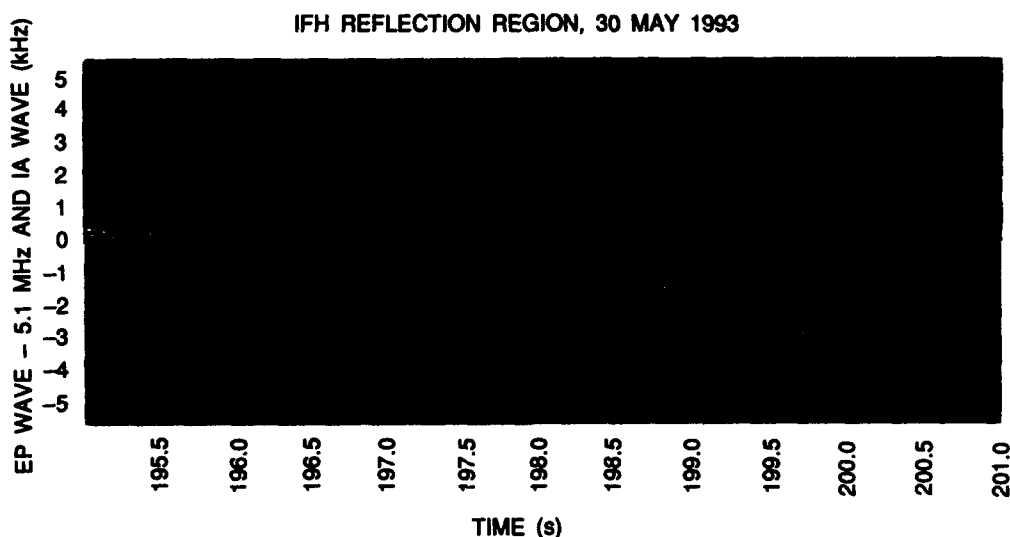


Fig. 9 — Low-frequency ion acoustic waves and high-frequency Langmuir waves near the HF reflection level inside the artificial ionospheric hole. The one-to-one correspondence of low- and high-frequency waves may indicate a parametric process.

from the 5.1 MHz electromagnetic pump (bottom). The time is relative to the launch of the IFH rocket. The close correspondence of these widely separated wave fields indicates a parametric instability in the plasma. Preliminary

interpretation of the data is that the electromagnetic pump wave focussed through the ionospheric hole decayed into a low-frequency ion acoustic (IA) wave and a high-frequency electron plasma (EP) wave.

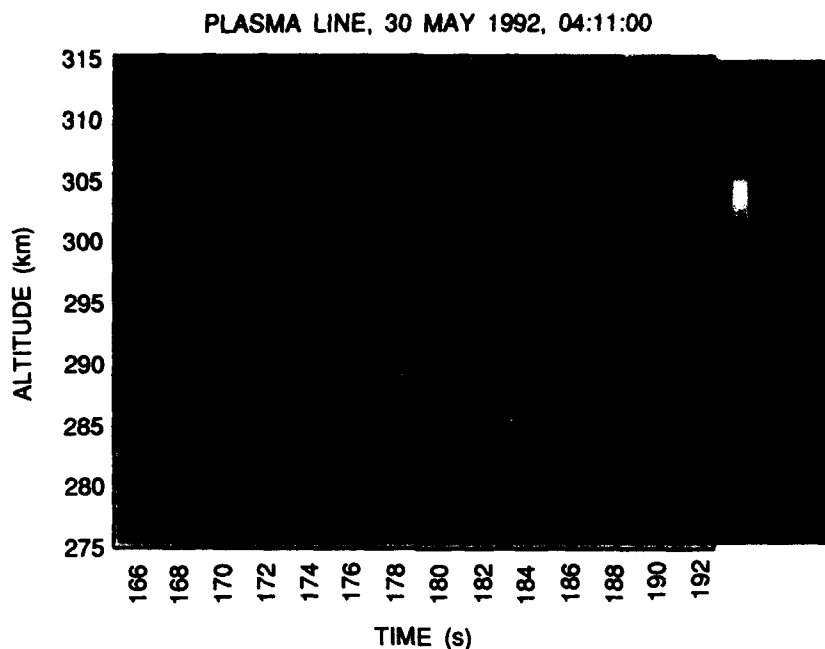


Fig. 10 — Radar measurements of backscatter from electron plasma waves. This "plasma line" shows the HF reflection layer before the release and a brief focal point after release in which the scatter from Langmuir waves is increased by 10 dB.

The 300-m reflector at Arecibo was used as an incoherent scatter radar during the IFH experiment. The 430 MHz Arecibo radar produced pulses to investigate the modified ionosphere. Figure 10 is an altitude-time signature of radar pulses scattered from the electron plasma oscillations generated by the high-power radio waves beam. Prior to the chemical release, the HF pump produced a turbulent, plasma-wave layer near 290 km altitude. Around 179 s after launch, 9 s after the chemical release, a turbulent "hot spot" was formed between 295- and 300-km altitude. The strength of the electron plasma oscillations was enhanced by a factor of 10 at this time. Later as the ionospheric lens became well developed, the strength of the plasma oscillations grew by a factor of 100.

Future: The highly successful IFH experiment has shown that the effective radiated power of any ionospheric modification (HF) facility may be increased by 20 dB by using an artificially created ionospheric lens. Experiments are being designed to repeat the experiment using the 1.2 GW HF facilities located in Tromsø

Norway and the DoD-sponsored HAARP facility under construction in Alaska. This technique will enable experiments to exceed the threshold for a number of nonlinear phenomena in plasmas including stimulation of broadband electromagnetic noise; acceleration of electrons; generation of artificial field aligned striations; and breakdown of the neutral gas.

[Sponsored by NASA and ONR] ■

Control of Interface Properties of GaSb/InAs Superlattices

R.J. Wagner, B.R. Bennett, B.V. Shanabrook, J.L. Davis, J.R. Waterman, and M.E. Twigg
Electronics Science and Technology Division

Motivation: Modern semiconductor devices with unique optical or electronic performance are constructed from stacks of thin semiconductor films. Precise control of film thickness, composition, and doping has been achieved in a number of vapor phase growth techniques, principal among them molecular beam epitaxy

(MBE). This technology has provided an avenue for scientists to create materials that do not occur in nature and exhibit properties that are ideally suited for a particular technological application. As an example of the flexibility of material design that this technology has spawned, recent theoretical work has suggested that repeated strained thin layers (superlattices) of InAs and $\text{Ga}_{1-x}\text{In}_x\text{Sb}$ can be prepared so that photons with energy less than 0.1 eV can be absorbed [1]. This absorption is a necessary condition for infrared detectors operating in the 8-12- μm atmospheric transmission window. Currently, detectors for this spectral region are constructed from the alloy semiconductor $\text{Hg}_{1-y}\text{Cd}_y\text{Te}$. This material is difficult to grow and easily damaged in device preparation. Therefore, $\text{Ga}_{1-x}\text{In}_x\text{Sb}/\text{InAs}$ superlattices could provide a more flexible and reliable material system from which to construct infrared detector focal plane arrays. However, before such technological breakthroughs can occur, it must be proved that it is feasible to construct this superlattice with advanced growth techniques.

Growth of GaSb/InAs Superlattices: We have used MBE techniques to prepare $\text{Ga}_{1-x}\text{In}_x\text{Sb}/\text{InAs}$ superlattices and have explored a variety of applied and basic science issues. Of

particular interest is the fact that the interface between the GaSb film (all that follows applies to $\text{Ga}_{1-x}\text{In}_x\text{Sb}$ as well; for experimental simplicity, the work we describe here emphasizes GaSb) and InAs can be formed in two different ways. As shown in Fig. 11, the interface can either be InSb-like (left panel) or GaAs-like (right panel). The goals of our work have been to create samples with either InSb-like interfaces or GaAs-like interfaces, to invent probes that are sensitive to the differences in interface type, and to quantify the influence of the different interface type on the optical, structural, and vibrational properties.

In the MBE growth process, furnaces loaded with Ga, In, As, and Sb are placed in a high vacuum environment so that beams of atoms (or molecules) emitted from the furnace mouth can impinge on a substrate target and form a semiconductor film. We have calibrated the fluxes from these furnaces so that we know how long it takes to deposit exactly one atomic layer of each of the atomic species. Moveable mechanical shutters, placed at the furnace outputs, permit termination of growth at any time. In this way, we have built up superlattices with controlled numbers of atomic layers of GaSb and InAs and with either InSb-like or GaAs-like interfaces.

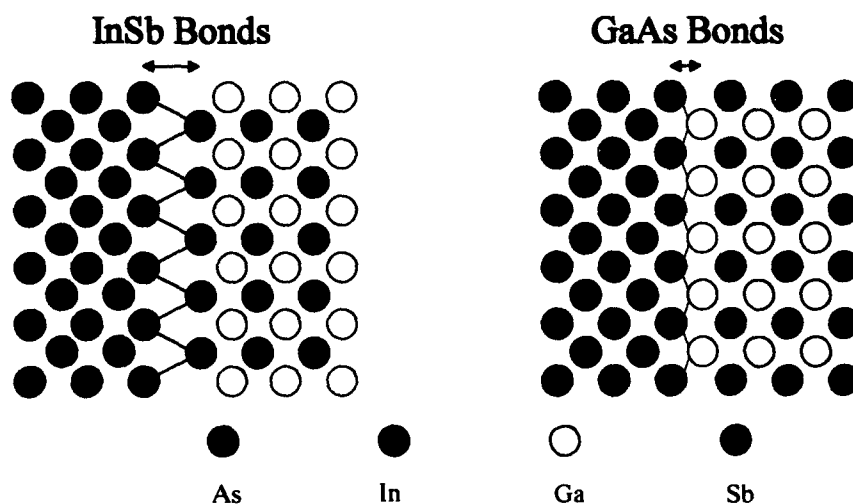


Fig. 11 — The interface between GaSb and InAs can either be formed with InSb-like character (left side) or GaAs-like character (right side). For reference, the lattice constants of GaAs, InAs, GaSb, and InSb are 5.653Å, 6.058Å, 6.095Å, 6.479Å, respectively.

Determination of Superlattice Properties: The interfacial bond lengths for the two types of interfaces will be quite different since the lattice constants of bulk InSb and GaAs differ by 14%. We have shown that these differences have a significant effect on the properties of the superlattices. In Fig. 12, we show that X-ray diffraction measurements are very sensitive to interface type. In this figure, superlattices A, B, and C each consisted of 40 repetitions of 8 monolayers (ML) of GaSb and 8 ML of InAs. However, for A, the interfaces were all InSb-like; for B, they were all GaAs-like; and for C, one half of the interfaces were GaAs-like and the other half were InSb-like. In addition to diffraction peaks due to the GaAs substrate and a thick buffer layer of GaSb, the multiple peaks labelled 0, ± 1 , ± 2 ,... are due to the superlattice. The position of peak 0 arises from the average lattice constant of the GaSb and InAs films *and* the interface (either GaAs-like or InSb-like) layers. Thus the peak shift between the three data sets is a consequence of the difference in interface bond length. The difference

in average lattice constant is in excellent agreement with theoretical predictions.

We have found that Raman spectroscopy can also be used to examine the structural differences between the two superlattice types. Typically this technique has been used to examine the vibrational properties of the major constituents of the sample under study. And, as seen in Fig. 13, the strongest scattering peak in each sample is due to vibrational modes of the GaSb and InAs layers at 236 cm^{-1} . In addition, however, the samples with GaAs-like interfaces have a new vibrational mode at 252 cm^{-1} . This vibrational mode occurs at an energy that is in excellent agreement with theoretical predictions and arises from a vibration that is localized at the planes of Ga and As atoms that make up the interface. Furthermore, we do not see this mode in samples with InSb-like interfaces. This further substantiates that we are able to grow samples with controlled interface type [2].

Direct lattice images obtained with high-resolution transmission electron microscopy also show that GaAs-like and InSb-like interfaces are

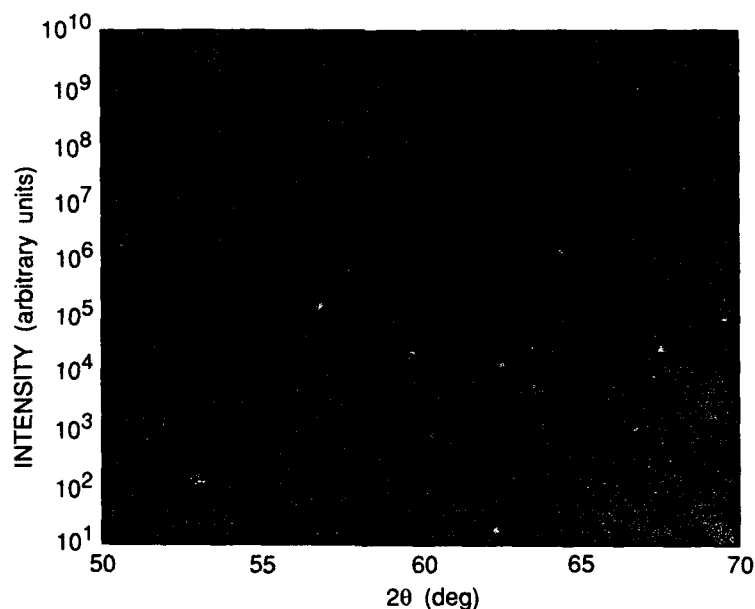


Fig. 12 — X-ray diffraction data for three superlattices, each consisting of 40 periods of 8 ML of GaSb and 8 ML of InAs (2 monolayers per lattice constant). Sample A has only InSb-like interfaces. Sample B only has GaAs-like interfaces. Sample C has alternating InSb-like and GaAs-like interfaces. The position of peak 0 in Sample A is at the average of $+1$ and -1 peaks.

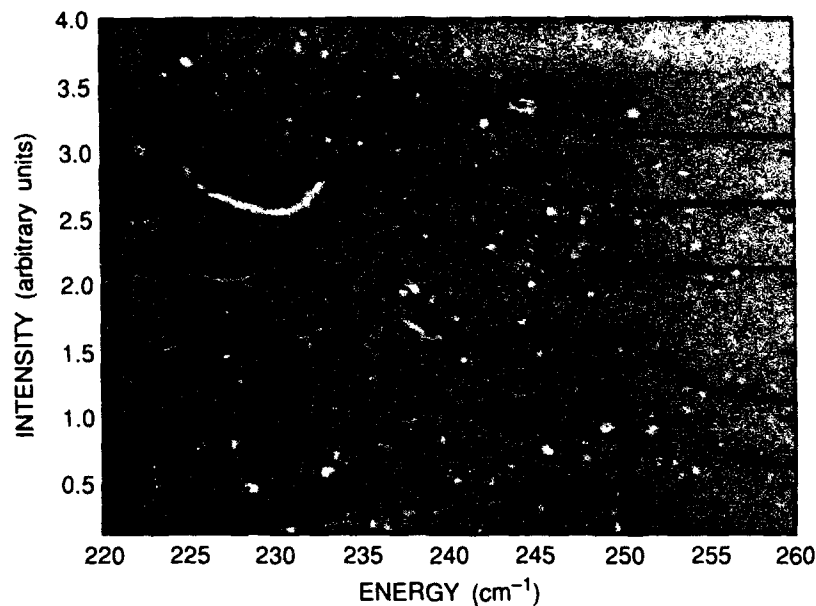


Fig. 13 — Raman spectra for a set of GaSb/InAs superlattices. In the sample designation 12-8-1 InSb, the first number, 12 in this case, refers to the number of InAs monolayers; the second number 8, refers to the number of GaSb monolayers.

distinguishable. Finally, we have shown with a number of infrared spectroscopic techniques that the interface structure can change the superlattice energy gap as much as 50 meV; this is a substantial shift when compared to a total band gap of 100-200 meV.

Summary: From this work we have learned that MBE growth techniques can be used to form either GaAs-like or InSb-like interfaces in GaSb/InAs superlattices. Further work will address the role of the interface bond type in determining the electronic and optical properties relevant to the use of these materials as high-performance infrared detectors. Although our work has not yet established that $\text{Ga}_{1-x}\text{In}_x\text{Sb}/\text{InAs}$ superlattices will be useful as infrared detectors, we have determined that

interfacial properties will play a large role in exploiting this material system to our technological advantage.

[Sponsored by ONR]

References

1. D.L. Smith and C. Mailhot, "Proposal for Strained Type II Superlattice Infrared Detectors," *J. Appl. Phys.* **62**, 2545 (1987).
2. B.R. Bennett, B.V. Shanabrook, R.J. Wagner, J.L. Davis, and J.R. Waterman, "Control of Interface Stoichiometry in InAs/GaSb Superlattices Grown by Molecular Beam Epitaxy," *Appl. Phys. Lett.* **63**, 949 (1993). ■

**ENERGETIC
PARTICLES,
PLASMAS,
AND
BEAMS**

- 153 **Missile Hit-Points on the D7G-53**
Dale A. Zolnick and Harold L. Toothman
- 154 **Capillary Optics for X-ray Lithography**
Charles M. Dozier, Michael I. Bell, and Dan A. Newman
- 156 **Ultra-Intense Laser Physics Research at NRL**
Phillip A. Sprangle, Antonio C. Ting, Eric H. Esarey, and Jacob Grun
- 159 **HRT's Ultraviolet Observations of a Solar Active Region**
Kenneth P. Dere, Clarence M. Korendyke, and Guenter E. Brueckner
- 162 **LIDAR Backscatter from a Rocket Plume**
T. Charmaine Gilbreath, Anne R. Peltier, and Anne E. Clement

Missile Hit-Points on the DDG-53

D.A. Zolnick and H.L. Toothman
Radar Division

Background: All new weapon systems and platforms are required by law to undergo "live fire" testing. The U.S. Navy has begun the process of "live fire" testing for its new *Arleigh Burke*-class destroyer by using the DDG-53. One aspect of this process, which directly relates to overall ship survivability in the modern combat environment, is estimating the damage that would occur *if* the ship were hit by a radar-guided anti-ship missile. Since actually shooting missiles at the real DDG-53 to determine battle damage was not judged to be a viable option, a sophisticated digital simulation system was developed at NRL to generate the realistic missile hit-point statistics for the DDG-53 that are needed to make accurate estimates of battle damage. More specifically, as modern radar-guided anti-ship missiles home on a target by tracking the returned radar signal, the digital system for generating hit-point statistics requires advanced techniques for accurately calculating the radar signature of ships (such as the DDG-53). These techniques are also needed to realistically simulate the trajectories flown by anti-

ship missiles (like the Exocet) as they home-in on a ship.

Methodology: As the front end of the simulation system, the Radar Analysis Branch in the Radar Division has developed a set of analytical computer programs to model complex objects such as the DDG-53 and to calculate and analyze their radar signature. Collectively this is called the Radar Target Signature model or simply RTS. Briefly, the RTS model begins with a detailed geometrical description of the ship in terms of a large number of basic geometrical shapes such as polygons, cones, and cylinder that are determined from a combination of design drawings and photographs of the actual ship. The RTS model then identifies all the possible multiple-bounce sequences among the basic shapes in the model and adds them to the geometrical description of the ship. Next, the RTS model calculates the radar signature of ship using high-frequency, scattering center techniques; the total signature of the ship is just the coherent summation of the contributions of each of the individual basic shapes plus the contributions of the multiple-bounce interactions among the basic shapes. For the DDG-53, the geometric description consists of roughly 200,000 basic geometrical shapes (Fig. 1) and

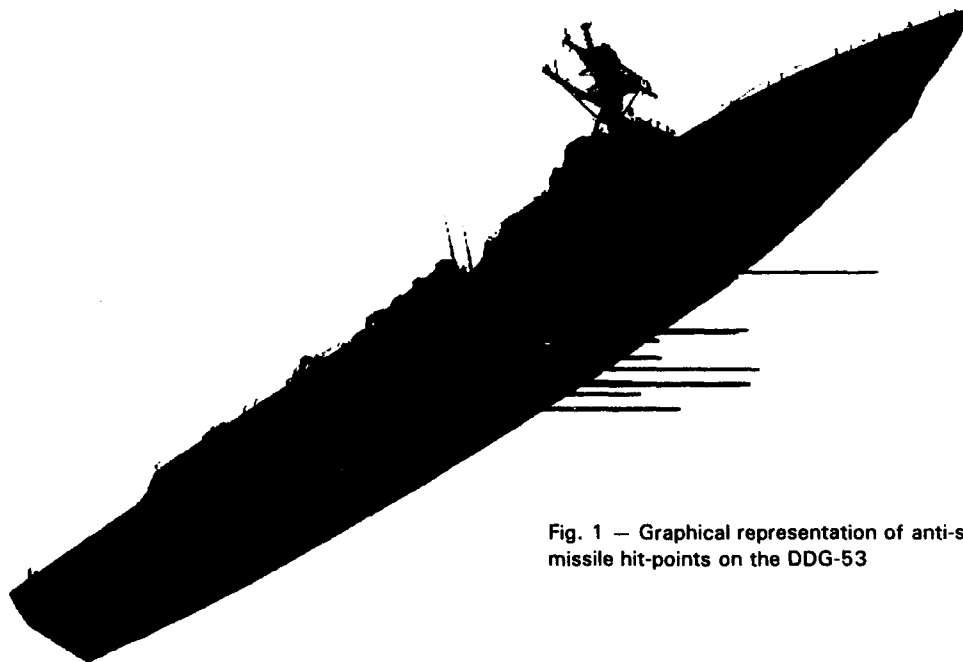


Fig. 1 — Graphical representation of anti-ship missile hit-points on the DDG-53

about 250,000 multiple-bounce sequences. The calculation of its radar signature for a single radar position takes approximately 100 seconds.

As the next step in the process, the Advanced Techniques Branch of the Tactical Electronics Division (TEWD) has developed an electronic warfare simulation program called *CRUISE Missiles*. This program uses the radar return of the target in conjunction with complex models of the missile radar-seeker hardware to determine the actual trajectory followed by a missile as it homes-in on a ship in a dynamic environment with respect to ship motion and sea multipath [1].

Unfortunately, because the *CRUISE Missiles* simulation requires radar signature update rates on the order of milliseconds, the radar signature of the ship cannot be obtained directly from the RTS model. To overcome this problem, a technique was developed by TEWD that uses the results of the RTS model (which, in addition to total radar signature, includes the ordered ranking, locations, and type of all contributors to the signature) to derive a simpler ship representation.

This representation typically consists of around the 1000 largest scatterers plus a carefully formed, discrete background "cloud" to account for the residual signature not represented by the top scatterers. By using the *CRUISE Missiles* simulation, the trajectories of an anti-ship missile can be found for varying launch positions and dynamically changing conditions with respect to ship motion and sea multipath. However, since the simplified model of the ship does not accurately represent the full ship geometry, the missile simulation is terminated after the missile has gone ballistic (i.e., travels in a straight line with no further changes in course or speed) but before it penetrates an envelope enclosing the ship proper.

At this point, the positions and velocities of the incoming missiles are passed back to the RTS model, which uses the full geometric description of the ship to track the missiles to the hit-points on the ship. The hit-point distributions (including terminal velocities) are then transferred to the Naval Surface Weapons Center, Carderock Division, for input into their battle damage assessment model. Additionally,

to more fully understand the results, the hit-points can be graphically displayed on the ship model itself. As an example, a set of fictitious hit-points generated by using a Gaussian distribution in azimuth and elevation about an arbitrarily selected direction are displayed on the actual DDG-53 model in Fig. 1.

Summary: In conclusion, the Radar Division and the Tactical Electronics Warfare Division have jointly developed a digital simulation system to generate accurate, realistic, hit-point statistics for radar-guided anti-ship missiles on actual ships. The simulation system is currently being used as part of the DDG-53 "live-fire" test program.

[Sponsored by NAVSEA]

Reference

1. A.J. Goldberg and R.J. Futato, "*CRUISE Missiles* Electronic Warfare Simulation," 1993 NRL Review, pp.123-126. ■

Capillary Optics for X-ray Lithography

C.M. Dozier and M.I. Bell
*Condensed Matter and
Radiation Sciences Division*

D.A. Newman
SFA, Inc.

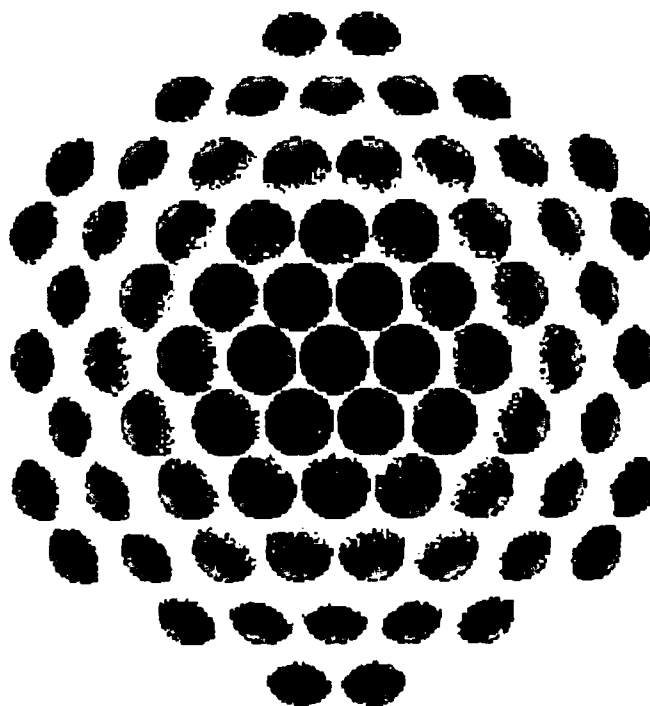
Future Navy systems will require micro-electronic circuits with very small feature sizes. The complexity and packing densities of such circuits are increasing rapidly. Feature sizes of currently manufactured electronic circuits already have submicrometer dimensions; these will approach a quarter of a micrometer in the next few years. Ultimately these features will be less than one tenth of a micrometer in size. If the Navy and our nation are to remain competitive in electronics, the skills and techniques necessary to fabricate smaller and smaller device structures must be developed.

A promising method of producing complex electronic circuits on silicon wafers involves the use of X-ray lithography. Circuit features, carefully imaged on a mask, are replicated onto a resist material, which is then used to fabricate portions of the circuit. Collimation of X rays from small, bright sources probably will be necessary to make this lithographic imaging successful and economical. One practical collimator system makes use of X-ray transmission through glass capillaries. The collimation technique is based on total reflection of the X rays at the interior surfaces of the capillary tubes. Multiple reflections inside the capillaries are used to transport, redirect, and collimate the X rays into a nearly parallel beam with appropriate divergence characteristics to image circuit features on the mask onto the resists.

Work on X-ray transport in capillaries done at NRL several years ago showed the ability of capillaries to transport X-radiation effectively [1]. These results led to work by others who showed that both straight and bent capillaries were useful for X-ray transport [2]. When many capillaries are bundled together, lens-like optics can be constructed so that nearly parallel, collimated beams can be formed.

Significant progress has been made in the design and fabrication of collimating optics. Uniform intensities and a small divergence (5 to 6 mrad) are needed to produce good images on the resist. Capillary diameters, lengths, curvatures, tapering, and tubing materials have significant effects on the intensity and divergence of the output beam. In addition, source brightness, size, and X-ray photon energy are important when coupling the lens into the lithographic system. We have made many ray-tracing calculations and experimental measurements that show the effectiveness of capillary optic designs for X-ray lithography. Figures 2 and 3 show calculated images of the central portion of a 10-cm-long lithographic collimator using 10- μ m diameter capillaries. Figure 2 shows the X-ray output at the end of the collimator where it is not uniform. Because the small divergence in the nearly parallel beams from the individual capillaries fills the image field, it produces uniform illumination of the mask. Figure 3 shows improved beam characteristics nearer to the position of a mask and wafer, 20 cm beyond the end of the collimator. The actual collimator will contain approximately 10^5 to 10^6 capillaries. By using NRL's optical fiber drawing

Fig. 2 — Calculated image of the X rays at the exit of a collimator. After several reflections, the X-radiation collects near one edge of the curved capillaries.



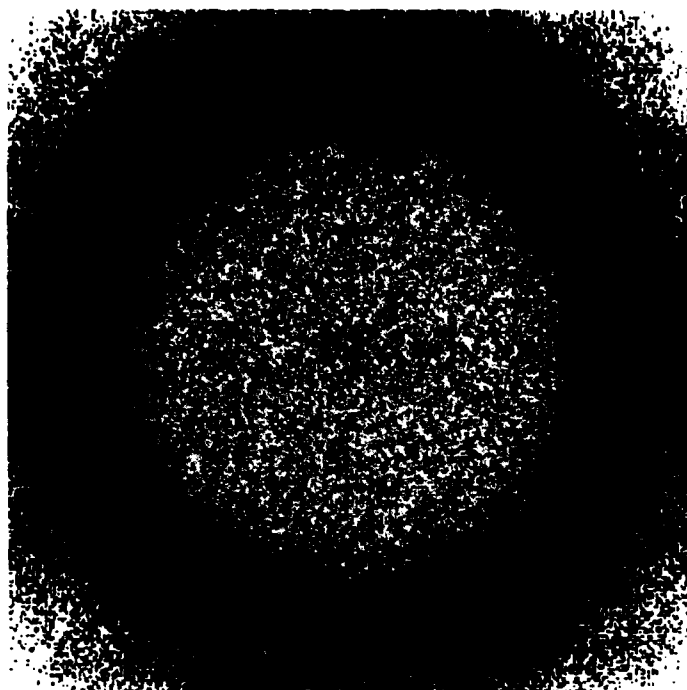


Fig. 3 — Calculated image of the X-ray beam 20 cm beyond the collimator. The small divergence in the beams fills the image area more uniformly.

capability, a prototype monolithic capillary optic has been fabricated. Techniques developed in its production are now being incorporated in the design and construction of more complex lenses using capillaries with 10 to 20 μm diameters.

X-ray transmission measurements of 1-mm-diameter single capillaries for comparison with modelled results are within 10 percent of theory for good quality capillaries. That is, these capillaries have very smooth, mirror-like interior surfaces. Although fabrication by using glass capillaries produces very smooth surfaces, glass is not the optimum reflecting surface for the X-ray photons needed for lithography, which have energies at or just below 1 keV. Additional modeling of the collimators suggest that other materials such as beryllium, boron, or carbon provide better reflecting surfaces than glass. Coating technologies for such small capillaries are currently being investigated.

The Department of Defense expects to have a complete X-ray lithography system ready for insertion into industrial production facilities by the end of 1995. Capillary collimators similar to the ones described here may play an important role in the success of such a system.

[Sponsored by ARPA]

References

1. D. Mosher and S.J. Stephanakis, "X-ray 'Light Pipes,'" *Appl. Phys. Lett.* **29**, 105 (1976).
2. M.A. Kumakhov and F.F. Komarov, "Multiple Reflection from Surface X-ray Optics," *Phys. Rep.* **191**, 289 (1990). ■

Ultra Intense Laser Physics Research at NRL

P.A. Sprangle, A.C. Ting, E.H. Esarey,
and J. Grun
Plasma Physics Division

Advances in laser science have made possible compact terawatt lasers capable of generating subpicosecond pulses at ultra high powers ($\geq 1 \text{ TW}$) and intensities ($\geq 10^{18} \text{ W/cm}^2$). These systems are commonly referred to as table-top-terawatt (T^3) lasers. The nonlinear interaction of ultra intense laser pulses with electron beams, plasmas, and matter is rich in a wide variety of phenomena [1]. The intensities that have been achieved by the NRL T^3 laser

system will form the basis of many exciting experiments in a new regime of nonlinear laser physics. These research areas include diverse subjects such as

- laser excitation of large-amplitude plasma waves (wakefields),
- relativistic optical guiding of laser pulses in plasmas,
- optical guiding in plasma channels,
- nonlinear optics,
- ultra wideband radiation generation for active remote sensing,
- stimulated backscattering from plasmas and electron beams,
- nonlinear Thomson scattering from plasmas and electron beams, and
- new laser fusion and X-ray source concepts.

T³ Laser Systems: T³ laser systems are based on a technique known as chirped pulse amplification (CPA), which was first applied to solid-state lasers in 1985. This technique allows picosecond and subpicosecond laser pulses having micron-range wavelengths to be amplified

efficiently in solid-state laser materials such as neodymium-doped glass, titanium-doped sapphire, and alexandrite (a chromium-doped mineral). In conventional laser amplification techniques, distortions that arise from saturation and nonlinear effects in the solid-state gain medium limit the intensity of the laser pulse. In the CPA technique, this limitation is overcome by taking a low-intensity ultra-short laser pulse, which has a small frequency variation, and stretching the pulse by using a pair of gratings. The pulse spreads because the different frequencies making up the pulse reflect from the grating at different angles. The stretched pulse is then amplified and compressed back to its original pulse length. Stretching the pulse before amplification keeps the intensity below levels that produce distortion effects. Figure 4 is a simplified schematic layout of a CPA laser system based on holographic transmission gratings.

NRL T³ Laser Facility: The Plasma Physics Division has acquired a T³ laser system that became operational in the fall of 1992; its parameters are listed in Table 1. An ideal laser

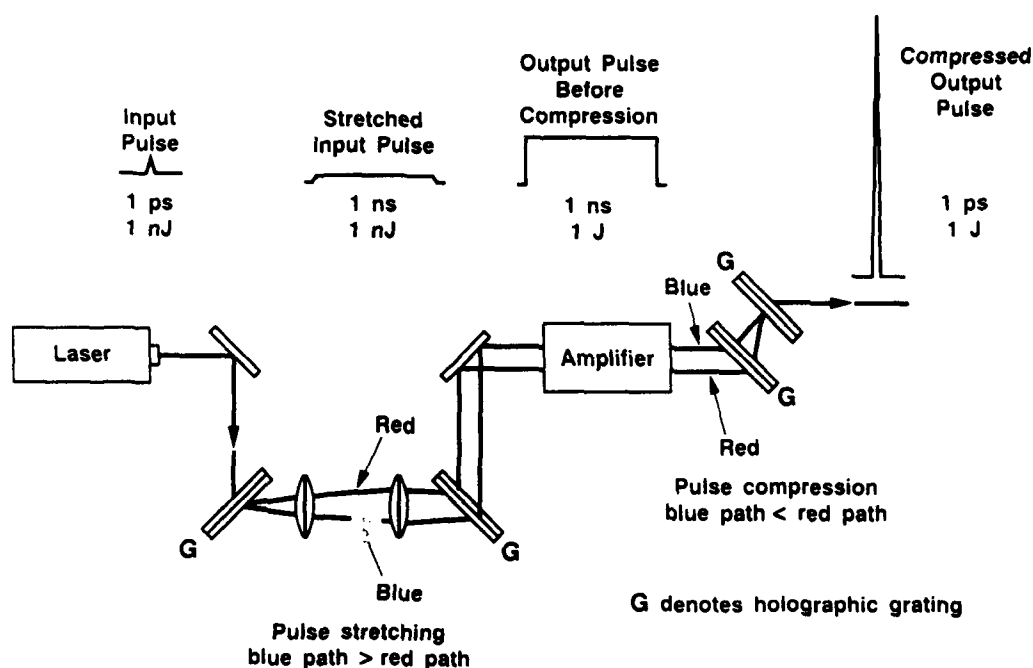


Fig. 4 — Chirped pulse amplification (CPA) configuration using transmission holographic gratings. The NRL T³ laser uses reflecting holographic gratings in its CPA process.

Table 1 — Parameters of the
NRL T³ Laser System

Wavelength	1.053 μm
Pulse power	> 1 TW
Pulse energy	1.3 J
Focused intensity	> 10^{18} W/cm ²
Pulse width	0.8 ps
Rep. rate	1 shot/4 min.
Contrast ratio	> 10^5 :1 (intensity) > 100:1 (energy)
Beam quality	$1.4 \times$ diffraction limit

beam having a Gaussian transverse spatial profile has an angular spread due to diffraction, given by $\Theta_D = \lambda/(\pi r_0)$, where λ is the wavelength and r_0 is the minimum spot size of the beam. If the beam contains higher order transverse modes, the angular spread will be greater than Θ_D . The NRL T³ laser beam quality is excellent at 1.4 times the diffraction limit or, in other words, has an angular spread 1.4 times Θ_D . The laser pulse, because of its high quality, can be focused to intensities greater than 10^{18} W/cm². Figure 5 shows the profile of the laser intensity, with a peak value of 2.2×10^{17} W/cm² and a 1/e full width of 21 μm .

The NRL T³ laser is being upgraded in several stages. The first upgrade, which will be completed in FY94, involves adding a more powerful final amplifier (a 45-mm-diameter neodymium-doped glass rod amplifier) to increase final energy per pulse to ~ 10 J and power to ~ 10 TW. The second upgrade will consist of shortening the 10-J laser pulse from 1 ps to 0.5 ps, thus increasing the power from ~ 10 TW to ~ 20 TW. This second upgrade will be accomplished by changing the amplifying medium of the regenerative amplifier from glass to Ti-sapphire (to increase gain bandwidth).

The Plasma Physics Division is presently evaluating the scientific issues involved in using one of the large amplifying stages of the NRL Pharos laser as a final amplifier for the T³ laser pulse. With a single amplifier from Pharos used to amplify the T³ laser pulse, an output power of ~ 100 TW and intensity of $> 10^{19}$ W/cm² could be generated.

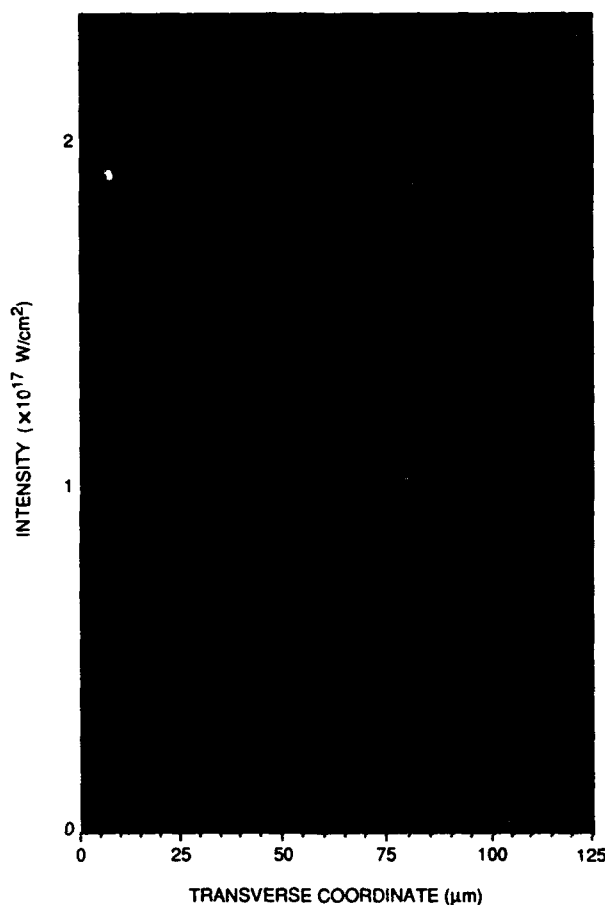


Fig. 5 — Intensity profile from the NRL T³ laser. The peak intensity is 2.2×10^{17} W/cm² and the 1/e full width is 21 μm .

Physics Experiments: The intense laser pulses associated with the NRL T³ laser system can provide the fields necessary to accelerate electrons to high energies in short distances. One of the candidates for such an advanced accelerator is the laser wakefield accelerator (LWFA). In the LWFA concept, an intense laser pulse is injected into a dense plasma. The radiation pressure causes the electrons to bunch behind the pulse, generating a large-amplitude electric field (wakefield), which travels with the laser pulse. The accelerating electric fields in the LWFA have been calculated to be in excess of 10^9 V/cm, which is thousands of times greater than the fields in conventional accelerators. Moreover, the intense laser light can modify the optical properties of the plasma. Relativistic optical guiding can result in the laser pulse

traveling extended distances in the plasma. Electrons could be accelerated by laser-induced wakefields to energies greater than 1 TeV in a distance of a few meters instead of tens of kilometers as in conventional accelerators.

The interaction of intense laser light with plasmas or electron beams can lead to very large frequency upshifts in the scattered light [1]. The scattered light, which can be either incoherent or coherent (depending on the particular properties of the scattering medium) could be a new source of tunable, short-pulse X rays. Ultra-short pulses of tunable X rays have a variety of Department of Defense and civilian applications, including time-resolved spectroscopy and microscopy, time-resolved analysis of fast chemical reactions (including explosions and shocks), material analysis, and biological and medical imaging. If the T^3 laser pulse is back-scattered off an energetic electron beam, the wavelength of the backscattered photons (in units of Å) is $650/(E_b + 1/2)^2$, where E_b is the electron beam energy in units of MeV. Scattering 1- μ m laser radiation off a 3.5-MeV electron beam can produce 40 Å photons (water window), which can be used for biological imaging.

[Sponsored by ONR]

Reference

1. P. Sprangle and E. Esarey, "Interaction of Ultrahigh Laser Field with Beams and Plasmas," *Phys. Fluids B* 4(7), 2241 (1992). ■

HRTS Ultraviolet Observations of a Solar Active Region

K.P. Dere, C.M. Korendyke,
and G.E. Brueckner
Space Science Division

The Sun continues to provide some of the most remarkable demonstrations of the interaction of magnetic fields and highly ionized gases. Solar magnetohydrodynamical (MHD) processes are responsible for a range of phenomena,

including a million-degree corona, solar flares, the solar wind, and eruptive plasmoids. Large-scale examples of the latter are coronal mass ejections, which travel through the heliosphere and often collide with Earth's magnetosphere. One of the underlying constraints of MHD is that the magnetic fields are "frozen-in" to the plasma. This occurs because the coronal gas is so highly ionized that the electrons are essentially free, and the electrical conductivity becomes exceedingly high. In this situation, the MHD equations require that plasmas flow only along magnetic field lines, or, conversely, that magnetic field lines cannot diffuse through the plasma, so that the fields are frozen-in to the plasma. If this were the last word on the dynamics of the solar atmosphere, it would be an extremely dull subject.

Most of the energy that is available to heat the corona, cause solar flares, or eject plasma is available in the energy stored in the Sun's magnetic fields. Only when the requirement that the fields be frozen-in can this magnetic energy be released. The most likely process for converting the magnetic energy into kinetic energy is magnetic reconnection, which produces a change in the topology of the magnetic field configuration. For example, a field line that connects a sunspot with its surrounding active region could, following reconnection, connect the sunspot with a region of magnetic flux entirely outside of its previous active region complex. Further consequences of magnetic reconnection include plasma heating, the acceleration of high-energy particles, and the ejection of plasma—often in an explosive manner. How these three aspects of the reconnection process are accomplished is not well understood, nor are the events that cause the initial breakdown that unleashes the stored energy. Because the MHD of the solar atmosphere is complex and difficult to model except for simple configurations, significant progress can often be made through the study of observations of the physical system in action.

A recent rocket flight of the NRL High Resolution Telescope and Spectrograph (HRTS) was designed to study the solar active region at the solar limb in an ultraviolet wavelength range

(185-265 nm). This wavelength range has rarely been used in the past because of instrument difficulties, but it offers a very useful set of spectral lines for diagnosing the density, temperature, and velocity patterns of the Sun over a wide range of temperatures (10^4 to 10^6 K). The HRTS consists of a 30-cm-diameter telescope, which focuses an image of the Sun onto the slit jaws of the tandem-Wadsworth ultraviolet spectrograph (invented by Drs. Brueckner and Bartoe at NRL).

The solar image is also reflected off the slit jaws and used by the ultraviolet spectroheliograph to form an image of the Sun in the lines of triply ionized carbon (C IV) produced at 10^5 K. Figure 6 shows one of the C IV spectroheliograms obtained during the flight, together with portions of one of the slit spectra showing lines of Si III, Fe II, and Fe XII. The two lines running nearly perpendicular to the solar limb are fiducial wires and help coalign the image with the spectra shown above. The spectra correspond to the plasmas that intersect the curved spectrograph slit, which was nearly parallel to the solar limb. One artifact of the

data can be seen as a sharp jump in intensity just below the slit. This is caused by the use of coatings with different reflectivities above and below this line.

The most intense emission in the center of the image is due to a surge that is being ejected from the Sun at a velocity of about 70 km s^{-1} . Also seen are a large nest of plasma strands and loops, which appear to be in a highly dynamic state. This is confirmed by the motions found in the doppler shifts of the spectra, which are seen as displacements of the line profiles from a straight horizontal line. The plasma structures to the left of the surge show motions on the order of 20 km s^{-1} ; the large flux tubes on the right show supersonic flows of 75 km s^{-1} . One very striking result is the difference between the hot coronal lines such as Fe XII, formed near 10^6 K, and the cooler lines of Si III and Fe II, formed below 10^5 K. The coronal lines do not show the high-velocity motions or the fine-scale structures apparent in the cooler lines.

A time series of C IV images (Fig. 7) shows several rapidly moving plasmas. This active region was not a major producer of

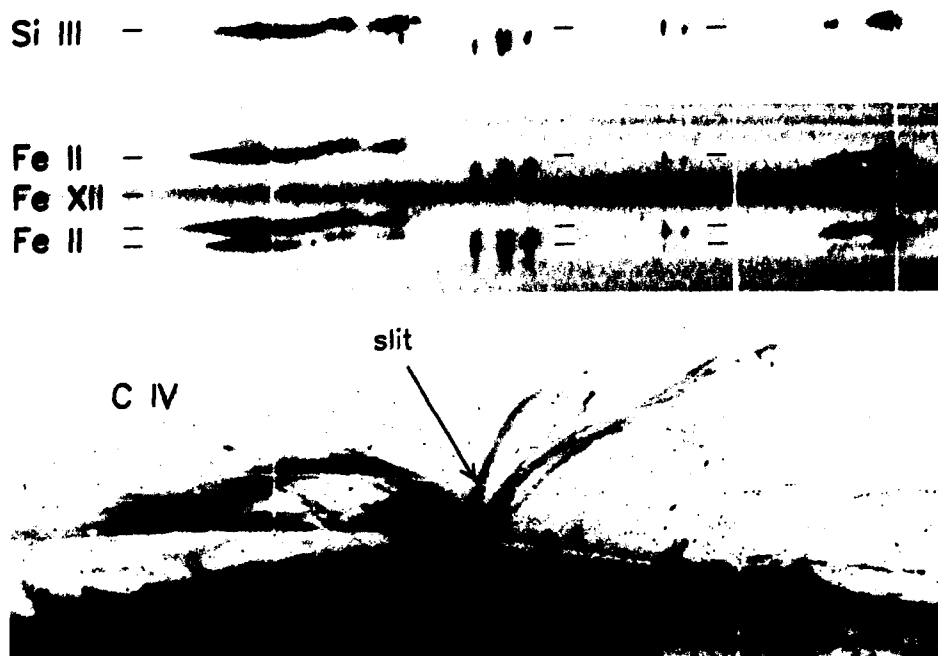


Fig. 6 — C IV ultraviolet spectroheliogram of a solar active region at the limb of the solar disk (bottom), and portions of the ultraviolet spectra of lines of Fe II (1×10^4 K), Si III (4×10^4 K), and Fe XII (1×10^6 K) (top)

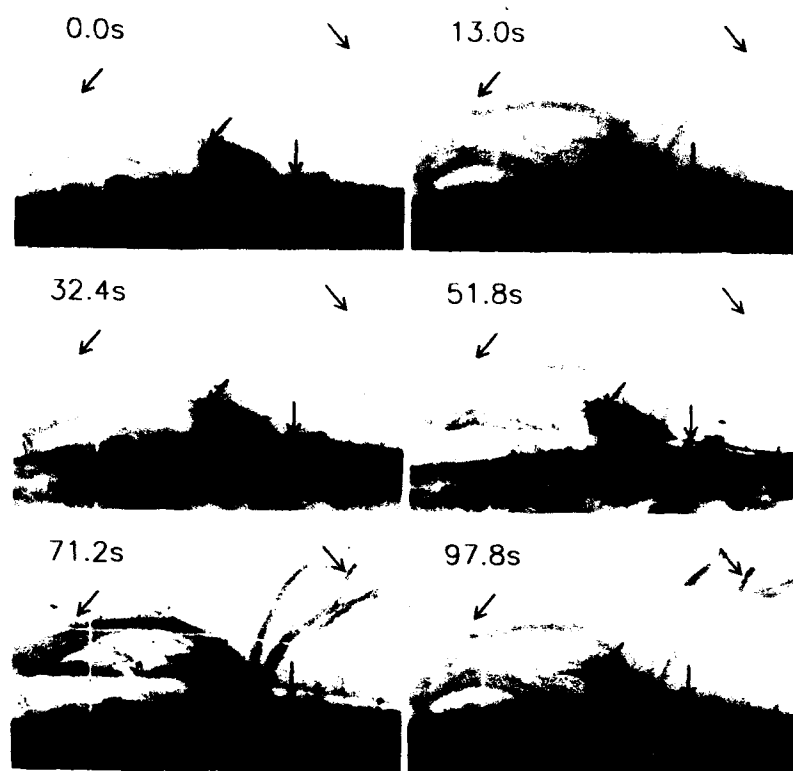


Fig. 7 — Time series of ultraviolet spectroheliograms showing the trajectories of several plasma ejecta

flares, and none occurred within several hours of the HRTS flight. Nevertheless, the continual rearrangement (reconnection) and ejection of magnetic flux tubes was observed for several days as the active region rotated across the solar disk. The elapsed time in seconds is displayed in the upper left corner of each image. The four arrows, fixed in place from image to image, point out rapidly moving structures. At the center is the surge, which has two straight legs that separate and a rapidly moving top that shows considerable fragmentation at the end. For a sense of scale, Earth could just fit between the legs of the surge. At the upper left is a simple plasmoid moving outward at 130 km s^{-1} , with little apparent connection to the rest of the active region. In the upper right, a small, round plasmoid appears to move along a flux tube at 40 km s^{-1} to join up with another stationary plasmoid on the same flux tube.

The HRTS observations demonstrate that a successful explanation of plasma acceleration

must fit a wide variety of situations. We see plasma jets flying unimpeded and intact through a solar active region filled with magnetic flux tubes as well as simple plasmoids accelerated along a single flux tube. The magnetic fields in the surge appear to be almost passive, as if a plasma loop had been grabbed by a shock and stretched beyond recognition. These data make it extremely difficult to interpret the acceleration and ejection of solar plasmas by means of magnetic reconnection, at least in terms of the two-dimensional geometries that are typically envisioned. The observations did show that a high degree of turbulence (not shown in Figs. 6 or 7) was present in the legs of the surge. This is perhaps an important clue because turbulence can produce enhanced resistivity and lead to a breakdown of the frozen-in field condition, allowing the initiation of magnetic reconnection and its consequent release of energy.

[Sponsored by NASA]

LIDAR Backscatter from a Rocket Plume

G.C. Gilbreath, A.R. Peltzer,
and A.E. Clement

Space Systems Development Department

The Naval Research Laboratory and the Air Force Phillips Laboratory, with support from Photon Research Associates, teamed to obtain the first calibrated LIDAR (laser infrared radar) signature from a rocket plume during its trajectory. The plume of the rocket was laser illuminated at a wavelength of 532 nm and was probed during the third stage of its boost phase. Returns were obtained from both the plume and post-boost debris. These significant results provide the plume phenomenology world with the first field test data to assess laser backscatter returns from particulates in rocket exhaust.

Experiment: The experiment was conducted by using the NRL laser ranging system integrated at the Air Force Optical Tracking Facility in Malabar, Florida. The third stage, a Minute Man rocket, was laser illuminated by using a frequency-doubled, Nd:YAG pulsed laser at $\lambda = 532$ nm. The laser had a pulse width of 250 ps and an output energy of 300 mJ, at a 10 Hz repetition rate, with 70 μ rad of divergence. The rocket was acquired, tracked, and its plume laser illuminated in a monostatic mode, using a 0.61-m primary telescope, Transmitter-1 (T1). The rocket was tracked by using a video-driven automatic tracker called the Advanced Modular Tracker (AMT). Figure 8 is a block diagram illustrating how the plume was acquired, tracked, and laser illuminated. The residue from the illuminated rocket fuel was solid and aluminum-based.

Measurements: Data were obtained on a gated Xybion-intensified CCD camera. This camera was gated at 20 μ s and optically filtered at 532 nm with a 10-nm notch filter. The camera was placed in the image plane of a 17.78-cm telescope that was co-aligned with the optic axis of the primary telescope, T1. A second CCD camera was located in the image plane of another 17.78-cm telescope, also co-aligned with the

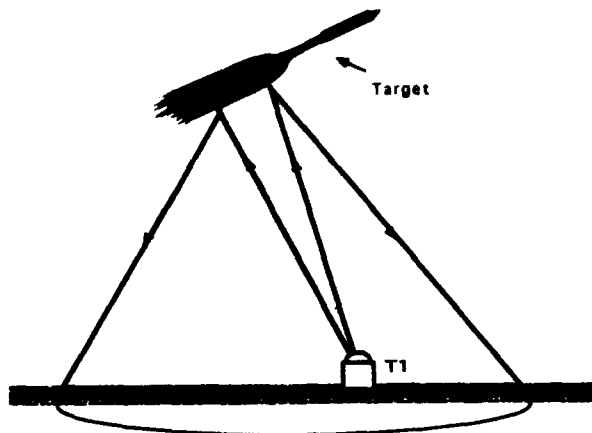


Fig. 8 — Diagram of acquisition and tracking of target using monostatic laser ranging at transmitter-1 during Red Tigress

optic axis of T1, to provide a visual record of acquisition and was used for the AMT. Figure 9 shows the plume illuminated by the laser. Data were obtained throughout the calibrated region on the Xybion-intensified camera from 117 to 135 s time after liftoff (TAL). The calibrated rocket range interval was 117 to 155 km, and the elevation interval was 41.5° to 47.5°. As the separation between the rocket and the laser site increases, the footprint of the laser beam increases, subtending a larger area of the plume. The diameter of the laser beam at the plume varied from 8.2 to 9.5 m over the data acquisition period.



Fig. 9 — Red Tigress plume illuminated by Nd:YAG laser

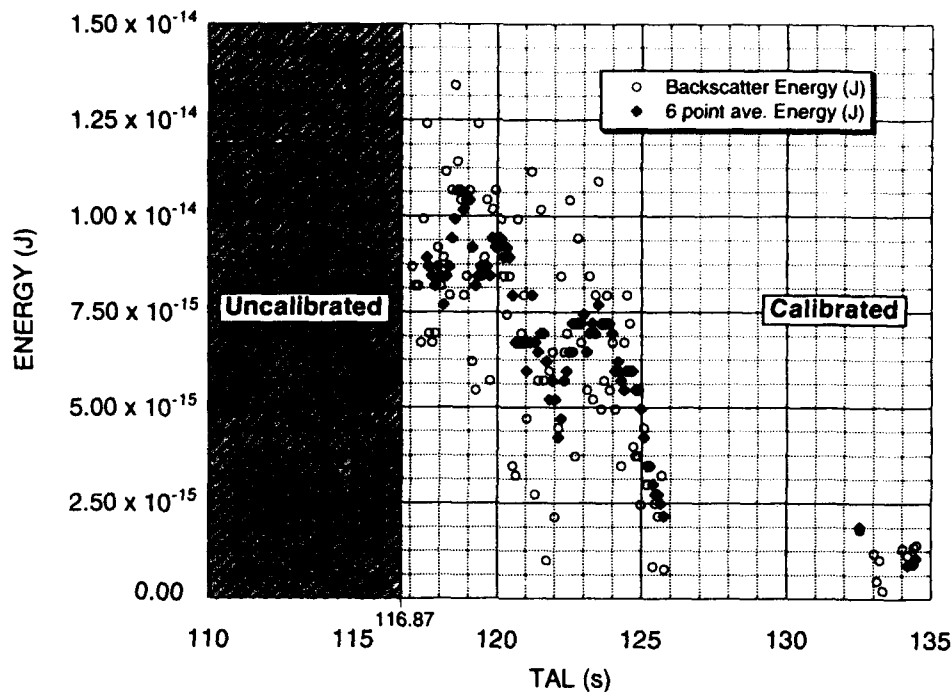


Fig. 10 — Energy vs TAL during calibrated segment of backscatter returns

Results: Figure 10 shows the laser backscatter energy from the rocket plume in the experiment. As can be seen, calibrated backscatter energy varied from 1.8×10^{-15} J to 1.34×10^{-14} J, obtained over a distance of 11 to 19 m from the rocket nozzles. This distance is significant because to date the only other calibrated backscatter that has been reported has been from chamber measurements taken from 1 to 2 m from the nozzles. At ~ 126 s TAL, third-stage engine burnout, the beam was directed toward the nozzles. No backscatter was detected in this region, possibly due to significant reduction in intensity from the Gaussian amplitude envelope of the laser beam. The beam was then directed away from the nozzles, back toward the original region. An interesting result can be seen between 133 to 135 s TAL—the observation of faint returns from the laser. It is possible that these returns are from secondary

rocket and fuel debris. Self-emission from the plume did not contribute significantly to the results obtained.

Acknowledgments: A special thanks to Christopher Falkowski of NRL and M.T. Adams of Photon Research Associates, for their help in data reduction and analysis.

[Sponsored by Ballistic Missile Defense Organization]

Reference

1. C.G. Gilbreath, M. Adams, A.R. Peltzer, A.E. Clement, and H.D. Newby, "LIDAR Backscatter at 532 nm from NRL/PL Field Test Experiment," Proceedings of IRIS Active Systems Symposium, 2-4 November, 1993. ■

**INFORMATION
TECHNOLOGY
AND
COMMUNICATION**

- 167 **Secure Information Through Replicated Architecture (SITRA)
Database System**
 Judith N. Froscher and John L. McDermott
- 168 **Embedded Training Methods for Command and Control Systems**
 Gene E. Layman
- 170 **Historical Perspective on the NAVSTAR Global
Positioning System**
 Ronald L. Beard

Secure Information Through Replicated Architecture (SINTRA) Database System

J.N. Froscher and J.P. McDermott
Information Technology Division

Security requirements are often seen as constraining system performance, and the technology used in secure systems typically lags hardware advances. Future Navy information systems will be more highly interconnected, contain more complex data, and be more accessible to users with diverse backgrounds and clearances. These new systems will need high-assurance, multilevel secure (MLS) database systems (DBS) that will allow more flexible sharing of information in future Navy information systems, without constraining their performance.

Progress in the development of high assurance, multilevel secure database systems has been rather limited because previous approaches provided access mediation to single-level fragments that make up an apparent multilevel database value or object. These single-level fragments were managed by instantiations of a lower-assurance database system at each security level. Because communication between levels introduces covert signaling channels, providing consistent views of and concurrent access to data to users at different security levels has not been entirely correct. Composing responses to users' queries on single-level fragments and decomposing updates to satisfy fragmentation

constraints present both usability and performance restrictions. Because previous approaches rely on porting a database product to a high-assurance operating system, the introduction of new database technology is quite cumbersome and difficult. This article describes an approach that alleviates some of these problems and provides MLS database capability through physical separation and replication. One result has been the development of the first prototype MLS database system with B3 assurance.

The Replicated Architecture: The Secure Information Through Replicated Architecture (SINTRA) project at NRL seeks to achieve a high-performance, fully functional, trusted database management system by applying a new approach to serving users with different clearances [1]. In the SINTRA approach, a database exists for each security level and contains not only data at that level but also mutually consistent copies (replicas) of all data from lower security levels. Users or client programs access only the database at their login security level. Access to these databases is controlled through a high-assurance trusted front-end processor. Because each database to which a user can have legitimate access contains only information for which the user is cleared, untrusted database management systems can provide the database operations. However, when a user updates the database, the update must be propagated securely and consistently to higher level databases. Figure 1 illustrates the basic SINTRA architecture for a simple security-class chain with classes *high*, *middle*, and *low*.

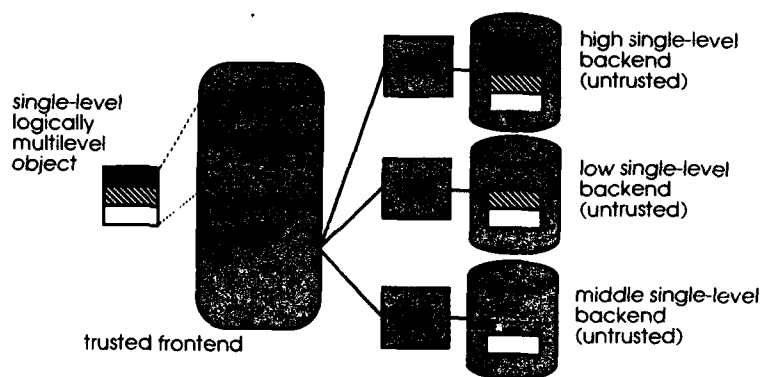


Fig. 1 — Basic SINTRA architecture

Transaction Management: The challenge for this approach is to provide correct replication and allow concurrent access to data without introducing security flaws. The DBS must control update propagation so that users access mutually consistent data at each security level. The criterion for correctness is one-copy serializability and conformance to a Bell-LaPadula security model. Project members have discovered and proved correct eight replica control algorithms [2, 3]. An analytic performance model demonstrates that choice of replica control algorithm does not impact performance for this approach [3].

SINTRA Prototype: The goal of this work is to develop a prototype MLS database management system. Performance, as well as minimization of trusted code and strength of mechanism are important issues for this project. This approach requires less trusted code, provides the opportunity for higher performance through optimization and parallelization on the backend processors, and permits the use of untrusted commercial database systems, without modification. This result strengthens the claim that other kinds of transactions processing systems can be secured through replication. Perhaps the most important lesson learned from the prototype is that security and good performance do not have to be mutually exclusive.

Future Directions: Although the SINTRA project has focused on the relational data model, the replicated architecture can also secure database systems based on other data models. A trusted database system designed around an extended relational model could provide, in addition to the usual relational database system features, management of complex (i.e., nested) objects, management of very-large-scale objects, user-defined types and functions, and user-defined logic-based rules to activate the database. Work in this area would develop an extended multilevel relational data model, algebra, query language, etc., and add these extensions to the SINTRA testbed. An extended relational model database system would provide better support for the more complex Navy command and control applications of the future.

[Sponsored by NSA and SPAWAR]

References

1. J. Froscher and C. Meadows. "Achieving a Trusted Database Management System Using Parallelism," in *Database Security II: Status and Prospects*, ed. C.E. Landwehr (North-Holland. Amsterdam, 1988), pp. 253-261.
2. M. Kang, J. Froscher, and O. Costich. "A Practical Transaction Model and Untrusted Transaction for Multilevel-secure Database Systems," in *Database Security VIII: Status and Prospects*, ed. C.E. Landwehr (North Holland. Amsterdam, 1993), pp. 249-265.
3. J. McDermott. "Transaction Management in Replicated-architecture Multilevel-secure Database Systems," Ph.D. dissertation, George Mason University, 1993. ■

Embedded Training Methods for Command and Control Systems

G.E. Layman

Tactical Electronic Warfare Division

Naval Command and Control training ranges from very high level, coordinated team training that occurs during Fleet exercises down to basic skills taught by training commands. On-the-job training must also be provided afloat and ashore to upgrade job skills and provide instruction for new Command and Control (C2) systems and system upgrades. We are applying novel, embedded training techniques to these various levels of training. A Training Module and a tactical Reconstruction Module have been developed for the Naval Tactical Command System - Afloat (NTCS-A) and are currently being evaluated by several Fleet and system development organizations.

Design: The training software program is included as an integral part of the NTCS-A C2 system and uses the functionality of the system to provide realistic training right on the operational equipment. This embedded training concept requires that the training software program

be able to take control of all the C2 system's functions during the training sessions. By substituting training scenarios for live operational data and controlling the C2 system's operations, the embedded training program is able to present training sessions that appear the same as if they were real, with all of the functionality of the C2 system being available to the trainee for training purposes.

We were confronted with several difficult design challenges:

- support concurrent real-time operations and training sessions within on-line operational systems,
- ensure that the embedded training programs can accommodate new C2 capabilities for future releases,
- provide a simple means to write comprehensive training sessions that can be created by a trainer with no programming experience, and

- provide a way to construct and present briefings of C2 analysis (e.g., reconstructed exercise analysis) performed within the C2 system.

Training Sessions: Training sessions range from simple operations, such as instructing a novice user how to perform a basic system function, up through tactics training involving complex, dynamic scenarios. These training sessions may be conducted at Navy Training commands or aboard any ship equipped with the NTCS-A C2 system.

Figure 2 is a simple example of creating a training session. Here, the Trainer uses the embedded Authoring Program contained within the Training Module to construct a training window that will automatically be recalled for display during a training session. Figure 3 is the display as it will appear to the trainee at that point in the session. In Fig. 3, the training window is in the lower left, and it displays the

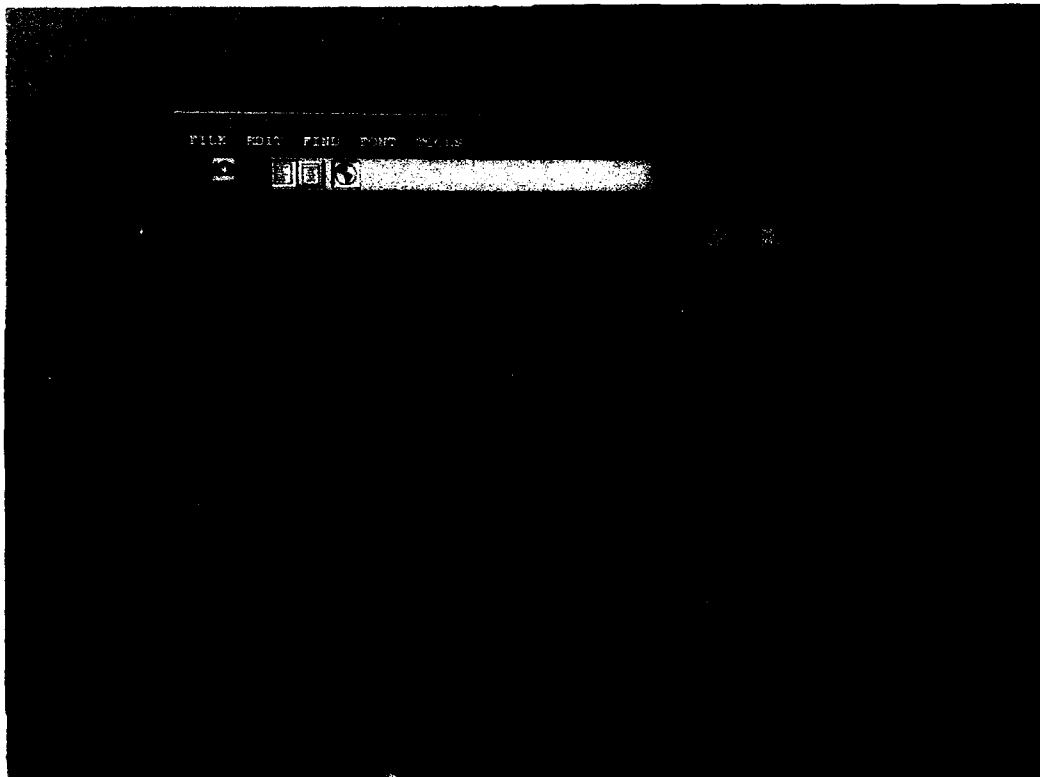


Fig. 2 — Sample training session creation

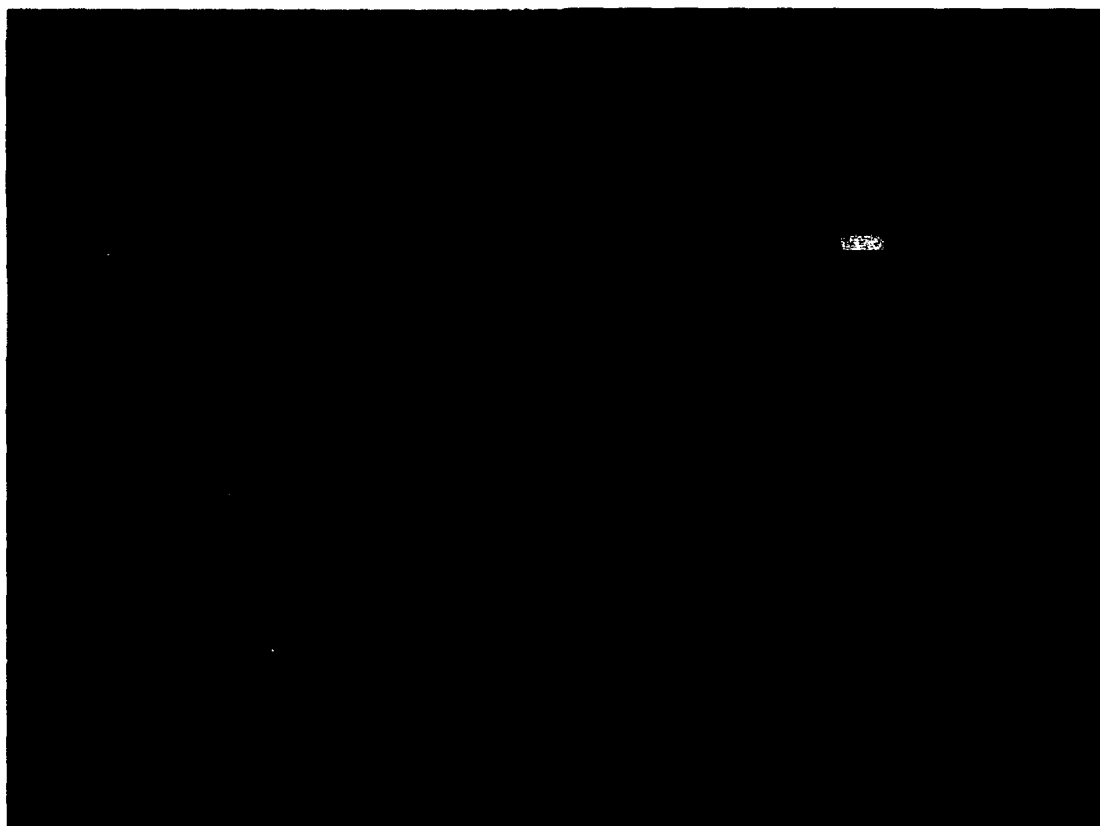


Fig. 3 — Sample training session

end product of the authoring session shown in Fig. 2. The slide inset in the upper left shows the trainee how the created display should look. The map, the function window shown in the upper right, and the track display are NTCS-A functions.

Exercise Reconstruction: The Reconstruction Module provides capabilities to collect and archive data, quickly recall data in ordered form for alphanumeric and/or geographic display for post-exercise analysis, and methods to sort or annotate the material for analytical or formal presentation purposes. Like the Training Module, this module uses the existing NTCS-A system software for collection and analysis. Major features added include a method for archiving tactical data, the control mechanisms for the playback of tracks and events, the means to apply NTCS-A analysis functions to the reconstructed exercise data, and a powerful

presentation capability based on PAL (Presentation and Annotation Language—a fourth-generation, computer-generated authoring language developed at NRL).

Current Research: The next phase of development is underway to incorporate a Simulation Enhanced Exercise Capability to allow simulated friendly and hostile tracks and events to be inserted during Fleet exercises. The Scenario Generator, which produces synthetic tracks for training sessions, will be used to control and insert simulated data into the C2 system. Figure 4 is an example of a dynamic, real-time simulation created with the Scenario Generator that could be inserted into an exercise and controlled through embedded training programs.

Summary: Embedded training methods provide a potential for more effective and



Fig. 4 — Scenario generator

efficient training of personnel who are being prepared to man operational systems. The major advantage is that a trainee can be trained in the shipboard environment on the actual equipment that is going to be used instead of on a generic trainer or stimulator. A significant advantage to the training community is that embedded training provides a tool to create and conduct very realistic training at low cost.

[Sponsored by ONR and SPAWAR] ■

Historical Perspective on the NAVSTAR Global Positioning System

R.L. Beard

Space Systems Development Department

The Naval Research Laboratory was among those recognized in 1993 with the 1992 Collier

Trophy in acknowledgement of more than 20 years of contributions to the NAVSTAR Global Positioning System (GPS). Development of the system concept and early technology demonstrations with the U.S. Air Force Joint Program Office (JPO) and the Aerospace Corporation combined the best aspects of the TIMATION (Time Navigation) project (initiated at NRL in 1964) with the Air Force 621B synchronous navigation satellite project. The multidisciplinary NRL project involved several NRL divisions and a number of contractors in precise clock and spacecraft technology developments. NAVSTAR GPS has become the premier navigation system; it is incorporated into virtually every military system and has many diverse civilian applications.

The TIMATION project, begun in 1964 by Roger L. Easton, evolved from a simplified method of navigation to a high-accuracy, three-dimensional system concept for the Defense

Navigation Satellite System in 1973. In the early 1970s, Department of Defense Navigation Satellite Executive Steering Group investigations of various advanced system concepts led to the formation of the Air Force Space Division Tri-Service Joint Program Office and subsequent GPS concept development. The early development and validation of the system concept encompassed two NRL-built experimental satellites, Navigation Technology Satellites (NTS) 1 and 2 (launched in 1974 and 1977, respectively), an experimental ground tracking network, and the spacecraft cesium and hydrogen maser atomic clock development. NTS-2 was the first NAVSTAR satellite to embody all the technical features now becoming operational. Significant support was provided in precise orbit determination and tracking analysis for the NTS and Rockwell International Block I GPS satellites (starting with the first launch in 1978) by the Naval Surface Weapons Center Dahlgren Laboratory (NSWC/DL).

The TIMATION project's original objective was to speed up and simplify navigation by using passive ranging techniques from low-altitude satellites, rather than by the Doppler measurement technique that had been used in the earlier TRANSIT system. However, passive ranging required an accurate and stable satellite oscillator, since signal time of propagation provides the range measurement. The TIMATION project then concentrated on developing an improved satellite quartz frequency standard, thereby reducing the timing error. A side tone ranging (STR) technique was designed to measure the range between the satellite and the user with simplified receiving equipment. Celestial navigation techniques could be directly used for simple and accurate navigation and time determination. Two experimental low-altitude satellites were built and launched by NRL during this project. The third, which began as TIMATION 3 before the formation of the NAVSTAR GPS Program, was renamed Navigation Technology Satellite One (NTS-1) at launch. This satellite's purpose was to experimentally examine facets of advanced system concepts and an evolutionary concept to bridge the gap between

TRANSIT and an advanced system. The NTS-1 satellite, built and operated by NRL one year after the start of the GPS Program, examined the first two experimental rubidium frequency standards operating in space.

NTS-2, the second GPS technology satellite built by NRL and launched in 1977, contained features used by the Rockwell International developmental, and later operational, NAVSTAR satellites [1]. NTS-2 flew the first two space-qualified prototype cesium frequency standards and led to the operational NAVSTAR satellites production cesium units. The two NTS-2 ranging systems were a TIMATION-type STR subsystem and a NAVSTAR Joint Program Office-provided Pseudorandom Noise Signal Assembly, so that NTS-2 could be operated in parallel by the GPS control stations and NRL-operated stations. The NTS-2 laser retroreflector, which provided precise, independent tracking for ranging accuracy comparison, experienced limited success because of limitations of the then-existing laser tracking network. NTS-2 compatibility with the GPS Control Segment allowed the network to be evaluated before the first NAVSTAR satellites were launched, about a year later. Figure 5 shows various technologies contributed by the NRL program.

After operational system approval in 1979, the NRL Program was redirected to emphasize the key GPS system technology of spaceborne atomic clocks [2]. Results of the first clocks flown showed that clock technology was crucial to the success of GPS, and adequate clocks and sources of clocks were not available. A joint clock technology program was established with the JPO to complete the NRL operational unit cesium development, develop alternate cesium clock sources, develop the new space-qualified hydrogen maser technology, and establish a testing facility where long-term space simulation data on flight clocks could establish a performance and reliability database. As a result, alternate source cesium standards, built by Kernco, Inc., and Frequency Electronics Inc. are currently being flown on NAVSTARs 26 - 32 for validation of operation and qualification of the units.

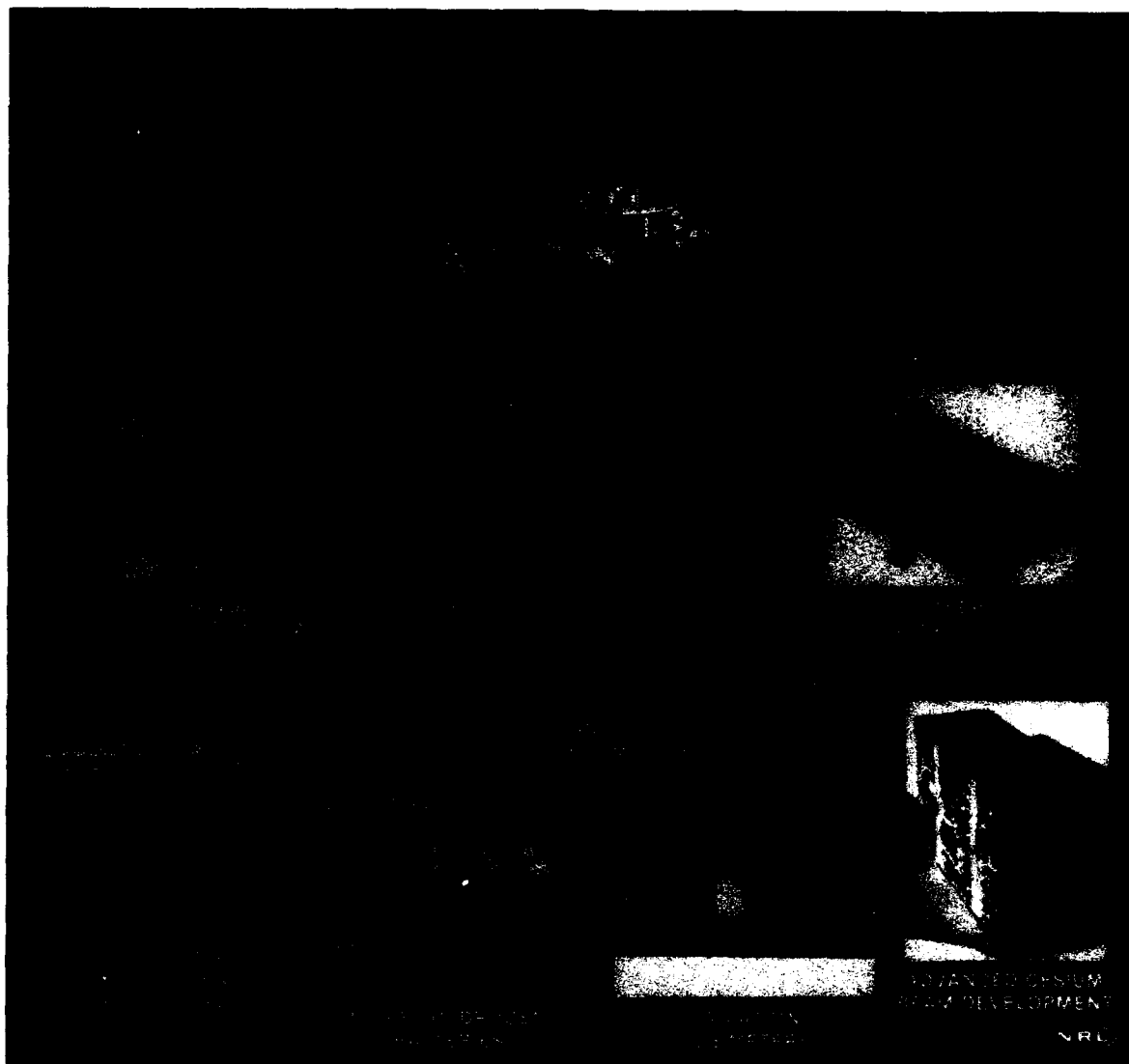


Fig. 5 — NRL GPS Technology Program

NRL continues to support the NAVSTAR GPS program through research and development on space and ground atomic clocks, consultation, and evaluation of these specialized devices for operational Block II satellites and replenishment Block IIR satellites. Special experiments, such as the Laser Retroreflector Experiment launched on NAVSTAR 35 in August 1993, allow independent, high-precision ranging to calibrate the GPS signals and continues NRL's role in GPS advanced technology.

[Sponsored by NAVAIR, NAVELEX, SPAWAR, and Air Force Space and Missile Center]

References

1. R. Easton et. al., "The Contribution of Navigation Technology to GPS," NRL Report 8360, Jan. 1980.
2. R.L. Beard, J.A. Murray, and J.D. White, "GPS Clock Technology and Navy PTTI Programs at the U.S. Naval Research Laboratory," Proceedings of the Eighteenth Annual Precise Time and Time Interval (PTTI) Applications and Planning Meeting, December 1986. ■

**MATERIALS
SCIENCE
AND
TECHNOLOGY**

- 177 **Simulation and Visualization of Ultrasonic Waves in Solids by Using Parallel Processing**
Richard S. Schechter, Henry H. Chaskeles, Richard B. Mignogna and P.P. Delsanto
- 181 **Ultimate Strength of Ultrafine Polycrystalline Materials**
Chandra S. Parule and Robert A. Masumura
- 182 **Element-Specific Magnetometry**
Jos U. Idzerda and Gary A. Prinz
- 184 **Origins of Magnetic Anisotropy in Magneto-optical Storage Materials**
William T. Elam, Vincent G. Harris, and Norman C. Koon

Simulation and Visualization of Ultrasonic Waves in Solids by Using Parallel Processing

R.S. Schechter, H.H. Chaskelis,
and R.B. Mignogna
*Materials Science and
Technology Division*

P.P. Delsanto
Politecnico di Torino, 10129 Torino Italy

The ability to understand wave propagation is important for many scientific areas. Our particular interest is in ultrasonic nondestructive evaluation (NDE), which is based on the propagation of elastic waves in solids. Some analytic solutions exist for certain problems in elastic wave propagation and scattering. However, the ability to model and visualize the full complexity of an ultrasonic transducer radiating into a solid, and the extremely complex wavefield resulting from scatterers, requires a large numerical simulation. The simulation must be both fast, so that large problems spanning many wavelengths may be done, and accurate, to capture the complexity in a real material. To accomplish this, a parallel processing approach has been developed.

Use of the Connection Machine propagation is rooted in two basic ideas. First, physical phenomena described by fields are inherently parallel, in that each field point obeys the same physical law (or in our case, the elastic wave equation). Second, the time evolution of the basic field quantities depends only on their values and those of their immediate neighbors. Based on this viewpoint there is strong motivation for using fine-grain massive parallelism for wave propagation.

Parallel Computer: The parallel computer used in this work is the Connection Machine-200 manufactured by Thinking Machines Corporation. The computer operates in SIMD (Single Instruction Multiple Data) mode. This means that the same instruction stream is

broadcast to every processor. NRL has a 16k processor version of the full CM-200, which has 64k processors.

Computation: The inhomogeneous elastic wave equation governs ultrasonic wave propagation in heterogeneous solids. This form of the wave equation allows spatial changes in material properties and permits a natural conversion to finite-difference equations incorporating internal boundaries. Thus materials with internal structure can be modeled. The resulting difference equations are explicit step-ahead central-difference equations. They have proven to be more accurate than any previously used finite-difference equations for this problem [1] and capture all wave effects in solids such as reflection, refraction, and mode conversion. The form of the difference equations is completely parallel in space variables, and therefore displacements can be simultaneously updated at every gridpoint. Only nearest neighbors in space, corresponding to neighboring processors, are involved, greatly minimizing interprocessor communication (a good condition for speed in parallel computations). The discretization in space is based on a nodes per wavelength requirement, while the size of the time step is based on a stability requirement for the difference equations. The difference equations execute at about 3.8 Gflops on a 64k processor CM-200 machine.

In addition to updating the difference equations in parallel, a parallel graphics device (frame buffer) is used to visualize and create video movies of the developing wavefield, in near computing real time. The entire process of reading the material properties for each cell, feeding the source wave in, updating the difference equations, and displaying the results 1000 times, takes only seconds to several minutes—depending on gridsize. The complexity of the material plays no role in the speed. Thus, once the difference equations are known and expressed in a form suitable for parallel computations, arbitrarily complicated problems in elastic wave propagation can be computed and the accompanying huge data sets visualized in near real time.

Results: The results shown here are images of the scattering of ultrasonic pulses from cracks and inclusions. These cases are of great interest to the NDE community, where detection and sizing of flaws is of the utmost importance. The images shown are gray scale, 256 by 256 pixels, and represent snapshots of the amplitude of the displacement field. Movies have been produced that consist of about 1000 time steps

or snapshots generated in real time as the computation proceeds. They show the dynamic evolution of the entire wavefield, illuminating in detail the formation of all waves that arise in the process of scattering.

Figure 1 shows a series of images or snapshots at four selected times, of a narrow Gaussian pulse of $0.423\text{-}\mu\text{s}$ duration scattering from a crack 5 mm long and .083 mm wide in glass.

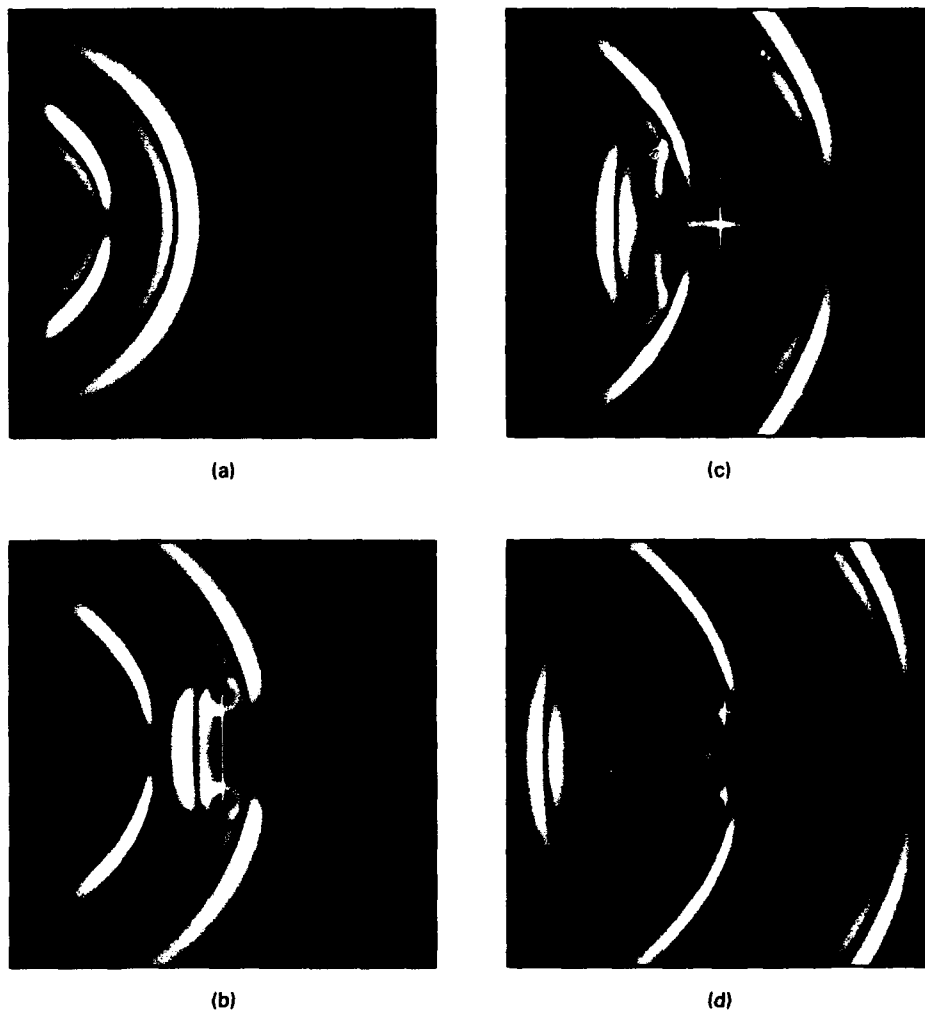


Fig. 1 — Simulated images showing the scattering of a longitudinal ultrasonic pulse from a crack in glass

There is a broad longitudinal wavefront; trailing behind are two smaller shear fronts caused by the finite extent of the pulse. One can see the incident wave scatter off the front crack tip edge and then the back crack tip edge, and the reflected longitudinal and shear waves from the front crack face. The circular longitudinal and shear waves excited at each tip spread out until they later meet and rescatter from the opposite tip. This process of multiple scattering continues. Experimental visualizations obtained

through dynamic photoelasticity using a pulsed laser [2] show a wavefield very similar to this computed image.

Figure 2 shows the experimental images. The differences in the images are due to the fact that the source wave and crack in the simulation are not identical to the experimentally used values. Note, however, the excellent qualitative agreement of the phenomena depicted in the simulation with that shown in the experimental visualization.

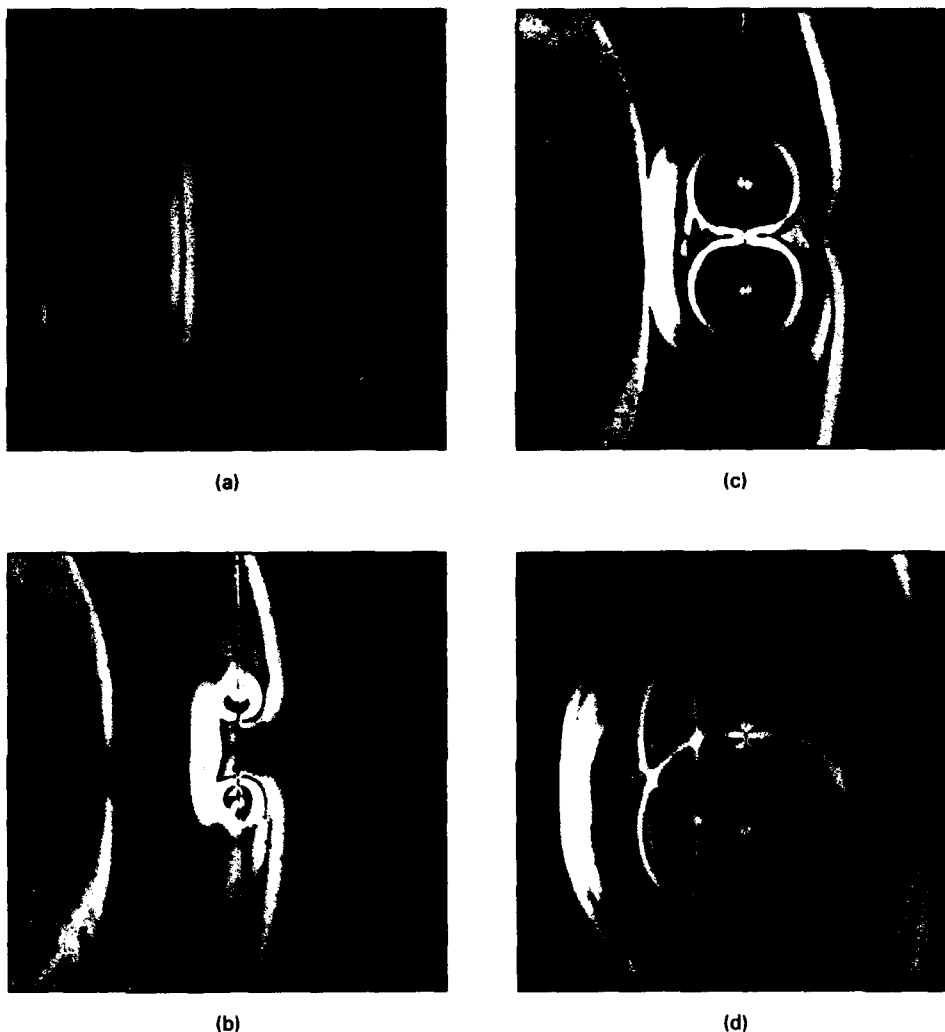


Fig. 2 — Experimentally obtained dynamic photoelastic images of scattering of a longitudinal ultrasonic pulse from a crack in glass

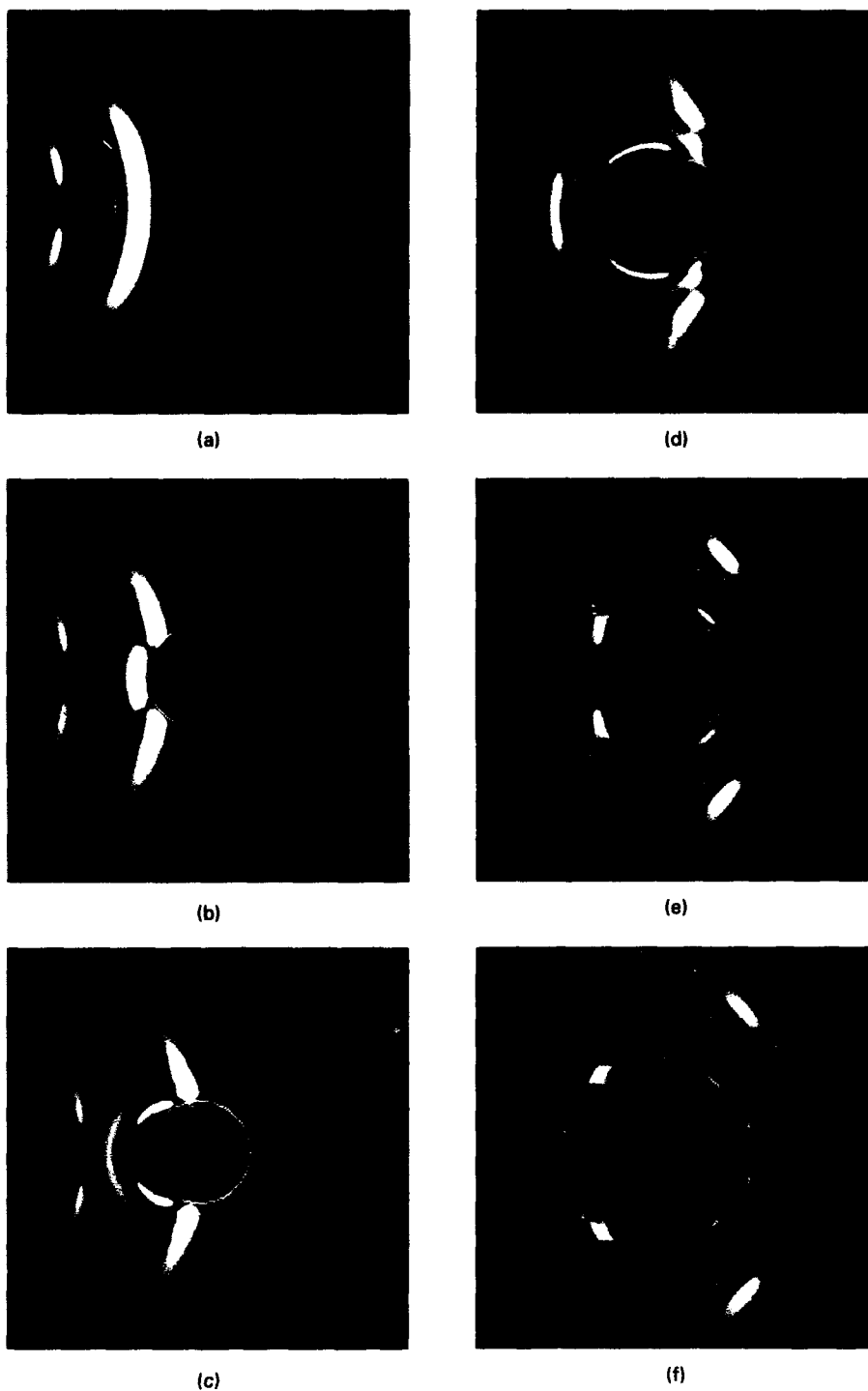


Fig. 3 — Simulated scattering of a longitudinal ultrasonic pulse from a cylindrical aluminum inclusion embedded in plexiglas

Figure 3 shows a series of images of a 1- μ s Gaussian pulse in plexiglas scattering off an aluminum circular inclusion with a diameter of 4.66 mm. There are scattered cylindrical, longitudinal, and shear waves and creeping waves circumnavigating the inclusion. There are transmitted waves penetrating the inclusion, waves creeping on the aluminum side of the circumference, and reflected and transmitted waves at the far side of the inclusion. The scattered wavefield produced by the inclusion is very complicated, with many mode conversions from longitudinal to shear and vice versa. The authors have been unable to find any photoelastic images in the plexiglas of this case. Other cases where experimental visualizations have been found, such as scattering from voids, agree equally as well.

Conclusions: The parallel processing approach described allows many wave phenomena to be investigated very quickly and the resulting huge data sets to be viewed in near real-time. The video taped movies can be of great value in providing insight to the properties of elastic waves. This model is intended to be used with ultrasonic tomographic algorithms.

Acknowledgments: We gratefully acknowledge the Naval Research Laboratory Connection Machine Facility for support and use of its Connection Machine and the ONR Multi-System Materials Program for support. [Sponsored by ONR]

References

1. P.P. Delsanto, R.S. Schechter, H.H. Chaskelis, and R.B. Mignogna, "Connection Machine Simulation of Ultrasonic Waves in Materials II: The Two-dimensional Case," to be submitted to *Wave Motion*.
2. C.F. Ying, "Photoelastic Visualization and Theoretical Analyses of Scatterings of Ultrasonic Pulses in Solids," in *Physical Acoustics: Ultrasonic Measurement Methods*, Vol. XIX, R.N. Thurston and A.D. Pierce, eds. (Academic Press, New York, 1990), p. 291.

Ultimate Strength of Ultrafine Polycrystalline Materials

C.S. Pande and R.A. Masumura
Material Science and Technology Division

For a polycrystalline material, the relationship between average grain size and strength has been known experimentally for several decades, and it has been quantified by using dislocation theory. This relationship (known as Hall-Petch) states that the strength varies inversely as the square root of the grain size. Hence, the smaller the grain size, the greater the strength. It was pointed out that if the Hall-Petch relation were valid for ultrafine grain sizes, the strength of the material could reach the theoretical elastic limit. With the use of recent novel experimental techniques, ultrafine grain materials have been produced whose sizes are smaller than normally used in commercial applications. Thus the central question becomes: Is the Hall-Petch relation in predicting the ultimate strength still valid when the average grain size is of nanoscale dimensions?

Theory: We have therefore re-examined the dislocation theory of strength of polycrystals for ultrafine grain sizes. Although several models of grain strengthening by using dislocations have been proposed, we have considered only the dislocation pile-up since it has been successfully used for the "classical" Hall-Petch model. The mobile or free dislocations on a slip plane are impeded by another locked dislocation at or near the grain boundary. An ever-increasing applied stress (hence greater strength) is needed to overcome the locked dislocation.

The equilibrium position of each free dislocation under an applied stress can be analytically determined and is given by the zeroes (roots) of a generalized Laguerre polynomial. The length L of the pile-up, e.g., the distance from the last to the locked dislocation, can be identified with the grain size. For large number of dislocations, $n > 20$, L can be obtained numerically or as an asymptotic formula. However for $n < 20$, an explicit relationship is required. This has been accomplished by using a property of Laguerre polynomials [1]. This

leads to a relationship between grain size and number of dislocations of any grain size. When combined with an appropriate condition for failure, the desired functionality between grain size and strength of the polycrystal is obtained. Figure 4 shows the results of our calculation for small grain sizes together with the "classical" Hall-Petch relation. There is an increase in strength with a decrease in grain size, as expected. However, in agreement with experiments the calculated results are lower than given by the usual Hall-Petch relation.

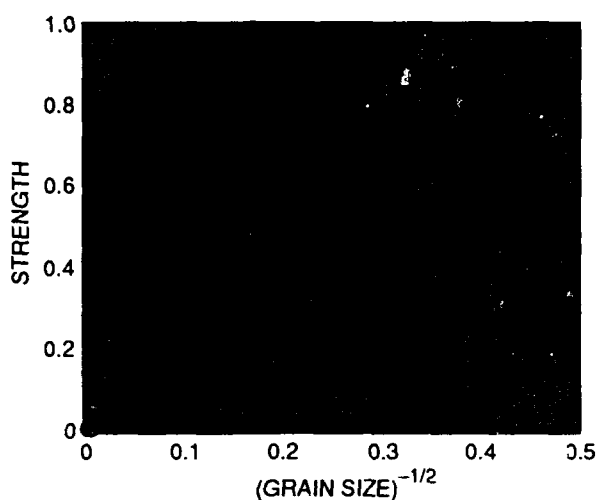


Fig. 4 — Comparison between ultrafine material and classical Hall-Petch relation (both strength and grain size are in normalized units)

This calculation should apply as long as the interior of the grains are able to sustain dislocations. For even finer grains, the dislocations can only move on grain boundary interfaces. Preliminary calculations indicate that in that situation the strength of the polycrystal can in fact decrease on further grain refinement [2].

Discussion: On the basis of these considerations, we predict that the plot of strength as a function of grain size should have three different regions: (1) a region from single crystal to grain size of about a micron where the classical Hall-Petch is valid; (2) a region of grain sizes ranging from about a micron to a few nanometers where the strength is less than that predicted by the Hall-Petch relation; and (3) a

region of ultrafine grain sizes where further grain refinement may actually decrease the strength of the material.

In recent years, experiments have shown the increase of the strength by grain refinement for a wide group of materials. However the measured strength is always less than that predicted by the classical Hall-Petch relation; in some cases where the grain sizes are extremely fine, a decrease in strength has been observed.

[Sponsored by ONR]

References

1. C.S. Pande, R.A. Masumura, and R.W. Armstrong, "Pile-up Based Hall-Petch Relation for Nanoscale Materials," *Nano-Structured Materials* 2(3), 323 (1993).
2. A.G. Evans and J.P. Hirth, "Deformation of Nanoscale Cermets," *Scripta Metallurgica et Materialia* 26(11), 1675 (1992). ■

Element-Specific Magnetometry

Y.U. Idzerda and G.A. Prinz

Material Science and Technology Division

The most traditional and informative characterization tool for magnetic materials is magnetometry—the measurement of the size of the magnetic moment as a function of an applied magnetic field. Currently all magnetometry measurements reflect the total, average moment of the entire sample. By using soft-X-ray magnetic circular dichroism (MCD) [1], we have developed a method to obtain independent magnetometry measurements (magnetic hysteresis curves) for each element in a heteromagnetic overlayer, multilayer, and alloy with limited spatial and variable depth resolution [2]. This new technique measures the difference between the X-ray absorption of left- and right-circularly polarized soft X rays (positive and negative helicity photons) at the 3d-electron transition metal L_3 and L_2 absorption white lines. This difference is proportional to the average moment of that particular transition metal in the

region illuminated by the small-spot X ray. Helicity-dependent X-ray absorption spectroscopy (XAS) spectra can be measured in a changing applied magnetic field by a fluorescence yield method [2], and the total magnetic hysteresis curve measured by classical techniques can be dissected into independent curves. These curves are associated with each different magnetic element in the sample. These measurements are made at the AT&T Dragon monochromator of the National Synchrotron Light Source, which is capable of simultaneously generating high fluxes of circularly polarized soft X rays of both circular polarizations.

Heteromagnetic Trilayer Film: To demonstrate the utility of element-specific magnetometry, we have measured the element-specific hysteresis curves and compared them to the total hysteresis curve for a multilayer sample consisting of a Co (51Å)/Cu (30Å)/Fe (102Å) trilayer structure deposited on a glass substrate and capped with an additional Cu film (40Å) to prevent oxidation. Multilayer films of this type have important applications in magnetic read-heads and as elements in ultra-dense, nonvolatile memory. The top panel of Fig. 5 shows the measured MCD intensity for the Fe L_3 and Co L_3 absorption edge as a function of the applied magnetic field, as supplied by an in situ, liquid-nitrogen-cooled electromagnet. These are the element-specific hysteresis loops. The bottom panel shows the total moment hysteresis curve as measured by vibrating sample magnetometry (shown as a solid line labeled VSM). Superimposed on the VSM hysteresis curve of the middle panel is the scaled sum of the two individual Fe and Co element-specific magnetic hysteresis curves (shown as a dashed line labeled Fe + Co). The agreement is nearly perfect. From these scaling values, the known Co and Fe film thicknesses, and the total magnetic moment value as measured by VSM, the average elemental atomic magnetic moment of the Fe and the Co can be extracted. Our best fit determines the average moments to be $2.1 \pm 0.08 \mu_B$ for the Fe and $1.2 \pm 0.05 \mu_B$ for the Co.

Conclusions: The flexibility of the measurement process allows for elemental dissection

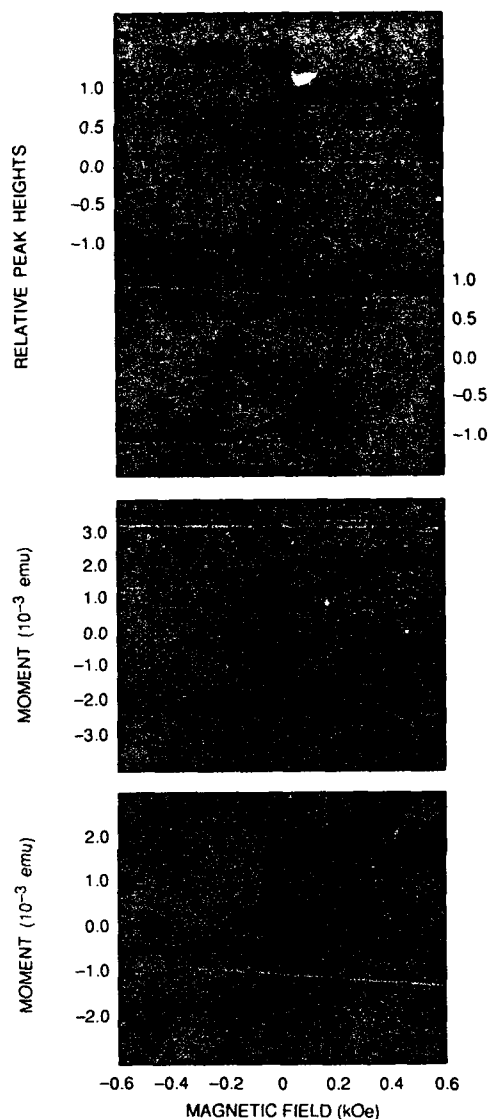


Fig 5 — TOP PANEL — The L_3 absorption edge intensities (white lines) using circularly polarized soft X rays as a function of applied magnetic field for the Fe and Co layers of a trilayer sample. MIDDLE PANEL — Comparison between the conventional hysteresis curve obtained from vibrating sample magnetometry (solid line, labeled VSM) and a least-squares best-fit linear combination of the element-specific magnetic hysteresis curves of the Fe and Co (dashed line, labeled Fe + Co). BOTTOM PANEL — The best-fit scaled element-specific magnetic hysteresis curves for the constituent Fe and Co used in the sum.

of hysteresis loops and also for variation of the analysis direction with respect to the applied field, another strength over the typical total-moment magnetometry studies. This type of angular study can be used to understand the

mechanism underlying the switching of the magnetic moment directions of the individual film components. Element-specific magnetometry measurements are a new way of extracting magnetic information from complicated systems and promises to become a technique with wide applicability to the growing complexity of magnetic studies.

Acknowledgments: This work was done in collaboration with C. T. Chen, H.-J. Lin, G. Meigs, and G. Ho of AT&T Bell Laboratories. A. Chaiken, now at Lawrence Livermore Laboratories, made these samples while a post-doc at the Naval Research Laboratory.

[Sponsored by ONR]

References

1. Y.U. Idzerda, L.H. Tjeng, H.-J. Lin, C.J. Gutierrez, G. Meigs, and C.T. Chen, "Magnetic Structure of Fe/Cr/Fe Trilayers," *Phys. Rev. B* **48**, 4144 (1993).
2. C.T. Chen, Y.U. Idzerda, H.-J. Lin, G. Meigs, A. Chaiken, G.A. Prinz, and G.H. Ho, "Element-specific Magnetic Hysteresis as a Means for Studying Heteromagnetic Multilayers," *Phys. Rev. B* **48**, 642 (1993). ■

Origins of Magnetic Anisotropy in Magneto-optical Storage Materials

W.T. Elam

*Condensed Matter and
Radiation Sciences Division*

V.G. Harris and N.C. Koon

Materials Science and Technology Division

Amorphous TbFe-based films are key materials for use in the latest generation of high-capacity magneto-optic memory storage devices. One of the most important features is their intrinsic perpendicular magnetic anisotropy, which maintains the direction of magnetization perpendicular to the plane of the film, thus enabling very high storage densities to be ob-

tained. Perpendicular magnetic anisotropy in thin films is unusual because a large demagnetizing energy arising from surface magnetic dipoles causes the magnetization direction to align parallel to the film plane.

Although extensive experimental studies have been performed on this class of materials for more than two decades, the underlying mechanisms responsible for this property have yet to be unambiguously established. This is largely due to the difficulties encountered in probing the atomic structure of thin amorphous films.

Approach: We have used extended X-ray absorption fine structure (EXAFS) and the polarization properties of synchrotron radiation to probe the local structure around the Fe and Tb atoms, both parallel and perpendicular to the film plane for several TbFe films. Comparing the in-plane structure to the out-of-plane structure shows an anisotropy around both the Fe and Tb atoms. EXAFS modeling procedures were used to estimate the coordination, radial distance, and chemistry of the near-neighbor atomic shells around each specie, thus enabling us to describe this anisotropy. These results were then correlated with magnetic properties before and after heat treatment in hopes of identifying the physical origin of the magnetic anisotropy in this material. [EXAFS measurements were performed by using NRL's materials analysis beamline (X23B) at the National Synchrotron Light Source at Brookhaven National Laboratory (Upton, NY).]

Results: In typical fashion, the EXAFS data were Fourier transformed to radial coordinates. In this form, the EXAFS data are useful in identifying features of the local environment around the absorbing atom. Figure 6(a) represents Fourier-transformed Fe EXAFS data for an as-deposited Tb₂₆Fe₇₄ film collected by using normal incident and glancing angle radiation. The large peak appearing near 2 Å contains information of the number and type of near-neighbor atoms, their radial distance, and the static and dynamic disorder of their atomic shells. The solid curve represents the structure in-plane; the dashed curve represents structure

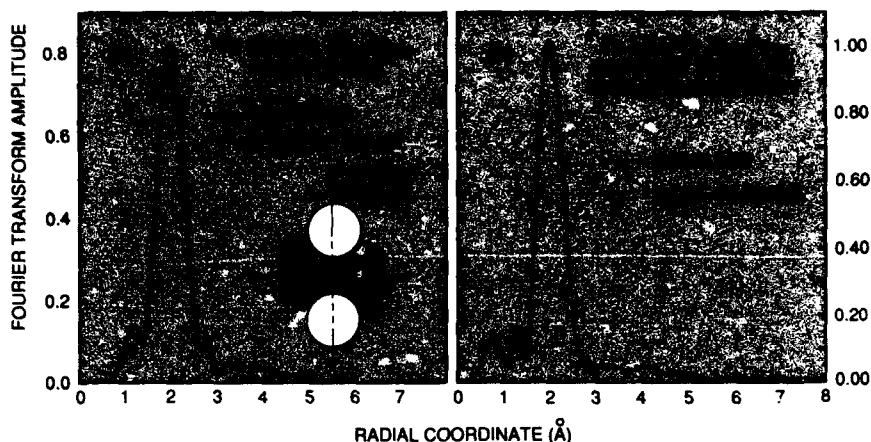


Fig. 6 — Fourier-transformed Fe EXAFS data for the $\text{Tb}_{26}\text{Fe}_{74}$ sample in its (a) as-deposited state, and (b) after a heat treatment at 300°C for 1 h. The radiation's electric field vector is aligned parallel and perpendicular to the film plane. Anisotropy is seen as a difference in the near-neighbor peak amplitude (located near 2.0 \AA). The inset drawing illustrates an atomic environment around the absorbing Fe atom, which is consistent with the results of the EXAFS modeling.

perpendicular to the film plane. The differences between data sets illustrate that a short-range structural anisotropy exists around the Fe atom. A similar anisotropy was seen in the Tb EXAFS data (not shown).

Model calculations that use shells of atoms having varying occupation numbers and chemistry, radial distances, and Debye-Waller factors (which describe the atomic disorder) allowed us to describe the anisotropy. We found that an anisotropic arrangement of atoms, where a greater number of like atom pairs (Fe-Fe, Tb-Tb) are aligned parallel to the film plane and a greater number of unlike atom pairs (Tb-Fe) are aligned perpendicular to the film plane, is responsible for the anisotropy in the Fourier-transformed EXAFS data. The inset to Fig. 6(a) is an illustration of the atomic configuration that is consistent with the modeling results.

A significant test of these data and our interpretation is to determine what happens to the structural anisotropy when the samples are annealed. Heat treatments at temperatures ranging from 200 to 300°C are known to substantially reduce the degree of perpendicular magnetic anisotropy without crystallizing these alloys. If the observed structural anisotropy is the dominant contributing mechanism to the magnetic anisotropy, then a heat treatment at these temperatures should also reduce the structural anisotropy.

After annealing the $\text{Tb}_{26}\text{Fe}_{74}$ film at a temperature of 300°C for a period of one hour, the magnetic anisotropy was reduced by more than 80%. Corresponding EXAFS measurements and analysis of the annealed sample are shown in Fig. 6(b). The anisotropy previously seen in Fig. 6(a) for the as-deposited sample has been completely eliminated by the 300°C anneal, thus supporting our interpretation that the magnetic anisotropy in these materials is associated with the structural anisotropy.

The structural anisotropy likely causes the magnetic anisotropy through a crystal field interaction on the Tb site via the coupling of its aspherical 4f charge cloud to the anisotropic electrostatic environment provided by the anisotropy described above.

This improved understanding of the relationship between local structure and magnetic properties in this class of materials points the way to new materials and artificial structures for the next generation of high density storage devices.

[Sponsored by ONR]

Reference

1. V.G. Harris, K.D. Aylesworth, B.N. Das, W.T. Elam, and N.C. Koon, "Structural Origins of Magnetic Anisotropy in Sputtered Amorphous TbFe Films," *Phys. Rev. Lett.* **69**, 1939 (1992). ■

**NUMERICAL
SIMULATING,
COMPUTING,
AND
MODELING**

- 189 **Reactive Flows in Ram Accelerators**
 Chiping Li, Kuzhikathra Kallasanath, Elamin S. Oran, and Jay P. Boris
- 190 **Numerical Ocean Models**
 NRL Global Modeling Team

Reactive Flows in Ram Accelerators

C. Li, K. Kailasanath, E.S. Oran,
and J.P. Boris
*Laboratory for Computational Physics
and Fluid Dynamics*

The ram accelerator is a new propulsion concept to accelerate projectiles to very high velocities (up to 8-10 km/s). The basic working principle of the ram accelerator is to use shock-induced combustion to generate high pressures to propel the projectile. A ram accelerator consists of a projectile moving in a launch tube filled with gaseous propellants such as premixed hydrogen-oxygen or methane-oxygen mixtures. When the projectile travels through the fuel-oxidizer mixture at supersonic speeds, shock waves generated by the projectile can significantly increase the temperature of the mixture behind the shocks and cause combustion to occur. Since the high-pressure region resulting from the shock-induced combustion is on or closely behind the projectile and no propellant is carried on the projectile, a higher launch speed and greater energy-conversion efficiency can potentially be achieved compared to conventional launching devices such as guns and rockets. A device of this type can be either land- or ship-based.

Time-Accurate Simulations: The flow field and combustion process in the ram accelerator are complex and highly transient because of the projectile acceleration. Understanding these related physical and chemical processes is crucial to the development of the ram accelerator. At the Laboratory for Computational Physics and Fluid Dynamics, multidimensional, time-accurate, numerical simulations are used to study the reactive flow field and the combustion process in the ram accelerator. The code used in our studies is based on the Flux-Corrected Transport Algorithm [1]. This algorithm is conservative, accurate, stable, monotonic, and ideally suited for studying strong discontinuities such as shocks and detonations. The acceleration of the projectile is coupled into the flow computation by using the noninertial source (NIS) technique [2]. Tests of this technique show that

changes in the flow field due to projectile acceleration can be smoothly computed for acceleration values up to 10^8 G. In addition, the virtual cell embedding (VCE) method [3] is used to efficiently represent complex projectile shapes on Cartesian grids. The combination of the NIS and VCE methods provides accurate and efficient simulations for highly transient flows around accelerating bodies. It is an ideal tool for studying the performance of the ram accelerator and similar propulsion systems in the acceleration process under various flow and geometric conditions.

Combustion Mechanism and Projectile Acceleration: Simulations show that the reactive flow field in the ram accelerator is highly transient. During acceleration, the flow field and the shock structure change rapidly and so does the combustion process. Figure 1 shows the reactive flow field around an accelerating projectile traveling at about 1200 m/s. This velocity is lower than the propagating velocity of a free detonation (the Chapman-Jouget or C-J velocity). In this case, the shock-induced combustion is maintained in the recirculation region behind the projectile and separated from the shock front. The energy released from the combustion process chokes the flow behind the projectile and supports a nonreactive normal shock on the projectile. The high pressure behind this shock provides the necessary thrust to propel the projectile. Also, large-scale, reactive flow structures generated in the recirculation region behind the projectile cause strong flow unsteadiness and pressure fluctuations on the projectile. Simulations show that significant accelerations, ranging from 10^4 to 10^5 G, can be achieved and a velocity gain of 400 m/s is obtained.

Figure 2 shows the reactive flow field around an accelerating projectile traveling at about 3500 m/s. This velocity is higher than the C-J velocity of the mixture. At this velocity, shock-induced combustion is closely coupled to the shock front to form a detonation on the projectile. Detonation is a very efficient form of combustion and generates very high pressures on the widest part of the projectile body. In this case, the detonation on the projectile is very



Fig. 1 — Reactive flow field around an accelerating projectile traveling at 1200 m/s. In this case, the shock-induced combustion is maintained in the recirculation region behind the projectile and separated from the shock front.

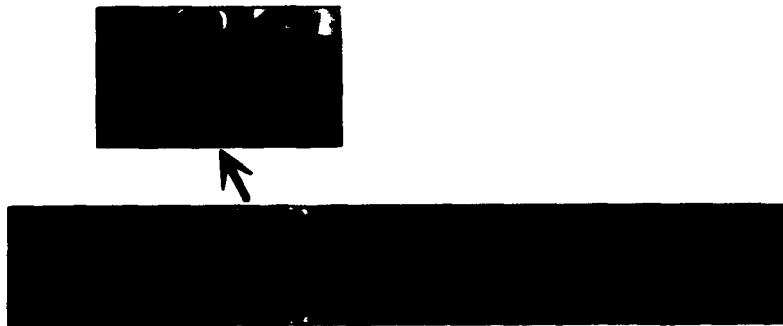


Fig. 2 — Reactive flow field around an accelerating projectile traveling at 3500 m/s. At this velocity, the shock-induced combustion is closely coupled to the shock front to form a stable detonation on the projectile.

stable, and the high pressure generated by the detonation accelerates the projectile at a rate between 2×10^5 and 3×10^5 G from 3200 to 4200 m/s.

Summary: The ram accelerator is a promising propulsion concept. A numerical capability has been developed to simulate transient, reactive flows around accelerating projectiles in ram accelerators. The numerical simulations show that a significant velocity gain can be obtained for a ram-accelerator projectile. These simulations also provide insights to the reactive flow field and the combustion process in the ram accelerator.

[Sponsored by AFOSR and NRL]

References

1. J.P. Boris, and D.L. Book, "Solution of Continuity Equations by the Method of Flux-Corrected Transport," in *Methods in Computational Physics*, Vol. 16 (Academic Press, N.Y., 1976), pp. 85-129.
2. C. Li, A.M. Landsberg, K. Kailasanath, E.S. Oran, and J.P. Boris, "Numerical

Simulations of Reactive Flows in Ram Accelerators," *CPIA* **293**, 279 (1992).

3. A.M. Landsberg, J.P. Boris, W. Sandberg, and T.R. Young, "Naval Ship Superstructure Design: Complex Three-Dimensional Flows Using an Efficient, Parallel Method," *Proceedings from High Performance Computing 1993: Grand Challenges in Computer Simulations* 1, 15, Society for Computer Simulations, San Diego, 1993. ■

Numerical Ocean Models

NRL Global Modeling Team*
Oceanography Division

The oceans manifest intense variability on space scales largely ranging from ~ 100 to 1000 km and on time scales from interannual (i.e., multi-year) to a few months, which is analogous

*Team includes J. McCaffrey, J. Mitchell, H. Hurlburt, J. Kindle, D. Fox, M. Carnes, R. Rhodes, G. Jacobs, Z. Hallock, W. Teague, T. Townsend, J. Metzger, J. Dastugue, and A. McManus.

to atmospheric "weather." Much of the energy of this oceanic "weather" is concentrated in the ocean's so-called *mesoscale* (~ 100 km, ~ 1 month). The ocean's mesoscale dominates variability in both the currents and density fields in the most of the major ocean current systems (Gulf Stream, Kuroshio Extension, etc.). Most of these major ocean currents are located on the boundaries of the major basins and are immediately adjacent to coastal regions of high Navy interest (Arabian Sea, Yellow-East China Sea, etc.).

Our ability to numerically model the ocean's variability on synoptic space and time scales is at a level of development much like that of numerical weather prediction several decades ago. Numerical modeling of ocean variability presents a greater challenge than numerical weather prediction in two major respects:

First, the spatial scales of baroclinic instability in the ocean (which is the process largely giving rise to the ocean mesoscale variability) are about 1 to 2 orders of magnitude smaller than those within the atmosphere (~ 100 km in the ocean vs ~ 1000 km in the atmosphere). As a result, much higher spatial resolution is required of ocean models than of their atmospheric counterparts. As a result, numerical ocean modeling is one of the "grand challenges" for high-performance computing. During FY93 alone, this team used the equivalent of 50,000 single processor Cray Y/MP hours on this grand challenge.

Second, there has historically been a lack of pertinent oceanographic data over the vast expanses of the world's oceans. This has been alleviated somewhat with the recent Navy Geosat-Exact Repeat Mission (Geosat-ERM) altimetric satellite, the European Space Agency ERS-1 satellite (which includes both an altimeter and a scatterometer), and the NASA/CNES TOPEX/Poseidon precise altimetric satellite. Sea surface height (SSH) measured by these satellite altimeters provides rich data sets for observing interannual changes in ocean circulation. For example, a comparison of recent satellite altimetry (ERS-1 and TOPEX/Poseidon) relative to the earlier Geosat-ERM data set used multiple-mission satellite altimetry for monitoring decadal changes in the global ocean circulation.

NRL has led the way in applying state-of-the-art supercomputer technology to numerical ocean modeling, in developing highly efficient numerical formulations (i.e., layered, primitive equation ocean models) to optimize the results possible from present day supercomputers, and in objectively assimilating satellite data into these numerical ocean models.

Global Ocean Model: NRL has developed the world's first $1/8^\circ$ eddy-resolving global ocean model, which promises to revolutionize our understanding of the important role of the ocean mesoscale in the global general circulation of the oceans (see Fig. 3). These initial simulations were carried out on the Department of Defense High Performance Computing Initiative Cray C90 at Vicksburg, Mississippi, and will be continued on the NRL CM-5. As a result, NRL is on the cutting-edge in its development of global ocean monitoring and prediction systems.

Global ocean monitoring and prediction systems have applications ranging from military operational support to studies of global environmental change, including: military operations, such as sealift ship-routing, search and rescue, antisubmarine warfare, coastal and mine warfare; commercial applications, such as ship-routing, fisheries forecasts; global environmental monitoring and prediction, such as pollutant-spill risks, El Niño forecasting, ocean observing system simulations.

Decadal Scale Effects of the 1982-83 El Niño: By using a combination of satellite altimeter measurements of SSH, satellite infrared measurements of sea surface temperature (SST), and a global ocean model, NRL has discovered evidence that the 1982-83 El Niño spawned a Rossby wave along the coast of North America. This Rossby wave lasted more than a decade, crossed the entire Pacific, and in 1991-92 interacted with the Kuroshio Extension (see Figs. 4 and 5). This interaction routed a portion of the Kuroshio Extension's transport to a more northern path, causing the major warm anomaly seen in the satellite SST measurements. In 1992-93, anomalies in SSH and SST spanned the northern Pacific from Japan to Alaska.

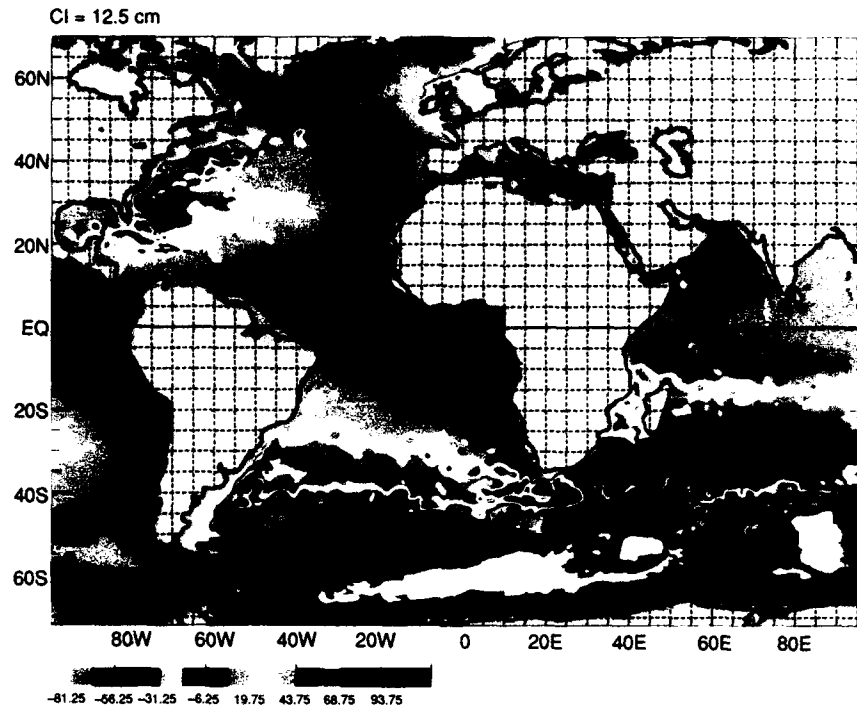


Fig. 3(a) — Sea surface height snapshot for the Atlantic and Indian Oceans from the NRL 6-Layer Global Ocean Model

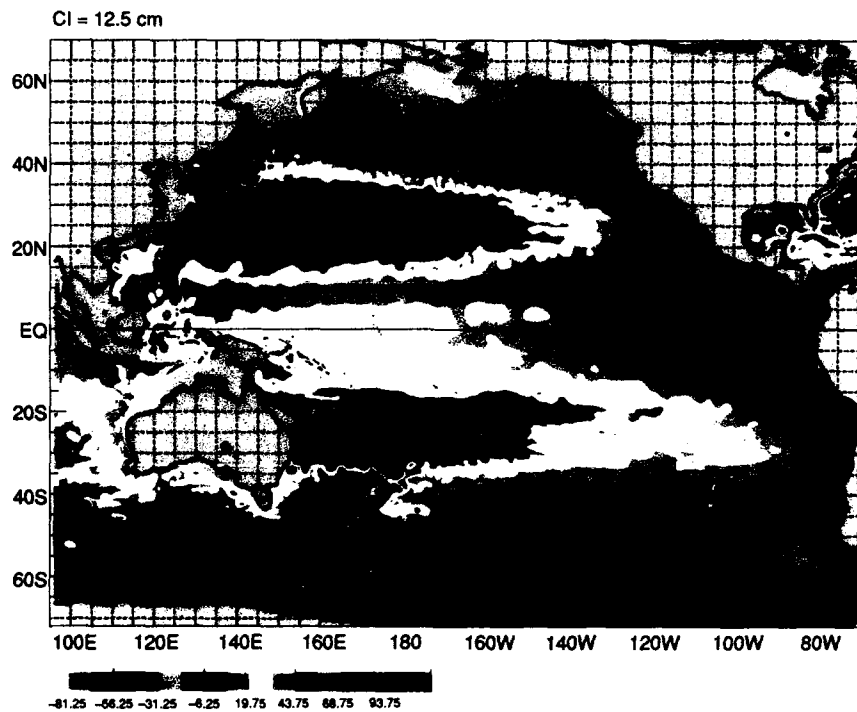


Fig. 3(b) — Sea surface height snapshot for the Pacific Ocean from the NRL 6-Layer Global Ocean Model

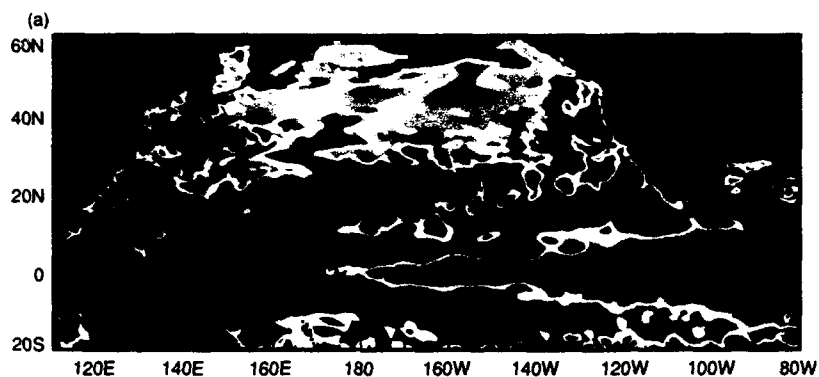


Fig. 4(a) — Model SSH deviation in Aug. 1982 from a mean over Jan. 1981 to Dec. 1992. The SSH along the equator and along the coast of the American continent is a signature of the 1982 El Niño.

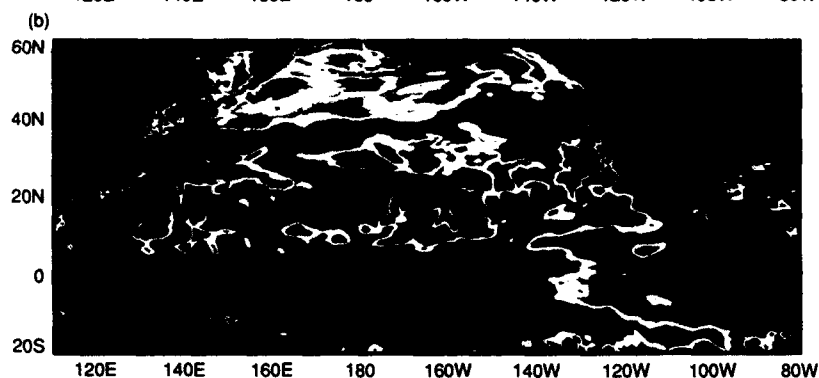


Fig. 4(b) — Model SSH deviation 5 months after the time of Fig. 4(a). The SSH high along the equator has diminished significantly, but a Kelvin wave, which propagated along the North American coast has left a SSH high along the entire coast.

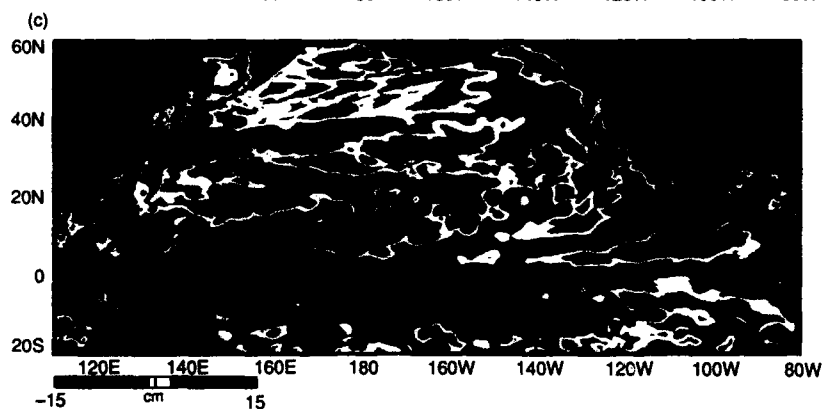


Fig. 4(c) — Model SSH 9 months after Fig. 4(a). The SSH high along the North American coast begins to peel away from the coast as a westward-propagating Rossby wave.

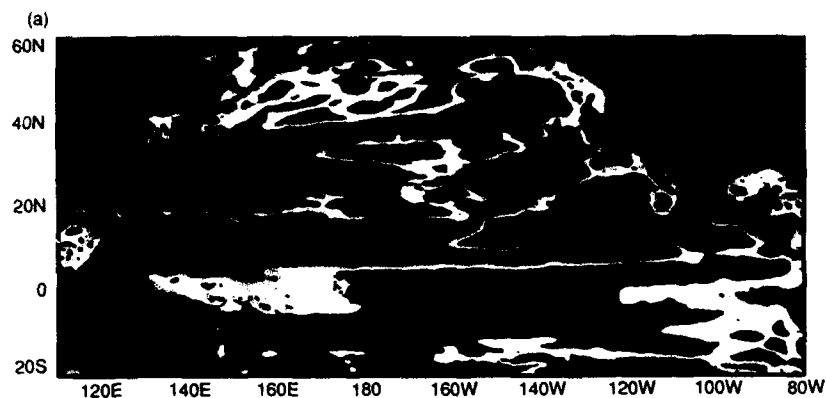


Fig. 5(a) — Model SSH deviation 2 years after the 1982-83 El Niño. The Rossby wave shown in Fig. 4(c) propagates away from shore. A dashed line is drawn on the Rossby wave to delineate its position.

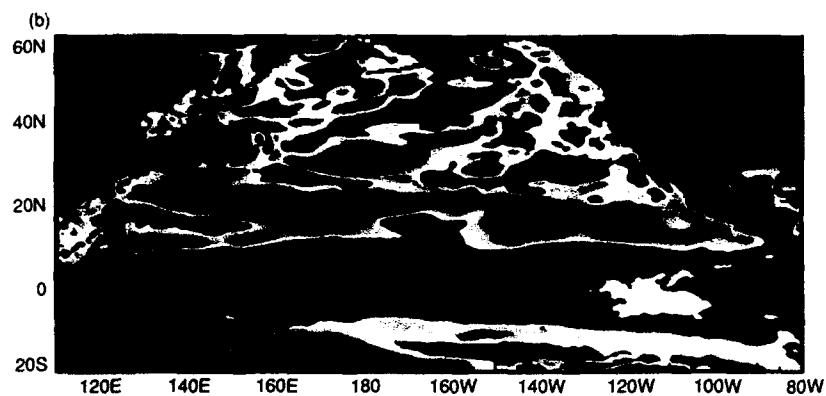


Fig. 5(b) — Model SSH deviation 5 years after the 1982-83 El Niño. The Rossby wave now extends from Taiwan to the Gulf of Alaska.

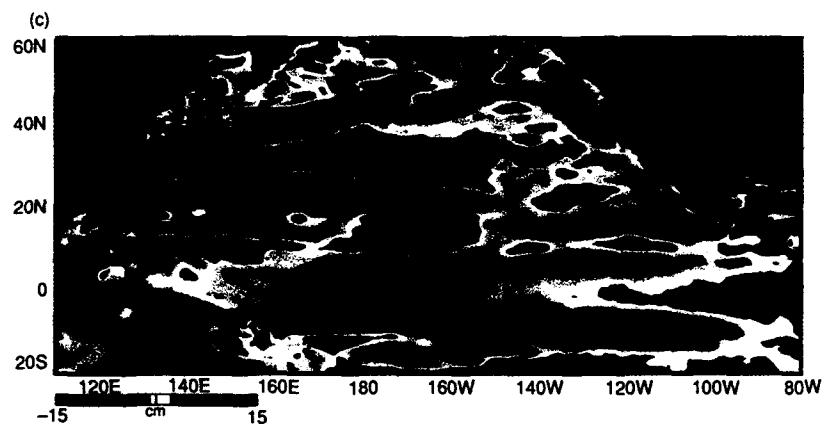


Fig. 5(c) — Model SSH deviation 10 years after the 1982-83 El Niño. The Rossby wave has moved to a position from the southern edge of Japan to the Gulf of Alaska.

This investigation provides an exciting example of how a realistic ocean model can be used to help interpret observations. In this case, the model is used to identify the origin of a major decadal anomaly and the sequence of events that led to an observed impact 11 years later. Taken individually, the observed or model data sets might yield inconclusive results. For example, satellite altimeter measurements are subject to many environmental corrections and errors. Furthermore, the effects of these errors may be increased by differences between the Geosat-ERM and ERS-1 satellites. The model results alone are not conclusive because they are a simulation that uses simplifications of the ocean with respect to physics, resolution, and atmospheric forcing functions. These simplifications make it possible to run the model on existing

supercomputers and facilitate the interpretation of the model results. In this study, it was essential that the model: maintain the wind-generated anomaly without dissipation or dispersion; propagate it to the observed location; and do both of these over a decadal time scale.

The remarkable sequence of events uncovered by this investigation indicate the surprising long-term oceanographic effects of the major 1982-83 El Niño. The methods used in this investigation, numerical modeling and satellite oceanography, aptly illustrate the utility of the critical components of a Global Ocean Monitoring and Prediction System. The far-reaching and long-term effects of major El Niños are just one example of the need for such a system.

[Sponsored by ONR, SPAWAR, and ARPA] ■

**OCEAN
AND
ATMOSPHERIC
SCIENCE
AND
TECHNOLOGY**

- 199 Use of Surface Temperature Retrievals from Satellite
Douglas A. May
- 200 Events Leading to the 1991-92 El Niño
John C. Kindle and Patricia A. Phoebus
- 203 Field Tests of the DOLPHIN—A Remotely Operated
Survey Vehicle
Maria T. Kalchauer and Edlt J. Kaminsky
- 206 Impacts of Weather Model Forecasts on Tactical
Environmental Decision Aids
Gary G. Love and John Cook

Sea Surface Temperature Retrievals from Satellite

D.A. May
Remote Sensing Division

Accurate representation of large-scale and mesoscale sea surface temperature (SST) patterns is important for many U.S. Navy operations. Detection of ocean feature locations and thermal characteristics is important for optimum ship track routing, acoustic surveillance, search and rescue activities, and weather prediction. The Navy's large operational domain requires that ample SST information be available throughout the world. Global in situ SST observations from ships, buoys, and expendable bathythermographs are relatively sparse and regionally located. However, satellite SSTs generated from National Oceanic and Atmospheric Administration (NOAA) polar-orbiting satellites provide more than 120,000 daily observations from all global regions. Through NRL direction and research support, this SST retrieval generation capability has been recently transitioned into operation at the Naval Oceanographic Office (NAVOCEANO). The processing system became fully operational in June, 1993.

Technique: Global multichannel sea surface temperature (MCSST) information from satellite are retrieved each day on an orbit-by-orbit basis from properly cloud-screened global area coverage (GAC) data at a spatial resolution of 8 km [1]. Accurately estimating SST from satellite requires correcting for atmospheric effects. These effects are caused primarily by atmospheric water vapor in the spectral bandwidths available on the polar-orbiting satellites. The MCSST algorithm is based on the differential absorption properties of water vapor in two or three infrared channel bandwidths. Operational retrieval algorithms are empirically derived at NRL by regressing satellite channel brightness temperatures to global drifting-buoy SST measurements within specified time and distance constraints. The accuracy of the derived algorithm is then continuously monitored on a monthly basis; it has been found to require few changes throughout a satellite's lifetime. Figure 1 depicts the general pattern of SST found in the Gulf Stream and Gulf of Mexico regions.

Research Efforts: NRL's Remote Sensing Applications Branch has been designated the lead agency for research and development affecting satellite SST production. The Algorithm

Fig. 1 — Color-enhanced NOAA-11 sea surface temperature image from May 2, 1992 depicting the location of major ocean frontal gradients associated with the Gulf Stream and Gulf of Mexico Loop Current.



Research Panel for SST has been formed to provide scientific guidance and recommendations for SST quality. It also develops and examines new satellite retrieval algorithm techniques for SST product improvements. This panel is chaired by NRL and includes members from several agencies and academic institutions with SST interests. The positive impact that satellite SSTs have on operational thermal analyses has been demonstrated, providing improved analysis delineation of ocean features and ocean frontal strengths and positions. Research has also demonstrated the comparative improvement in retrieval accuracy available by using a nonlinear multichannel algorithm instead of the standard linear algorithm technique [2]. Root-mean-square difference statistics relative to global drifting buoys now demonstrate satellite SST retrieval accuracies within 0.6°C , with accuracies of 0.4°C possible if all three infrared channels are used. Investigations for retrieval accuracy improvement now focus on examining remotely sensed global water vapor data and/or atmospheric sounder information for atmospheric correction improvements.

Summary: With implementation of the satellite SST retrieval processing capability at NAVOCEANO, U.S. Navy operations dependent on accurate global SST information now have access to numerous observations on a very timely basis. NRL and NAVOCEANO are working to maintain a consistently accurate product and improve the atmospheric correction accuracy, cloud screening capability, and quantity of retrievals.

[Sponsored by SPAWAR]

References

1. E.P. McClain, "Global Sea Surface Temperatures and Cloud Clearing for Aerosol Optical Depth Estimates," *Int. J. Remote Sens.* **10**, 763 (1989).
2. D.A. May, "Global and Regional Comparative Performance of Linear and Nonlinear Satellite Multichannel Sea Surface Temperature Algorithms," NRL Memorandum Report NRL/MR/7240--93-7049, 1993. ■

Events Leading to the 1991-92 El Niño

J.C. Kindle
Oceanography Division

P.A. Phoebus
Marine Meteorology Division

The El Niño Southern Oscillation (ENSO) describes a group of cyclical, interrelated atmospheric and oceanic events that occur in the tropical Pacific. The extreme warm and cold ocean events are accompanied by shifts in ocean currents, changes to biological populations, and anomalous weather patterns around the globe. Efforts to effectively determine the global environment must carefully account for these changes, not only for climatic time scales, but also for synoptic time scales where everyday decisions made by both military and civilian communities rely on accurate environmental information.

Although a number of ideas have been proposed about the origin of the El Niño, recent attention has focused on anomalous westerly winds that occur in the equatorial western Pacific. These westerly wind bursts (WWB) appear as bands of strong westerly winds imbedded in the easterly trade winds. WWB are of interest because of their potential role in generating equatorially trapped ocean Kelvin waves that propagate eastward along the equator to the South American coast and may be related to the development or enhancement of the El Niño.

Atmospheric Events: Model-enhanced fields provide a more complete picture of atmospheric behavior than is available from observations alone. The 10-m wind fields from the Naval Research Laboratory's global analysis and prediction system (NOGAPS) clearly depict several WWB from October 1990 through January 1992, the period leading to the 1991-92 El Niño. Most of these WWB last from a few days to two weeks, and wind speeds as high as 10-15 m/s are common.

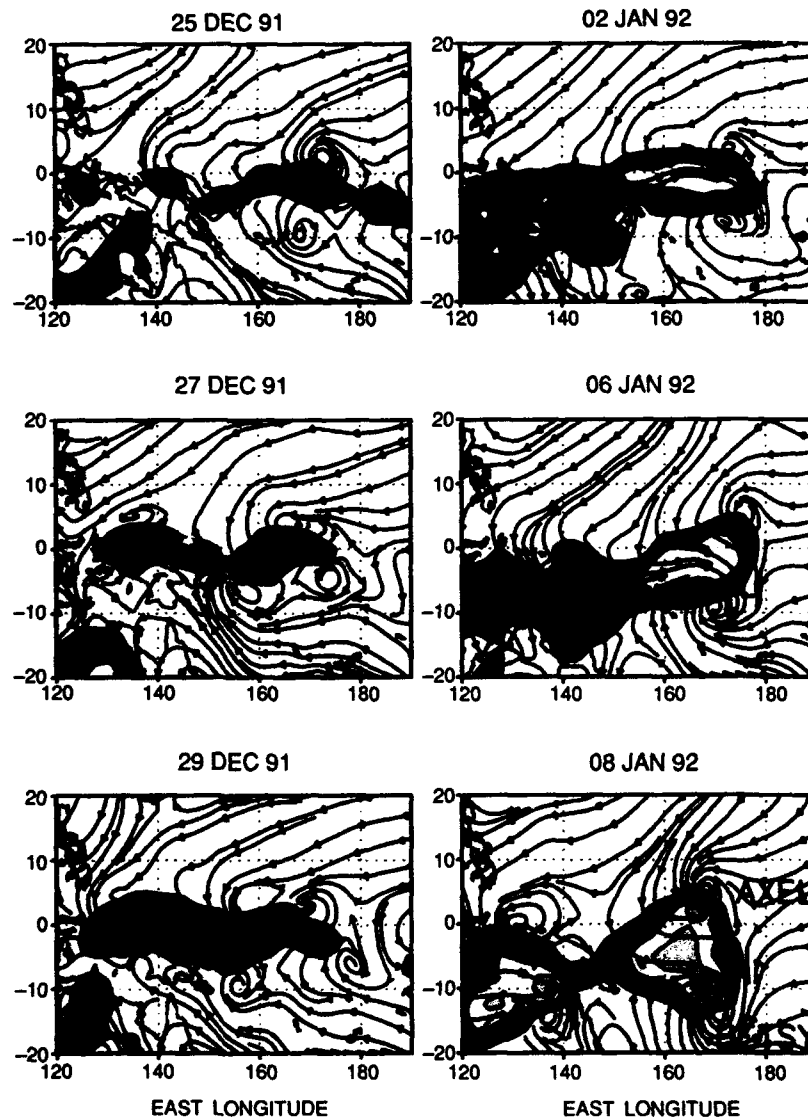
Most of these WWB are accompanied from their inception by cyclonic circulations that develop into tropical cyclones while very close to

the equator (Fig. 2). In 1991, storms forming south of 10°N and east of 145°E were usually accompanied by equatorial westerlies, with the strongest events occurring between northern/southern hemisphere cyclone couplets, such as the one shown. We see a similar equatorward and eastward shift in tropical cyclone development during other years marking the beginning of warm events in the eastern Pacific.

Ocean Events: The forcing for the ocean model simulations is provided by NOGAPS surface wind stresses updated every 12 hours. A suite of experiments, performed with the NRL global multi-layer ocean model, demonstrates an ability to accurately simulate the eastern Pacific

sea level variations (Fig. 3) [1,2]. During the period studied, the model reveals the following scenario for the onset of the 1991-92 El Niño. The eastern boundary sea level exhibits three distinct pulse-like events superimposed on a general rise beginning in October, 1991. The first pulse is generated by wind anomalies in the central Pacific; the latter two pulses are the result of three powerful WWB events. The Kelvin wave arriving in the eastern Pacific in mid-late December was generated by a strong WWB in November (Fig. 4), which was associated with a typhoon couplet. A second Kelvin wave is generated in the western Pacific in early January by the Axel-Betsy WWB shown in Fig. 2. This wave is reinforced by a strong central

Fig. 2 — NOGAPS 10-m streamline analyses depicting the westerly wind burst associated with the development of Typhoon Axel and Tropical Cyclone Betsy from December 25, 1991 to January 8, 1992. Westerly wind components greater than 2.5 m/s are contoured every 2.5 m/s.



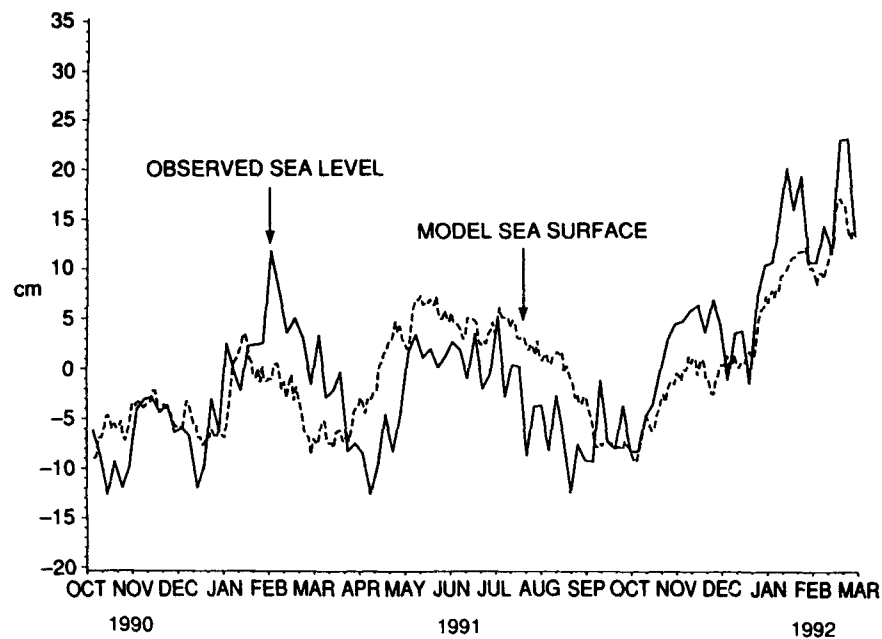


Fig. 3 — Variations of model sea surface (dashed line) and observed sea level (solid line) vs time in the eastern equatorial Pacific (Baltra, Galapagos)

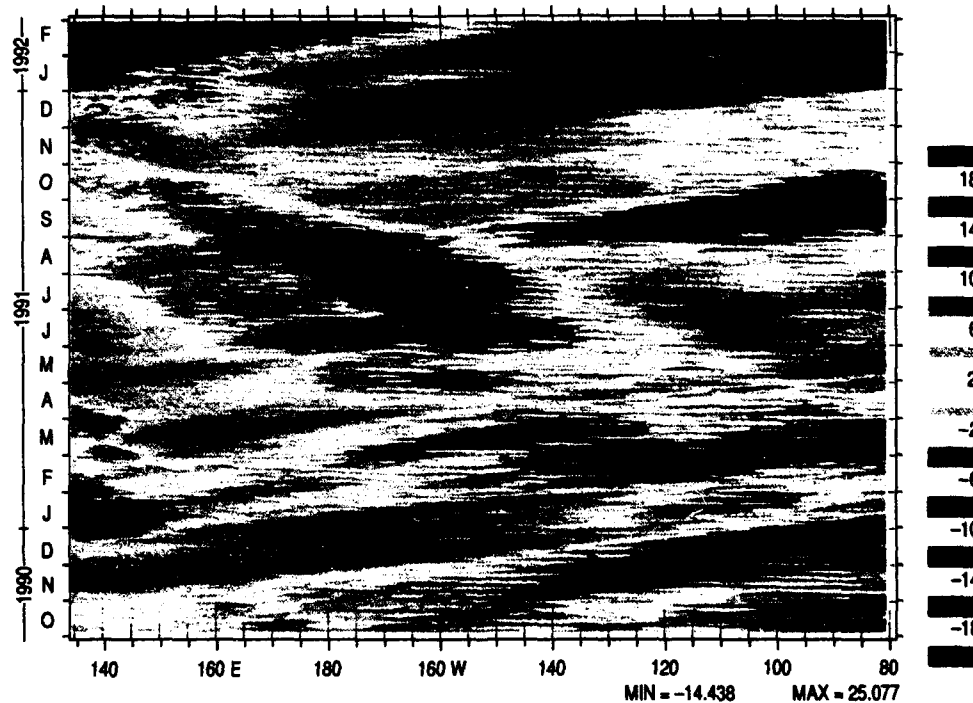


Fig. 4 — Longitude vs time diagram of model sea surface anomalies (cm) along the equator. Yellow to red values denote positive anomalies; blue indicates negative anomalies. The characteristic Kelvin wave propagation is seen as a band of color slanting upward from left to right, representing a phase speed of approximately 2.5 m/s.

Pacific westerly wind anomaly in mid-January, when Typhoon Ekeka developed east of 160°W. Taken together, these three pulses account for much of the sea-level rise and subsequent equatorial warming observed in the eastern Pacific.

Summary: Several important implications should be noted. First, long time-scale events in the tropical ocean are driven, at least in part, by highly energetic but short-lived atmospheric anomalies. Thus, long-range predictions of ENSO may suffer if the models used are too coarse to resolve these scale interactions. On the other hand, high-resolution global oceanic and atmospheric models can be used to understand complex, large-scale interactions that influence events far from the source of the original anomalies. Such knowledge will lead to improved, longer-range forecasts of both climatic and synoptic scale events around the globe.

[Sponsored by ONR]

References

1. P.A. Phoebus and J.C. Kindle, "Events Preceding the 1991-92 El Niño, Part I: A Study of Westerly Wind Bursts Depicted by an Operational Analysis/Forecast System," submitted to *J. Geophys. Res.*, 1993.
2. J.C. Kindle and P.A. Phoebus, "Events Preceding the 1991-92 El Niño, Part II: The Ocean Response to Operational Westerly Wind Bursts," submitted to *J. Geophys. Res.*, 1993. ■

Field Tests of the DOLPHIN—A Remotely Operated Survey Vehicle

M.T. Kalcic
Marine Geosciences Division

E.J. Kaminsky
Sverdrup Technologies

Remotely operated vehicles (ROV) instrumented with state-of-the-art ocean survey systems are a potential force multiplier for the

Navy's reduced fleet of oceanographic survey ships. The Oceanographer of the Navy (N096) tasked the Naval Research Laboratory (NRL) to test and evaluate the Deep Ocean Logging Platform with Hydrographic Instrumentation and Navigation (DOLPHIN) as a Navy survey platform. DOLPHIN is a diesel-powered semisubmersible developed by International Submarine Engineering (ISE). NRL, in conjunction with the National Oceanic and Atmospheric Administration (NOAA), the Naval Oceanographic Office (NAVOCEANO), and the Canadian Hydrographic Service (CHS) conducted DOLPHIN field tests in August 1992. The joint survey was conducted with NOAA's ship *Whiting*, NAVOCEANO's ship USNS *Littlehales*, and CHS's DOLPHIN over the Norfolk Canyon, 62 nmi east of Cape Charles, Virginia.

DOLPHIN: The DOLPHIN vehicle, Fig. 5, is constructed of aluminum alloy, weighs approximately 3500 kg (dry), and measures 7.44 m in length. It has a Sabre 212-hp turbocharged, diesel engine with endurance up to 26 h at 12 kt (or 312 nmi) on 90 gal of diesel fuel. The vehicle uses differential Global Positioning System (DGPS), attitude sensors, and a gyrocompass for navigation. The DOLPHIN's DGPS and radio link antennas are attached to a snorkel at the mast's top (Fig. 5). The DOLPHIN's submerged draft is 4.57 m. The vehicle performs automatic linekeeping; manual override is available for stopping, turning, or maneuvering. The DOLPHIN requires a 20-ton crane and approximately five people for launch and retrieval. Brooke Ocean Technology (BOT) designed a ship-based, articulated crane specifically for DOLPHIN that can launch and retrieve the ROV in up to sea state 5.

Multibeam Systems: The DOLPHIN tested has a Simrad EM-100, a 95 kHz multibeam sounding system [1]. The DOLPHIN transmits the EM-100 bathymetry data to the ship at 9600 baud over a UHF radio link. The EM-100 operates in three different modes: narrow, wide, and ultrawide, covering depths from 10 to 600 m. The EM-100 operates with a maximum of 32 receiving beams and athwartship beam apertures of 3.75, 2.5, or 2.0 deg.

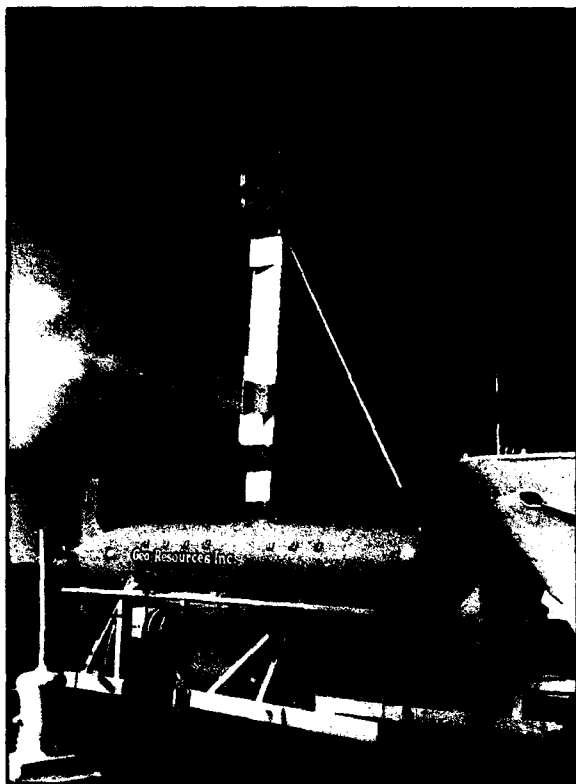


Fig. 5 — The deep ocean logging platform with hydrographic instrumentation and navigation (DOLPHIN)

The maximum coverage is 100 deg, corresponding to 2.4 times the water depth. The *Whiting* has General Instrument Corporation's Hydrochart II (HC), a dual-transducer multibeam-sonar system that operates at 36 kHz. The system uses a cross-fan transducer array to form 17 beams, 9 each for port and starboard, with overlapping near-nadir beams. The swath coverage of the Hydrochart II is 2.5 times the water depth or 105 deg. The *Littlehales*, like DOLPHIN, has a hull-mounted EM-100.

Test Survey of Norfolk Canyon: The ships and ROV collected data along the contours of the Norfolk Canyon, with several cross tracks. Patch tests were run to evaluate the system's attitude and handling. The platforms collected data over the same lines on two different days, surveying approximately 30 nmi. The DOLPHIN's automatic linekeeping worked well except when the DGPS position jumped to a location 100 m off the programmed track, making

the DOLPHIN respond with an abrupt turn in an effort to correct its course. The DOLPHIN's sensors detected the excessive acceleration and therefore shutdown and surfaced the ROV. The DOLPHIN was immediately restarted and on track within 5 min.

Survey Results: Figure 6 shows a comparison of pitch records for the DOLPHIN and *Whiting* over the same time interval. The DOLPHIN showed less pitch for line B03 (headed into prevailing seas) than the ship; however, results for line B04 (heading with the seas) showed more pitch for the ROV. DOLPHIN performance and stability are marginally superior when running into the seas as opposed to running with the seas. This is due to the response of the stabilizing planes, which produce a more rapid vehicle response in bow seas. Running with the seas, the DOLPHIN's relative speed is reduced, some surfing occurs, and less water is passing over the stabilizer planes. With a conventional monohull vessel, the converse is true; running into the seas produces thrusts on the bow at different intensities, resulting in pitching. A ship running with the seas results in less thrust and less pitch with a longer period.

Bathymetry analysis showed the HC-II root-mean-square (rms) noise levels to be about 0.28% of depth, DOLPHIN's EM-100 noise levels to be about 0.2% of depth, and the *Littlehales*'s EM-100 data to be about 0.17% of depth. The rms noise difference, 0.03% of depth, was not significant. Some noise on the DOLPHIN was attributed to the power supply, which was subsequently replaced with a quieter one.

Figure 7 shows georeferenced 50-m bathymetry contours from the three platforms over an area of the Norfolk Canyon. The rms depth differences between DOLPHIN and *Whiting* data were 1.9% of depth, and between DOLPHIN and *Littlehales*, the rms was 2.0% of depth. The rms depth difference between the two ships was 2.3% of depth. Although differences between the two ships varied more than between either ship and the ROV, the mean difference between the two ships was almost a meter smaller than for the DOLPHIN and the

Fig. 6 — Pitch observations for DOLPHIN (yellow) and NOAA *Whiting* (red) travelling into bow seas (top) and heading with the seas (bottom)

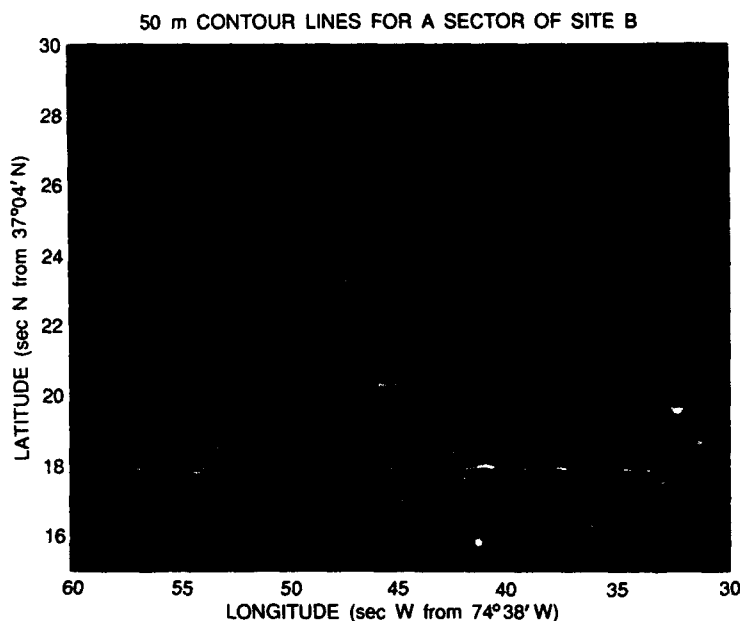
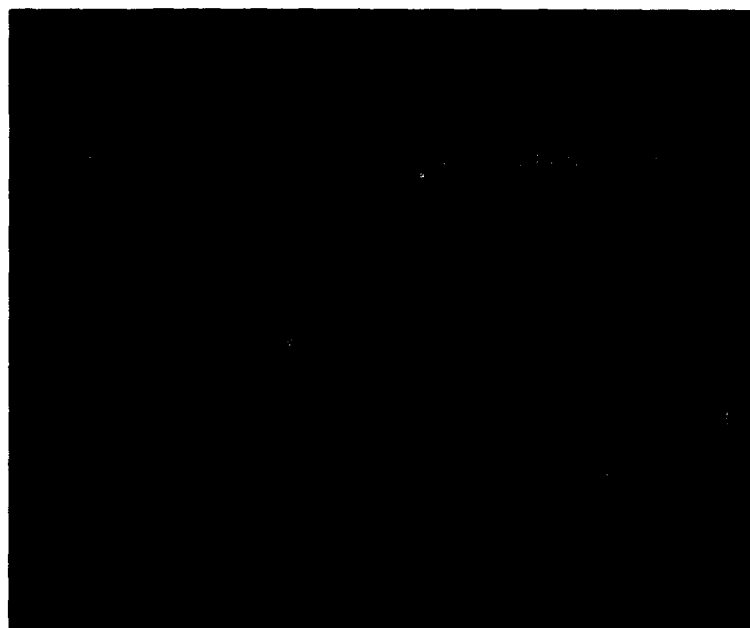


Fig. 7 — Bathymetry contours of the Norfolk Canyon for DOLPHIN, *Whiting*, and *Littlehales*

ships. Reference 2 shows that the mean difference between the ships was 0.48 m and was -1.7 and -1.3 m, respectively, between the DOLPHIN and *Littlehales* and DOLPHIN and *Whiting*. A calibration error in the DOLPHIN's depth setting caused the DOLPHIN to sound shallower than the two ships by about a meter.

Conclusions: One DOLPHIN surveying parallel to a survey ship could double the

amount of data collected per ship-survey mile. Tests conducted over the Norfolk Canyon showed the ROV to be robust to sea state, noise, and data dropouts. Plans to implement a DOLPHIN-like vehicle with an imaging-multi-beam, sediment classifier, and high-rate telemetry are underway between NRL's Marine Geosciences Division and NAVOCEANO. This system will be fielded in FY95 to provide the Navy with an advanced, data-collection platform

that will serve as a force multiplier to NAV-OCEANO's oceanographic survey fleet.

[Sponsored by the Oceanographer of the Navy]

References

1. D.R. Peyton, "The DOLPHIN/EM100 Ocean Mapping System," *The Hydrographic Journal*, No. 65 (July 1992).
2. E.J. Kaminsky and M.T. Kalcic, "Multi-beam Data Evaluation for DOLPHIN and Ship Collection Platforms," NRL/MR/7441--93-7034, July 1993. ■

Impacts of Weather Model Forecasts on Tactical Environmental Decision Aids

G.G. Love and J. Cook
Marine Meteorology Division

Although modern weapon systems are designed to be "all-weather," they are not immune to the effects of weather or environmental conditions. To mitigate the effects of environmental factors, the U.S. Navy has developed numerical weather prediction models that forecast meteorological conditions and Tactical Environmental Decision Aids that predict the performance of weapons and sensors. The bases for such decision aids are frequently computer-simulation models of weather-dependent physical processes, for example, transport and diffusion or propagation. Recently, we interfaced two computer models to weather model output to demonstrate weather effects on tactical systems. This evaluation of impacts on system performance, as influenced by atmospheric mesoscale phenomena will help to determine future weather model resolution and accuracy requirements.

The Weather Prediction Models: The U.S. Navy has developed both global and regional weather prediction models. The Navy Operational Global Atmospheric Prediction

System (NOGAPS [1]) is the large-scale global model that provides weather forecast guidance for up to 5 days. NOGAPS also provides high-quality forecast fields that are used as boundary conditions for higher resolution models that cover smaller domains. One such model, a vertically nested, second-order closure variant of NORAPS (Navy Operational Regional Atmospheric Prediction System) [2,3] is currently used to provide regional or mesoscale weather forecast guidance for up to 24 h. This research version of NORAPS is being used to examine detailed variations of the atmosphere in the southern and central California littoral region in participation with the Variability of Coastal Atmospheric Refractivity (VOCAR) experiment.

Figure 8 compares 2-h forecasts from NOGAPS and NORAPS (interpolated to 0700 PDT by using the analysis at 0500 and the 6-h forecast at 1100). The NOGAPS forecast shows winds flowing somewhat down the coast from the north, with a circulation over land and stable air near the surface. In contrast, the NORAPS forecast shows winds flowing down the coast, but with an eddy in the shelter of the southern California bight. The eddy was created by NORAPS at 2300 PDT the previous evening and verifies well with surface wind data observed at 0700 PDT. The air's buoyant instability is more varied for the NORAPS forecast with stable air over water except in the eddy where winds are weaker and over mountains (upper left) where air tends to be less stable.

Downwind Hazard Prediction: The first example of tactical impact is illustrated using the Vapor, Liquid, and Solid Tracking (VLSTRACK) [4] computer model recently developed by the Protection Systems Department at the Naval Surface Warfare Center. The VLSTRACK model estimates the transport and diffusion of a Gaussian plume to provide downwind hazard predictions for a wide range of chemical and biological agents and munitions.

Cumulative dosages predicted by VLSTRACK (Fig. 9) show the trajectory of the plume when driven by NOGAPS or NORAPS data. Both agents are released at the same point and time, but the NOGAPS and NORAPS winds

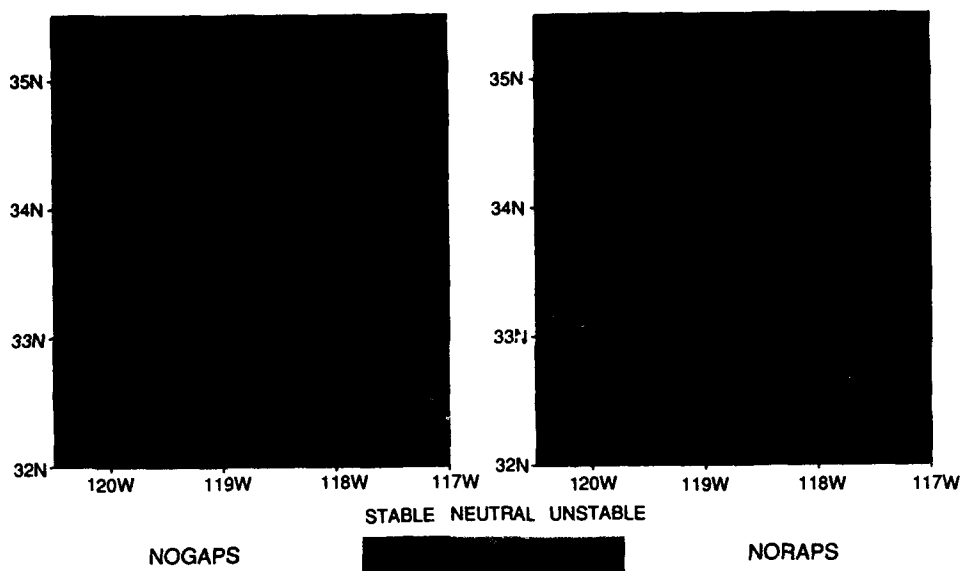


Fig. 8 — The surface winds and buoyant instabilities forecast by the NOGAPS and NORAPS weather prediction models show the relative increase in resolving power of the NORAPS model. The forecast for each model shown is a 2-h interpolation that uses the analysis and the 6-h forecast. The eddy forecast by NORAPS verifies well with the observed surface winds shown for 0700 PDT on 21 July 1992.

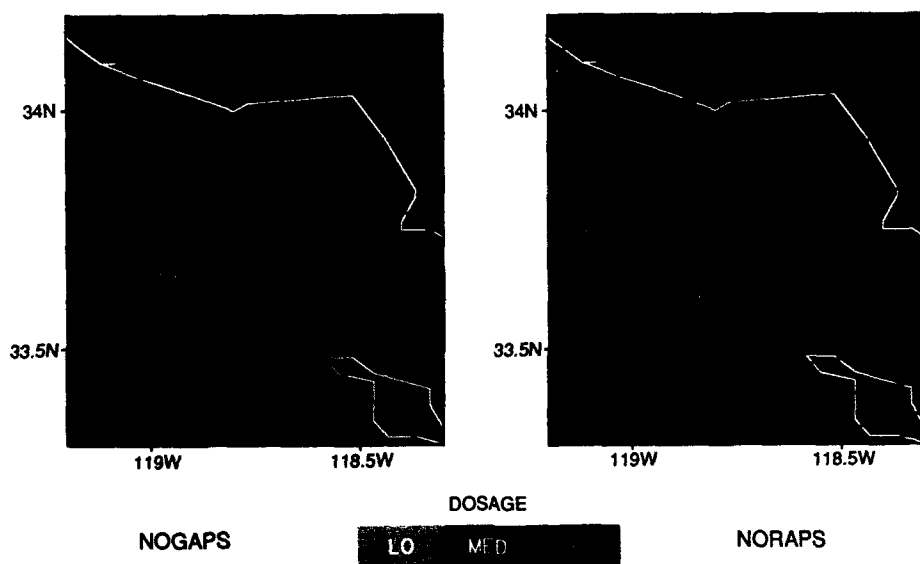


Fig. 9 — The predicted VLSTRACK cloud plume trajectory shows the cumulative dosage of the selected agent since the time of release at 0500 PDT on 21 July 1992. The trajectories show the integrated effect at 1100 PDT of the changing winds over the previous 6 hours. The difference in the two trajectories is primarily due to differences in the forecast winds obtained from the NOGAPS and NORAPS models.

and buoyant instabilities are very different. As a result, the cloud plume trajectories diverge. If the agent is released with the wrong winds, the downwind dosage may not be effective. The eddy resolved by NORAPS produced a local difference while it persisted, but once it subsided, both NOGAPS and NORAPS winds tended toward agreement. NORAPS also resolves diurnal flow patterns such as land/sea breezes that will produce similar differences in predicted plume trajectories near the coast.

Radio Propagation Prediction: The second example of tactical impact is illustrated by using the Radio Physical Optics (RPO) [5] computer program recently developed by the RDT&E Division at the Naval Command, Control and Ocean Surveillance Center to predict radio propagation. The RPO model is a hybrid of ray optics and parabolic equation methods that overcomes the high computational burden traditionally associated with solving parabolic equations.

Atmospheric conditions can significantly affect electromagnetic (EM) propagation. Figure 10 shows a 12-h forecast of the near-surface

trapping layer predicted by NORAPS for 0400 PST on 16 February 92. Trapping layers are regions in the atmosphere where the refractivity changes with height such that EM waves are refracted toward Earth's surface, and can cause extended detection and counterdetection ranges for radars. The height of the trapping layer is determined by the depth of the marine atmospheric boundary layer, and its strength is related to the refractivity vertical gradient and its thickness (not shown). The figure shows an environment with a trapping layer generally rising to the south and east, until the coastline is encountered. Over land, turbulent mixing causes the trapping layer to dissipate. Figure 11 is a series of panels showing propagation loss computed by RPO along the radial cross sections shown in the previous figure. This illustrates the effect of the forecast trapping layer on a rotating radar. The trapping layer results in extended ranges to the north and east; ranges to the south and west are near those for standard atmospheric conditions. Such variability is not uncommon in littoral areas, and use of the wrong refractive environment can lead to large differences between predicted and observed

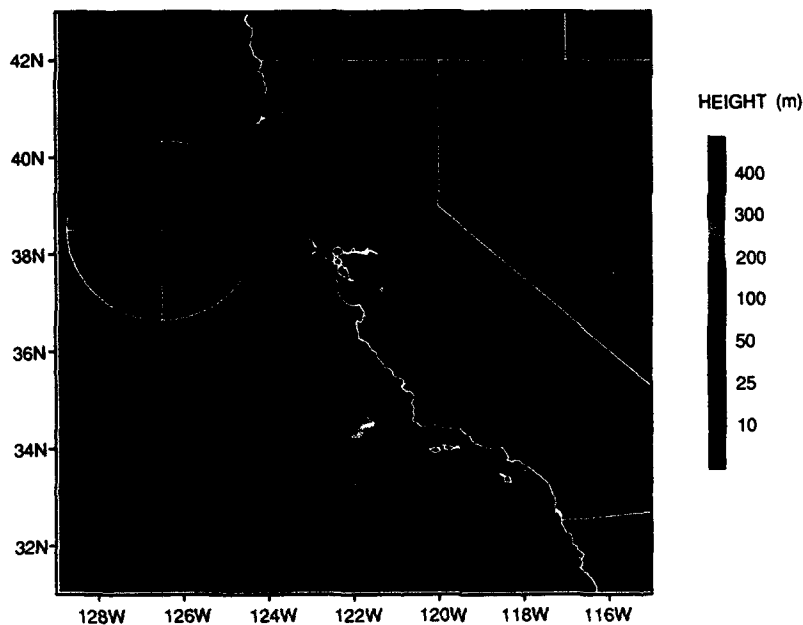


Fig. 10 — The height of the trapping layer 12-h forecast by NORAPS is shown to vary significantly off the California coast at 0400 PST on 16 February 1992. The topology of the trapping layer indicates the complexity of the associated refractive structure. The four radials along the compass points indicate the cross sections used for RPO predictions in Fig. 11.

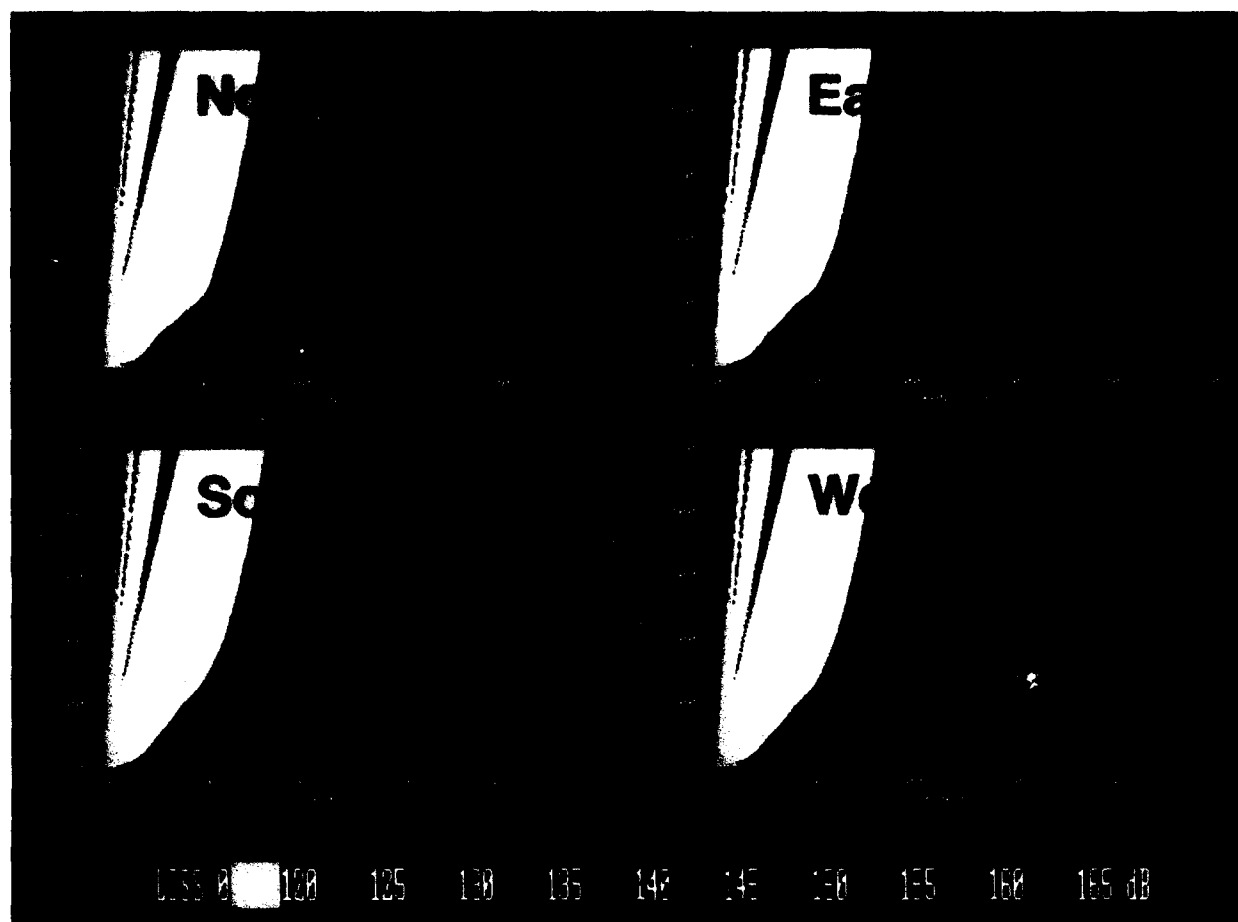


Fig. 11 — The predicted propagation loss for the radial cross sections shown in Fig. 10 are computed by RPO. The radar propagation is extended along the north and east radials as indicated by the lower propagation losses at heights near 100 meters. This difference is due to a trapping layer rising and strengthening locally from southwest to northeast.

radar performance. The VOCAR experiment mentioned earlier is a multiyear exercise, with intense observation periods designed to collect data on littoral zone processes that can be used to improve model physics, validate model forecasts, and diagnose anomalies.

Summary: These two examples have been animated in a video. They dramatically demonstrate environmental impacts on tactical systems. However, proper planning by using accurate weather conditions can increase system performance and operational effectiveness. These examples also clearly demonstrate the value of predicting system performance based on high-resolution weather model predictions. We hope to extend this research to other areas of warfare

by increasing weather model temporal resolution, comparing forecasts with observations, and examining new tactical decision aids.

Acknowledgments: This work is a collaborative effort of the authors with Dr. Stephen Burk and Mr. William Thompson of the NRL Marine Meteorology Division and is based on results using their research version of NORAPS. [Sponsored by ONR and SPAWAR]

References

1. T.E. Rosmond, "The Design and Testing of the Navy Operational Global Atmospheric Prediction System," *Wea. & Forecasting*, 7, 262-272 (1992).

2. R.M. Hodur, "Description and Evaluation of NORAPS: The Navy Operational Regional Atmospheric Prediction System," *Mon. Wea. Rev.* **110**, 1591-1602 (1982).
3. S.D. Burk and W.T. Thompson, "A Vertically Nested Regional Numerical Weather Prediction Model with Second-order Closure Physics," *Mon. Wea. Rev.* **117**, 2305-2324 (1989).
4. T.J. Bauer, Operator's Instruction Manual for VLSTRACK, Version 1.2, NSWC Draft Report, Naval Surface Warfare Center, Dahlgren, VA, 1991.
5. H.V. Hitney, "Hybrid Ray Optics and Parabolic Equation Methods for Radar Propagation Modeling," Proc. IEE International Radar Conf., Brighton, England, 1992. ■

**OPTICAL
SCIENCE**

- 213 High-Frequency Approximations to Physical Optics
William B. Gordon
- 215 Broadband Thermal Optical Limiter
Brian L. Justus, Alan L. Huston, and Anthony J. Campillo
- 217 High-Speed, Low-Loss Transmission Line on
Silicon Membrane
Michael Y. Frankel
- 220 Paramagnetic Resonance and Optical Studies of GaN
*William E. Carlos, Evan R. Glaser, Thomas A. Kennedy,
and Jaime A. Freitas, Jr.*
- 222 Interferometric "Seeing" Measurements on Mt. Wilson:
Power Spectra and Outer Scales
David M. M. Leitch and David R. Stetson

High-Frequency Approximations to Physical Optics

W.B. Gordon
Radar Division

Physical Optics (PO) is the classical technique for calculating electromagnetic scatter from electrically large reflectors, i.e., reflectors that are many wavelengths in extent. In PO theory, the scatter from a surface reflector is represented by a certain surface integral, which has the appearance of a two-dimensional Fourier transform. The calculation of this integral is onerous; this article discusses work devoted to reducing this integral to the sum of line integrals and/or closed-form expressions.

In the present discussion we consider the radar backscatter from a curved surface reflector S which is terminated by a boundary edge ∂S , as shown in Fig. 1. Incident radiation is assumed to be a monochromatic plane wave. In practical terms, the results can be applied to pulsed radars that are sufficiently narrowband. In PO theory, the far field backscatter is then proportional to the quantity

$$J_{po} = (1/\lambda) \int_{S_0} e^{i2ks \cdot X} (s \cdot \eta) dA, \quad (1)$$

where λ is the radar wavelength, $k = 2\pi/\lambda$, s is the "scatter vector" that points from the reflector to the radar, X is the position vector of a general point on S , η is the unit surface normal to S , dA is the infinitesimal element of area on S , and S_0 is the illuminated part of S . The actual radar cross section is related to J_{po} according to $\sigma = 4\pi |J_{po}|^2$. PO predictions based on Eq. (1) can be expected to be physically accurate provided that: the reflector is not electrically small; the radar line-of-sight does not make too small an angle ($< 45^\circ$) with the surface at the boundary edge; and the surface is not reentrant. (No multiple internal reflections, as in a cavity.)

We come now to the problem of reducing the calculation of Eq. (1) to something that is more tractable. At the turn of the century, the

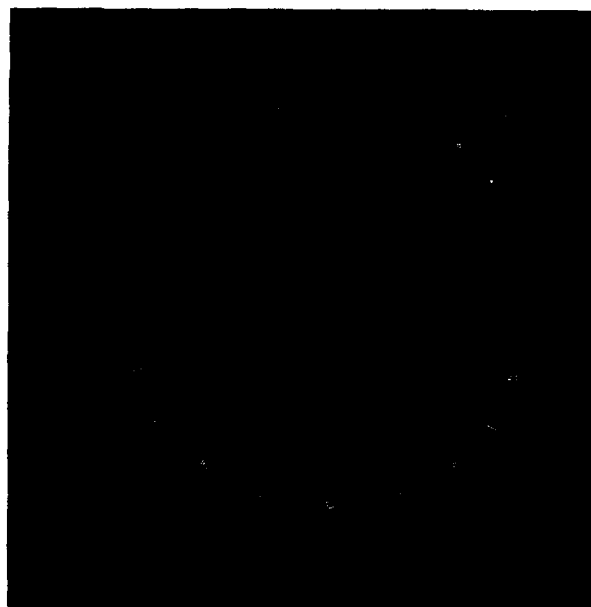


Fig. 1 — A general curved surface S with boundary edge ∂S and surface normal η

formulas for the near field (Fresnel) diffraction through an aperture were reduced to line integrals evaluated around the boundary [1]. Remarkably, these formulas were never applied to the calculation of far field scatter from flat plate reflectors, although this could easily have been done and the problem was of great practical interest. In 1975, the author showed how the scattering integral for flat plate scatter could be reduced to a line integral [2]. In addition for polygonal plates, the line integral can be reduced to a closed-form expression. According to this "Polygon Formula," each edge gives rise to a $\sin x/x$ term, and the total scatter from the polygonal plate is the sum of all the edge terms, appropriately phased.

The problem of scatter from curved surfaces is more complicated. However, as a consequence of Fermat's Principle, at sufficiently high frequencies one would expect scatter from a curved edged surface to be dominated by two effects: a specular effect and an edge effect. (Recall that a specular point is one at which the surface normal points toward the radar.) The amplitude of the specular effect is given by a well-known formula from Geometrical Optics (GO), and the author has recently obtained a

formula for the PO predicted edge effect [3], namely, the line integral

$$J_{\text{edge}} = \frac{1}{4\pi} \int_{S_0} \frac{s \cdot \eta}{1 - (s \cdot \eta)^2} e^{i2ks \cdot X} (s \times \eta) dX, \quad (2)$$

where ∂S_0 is the illuminated part of ∂S . An heuristic derivation of Eq. (2) can be obtained by decomposing S into a large number of small rectangular tiles as suggested in Fig. 1, applying the Polygon Formula to each tile, and then throwing out all the resulting edge terms except those lying on the boundary curve ∂S . In Ref. 3, Eq. (2) is also justified on other grounds.

A high-frequency approximation to J_{po} is obtained by adding (with phase) the specular effect to the edge effect J_{edge} . The specular effect is inversely proportional to $|K(p)|^{1/2}$, where $K(p)$ is the total Gaussian curvature at the specular point p . Hence the method breaks down if $K(p)$ vanishes. More generally, the approximations can be expected to break down if S has flat parts with zero curvature; the scatter from flat facets is large and would tend to dominate the specular and edge effects. In fact, we have found that our high-frequency approximations break down for smooth "inflected" surfaces for which the curvature attains both

positive and negative values—even though the set of points of zero curvature is an infinitely thin line. Figure 2 shows examples of inflected and noninflected surfaces.

Approximations using Eq. (2) are called "L-type" approximations (L for line integral). A second type of approximation can be obtained by applying the Stationary Phase Method to the integral (2). One thus obtains a closed-form expression consisting of certain terms evaluated at the "bright points" of ∂S , i.e., the points at which the scatter vector is perpendicular to ∂S . These will be called "S-type" approximations, (S for stationary phase).

Figure 3 shows an example. The surface S is a paraboloid of revolution terminated by a cutting plane perpendicular to the axis. The radar cross section σ is plotted on a logarithmic scale, and θ is the off-axis aspect angle. The "exact" values of σ were obtained from a straightforward two-dimensional quadrature of J_{po} ; with the exception of certain singularities, agreement with the high-frequency approximations is rather good. There are two types of singularity: caustic and noncaustic. Caustic singularities affect only S-type approximations, whereas noncaustic singularities affect both types. Noncaustic singularities occur when the specular point falls on ∂S . When this happens $s \cdot \eta = 1$, and the integrand in Eq. (2) becomes singular.

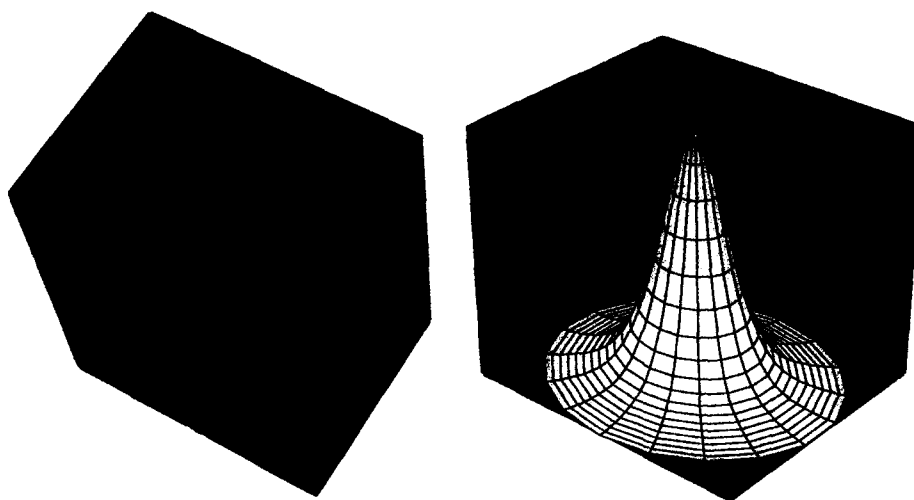


Fig. 2 — Examples of inflected (yellow) and noninflected (red) surfaces

Fig. 3 — Comparison of radar cross-section calculations. Yellow line, S-type approximation; blue dashed line, L-type approximation; red dashed line, exact 2-D quadrature.



The better accuracy obtained with the L-type approximations (over the S-type) is paid for by the necessity of numerically calculating Eq. (2). However, in terms of CPU time, the costs of numerically calculating the line integral (2) is orders of magnitude less than the costs for the double integral (1).

[Sponsored by ONR]

References

1. W.B. Gordon, "Vector Potentials and Physical Optics," *J. Math. Physics* **16**, 448 (1975).
2. W.B. Gordon, "Far Field Approximations to the Kirchhoff-Helmholtz Representations of Scattered Fields," *IEEE Trans. AP-23*, 590 (1975).
3. W.B. Gordon, "High Frequency Approximations to the Physical Optics Scattering Integral," *IEEE Trans. AP*, to appear. ■

Broadband Thermal Optical Limiter

B.L. Justus, A.L. Huston, and A.J. Campillo
Optical Sciences Division

The protection of eyes and sensors from damage due to exposure to sources of intense light, such as laser radiation, is a problem of

interest to the Navy. Although the problem remains largely unsolved, a significant degree of protection can be accomplished by a device called an optical limiter. The transmission of an ideal optical limiter would be constant for low-intensity light but would be dramatically reduced for high-intensity light. One type of optical limiter uses nonlinear optical materials as the protective element, exploiting intensity-dependent changes in the refractive index or absorption of such materials. Optical limiter material and device requirements include high transmission of low-intensity light over a broad range of wavelengths, wide field-of-view, a fast yet persistent temporal response, and the ability to recover from optical damage. We have recently demonstrated a thermal optical limiter that, when used with high optical gain optics (as typically found in binoculars and gunsights), provides a high degree of eye protection.

Thermal Refractive Nonlinearity: Thermal refractive optical nonlinearities arise as a result of changes in the refractive index of a material upon heating. Despite the fact that the thermal mechanism can achieve extremely large optical nonlinearities, use of the thermal mechanism for optical limiting had not been seriously considered previously. Researchers had assumed that the response time of the thermal mechanism was too slow to provide protection against typical nanosecond-duration *Q*-switched pulsed lasers. In fact, the thermal mechanism meets every important requirement, including

response time, for use in an optical limiter. A particular feature of the thermal limiter we developed is its extremely broad spectral response curve. Although engineered and tested at 532 nm, it will operate equally well at any wavelength—from the ultraviolet (UV) to the near infrared (IR). This is a vital characteristic for effective protection from frequency-agile laser threats.

Defocusing Optics: The broadband thermal optical limiter [1] is constructed (Fig. 4) by using a defocusing geometry that consists of a lens to focus the light into a partially absorbing sample and then a second lens to recollimate the light or direct it onto a detector. For low-incident fluences, all light transmitted by the sample reaches the detector. At high-incident fluences, the nonlinear sample expands the beam and redistributes the energy into a series of concentric rings. These rings are deflected outside the collection angle of the second lens and are conveniently blocked by an aperture, thereby dramatically reducing the transmission to the detector. The experiments were performed by using a solution of nigrosin dye dissolved in carbon disulfide. Nigrosin is characterized by an extremely broad and flat absorption over the entire visible and near-IR spectral regions. Figure 5 compares the transmission of nigrosin

to the daylight vision response curve of the eye. Carbon disulfide is a common laboratory solvent with an exceptional thermal figure of merit. By using $f/5$ optics and 6-ns-duration laser pulses at 532 nm, a limiting threshold was observed with a device transmission of 47% (Fig. 6). This corresponds to a fluence of only 100 mJ/cm² at the focus. The straight line represents the transmitted energy if no limiting occurs. The maximum transmitted energy is less than 400 nJ for input energies over 20 μ J, representing a net high-intensity transmission of only 2%. When optics with an area ≥ 1 cm² are used, this corresponds to a fluence < 0.5 μ J/cm² into the eye, which is considered a safe level of exposure.

Conclusions: The broadband thermal optical limiter, as engineered, could be incorporated into many optical imaging systems of Navy interest. In addition, we have investigated methods for improving the performance of the thermal limiter, for example, by using state-of-the-art intensity-dependent absorbing materials [2]. Such materials exhibit excited state absorption that enhances the heating of the thermal solution and, in turn, the thermal nonlinearity. We have also performed a comprehensive experimental and numerical analysis of the characteristics of thermal defocusing limiters [3].

[Sponsored by ONR]

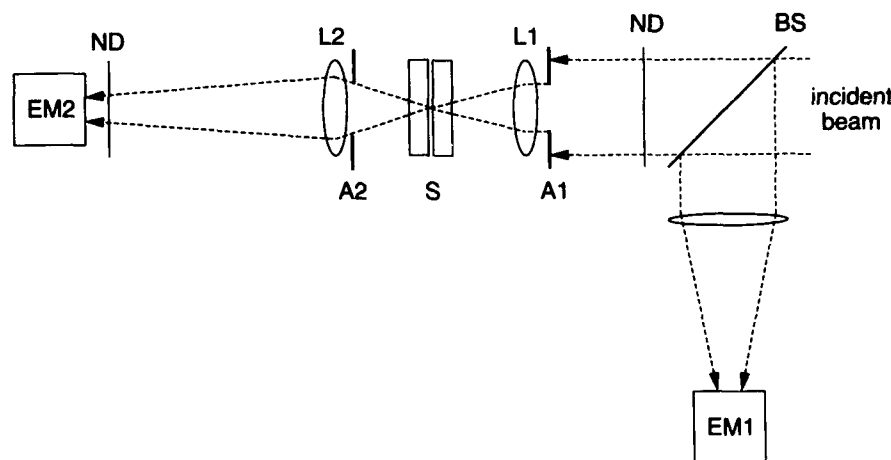


Fig. 4 — Schematic of broadband thermal limiter using $f/5$ defocusing optics. BS: beamsplitter; EM1: reference energy meter; ND: neutral density filter; A1: 10-mm diameter entrance aperture; L1: $f = 50$ -mm double-element focusing lens; S: sample cell containing 25- μ m thick nigrosin/CS₂ solution; A2: 10-mm-diameter collecting aperture; L2: $f = 50$ mm imaging lens; EM2: energy meter.

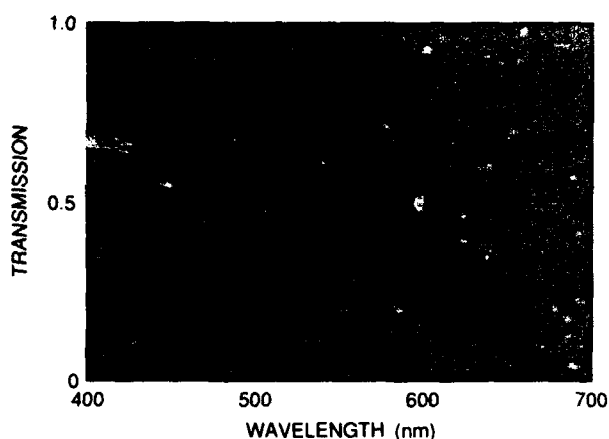


Fig. 5 — Transmission spectrum of a nigrosin/ CS_2 solution. The daylight vision response of the human eye is shown for comparison.

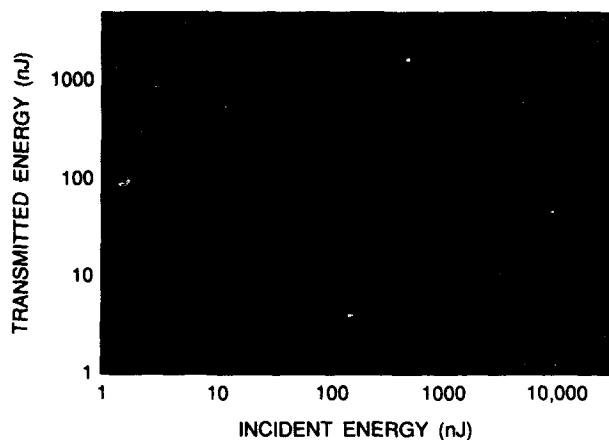


Fig. 6 — Logarithmic plot of transmitted energy vs incident energy for a nigrosin/ CS_2 solution ($\alpha = 0.76$). The solid line is the system transmission if no limiting occurred.

References

1. B.L. Justus, A.L. Huston, and A.J. Campillo, "Broadband Thermal Optical Limiter," *Appl. Phys. Lett.* **63**, 1483 (1993).
2. B.L. Justus, Z.H. Kafafi, and A.L. Huston, "Excited-state Absorption-enhanced Thermal Optical Limiting in C_{60} ," *Optics Lett.* **18**, 1603 (1993).
3. G.A. Swartzlander, B.L. Justus, A.L. Huston, A.J. Campillo, and C.T. Law, "Characteristics of a Low F -number Broadband Visible Thermal Optical Limiter," *Int. J. Nonlin. Opt. Phys.* **2**(4) (1993), in press. ■

High-Speed, Low-Loss Transmission Line on Silicon Membrane

M.Y. Frankel

Optical Sciences Division

High-speed, low-loss coplanar transmission lines are important for a variety of applications, including microwave integrated circuits, ultra-fast device characterization, and traveling-wave optical modulators. Conventional microwave coplanar transmission lines have conductors fabricated on thick substrates. Therefore, they possess relatively slow signal propagation velocities as determined by the average of the large substrate permittivity and air superstrate permittivity. In addition, deleterious effects that cause severe signal degradation as the result of strong velocity dispersion and rapidly increasing attenuation appear at frequencies above ~ 100 GHz. The reason for the high-frequency performance degradation can be traced to the large structural inhomogeneity caused by having a high-permittivity substrate and a low-permittivity air superstrate. Previous attempts to improve signal propagation characteristics suffer from limitations in substrate material or system applicability. In this work, we demonstrate a method for achieving high signal propagation speed, low velocity dispersion, and suppressed high-frequency losses on a structure that is compatible with a wide range of substrate materials and can be applied to a wide range of uses.

Experiment: The significant performance improvement is achieved by fabricating the electrodes of a coplanar strip (CPS) transmission line on an ultrathin silicon (Si) membrane (Fig. 7). The membrane is $\sim 8\text{-}\mu\text{m}$ thick (or one tenth the thickness of human hair), and substantially reduces structural inhomogeneities. The membrane has paper-like flexibility; a rigid mechanical support is made of an aerogel, which is a sponge-type microporous material fabricated of silica and consisting of up to 97% void spaces. Therefore, the aerogel serves as "solid air," and the electromagnetic signal propagating on the CPS experiences mostly air, with only a small fraction being in the Si membrane. For comparison purposes, we have also

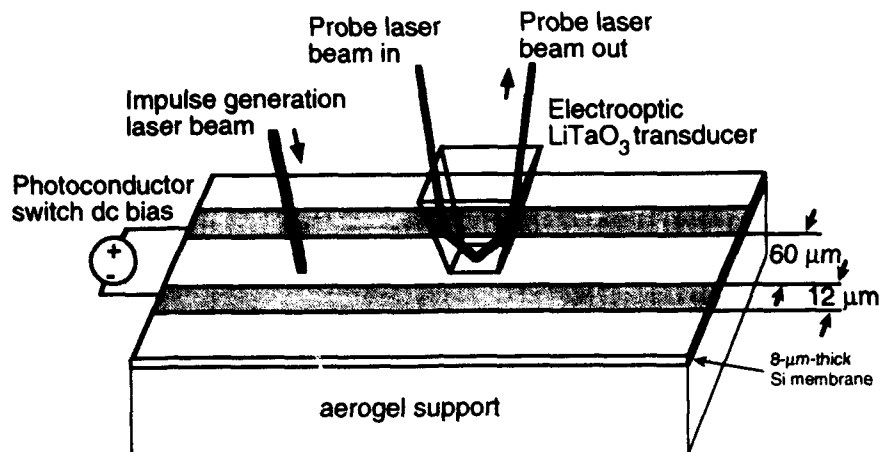


Fig. 7 — Typical generation and electro-optic measurement geometry for coplanar transmission line on membrane

measured propagation characteristics of an identical CPS fabricated on a conventional thick substrate.

We are interested in extremely high frequencies, spanning the range from near dc up to 1000 GHz (1 THz). It is impossible to achieve this kind of bandwidth by using conventional all-electronic instrumentation. We have developed an electro-optic characterization system that allows us to generate and measure subpicosecond electrical pulses containing frequency components from dc to more than 1000 GHz. The system includes a photoconductor optoelectronic switch embedded in the CPS. The switch generates a subpicosecond electrical pulse when excited by a 100-fs optical pulse from a mode-locked dye laser. The electrical signal propagates along the CPS and suffers frequency-dependent dispersion and attenuation. An electro-optic electrical signal transducer is positioned at a point along the transmission line where a measurement is desired, and the transducer is interrogated by another 100-fs optical pulse synchronized to the excitation one. We observe the electrical signal evolution as it propagates along the CPS with subpicosecond resolution and millivolt sensitivity and obtain both time- and frequency-domain CPS propagation characteristics.

Results: The initial transmission line designs were based on an approximate analytic

model. Further analysis of the thin-substrate transmission lines was done with the aid of a finite-difference transmission-line-matrix (FD-TLM) numeric simulation algorithm developed by Prof. Voelker at the University of Nebraska and implemented on a Cray supercomputer.

Figure 8 shows the time-domain signals measured at increasing propagation distances along the CPS. The effects of the finite propagation velocity, attenuation, and dispersion are clearly seen. Qualitatively, we observe the decaying signal amplitude caused by attenuation as well as the broadening of the rising edge and the ringing on the tail of the pulses caused by frequency dispersion.

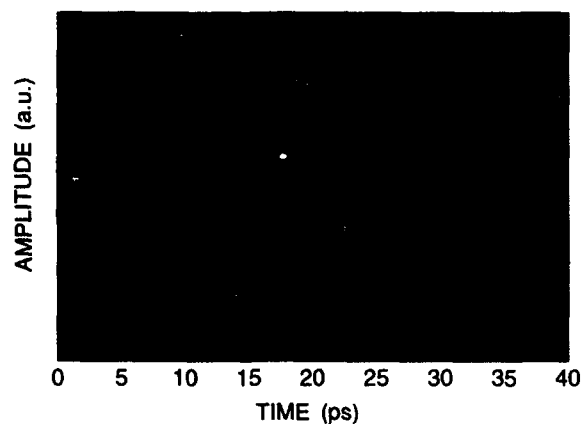


Fig. 8 — Measured time-domain picosecond electrical pulse propagation on a transmission line with 12-μm electrodes and 60-μm separation on thick sapphire substrate

Quantitative frequency-domain characteristics are obtained from the time-domain data by taking the ratio of the Fourier transforms of any pair of measured pulses. Indeed, the tremendous power of the electro-optic measurement technique is startlingly obvious when one looks at the frequency-domain data. Figure 9 shows the measured frequency-domain phase velocity and attenuation coefficient over an extraordinary 1 to 1000 GHz frequency range—a single measurement provides complete propagation characteristics in an otherwise inaccessible frequency range.

In the quasistatic limit for frequencies up to 100 GHz, phase velocity is constant and attenuation is small. For the thick-substrate CPS, the electric-field distributions are identical in the substrate and in the air, and the phase velocity is determined by an average of the substrate and air permittivities. For the membrane CPS, the electric field extends around the membrane and a much larger fraction is contained in the air. Hence, the propagation velocity is increased by ~40% compared to that of the thick-substrate CPS. This feature reduces the propagation delay and benefits time-critical paths in high-speed integrated circuits. The attenuation coefficient is dominated by resistive losses, increases slowly as a square root of frequency, and is

similar for both CPS lines. The simulations agree with the measurements, validating the simulation algorithm in the quasistatic limit.

At frequencies greater than 100 GHz, the quasistatic approximations no longer apply for our CPS structures. A larger fraction of the electric field is preferentially confined into the high-permittivity material for both CPS lines. This effect causes a continuous decrease of the phase velocity. For the thick substrate CPS, an additional parasitic effect appears to be caused by coupling of the propagating electrical signal to a shock wave radiated into the substrate. This shock wave is analogous to a wake seen after a boat that is moving faster than the wave-propagation velocity in water. The radiative-loss attenuation coefficient increases as frequency cubed, and the radiative loss rapidly overtakes the resistive loss above 200 GHz. However, for the membrane CPS, the radiative loss is suppressed as the radiated signal is effectively forced back into the guided one as a result of the thinness of the membrane, and the resistive loss remains dominant. The frequency-domain ripples are due to residual experimental inaccuracies. The simulations are in agreement with the measurements in this strongly nonquasistatic region up to 500 GHz, again indicating the validity and usefulness of the calculations.

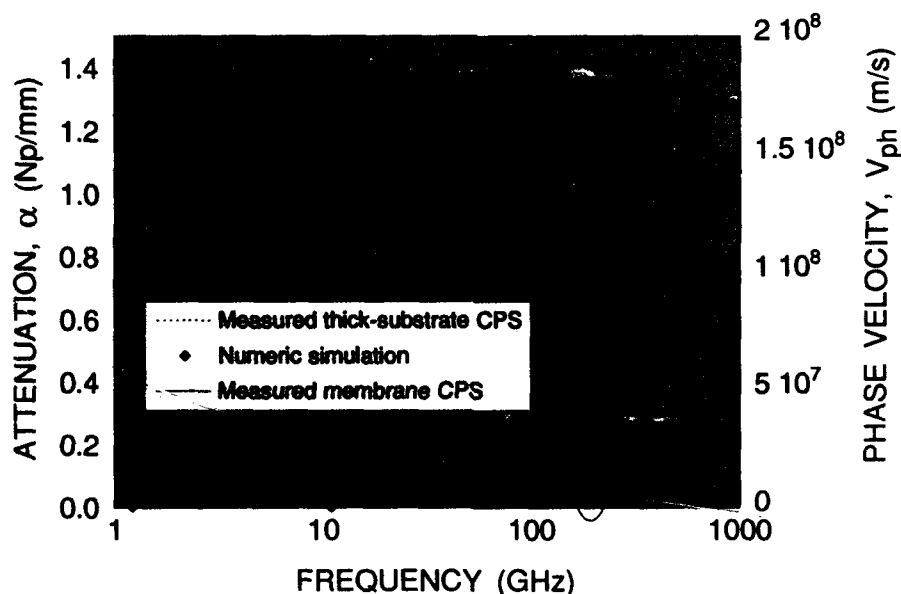


Fig. 9 — Measured and simulated frequency-domain phase velocity and attenuation coefficient for thick substrate and membrane transmission lines

We have developed a new coplanar transmission line structure fabricated on a membrane substrate supported by aerogel. An electro-optic characterization system capable of subpicosecond time resolution or 1000 GHz bandwidth has been constructed and applied to the characterization of the novel membrane transmission line. The measured characteristics show increased propagation speed and suppressed radiative loss mechanism relative to comparable conventional transmission lines. Applications of this transmission line to high-speed circuits and traveling-wave electro-optic modulators are being explored.

[Sponsored by ONR]

Reference

1. M.Y. Frankel, R.H. Voelker, and J.N. Hilfiker, "Coplanar Transmission Lines for High-Speed Low-Loss Propagation," to appear, *IEEE Trans. Micr. Theor. Techn.* ■

Paramagnetic Resonance and Optical Studies of GaN

W.E. Carlos, E.R. Glaser, and T.A. Kennedy
Electronics Science and Technology Division

J.A. Freitas, Jr.
SFA, Inc.

Semiconductors for red/infrared electro-optic applications are well established; however, materials for blue to near-ultraviolet (UV) applications have proved more elusive. Recent advances in gallium nitride (GaN) deposition techniques have made this a serious candidate for such applications. The broad motivation for our studies of wide bandgap materials is the understanding and eventual control of residual defects and impurities so that they can reach their full potential. Specifically, we have used electron spin resonance (ESR), low-temperature photoluminescence (PL), and optically detected magnetic resonance (ODMR) measurements on GaN films grown on sapphire substrates.

Excess Donor Densities: From the position of the ESR signal (shown in the inset to Fig. 10) and the magnitude and temperature dependence of its linewidth we can identify this resonance with a band of interacting shallow donors. The intensity of the low-temperature ESR measures the concentration of uncompensated donors by determining the number of neutral donors at close to complete freeze out. Figure 10 shows a monotonic increase in the uncompensated donor density with film thickness for films with aluminum nitride (AlN) buffer layers, whereas for films with GaN buffer layers, this density is almost constant. We suggest that the increase in excess donor density with thickness for the films with AlN buffer layers is due to a decrease in the density of compensating acceptors rather than to an increase in the density of donors. This indicates inhomogeneity along the growth direction of the films.

Photoluminescence Results: To investigate the question of homogeneity further, we

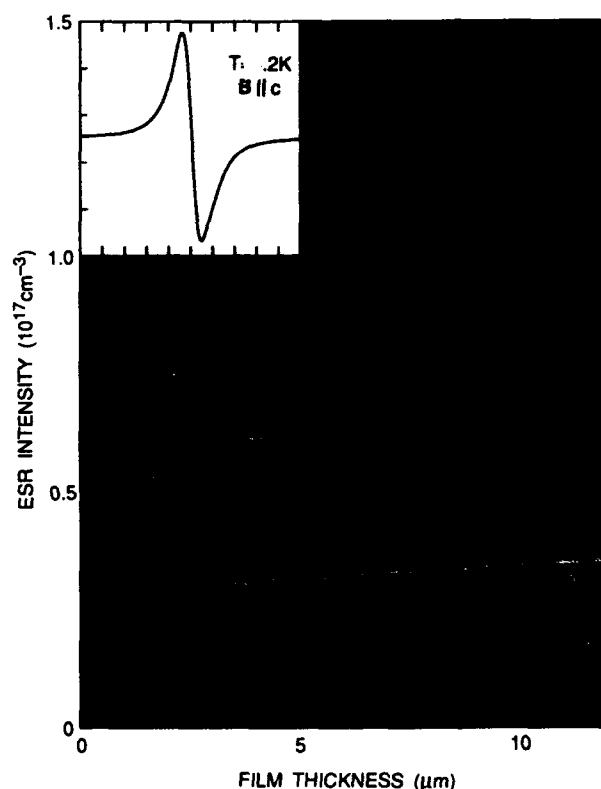


Fig. 10 — Concentration of uncompensated donors as a function of film thickness. The ESR signal is shown in the inset.

measured the PL with excitation at both the free surface and at the film-sapphire interface. The PL is primarily due to the GaN within a penetration depth ($\leq 1 \mu\text{m}$) of the appropriate interface. Figure 11 shows that the spectra are characterized by an intense sharp line near the bandedge and a broad yellow band that peaks at $\sim 2.2 \text{ eV}$. The former is due to excitons bound to neutral donors; the latter may be associated with carbon impurities and/or structural defects. With thick films, we obtain approximately equal PL intensities for excitation at either interface. However, for both bands the thinner films show 1 to 2 orders of magnitude less intensity for excitation at the film-sapphire interface than for excitation at the free surface. This clearly shows that the thin films are not homogeneous but that their homogeneity improves as the films grow thicker, presumably due to annealing at the growth temperature.

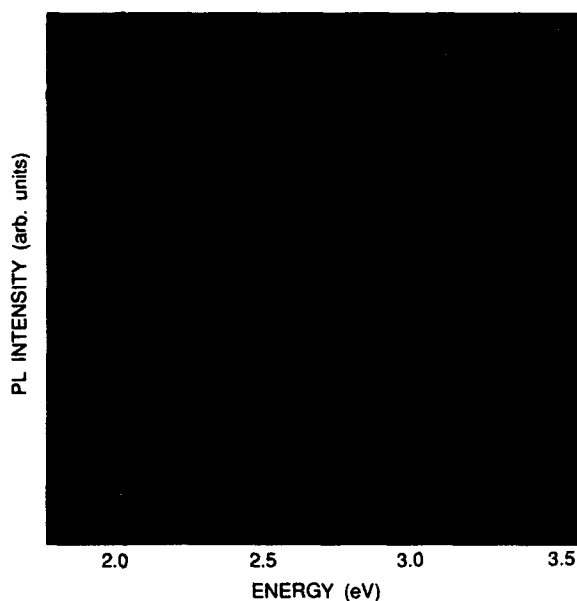


Fig. 11 — Photoluminescence spectra of a GaN film. Note that the spectrum with excitation through the substrate required ~ 100 times more power.

ODMR Results: ODMR combines PL with ESR in monitoring the effects of a magnetic resonance on the PL intensity. Figure 12

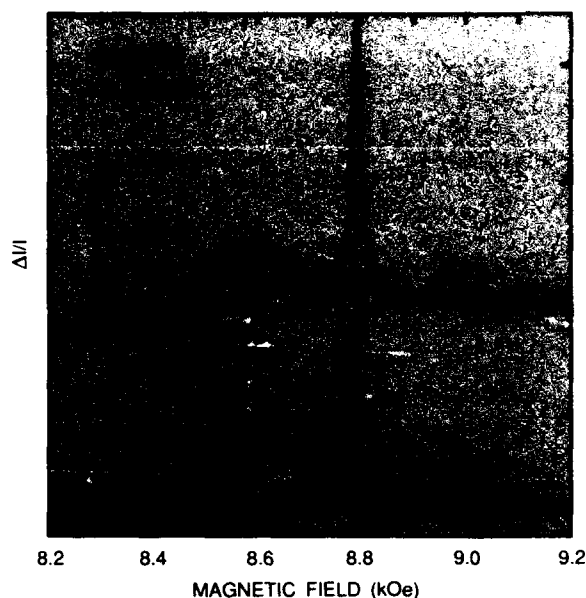


Fig. 12 — ODMR spectra of a GaN film. Sharp lines are due to the donor resonance observed in ESR, broad lines are due to a deeper state.

shows two PL increasing signals, which spectral studies indicate arise exclusively from the yellow band. The first is the sharp resonance observed in ESR and identified with delocalized donor electrons; the second, broader ODMR is associated with a deep state. Carbon, perhaps complexed with a vacancy as a deep acceptor, has been associated with the 2.2 eV band and is certainly present in large quantities in the trimethylgallium used in deposition. It has been argued that the shallow residual donors in GaN arise from N vacancies. One possibility is that the two resonances arise from the recombination of an electron in the shallow state of a nitrogen vacancy and a hole in a somewhat deeper state of the same vacancy, followed by the subsequent recombination with a hole on a deep carbon acceptor yielding the yellow luminescence. This model explains many details of the three measurements.

Acknowledgment: The GaN films used in this work were generously provided by M. Asif Khan of APA Optics.

[Sponsored by ONR]

Interferometric "Seeing" Measurements on Mt. Wilson: Power Spectra and Outer Scales

D. Mozurkewich
Remote Sensing Division

D.F. Buscher
Universities Space Research Association

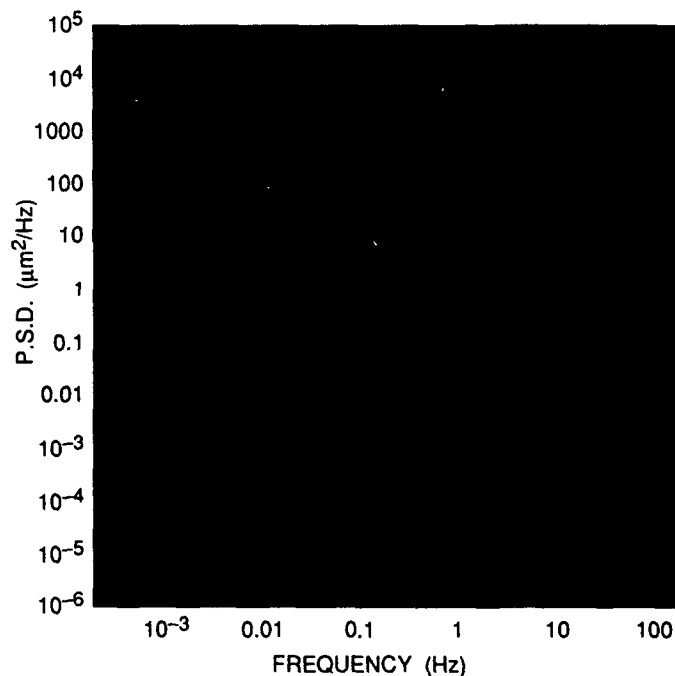
High-resolution imaging techniques, such as adaptive optics and long-baseline interferometry, will revolutionize ground-based optical astronomy by circumventing the one-arcsecond angular resolution limit imposed by atmospheric "seeing". Although these techniques make the resolution of a modern observatory independent of the seeing, the sensitivity of these techniques depends very strongly on the seeing quality. As a result, we require a more detailed understanding of the phenomena.

Turbulent mixing of warm and cold air in Earth's atmosphere causes refractive index inhomogeneities that distort a wavefront passing through it. The standard Tatarski model for atmospheric turbulence is based on two assumptions: the turbulence obeys Kolmogorov statis-

tics, and the wind blows the turbulence past the observer faster than it evolves. With these assumptions, the temporal turbulence power spectrum will vary as the $-8/3$ power of the frequency. This will be valid for spatial frequencies smaller than the "outer scale", the scale on which energy is injected into the system. For larger spatial frequencies (lower temporal frequencies), the power spectrum will saturate, although details of this saturation are not understood. The phase fluctuations we measure with an interferometer are the difference between the turbulence measured at two points separated by the baseline length. At high frequencies, this is just twice the turbulence spectrum. At lower frequencies, the power varies as the $-2/3$ power of the frequency. The break between these behaviors occurs at $f = 0.2V/B$, where V is the wind speed and B is the baseline length. The total power scales as the $5/3$ power of the baseline length.

We measured temporal power spectra of atmospheric phase fluctuations with the Mark III stellar interferometer on Mt. Wilson under a wide variety of seeing conditions. (Examples are shown in Fig. 13.) We used baselines between 4 and 31 meters. On all nights, these power spectra closely match the predicted

Fig. 13 — Power spectra of stellar fringe motion taken by the Mark III interferometer. The upper curve is from February 20, 1991, on the 31.5-m baseline; the lower curve is from July 3, 1989, on the 12-m baseline. The fitted curves are atmospheric models with coherence times of 5.5 ms and 12.3 ms, respectively, and isoplanatic patch diameters of 14 and 57 cm, respectively.



shape. On a few nights, the spectra clearly saturate at low frequencies, implying an outer scale length of order 30 to 100 meters. However, on most nights, the shape of the individual spectra are consistent with an outer scale greater than a few kilometers in size. On some of the nights, we obtained temporal power spectra on two different interferometer baselines. Although the shape of individual spectra are consistent with an infinite outer scale, the power does not increase rapidly enough with baseline length. On these nights, this saturation of the spatial structure function is consistent with the assumption of an outer scale length similar to that derived for the nights where low-frequency flattening of the spectra is clearly seen.

Our power spectra are in good agreement with the standard model for spatial scales up to several meters and timescales of a few seconds. Thus the designer of an adaptive optics system for a moderately sized telescope will be safe in basing the design on the standard model. Simi-

larly, implementing predictive fringe-tracking systems in long-baseline optical interferometers (such as the Navy Prototype Optical Interferometer currently under construction outside Flagstaff, Arizona) is a reasonable approach. The spectrum of fluctuations is much steeper than "white noise" for timescales considerably longer than the basic coherence time of the fringes.

There is good evidence for an outer-scale type of phenomenon occurring at spatial scales of 30 to 100 meters. This may imply an increase in astrometric precision of a factor of 5 to 30 (over measurements at baselines smaller than the outer scale) for the next generation of interferometers with baselines of 0.1 to 1 km. However, we do not have clear evidence that the structure function does indeed become independent of baseline. It may change slope but not completely flatten out, an effect seen in radio astronomical data.

[Sponsored by ONR] ■

**SPACE
RESEARCH
AND
SCIENCE
TECHNOLOGY**

- 227 Double Space Telescope Image Reconstruction on the
TRL Connection Machine

Paul L. Hertel and Michael L. Cobb

- 229 Impedance Mode Study for the Common Pressure
Vessel Battery

*Daniel J. Shortt, William E. Baker, Jr., James C. Garner,
and George Barnard*

- 231 Advanced Release Technologies Program

William J. Purdy

- 233 Vibration Excitation Test of the LACE Satellite as
Observed by a Ground-based Laser Radar

Shalom Elshor, K. S. Schuler, and T. W. Ryley, Jr.

Hubble Space Telescope Image Reconstruction on the NRL Connection Machine

P.L. Hertz
Space Science Division

M.L. Cobb
Remote Sensing Division

The problem with the primary mirror of the NASA/ESA Hubble Space Telescope (HST) has certainly been well reported. The very first image taken a few weeks after launch showed evidence of spherical aberration in the HST optics. Independent measurements in space and from the flawed ground test equipment show that the HST primary mirror is too flat. The aberration in the mirror, which is less than $2.3\text{ }\mu\text{m}$, causes light from the center of the mirror to be focused 4 cm in front of light from the edge of the mirror. The resulting images have a small bright core containing about 20% of the light surrounded by a broad unfocused halo containing the remaining 80% of the light [1].

The core, or Airy disk, of stellar images is the size of the diffraction limit of the HST mirror, and diffraction-limited information is contained in the aberrated images. For bright objects, deconvolution techniques can restore the images to the full diffraction limit, creating images comparable to the unaberrated optical system.

Deconvolving Images: Images that have been blurred in a predetermined and known manner can be restored through an iterative process called deconvolution. Iterative deconvolution techniques take a guess of the true image. This guess is then blurred by using the known blurring function and compared with the data. A correction term based on the difference between the data and the blurred guess is determined, and it is used to update the guess. The process continues until some convergence criteria are met.

From a deconvolution point of view, HST images are atypical. The re-imaging optics in the Wide Field/Planetary Camera imaging system distort the blurring of the image by a differ-

ent amount in different parts of the image. The mathematical operation that blurs an image, called convolution, requires that the blur function be constant over the entire image. Standard deconvolution techniques cannot handle the spatially varying blur function of HST.

A Parallel Solution: The NRL Connection Machine CM-200 is a massively parallel computer. It has 16384 processors and 2 Gbytes of memory. We have implemented parallel deconvolution codes that explicitly apply a spatially varying blur function.

The image is divided into small patches, each of which is small enough so that the blur function is constant over the patch. Each patch is assigned its own processor and enough memory to contain its own blur function. When the guess image is blurred, the parallel convolution routine simultaneously applies the appropriate blur function to each patch of the image [2,3]. The result can then be compared to the HST image data and correction terms can be derived that are fully consistent with the spatially varying blur function.

HST Images Deconvolved on the CM-2: The parallel deconvolution code has been programmed efficiently, and it runs extremely fast. The solution of a deconvolution problem typically takes 20-100 iterations. On standard SUN-class workstations, a deconvolution code using a constant blur function might take many minutes; the entire solution can take more than an hour. The CM-2 requires less than 5 seconds per iteration, so an entire image can be deconvolved in only a few minutes. This is critical for the astronomer who wants to try many iterations with different initial guesses, trial blur functions, background terms, etc.

In Figs. 1 and 2 we show the result of using the CM-2 deconvolution program on HST data. The test images were provided to us by Jim Westphal and the WF/PC instrument team. Figure 1 shows the raw and deconvolved HST images for the star cluster NGC 1850. Figure 2 shows the raw and deconvolved HST images for Saturn. Each image required less than 90 seconds on the CM-2 to deconvolve.

[Sponsored by ONR]

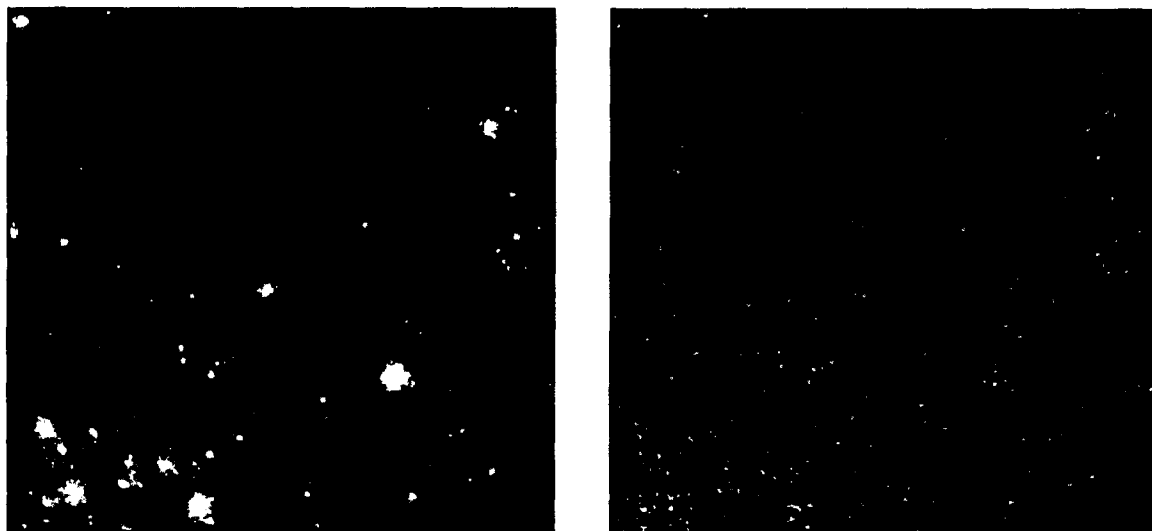


Fig. 1 — An example of image deconvolution on the Connection Machine. The left figure is the HST image of the star cluster NGC 1830. The right figure is the image after deconvolution on the CM-2.



Fig. 2 — Similar to Fig. 1, but with an HST image of the planet Saturn

References

1. R.L. White and R.J. Allen, eds., *The Restoration of HST Images and Spectra* (Space Telescope Science Institute, Baltimore, 1990).
2. P. Hertz and M.L. Cobb, "Rapid Deconvolution of Hubble Space Telescope Images on the NRL Connection Machine," in *The First Year of HST Observations*, A.L. Kinney and J.C. Blades, eds. (Space Telescope Science Institute, Baltimore, 1991).
3. M.L. Cobb, P.L. Hertz, R.O. Whaley, and E.A. Hoffman, "Space Variant Point Spread Function Deconvolution of Hubble Imagery Using the Connection Machine," in *Proc. SPIE Conf. on Image Analysis*, San Diego, July 1993, in press. ■

Impedance Model Study for the Common Pressure Vessel Battery

D.J. Shortt, W.E. Baker, Jr.,
J.C. Garner, and G. Barnard
Space Systems Development Department

The Naval Research Laboratory (NRL) is using the Common Pressure Vessel (CPV) NiH_2 battery for the Deep Space Probe Science Experiment (DSPSE). The energy density of this battery is higher than either the NiCd batteries or the Individual Pressure Vessel (IPV) NiH_2 batteries. To evaluate the performance of the electrical power subsystem (EPS), an impedance model for the CPV battery was developed. The model is based on measurements taken on the NRL qualification unit and uses passive circuit elements.

Introduction: Reference 1 describes a passive circuit model for a CPV battery. This paper extends the modeling concept of Ref. 1 to reflect a more accurate representation of the battery. The tested battery is the qualification unit for an NRL space experiment. It is a NiH_2 CPV battery consisting of 22 cells, rated for 10.5 ampere-hours (AH) and manufactured by Johnson Controls, Inc. A similar battery is being used on the Deep Space Program Science Experiment (DSPSE) described in Ref. 2. Reference 3 provides a more detailed description of the battery.

NRL's testing of the battery is based on the duty cycle that has been observed in past missions and projected mission load profiles. A unique testing condition was determined that required the battery to be able to supply load current during some operations in sunlight. Thus, the CPV battery would be charging and then discharging at frequencies approaching 100 Hz. The battery would also have to supply (discharge only) a pulsing load current in a similar range of frequencies.

The battery was subjected to a series of sinusoidal waveforms in the .01 to 1000 Hz frequency range. Table 1 shows the average and amplitude values of the waveforms. During tests that resulted in a concurrent battery discharge, the charger replenished the battery prior

Table 1 — Parameters for Figs. 4 and 5

	Curve	Avg. (A)	Ampl. (A)	°C
Discharge Mode	1	-1.25	1.25	25
	2	-5	5	25
	3	-3.75	3.75	25
Mixed Mode	A	0.5	1.5	25
	B	0.5	1.5	25
	C	0.5	1.5	10
	D	-0.5	1.5	10
	E	0.5	1.5	-10
	F	-0.5	1.5	-10
	G	0.5	1.5	35
	H	-0.5	1.5	25
	I	0.5	1.5	25
	J	-0.5	1.5	35

to each impedance measuring sweep. For tests that resulted in a net battery charge, the battery was discharged by an equivalent number of ampere hours prior to each measurement sweep. At each significant test phase, a run was first performed on a power supply simulating the battery to reduce the chance of battery damage and to validate the test set configuration.

Simulation: In Ref. 4, p. 349-353, a battery is modeled by the circuits shown in Fig. 3. (Reference 4 provides a detailed discussion of the items represented by the circuit parameters.) Our results indicate that both of these circuits can represent the CPV battery performance under different conditions.

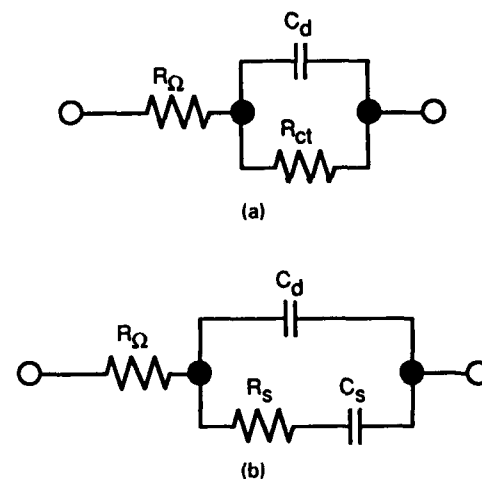


Fig. 3 — Battery model using passive circuit elements

Two cases were simulated. First the battery was modeled as a large capacitance with small series and charge transfer resistances ($R_0 = 0.055\Omega$, $R_{ct} = 0.1\Omega$, $C_d = 3500$ F). The frequency range for the simulations is 0.01 to 1000 Hz. This is the expected impedance for a 10.5 AH CPV NiH₂ battery. The second case used the following values: $R_0 = 0.055\Omega$, $R_s = 0.07\Omega$, $C_s = 330$ F, $C_d = 2$ F, where C_s represents the Warburg Impedance [4]. This represents a battery in which the frequency range for mass transfer is very limited, as contrasted with the previous case in which mass transfer has a very wide frequency range. For a battery to exhibit both of these characteristics under different ambient conditions implies that it loses capacity (note the difference in the value for C_d) as a function of temperature.

Results: Figures 4 and 5 show the CPV battery impedance data in the discharge and mixed (discharge and charge) mode, respectively. The data in Fig. 4 were taken at 25°C, which matches the simulated performance. However, the data in Fig. 5 show (for the lower temperatures, -10° and 10°C) performance that matches that of Fig. 3(b). The obvious conclusion is that the CPV battery is losing capacity as the temperature is lowered. This loss in capacity has been verified by measuring the energy discharged by the battery into a resistor

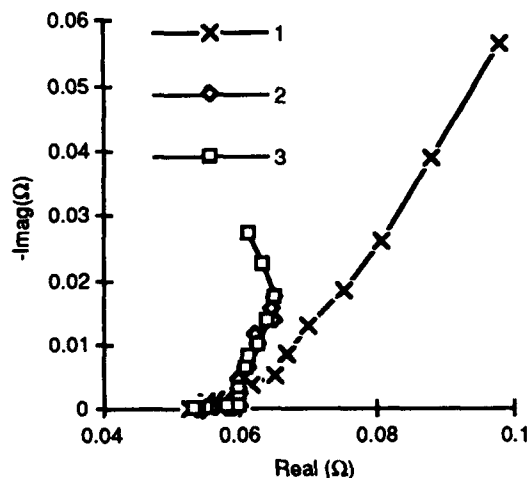


Fig. 4 — CPV battery discharge mode impedance data

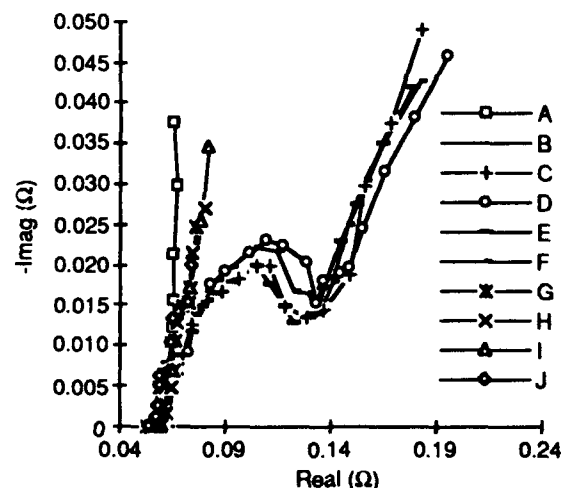


Fig. 5 — CPV battery mixed-mode impedance data

in a separate experiment. J.P. Zagrodnik of Johnson Controls, Inc., has confirmed that the loss of capacity was caused by contamination during the manufacturing process. The source of contamination has been removed and is no longer a concern.

An active or nonlinear circuit element, such as a frequency-dependent resistor, plays a significant part in the CPV battery performance at low temperatures (< 10°C). A nonlinear series element or charge transfer characteristic or a combination of both could account for the previously mentioned effect. This is a topic for a future paper.

Summary: A CPV battery impedance study was done to gain insight into the performance of the DSPSE EPS. The battery model simulation indicated that a loss of battery (10.5 AH) capacity occurs as the temperature is lowered. Additional data must be taken on other CPV NiH₂ batteries for the DSPSE EPS to determine the circuit element (series and/or charge transfer characteristic) that can cause the loss of capacity described.

[Sponsored by BMDO]

References

1. D.J. Shortt and W.E. Baker, Jr., "Battery Impedance Effects on Spacecraft Electrical Power System Stability," 26th IECEC Proceedings, 1991.

2. W.E. Baker, Jr., J.C. Garner, and D.J. Shortt, "The DSPSE Electrical Power System," 28th IECEC Proceedings, 1993.
3. J.P. Zagrodnik and K.R. Jones, "NiH₂ Multi-cell CPV Battery Development Update," 27th IECEC Proceedings, 1992.
4. A.J. Bard and L.R. Faulkner, *Electrochemical Methods: Fundamentals and Applications* (J. Wiley and Sons, 1980). ■

Advanced Release Technologies Program

W.E. Purdy

Spacecraft Engineering Department

Overview: The Advanced Release Technologies (ARTS) program, managed by the Naval Research Laboratory's Naval Center for Space Technology, is tasked with reducing the cost and weight of spacecraft by developing improved release mechanism and ordnance systems. These systems can be greatly improved by using the emerging technologies of high-power laser diodes and nonexplosive release mechanisms. One laser-diode-based ordnance firing system and two nonexplosive release mechanisms were developed under this program. Another nonexplosive release mechanism was tested and approved for flight.

Background: The ARTS program was motivated by the high costs associated with using electrically activated ordnance on present day spacecraft. The cost savings generated by these advanced components result from:

- reducing the safety issues of ordnance systems,
- eliminating the need for heavy electromagnetic interference (EMI) and radio frequency interference (RFI) shielding of ordnance systems, and
- greatly reducing the pyroshock environment for spacecraft.

A quantitative cost analysis showed that implementing the ARTS components into a large spacecraft would result in a savings of \$500 K for each satellite built. The development of these systems into flight-qualified components took place from October 1991 to December 1993. This process culminated in the production of a space flight experiment containing two of each of these components. The following is an overview of each of the components that were developed and used in the flight experiment.

Frangibolt™: The Frangibolt™ release mechanism, developed by the TiNi Alloy Company in Oakland, California, and the Naval Center for Space Technology, uses the shape memory alloy, nitinol, to break a notched bolt in tension on command to effect a release operation (Fig. 6). The nitinol collar is compressed so that when heated it elongates to its original length, stretching the bolt until it fails in tension at the notch.

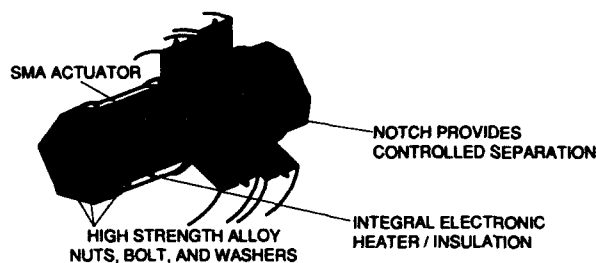


Fig. 6 — Frangibolt™

Nonexplosive Separation Nut: The nonexplosive separation nut, developed and qualified independently by G&H Technologies Special Products Division in Santa Monica, California, uses their previously qualified Non-Explosive Actuators (NEAs) to unlatch a spring-powered separation nut (Fig. 7). Current is passed across the bridgewire of the NEA. This releases it, and in turn unlocks the release housing of the separation nut, which is driven upward to disengage the thread segments, which releases a preloaded bolt.

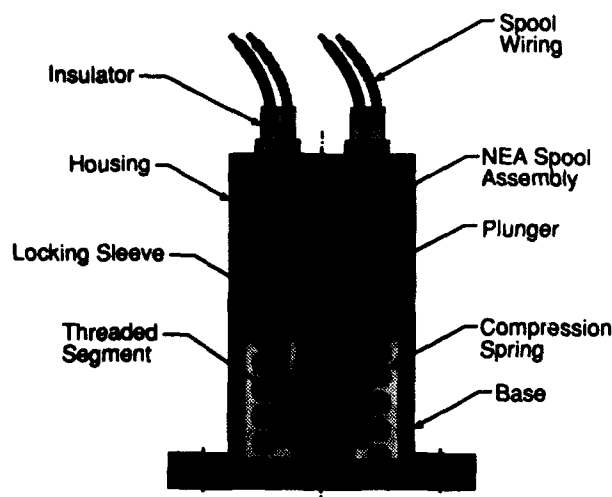


Fig. 7 - Nonexplosive separation nut

Fusible Link: The Fusible Link, jointly developed by Boeing Space and Defense Mechanisms Research Department, in Seattle, Washington, and the Naval Center for Space Technology, fuses a strap made of nitinol to unlock a preloaded link to perform a release operation (Fig. 8). When a 30 amp, 3 V ac current is applied to the nitinol fusing element, it burns through within 300 ms, unlatching the jaws. This allows the tensioned link to be pulled out of the separable joint. Nitinol is used as the fusing element because of its properties of high strength, high electrical resistivity, and excellent corrosion resistance, rather than for its shape memory effect.

Laser Ordnance System: The laser ordnance system, jointly developed by Ensign Bickford Aerospace Corporation in Simsbury, Connecticut, and the Naval Center for Space Technology, ignites explosive cartridges that use lasers rather than electrically heated bridge-wires. A 2-W laser diode fires down a fiber-optic harness into an explosive cartridge, igniting the explosive mix.

Flight Experiment: A flight experiment containing all of the ARTS devices is in production at NRL and will have completed protoflight acceptance testing by December 1993. The experiment will then be installed on a host spacecraft and will await launch. The experiment

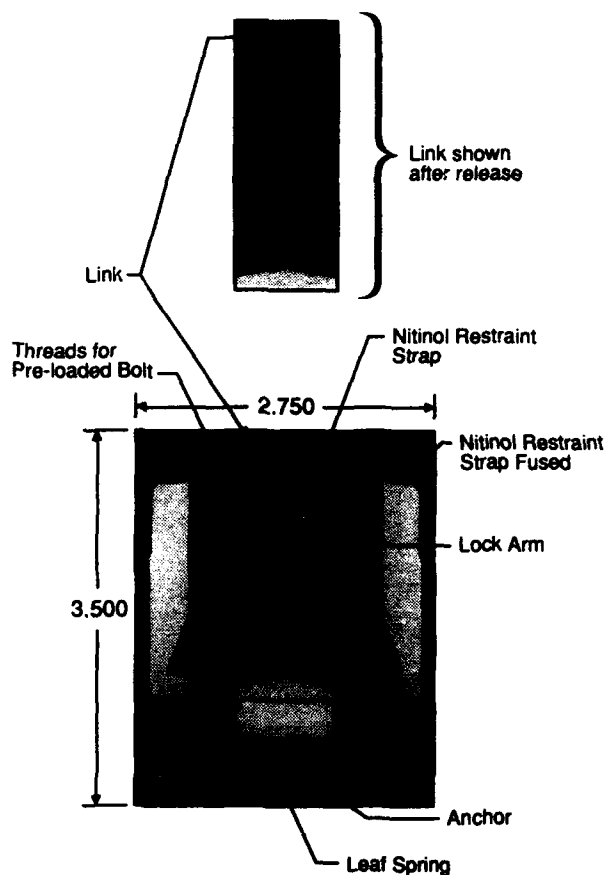


Fig. 8 - Fusible link

contains two laser-ordnance-fired bolt cutters, two Frangibolts™, two nonexplosive separation nuts, two Fusible Links and their dc to ac power converter. The experiment has eight small preloaded plates, which are individually deployed upon release of the ARTS devices. The deployment is verified by Hall effect sensors. One of each of the two devices will be operated within two months of launch; the second of each of the devices will be operated approximately one year after launch.

Conclusion: All of the tasks of a spacecraft ordnance system can be performed with a lighter, more economical system by using the ARTS-developed components. The implementation philosophy is to replace all pyrotechnically driven release devices with nonexplosive release devices and to fire the remaining ordnance with the laser ordnance system. The primary thrust of the ARTS program has been

to create economic savings, including the inherent cost savings of weight reductions. The ARTS program will conclude with flight-proven spacecraft components ready for implementation on production spacecraft with minor resizing of the components as required. Implementation of these components is taking place on Navy satellites that are being designed. The Frangibolt™ is being used to release the solar arrays on the Deep Space Probe Science Experiment (DSPSE) spacecraft to be launched in January 1994. Several other Department of Defense and National Aeronautics and Space Agency space programs are looking at implementing these components.

[Sponsored by SPAWAR] ■

Vibration Excitation Test of the LACE Satellite as Observed by a Ground-based Laser Radar

S. Fisher

Spacecraft Engineering Department

K.I. Schultz

*Massachusetts Institute of Technology
Lincoln Laboratory*

L.W. Taylor, Jr.

*National Aeronautics and
Space Administration*

A thorough knowledge of the response of orbiting systems to disturbances is essential to the design, construction, and operation of modern spacecraft. The very lightweight construction of space structures and the effects of the space environment such as weightlessness require on-orbit data measurements to establish an understanding of the behavior of structures in space. Pursuant to this goal of obtaining on-orbit satellite data, the Low Power Atmospheric Compensation Experiment (LACE) dynamics experiment measured vibrations of a large, orbiting satellite by means of the 10.6- μm CO₂ Firepond laser radar operated by the Massachusetts Institute of Technology (MIT) Lincoln

Laboratory in Westford, Massachusetts. Successful tests were conducted in January 1991 and August 1992. The 1991 tests measured vibration velocity amplitudes to within 2 mm/s, thereby demonstrating the feasibility of this ground-based vibration-detection technology. The 1992 tests observed open-loop augmentation and damping of vibration amplitudes by a timed sequence of preprogrammed impulses applied to the LACE spacecraft by boom movements. Also in 1992, improvements in the Firepond system allowed Doppler velocity measurements to 0.5 mm/s precision. Because of the high cost of space experiments, only two other on-orbit vibration experiments have been conducted: the Solar Array Flight Experiment (SAFE) [1], and the Middeck Zero-Gravity Dynamics Experiment (MODE) [2]. Both of these experiments were mounted on the space shuttle. The LACE dynamics experiment, performed on a free-flying satellite, has provided an opportunity to obtain valuable on-orbit structural dynamics information at relatively low cost. The dynamics experiment rode "piggy-back" as an experiment secondary to the primary objective of the LACE satellite. We used the novel technique of using ground-based measurements of vibrations of the orbiting satellite.

Description of the Dynamics Experiment: The LACE satellite was launched on February 14, 1990, into a 540-km-altitude, circular, 43° inclination orbit. The spacecraft, (Fig. 9) was built for the Ballistic Missile Defense Initiative Organization (BMDO) by the Naval Research Laboratory. The 1,400-kg Earth-pointing LACE spacecraft has three deployable/retractable booms of maximum length 45.72 m (150 ft). The zenith-directed gravity gradient boom, mounted on the top of the bus with a magnetic damper at its tip, controls pitch to within about 1° libration amplitude. A constant-speed momentum wheel controls roll and yaw motion. The forward or retro-boom is deployed along the velocity vector; an array of glass retro-reflectors is installed at its tip to enable atmospheric compensation experiments. The balance boom is deployed counter to the velocity.

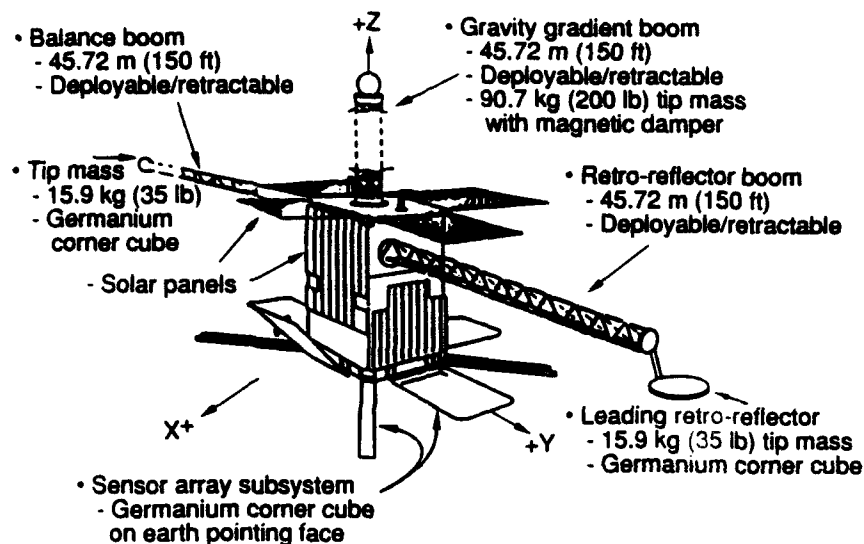


Fig. 9 — LACE satellite showing placement of retro-reflectors

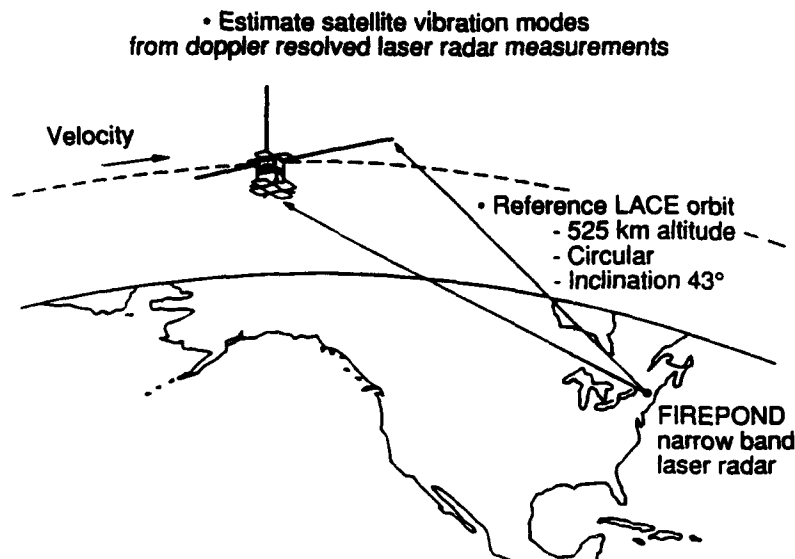


Fig. 10 — LACE dynamics experiment showing targeting from Firepond

Flight hardware for the secondary dynamics experiment consists of infrared (IR) germanium retro-reflectors mounted on the tip of the lead boom, the bottom of the satellite body, and the tip of the trailing boom. After acquisition and track initiation by a visible light argon-ion laser, the Firepond system targets the germanium reflectors with the 10.6- μm CO₂ laser radar (Fig. 10). The beamwidth at the LACE altitude is about 5 m. Two of the reflectors are illuminated simultaneously to provide differential

Doppler measurements of relative retro-reflector motion. This motion is generated by the vibrations of the boom tip relative to the body, by the rigid-body satellite motion, and by retraction of the lead boom.

In the 1991 tests, the lead boom was retracted from 24.4 m (80 ft) to 4.57 m (15 ft) during illuminations from the 10.6- μm IR laser radar. The trailing boom and gravity gradient booms were fixed at 45.72 m (150 ft). Forced vibrations of the LACE structure were observed

during the retraction, and free-damped system vibrations were observed after the retraction was stopped. The results demonstrated the importance of in situ verification of initial finite-element modeling (FEM). A mode not previously predicted was observed, and the identified frequencies were shifted somewhat from predicted values. The initial model had been based on static ground tests [3].

Open-Loop Control: In the 1992 tests, vibration modes were excited by a preprogrammed series of impulses to demonstrate open-loop vibration excitation and damping. The impulses were provided by movements of the gravity-gradient boom with single 0.15-m (6-in.) bay retractions and deployments. Its nominal length is 45.72 m (150 ft). The lead boom was fixed at 5.5 m (18 ft), and the trailing boom was fixed at 45.72 m (150 ft). Each retraction and/or deployment of the gravity-gradient boom effectively gives two 0.5-s-duration impulses of equal magnitude and opposite direction to the satellite body. Timing of repeated retractions/deployments excites or quenches vibrations, depending on the phasing of the maneuvers. A maximum vibration amplitude of about 10 mm/s is thereby obtained. Computer simulations were performed to determine an appropriate sequence of deployment/retraction maneuvers to both

excite and inhibit boom vibration modes. The sequences were preprogrammed 24 h before the test and uplinked to LACE. After target acquisition and track initiation from Firepond, a voice command was given to the ground-control site to initiate the boom maneuver sequence.

In the first part of the 1992 tests, on Julian day 239, the gravity-gradient boom was commanded to retract and deploy at 20-s intervals. The goal was to excite vibrations large enough to be observable by the Firepond system. An early analysis of the data showed that two modes were observable: 0.13 Hz and 0.31 Hz. Therefore on subsequent days, a deployment/retraction pattern was set up to excite and damp vibrations. Observations of damping were made on Julian day 242.

Comparison of Simulations with Observations: To better simulate the observations, structural parameters of the FEM model of the system were slightly modified. The bending stiffness of the booms was increased, the torsional stiffness was increased, and the cannister stiffness was decreased. Figure 11 shows the resultant simulations compared with day 239 observations. The plot shows the measured vibration velocity amplitudes, with the amplitude of the simulated velocities rescaled. It can be seen that the simulated vibration matched the

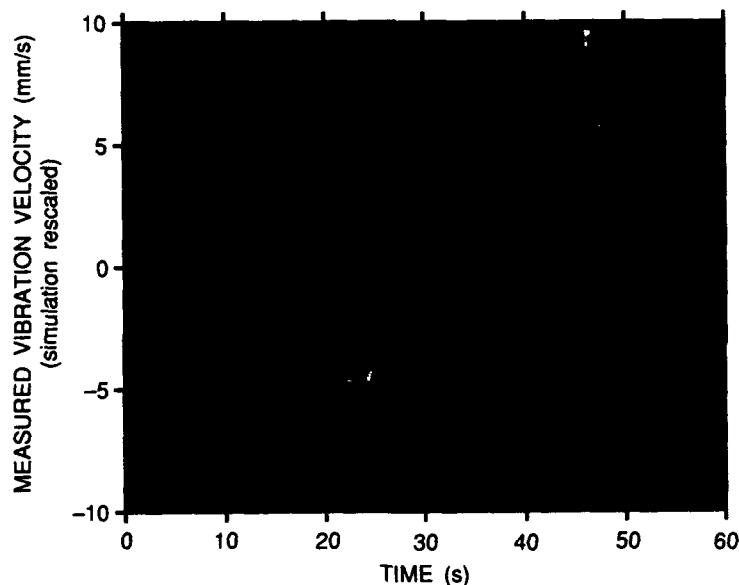


Fig. 11 — Comparison of observed vibrations vs simulation, day 239

phasing of the observed vibration quite well over many cycles, thereby giving confidence in the fidelity of the revised FEM model.

Conclusion: The LACE dynamics experiment demonstrated the feasibility of remote sensing as a relatively low-cost technique for health monitoring and vibration measurements of orbiting structures. The space hardware requirements are minimal: germanium retro-reflectors, which cost about \$5 K each. An array of the reflectors onboard an orbiting structure would allow for periodic assessment of structural health.

The experiment has enabled a considerable improvement in the FEM structural model and has demonstrated open-loop vibration excitation and damping of vibrations of an orbiting structure. The Firepond laser radar has measured vibration amplitudes with a precision of 0.5 mm/s.

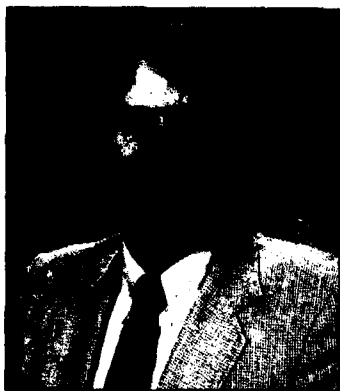
[Sponsored by NASA]

References

1. Lockheed Missiles and Space Co., "Solar Array Flight Experiment Final Report," Marshall Space Flight Center, Huntsville, Ala., Contract NASA-31352, Report No. LMSC-F087173, April 1986.
2. E.F. Crawley, M.S. Barlow, M.C. Van Schoor, B. Masters, and A.S. Bicos, "Mid-deck Zero-Gravity Dynamics Experiment: Comparison of Ground and Flight Test Data," Presented to the 43rd Congress of the International Astronautical Federation, Washington, DC. 28 Aug.-5 Sept. 1992. McDonnell Douglas Space Systems Company, MDC 91H1160, August 1992.
3. K.I. Schultz and S. Fisher, "Ground-based Laser Radar Measurements of Satellite Vibrations," *Appl. Opt.* 31(36), 7690 (1992). ■

**AWARDS
AND
RECOGNITION**

239	Special Awards and Recognition
247	Individual Honors
259	Allen Berman Research Publication and Edison Patent Awards
264	Awards for <i>NRL Review Articles</i>



Dr. Michael Collins
Acoustics Division

**ACOUSTICAL SOCIETY OF AMERICA
1993 R. BRUCE LINDSAY AWARD**

Dr. Collins was cited "for his exceptional contributions to numerical modeling of complex acoustical phenomena and nonlinear inversion methods...Dr Collins' research cuts across many state-of-the-art areas of ocean acoustics, including elastic and two-way parabolic equation, simultaneous localization, and environmental search (focalization)."



Dr. Richard J. Colton
Chemistry Division

**CHEMICAL SOCIETY OF WASHINGTON
1992 HILLEBRAND PRIZE**

Dr. Colton was recognized for "his outstanding original contributions to the science of chemistry, which have been recognized nationally and internationally." According to the nomination, "Dr. Colton has been a major force in promoting surface science and especially nanometer-scale science and technology..."



Dr. Norman Koon
*Materials Science and
Technology Division*

E.O. HULBURT SCIENCE AND ENGINEERING AWARD

Dr. Koon received NRL's highest civilian honor for his "sustained, important, and continuing contributions to the science and technology of rare Earth-transition metal materials. It is important to note that he has contributed not just to the science and not just to the technology, but to both, in great measure."

Special Awards and Recognition

NRL is proud of its many distinguished scientists and engineers. A few of these have received exceptional honors for their achievements.



1992 ROBERT J. COLLIER TROPHY

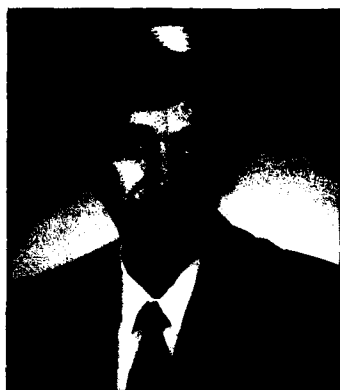
NRL was honored by the National Aeronautic Association (NAA) for significant contributions to the development of the NAVSTAR Global Positioning System (GPS). ADM Stanley R. Arthur, Vice Chief of Naval Operations, accepted the trophy on behalf of NRL and the Navy. NAA recognized the GPS team for "the most significant development for safe and efficient navigation and surveillance of air and spacecraft since the introduction of radio navigation 50 years ago." From left to right are CAPT Paul Gaffney, Mr. Roger Easton, Dr. Timothy Coffey, Mr. Peter Wilhelm, and RADM William Miller. Mr. Easton, a former NRL employee, was the founder of the NRL program that led to the GPS.



Dr. Robert F. Brady, Jr.
Chemistry Division

1992 ROON FOUNDATION AWARD

Dr. Brady co-authored a paper that was judged to be the best paper presented at the annual meeting of the Federation of Societies for Coatings Technology. His research work for the paper was done at the Materials Research Laboratory in Australia while Dr. Brady was there on assignment as a visiting scientist.



Dr. Warren E. Pickett
*Condensed Matter and
Radiation Sciences Division*

SIGMA XI 1993 PURE SCIENCE AWARD

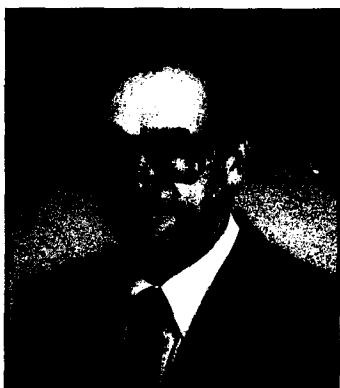
Dr. Pickett was cited "for his outstanding theoretical efforts that contributed to a better understanding of the properties of high-temperature superconductors."



Dr. Alan D. Kersey
Optical Sciences Division

SIGMA XI 1993 APPLIED SCIENCE AWARD

Dr. Kersey was cited "for innovative research in fiber-optic sensor technology, which has led to significant advances in signal processing, multiplexing, polarization phenomena, fiber gyroscopes, and smart structures and other areas of particular use to the Navy."



Dr. James D. Kurfess
Space Science Division

NATIONAL AIR AND SPACE ADMINISTRATION (NASA) EXCEPTIONAL SCIENTIFIC ACHIEVEMENT MEDAL

NASA, which awards this medal for "unusually significant scientific contributions toward achievement of aeronautical or space exploration goals," recognized Dr. Kurfess for his "outstanding achievements as principal investigator of the Oriented Scintillation Spectrometer Experiment (OSSE) instrument and the discovery of Cobalt-57 emission from Supernova 1987A and of the nature of the gamma ray emission from the Galactic Disk."



Dr. Gerald Share
Space Science Division

**AMERICAN ASTRONOMICAL SOCIETY
1992 BRUNO ROSSI PRIZE**

Dr. Share was cited for his "wide-ranging contributions to the understanding of solar and cosmic gamma radiation," particularly recognizing his "ingenuity and leadership" in the use of broad field-of-view gamma-ray spectrometer on NASA's Solar Maximum Mission.



Mr. Peter G. Wilhelm
*Director of the Naval Center
for Space Technology*

**ROTARY NATIONAL AWARD
FOR SPACE ACHIEVEMENT FOUNDATION
1993 STELLAR AWARD**

Mr. Wilhelm was recognized for his "career-long contributions to America's space program" and received the Stellar Award in the Program Management Category. During his leadership of NRL's space technology program, NRL has become the Navy's leading laboratory in space technology and is credited with the design, development, and operation of 80 scientific and Fleet-supported satellites.



Dr. Donald U. Gubser
*Materials Science and
Technology Division*

**SENIOR EXECUTIVE SERVICE
MERITORIOUS RANK AWARD**

Dr. Gubser was cited for "his sustained outstanding leadership and achievements in materials science and technology." Under his leadership, the division has initiated new research projects in the areas of superconductivity, magnetism, composite materials, adaptive structures, processing science, and computational simulations.



Dr. David Bradley
Acoustics Division

NAVY SUPERIOR CIVILIAN SERVICE AWARD

Dr. Bradley was cited for "his innovative research and development leadership in serving the Navy, DoD and the nation throughout his career...Dr. Bradley has enabled the Navy to best perform its mission in a diverse set of warfare areas, including antisubmarine warfare, mine warfare, mine countermeasures, Navy special warfare, and in nuclear submarine security."



Dr. Joel M. Schnur
*Center for Bio/Molecular
Science and Engineering*

NAVY SUPERIOR CIVILIAN SERVICE AWARD

Dr. Schnur was recognized for "his sustained outstanding and pioneering leadership in the development of the field of bio/molecular science and technology for Navy, Department of Defense, and national applications."



Mr. Richard A. Hale
Information Technology Division

NAVY SUPERIOR CIVILIAN SERVICE AWARD

According to the award citation, "Mr. Hale's insight into the Navy's operational requirements for information security enabled him to generate specifications that resulted in the delivery of the first standard military computer with embedded cryptography and a multi-level operating system, database management system and network."



Ms. Halcyon Morris
Acoustics Division

NAVY MERITORIOUS CIVILIAN SERVICE AWARD

Ms. Morris was recognized for "her long-term career achievements and outstanding contributions to the advancement of women in the Navy research laboratory workplace, her establishment of educational programs to increase opportunities for women and minorities in scientific fields, her establishment and management of joint Laboratory-University programs to increase cooperation and interaction in graduate education and Navy research, and her overall efforts to enhance the Laboratory's facilities and external recognition."



Dr. Frederick W. Williams
Chemistry Division

NAVY MERITORIOUS CIVILIAN SERVICE AWARD

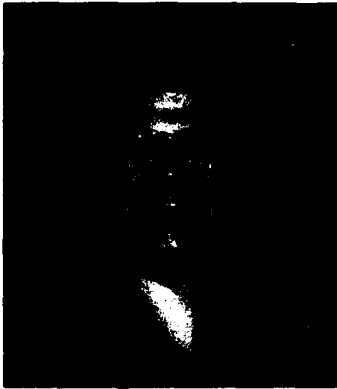
Dr. Williams received the award for "the great breadth and remarkable productivity of his scientific accomplishments and dedication to his work and to the Navy....for his mastery of the intricacies and complexities of combustion and fire processes, for his application of those insights toward the solution of very real and urgent Navy problems, and for his extension of those solutions toward the safety and well-being of society as a whole."



Mr. Joseph F. Thomason
Radar Division

**OFFICE OF NAVAL RESEARCH
OUTSTANDING EMPLOYEE WITH DISABILITIES AWARD**

Mr. Thomason was recognized for his work in the development of high-frequency radar and his efforts to solve wide-area surveillance problems. According to the nomination, "because of his handicap there were more obstacles to overcome than field assignments normally present. He dealt with these obstacles willingly and without complaint."



Dr. Bruce P. Gaber
*Center For Bio/Molecular
Science and Engineering*

**OFFICE OF NAVAL RESEARCH
EQUAL EMPLOYMENT OPPORTUNITY AWARD**

and

**NRL COMMANDING OFFICER'S AWARD FOR
ACHIEVEMENT IN THE FIELD OF EQUAL OPPORTUNITY
(Supervisory Category)**

Dr. Gaber was recognized for "making a major difference in equal employment opportunities both within and beyond NRL." According to the nomination, Dr. Gaber has been a "staunch advocate of EEO objectives at the Laboratory. He has worked diligently to establish an environment that provides advancement opportunities for women and minorities in science."



Mr. Eugene Kelley
Command Support Division

**OFFICE OF NAVAL RESEARCH
EQUAL EMPLOYMENT OPPORTUNITY AWARD**

and

**NRL COMMANDING OFFICER'S AWARD FOR
ACHIEVEMENT IN THE FIELD OF EQUAL OPPORTUNITY
(Nonsupervisory Category)**

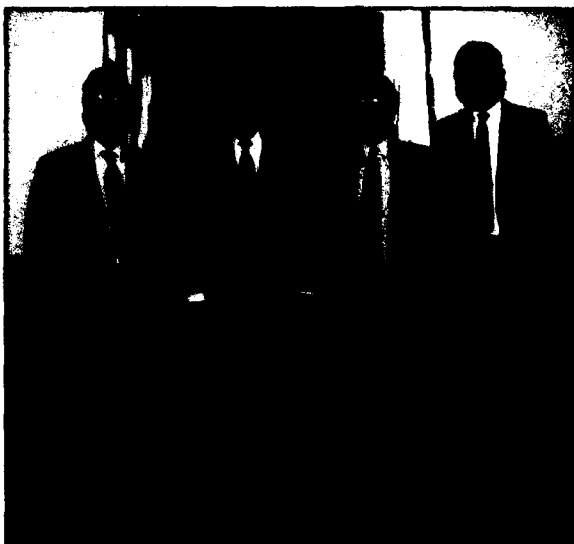
As a member of the Black Employee Subcommittee since 1989, Mr. Kelley is credited with reorganizing and revitalizing this important EEO organization in 1992. His efforts resulted in a dramatic increase in participation. He has also worked with the DC Metropolitan Police Department in an outreach program for troubled.



Dr. Carl Landwehr
Information Technology Division

**INTERNATIONAL FEDERATION FOR
INFORMATION PROCESSING (IFIP)
SILVER CORE AWARD**

Dr. Landwehr, who was the founding chairperson of IFIP's Working Group 11.3 on Database Security, received the award for his six years of service as chairperson. He has recruited members from industry, government, and universities. He has edited or co-edited six books reporting the results of those meetings, which have become fundamental references for researchers in database security.



THE TECHNICAL COOPERATION PROGRAM (TTCP) ACHIEVEMENT AWARD

This award is presented annually to United States participants in TTCP for excellence in collaborative research and development. Recipients of the award (left to right) are: Dr. Robert Pohanka, Office of Naval Research; Dr. Bhakta Rath, Associate Director of Research of the Materials Science and Component Technology Directorate, Naval Research Laboratory; and Dr. Robert Schwartz, Naval Warfare Center in China Lake. Mr. Jack Bachkosky of the Office of Director of Defense Research and Engineering (far right) presented the award.



NAVAL DISTRICT WASHINGTON PERSONAL EXCELLENCE PARTNERSHIP OF THE YEAR AWARD

NRL is the recipient of this award for the third consecutive year in the collaborative category for exemplary partnership with the following schools: Leckie and Patterson Elementary Schools, Harris Educational Center, and Ballou Senior High School. Through this award, NRL community outreach volunteers are recognized for their outstanding performance in support of the four partner schools. Shown are just a few of NRL's volunteers and school representatives: front row (left to right) Vivian Gibson, Counselor from Patterson; Dr. George Carruthers; Ruth Phillips; Beba Zevgoliz; Gabrielle Peace; Judy Hope; and Linda Shaw; back row (left to right) CAPT Paul Gaffney II, USN, NRL Commanding Officer; Michael Rugar; Dr. Robert Pellenbarg; RADM Edward Moore, Jr., USN, Commandant, Naval District Washington; Dom Panciarelli, Community Outreach Coordinator; and Dr. Edward Stone. RADM Moore presented the award to CAPT Gaffney who accepted on behalf of the volunteers.

Individual Honors

Laboratory employees received numerous scientific medals, military service awards, academic honors, and other forms of recognition, including election and appointment to offices in technical societies. The following is an alphabetical list of persons who received such recognition in FY 1993.



CAPT Gaffney presents Dr. Jerome Karle, Chief Scientist of the Laboratory for Structure of Matter and recipient of the 1985 Nobel Prize in Chemistry, with NRL's first Lifetime Achievement Award. CAPT Gaffney remarked, "NRL would like to recognize you with something that will mark this day in your lifelong contributions to this great Laboratory, that you have served so well for nearly five decades..."

Ahn, S., Executive Director, Korean-American Scientists and Engineers Association.

Aggarwal, I.D., Member, Program Committee, International Meeting on Halide and Chalcogenide Glass, May 1994, China; Chairman, DoD Panel on Fiber Optic Chemical Sensors at Air and Waste Management's International Symposium on Optical Sensing, October 1993.

Anderson, W.T., Technical Chairman, GaAs Reliability Workshop; Member, Scientific and Steering Committee of the Workshop on Expert Evaluation and Control of Compound Semiconductor Materials and Technologies (EXMATEC); Member, Technical Program Committee of the Advanced Mi-

croelectronics Qualification, Reliability, and Logistics Workshop; Member, Technical Program Committee of the European Symposium on Reliability of Electron Devices, Failure Physics and Analysis; Member, Advisory Board, NASA MMIC Reliability Assurance Group; Visiting Professor, University of Darmstadt, Germany.

Apruzese, J.P., Appointed to Program Committee, Sixteenth International Conference on Lasers and Applications; appointed to Program Committee, Fourth International Colloquium on X-ray Lasers.

Batra, N.K., Associate Technical Editor, *Materials Evaluation*; Finance Chairman, 1993 IEEE Ultrasonics Symposium; Member,

- IEEE Ultrasonics Symposium Technical Program Committee; Session Chairman, 1992 IEEE UFFCS Symposium, Tucson, Arizona; Session Chairman, 1992 QNDE Meeting, San Diego, California.
- Berkson, J.M.**, Appointed to Technical Committee on Underwater Acoustics, Acoustical Society of America.
- Bermudez, V.C.**, Invited talk at American Vacuum Society Meeting, Santa Fe, New Mexico, April 20, 1993.
- Bernhardt, P.A.**, Elected Senior Member of the Institute for Electronics and Electrical Engineers (IEEE); Elected Chairman of Commission II (Waves in Plasmas) for the International Union of Radio Science (URSI) for the United States National Committee (USNC); Member of the American Geophysical Union (AGU) Books Board; Associate Editor, *Journal of Geophysical Research* — Space Physics; Editor, Special Issue on Advances in Space Research (Active Experiments in Space).
- Binari, S.C.**, Asked to serve on 1993 GaAs IC Symposium Technical Program Committee.
- Blue, J.E.**, Fellow, Acoustical Society of America; Chairman, Membership Committee, Acoustical Society of America.
- Bogar, F.D.**, Elected First Vice Chairman, National Capital Section of The Electrochemical Society.
- Boos, J.B.**, Served as Area Chair, Electron Devices Area for the 1993 International Conference on InP and Related Materials; Served as Secretary, Steering Committee, International Conference on InP and Related Materials.
- Boris, J.P.**, Chair, APS Computational Physics Division Rahman Prize Committee; Program Subcommittee, 25th International Symposium on Combustion; AIAA Fluid Dynamics Technical Committee; Panel to Review NASA Ames CFD Program.
- Borsuk, G.M.**, Co-chairman — U.S. Delegation Co-chairman, TTG 3, COCOM; Chairman, DoD Panel on Electronics for COCOM.
- Brady, Jr., R.F.**, Technical Editor, *Journal of Coatings Technology*; Appointed U.S. National Leader, The Technical Cooperation Program (TTCP), Panel P-3 on Organic Materials; Member, Budget and Finance Committee, American Chemical Society.
- Brancato, E.L.**, Member, four standards committees of IEEE, ASTM, and International Electrochemical Commission.
- Broughton, J.Q.**, Editor of Materials Research Society's December 1992 proceedings on "Materials Theory and Modelling;" Editor of Special Issue of *Computational Materials Science*, "Issues and Perspectives for the 90s. A Global View."
- Brueckner, G.E.**, Elected Full Member of Section 1 (Basic Sciences) of the International Academy of Astronautics.
- Buckley, L.J.**, Appointed to National Research Council Committee for Materials Advisory Board Study on New Sensor Materials; Member, Editorial Board, American Institute of Physics, *Journal of Smart Materials and Structures*.
- Bultman, J.D.**, Member, Committee on Creosote and Creosote Solutions and Member, Committee for the Evaluation of Wood Preservatives, both of the American Wood-Preservers' Association; Associate Editor and Member of the Editorial Board of *El Guayulero* (published by the Association for the Advancement of Industrial Crops); Associate Editor, *Biotropica* (published by the Association for Tropical Biology); and Associate Science Editor (NRL) for Naval Research Reviews (published by the Office of Naval Research).
- Buot, F.A.**, Member, Advisory Committee, International Workshop on Computational Electronics, Leeds, U.K.; UNDP Consultant, University of the Philippines and University of San Carlos.
- Campbell, F.J.**, Eric O. Foster Award for Distinguished Service, IEEE/DEIS.
- Campillo, A.J.**, Elected Fellow of the Optical Society of America; Appointed Topical Editor of *Optics Letters*; Chaired Optical Sensors and Measurements Program Subcommittee of the 1992 Lasers and Electro-optics Society Annual Meeting; Served on the Program Committee of the Optical Society of America Annual Meeting.

- Cantrell, B.H.**, Letter of Commendation from Program Executive Office; Theater Air Defense.
- Carlos, W.**, Invited talk at International Conference on SiC and Related Materials, November 1-3, 1993.
- Carruthers, G.R.**, Editor, *National Technical Association Journal*.
- Chang, E.L.**, Elected President of the Society of Chinese Biophysicists in America.
- Cheng, C.C.**, Appointed by the Academia Sinica, Taipei, Taiwan, as a member of the Advisory Committee for the Institute of Astronomy and Astrophysics, Academia Sinica.
- Cogdell, G.B.C.**, Member, Program Committee, Lasers and Electro-Optics Society, IEEE, November 1993.
- Collins, M.D.**, Received the R. Bruce Lindsay Award from the Acoustical Society of America.
- Colton, R.J.**, Recipient, 1992 Hillebrand Prize awarded by the Chemical Society of Washington; Director, American Vacuum Society; Chairman, AVS Nanometer-scale Science and Technology Division.
- Cooper, K.P.**, Chairman, Washington, D.C. Chapter of ASM International; Co-Chair of Sub-Topic Area "Electron and Laser Beam Melting and Surface Modification" at First International Conference on Processing Materials for Properties, Honolulu, Hawaii, Nov. 7-10, 1993.
- Cooperstein, G.**, Fellow, American Physical Society; Technical Programs Chairman, 1995 IEEE International Pulsed Power Conference; Editor, *Proceedings of the 1992 International Conference on High Power Particle Beams*; Member, International Advisory Committee, 1994 International Conference on High Power Particle Beams.
- Cotell, C.M.**, Selected volume chairman of ASM Metals Handbook Volume 5: *Surface Engineering*; Elected scientific member of the Böhmische Physical Society with the citation "for outstanding contributions in the areas of pulsed laser deposition of bio-compatible ceramics and ion beam modification of materials;" Appointed member of



Dr. Herbert Friedman, Chief Scientist Emeritus at NRL's E.O. Hulburt Center for Space Research, has been elected an Honorary Fellow of the American Institute of Aeronautics and Astronautics. This is the highest accolade given by the Institute.

- the CLEO '93 (Conference on Lasers and Electro-Optics) Program Committee; Served on subcommittee and chaired session on Lasers in Electro-Optic Materials Growth and Processing.
- DeVore, C.R.**, Newsletter Editor, member of Publicity and Membership Committee, and ex officio member of Executive Committee, Division of Computational Physics, American Physical Society.
- Dobisz, E.A.**, Program Committee for American Vacuum Society National Symposium, Chicago, November 1992; Program Committee for SPIE Symposium on Electron Beam, X-Ray, and Ion Beam Submicrometer Lithographies for Manufacturing IV, San Jose, March 1993; Organizer of Nanofabrication Facilities Workshop, Oxon Hill, MD, January 1993.
- Drumheller, D.M.**, Sigma Xi.
- Elton, R.C.**, Member International Organizing Committee for 4th International Colloquium on X-Ray Lasers, Williamsburg, Virginia, May 18-20, 1994; Member, International Organizing Committee for Novel Lasers session at IQEC-94, Anaheim, California, May 8-13, 1994.



CDR Steven D. Harris (right), Chief Military Scientist for Human-System Integration in NRL's Information Technology Division, receives an award of appreciation from a National Transportation Safety Board official. CDR Harris was cited for "exemplary contribution to technology transfer for transportation systems and for insightful application of human engineering to marine systems."

Esman, R.D., Appointed to the Microwave Optoelectronics Workshop Committee sponsored by the Conference on Optical Fiber Communications.

Esterowitz, L., QELS, Technical Subcommittee, Physics of Coherent Light Sources; Member, LEOS '93, Subcommittees: Lasers in Medicine and Biology, and Solid State Lasers; NIH Special Review Panel on Laser Medicine; IEEE/LEOS Chairman, Solid State Laser Technical Committee; Medical Free Electron Laser Review Panel.

Farwell, R.W., Member, Administrative Committee, IEEE Oceanic Engineering Society; Associate Editor, *Journal of Oceanic Engineering*; Chairman, Technical Committee on Underwater Acoustics Technology, IEEE Oceanic Engineering Society; Member, Technical Committee on Acoustical Oceanography, Acoustical Society of America; Member, Medals and Awards Subcommittee, Acoustical Society of America.

Fedder, J.A., Chairman, Department of Energy, Basic Energy Science, Program Review Panel.

Feuillade, C., Fellow, Institute of Acoustics (U.K.); Appointed to Acoustical Society of

America, Technical Committee on Acoustical Oceanography; Invited paper, Special Session on Determination of Environmental Parameters by Matched-Field Processing, 125th Meeting of ASA.

Fliflet, A.W., Elected to Fellowship in the American Physical Society.

Flippen-Anderson, J.L., Elected Vice-chairman of the U.S. National Committee for Crystallography; Elected U.S. Delegate to XVI Congress and General Assembly of the International Union of Crystallography; Elected Secretary of the Small Molecule Commission of the International Union of Crystallography; Co-editor of American Crystallographic Association newsletter; Elected Secretary of the Small Molecule Commission of the International Union of Crystallography.

Friebele, E., Chairman, NATO Panel IV, Research Study Group 12, Nuclear Effects Task Group; Program Committee, Smart Structures and Materials Conference.

Friedman, H., Elected to Council for American Philosophical Society; Member, Space Studies Board, National Research Council (extended term); Member, Committee on International Programs of the SSB/NRC; reappointed to Report Review Committee, National Research Council; Elected Honorary Fellow of AIAA; Member of the Film Committee of the NAS/Production of the Space Age Film.

Garroway, A.N., Member, Editorial Board: *Journal of Magnetic Resonance and Applied Magnetic Resonance*.

Giallorenzi, T.G., IEEE LEOS Vice President for Publications; Elected IEEE LEOS Board of Governors; Associate editor: *IEEE Proceedings*, *IEEE Lightwave Communications*; *OSA Applied Optics*, and *Laser Focus*; Member, OSA Technical Council; IEEE/OSA Conference on Lasers and Electro-Optics Steering Committee.

Glembocki, O.J., Chairman, MRS Symposium K, "Diagnostic Techniques for Semiconductor Materials Processing," Chairman, SPIE Symposium "Spectroscopic Characterization Techniques for Semiconductor Technology V;" Chairman, "Joint U.S.-

European Workshop on Electronic Materials Characterization for Device Fabrication."

Gold, S.H., Appointed Secretary of the Executive Committee (ExCom) of the IEEE Plasma Sciences and Applications Committee; Member of the Subcommittee on Fusion Energy Funding Policy and the Constitution and Bylaws Subcommittee; Member of the Program Committees for the Twentieth and Twenty-first IEEE International Conferences on Plasma Science (1993 and 1994); Associate Editor of the *IEEE Transactions on Plasma Science*; Chair of plenary session on Chaotic Dynamics at the Twentieth IEEE International Conference on Plasma Science.

Gordon, D., Appointed, Program Committee for the 1993 National Conference on Artificial Intelligence (AAAI93).

Gray, J., Program Committee, IEEE Symposium on Security and Privacy.

Grefenstette, J., Appointed, Program Committee for the 1993 International Conference on Genetic Algorithms; Appointed, Program Committee for the 1993 International Conference on Machine Learning; Appointed, Served as Associate Editor for the journal *Evolutionary Computation*; Served on the Editorial Board for the journal *Machine Learning*; Served on the Editorial Board for the journal *Adaptive Behavior*.

Griffin, S.R., Received Arctic Award from Arctic Submarine Laboratory.

Griscom, D.L., Fellow of the American Ceramic Society and Chairman of the N.J. Kreidl Award Committee of the Society's Glass and Optical Materials Division; Member, Editorial Advisory Board, *Journal of Non-Crystalline Solids*; Co-editor, Proceedings of the 8th International Symposium on Halide Glasses (published as *J. Non-Cryst. Solids* 161 (1993); Co-organizer, "R.A. Weeks International Symposium on SiO₂ Related Materials" to be held at the American Ceramic Society's 1993 PAC RIM meeting.

Grun, J., Elected Fellow of American Physical Society.

Gubser, D.U., 1992 Meritorious Executive Senior Executive Service Award; Co-orga-

nizer/Chairman of International Superconductivity Meeting, "Physics and Chemistry of Molecular and Oxide Superconductors;" Appointed member of the External Advisory Board of the National Center for Excellence in Metalworking Technology (NCEMT).

Gursky, H., Reappointed to the Advisory Board of the Institute for Computational Sciences and Informatics, George Mason University (through 30 June 1994); Appointed Chairman, EUV Imagry Telescope Steering Committee; Reappointed Chairman, Ballistic Missile Defense Organization (BMDO) User Products Interest Group (UPIG).

Hale, R.A., Received the Navy Superior Civilian Service Medal.

Heitmeyer, C.L., Invited lecturer, NATO Advanced Study Institute, Real-Time Computing; Session chairman, 1993 COMPASS Conference, 1993 Real-Time Applications Workshop; Program Committee member, 1993 Real-Time Systems Symposium; Seventh International Workshop on Software Specification and Design; 1992 European Conference on Hypertext; Member, JDL computer science panel, DoD Software Technology Initiative.

Hembree, L.A., Member, Defense Modeling Simulation Office (DMSO) Distributed Interactive Simulation (DIS) Steering Committee; Chairman, DIS Atmospheric Subgroup.

Hornstein, J.S., First Vice President, National Capital Section of the Optical Society of America.

Jacob, R.J.K., Associate Editor, *ACM Transactions on Computer-Human Interaction*; Vice-chair of ACM/SIGCHI; Appointed Associate Papers Chair, ACM CHI '94 Conference on Human Factors in Computing Systems; Member of Advisory Board, Human-Computer Interaction Laboratory, University of Maryland; Appointed to International Coordination Committee, International Conference on Virtual Reality, Singapore; Invited Lecturer, NATO Advanced Study Institute on Man-Machine Communication for the Design of Educational Systems, Eindhoven, Netherlands.



Ms. Feng-Ling Lin of the Radar Division receives her 1992 Alan Berman Research Publication Award from CAPT Gaffney

Jonker, B.T., Editor of 1993 Spring Materials Research Society Proceedings, Vol. 313, *Magnetic Ultrathin Films* (856 pages); Co-chair for Spring 1993 Materials Research Society Symposium, "Magnetic Ultrathin Films."

Jordan, A.K., Elected Fellow of the Optical Society of America; Appointed Visiting Scientist, Research Laboratory of Electronics, Massachusetts Institute of Technology.

Joyce, G.R., Fellow of the American Physical Society.

Kabler, M.N., Fellow, American Physical Society; Spokesperson for Participating Research Team, Beamline X24C, National Synchrotron Light Source, Brookhaven National Laboratory.

Kailasanath, K., Associate Fellow, American Institute of Aeronautics and Astronautics (AIAA); Program Chair, The Combustion Institute (Eastern States Section); Invited presenter, short course on "Computational Methods in Combustion;" Member, Papers Subcommittee, 25th Symposium (International) on Combustion.

Kang, M.H., Program Committee, 1993 Conference on Information and Knowledge Management.

Kaplan, R., Technical Committee, International Conference on SiC and Related Materials, November 1-3, 1993, Washington, D.C.

Karle, I.L., Elected to American Academy of Arts and Sciences; Appointed to Editorial Board of *Peptide Science*; Included in *Who's Who in Science and Engineering*.

Kaufman, B., Elected Fellow, American Institute of Aeronautics and Astronautics (AIAA).

Kelner, G., Submitted a chapter, "Silicon Carbide Devices" for the review book *Properties of Silicon Carbide* that will be published by IEE in 1993. This is an international effort with contributions from American, Japanese, German, and Russian scientists.

Kersey, A.D., Winner of Sigma Xi Applied Science Award, 1993; Elected Fellow of the Optical Society of America; Appointed Associate Editor of the *IEEE Journal of Lightwave Technology*.

Kidwell, D.A., Received 1993 Office of National Drug Control Policy, Federal Laboratory Consortium Award of Excellence in Technology Transfer.

Kim, C., Elected Director of National Board and Chairman of Finance Committee, The Korean American Scholarship Foundation.

Krowne, C.M., Fellow, Washington Academy of Sciences; Member, Technical Program Committee, 1993 IEEE Microwave Theory and Techniques Symposium, Atlanta, Georgia, June 14-18, 1993; Organizer and Chairman of Workshop at 1993 MTT-S Symposium: "Combined Self-Consistent Particle Transport Simulation and Full Wave Dynamic Field Simulation for Monolithic Solid-State Device and Circuit Calculations;" Member, Joint Board on Science and Engineering Education, which coordinates secondary school educational activities in metropolitan Washington area; Member of the Board of Washington Academy of Sciences.

Kurfess, J., NASA award for Exceptional Scientific Achievement; Appointed member: NASA High Energy Astrophysics Management and Operations Working Group.



Dr. Robert Lehmberg (left) and Dr. Stephen Obenschain, both of the Plasma Physics Division, are the recipients of the 1993 American Physical Society's Award for Excellence in Plasma Physics

Landwehr, C.E., Chairman and U.S. National Leader, TTCP XTP-1 (Trustworthy Computing Technologies); Chairman, Working Group 11.3 (Database Security), International Federation for Information Processing (IFIP); Editorial Board Member, *Journal of Computer Security*; Editorial Board Member, *High Integrity Systems Journal*; Program Committee, First ACM Conference on Computer and Communications Security; Program Committee, Fourth IFIP Working Conference on Dependable Computing for Critical Applications.

Lean, J.L., Editor's Citation for Excellence in Refereeing, *Journal of Geophysical Research-Space Physics*.

Lee, J.N., Re-elected Chairman of Steering Committee for the *IEEE-OSA Journal of Lightwave Technology*; Co-editor for Special Issue of *Applied Optics* on Spatial Light Modulators.

Lee, T.F., The Institute of Electrical and Electronic Engineers, Inc., Geoscience and Remote Sensing Society, 1992 Symposium Prize Paper Award; Member, American Meteorological Society Committee on Satellite Meteorology and Oceanography; Selected as Co-chairman, 1994 Annual Conference.

Ligler, F.S., Appointed to the Editorial Board of *Applied Biochemistry and Biotechnology*.

Long, J.P., Representative for the Time-Resolved Spectroscopy Group at the National Synchrotron Light Source, Brookhaven National Laboratory; Member, Users Executive Committee, National Synchrotron Light Source.

Lowrey, A.H., Adjunct Professor, Uniformed Services University of Health Sciences; Treasurer, Molecular Graphics Society of the Americas.

Lubbes, H.O., Chosen by the Aerospace Computer Associates to deliver the Distinguished Lecture at the Ninth Annual Computer Security Applications Conference.

Marks, C.J., Elected National Vice President for Policy and Long Range Planning, Federally Employed Women (FEW).

McCafferty, E., Chairman, Honors and Awards Committee, The Electrochemical Society; Member, Corrosion Monograph Committee, The Electrochemical Society.

McCord, M., Selected for promotion to Lieutenant Commander in the Naval Reserve.

McLean, J., Program Chair, COMPASS; Associate Editor, *Journal of Computer Security*; Program Committee, IEEE Symposium on Security and Privacy; Program Committee,

IEEE Computer Security Foundations Workshop; Program Committee, IFIP Working Conference on Dependable Computing for Critical Applications; Program Committee, ACM SIGSAC New Security Paradigms Workshop.

McMahon, J.M., Co-chairman, TTG-6 Panel on Sensors and Lasers (OSD); Chairman, Reliance Sub-panel on Electro-optics; Navy Representative, Advisory Group on Electron Devices, Panel C; Acting Ambassador/President of Coordinating Committee for Multilateral Control of Exports (COCOM).

Meadows, C., Program Chair, IEEE Symposium on Security and Privacy; Editor, *ACM SIGSAC Review*; Associate Editor, *Journal of Computer Security*; Program Committee, IEEE Computer Security Foundations Workshop; Program Committee, IFIP Working Conference on Dependable Computing for Critical Applications.

Meier, R., Received *Journal of Geophysical Research*, "1993 Editor's Award for Excellence in Refereeing."



Dr. Wallace Manheimer of the Plasma Physics Division has been elected a Fellow of the Institute of Electrical and Electronics Engineers. Dr. Manheimer was cited for his "contributions to the analysis of nonlinear phenomena in plasmas and electron beams."

Melendez-Alvira, D.J., Group Achievement Award — NASA Administrator, 1993.

Metzbower, E.A., Chairman of the Joining Division Council of ASM International; Served on the Technical Divisions Board of ASM International; Served on the Board of Directors of the Laser Institute of America; Served on the Welding Research and Development Committee of the American Welding Society.

Meyrowitz, A., Member, Sigma Xi Honor Society; Appointed U.S. National Leader for Machine Intelligence (Technical Cooperation Program).

Middour, J.W., Elected member, American Astronautical Society Spaceflight Mechanics Committee.

Miller, J.B., Guest Editor of Special Issue of *Applied Magnetic Resonance*, to appear in fall of 1994.

Mosher, D., Editor, *Proceedings of the 9th International Conference on High Power Particle Beams*; Member, JDOST—Joint DoD-DoE Committee for the Design of the Jupiter Simulator Facility.

Mueller, G.P., U.S. Chairman, Subpanel 5, IEP US/UK-3 Electromagnetic Protective Materials; Navy representative, JDL/Reliance Subpanel of Technical Panel on Advanced Materials; Navy representative, Laser-Hardened Materials and Structure Group (ODDR&E).

Murday, J.S., Chairman, Development Committee of the American Institute of Physics; Past President, American Vacuum Society.

Namenson, A.I., Member, DNA Hardness Assurance Committee.

Natishan, P.M., Councillor, National Capital Section of the Electrochemical Society; Trustee, Baltimore-Washington Section of the National Association of Corrosion Engineers; Representative to the Individual Membership Committee, The Electrochemical Society; Member, Ways and Means Committee, The Electrochemical Society.

Neidert, R.E., Chairman, Computer-Aided Design Subcommittee of Microwave Ferrite Consortium.

- Nelson, H.H.**, DoD Congressional Fellowship, 1993-4; Congressional Fellowship Program, FY94-95.
- Nero, R.W.**, Member, Acoustical Society of America, Technical Committee on Acoustical Oceanography.
- Ngai, K.L.**, Chairman of the 2nd International Discussion Meeting on Relaxations in Complex Systems; Guest Editor, *Journal of Non-Crystalline Solids*.
- Numrich, S.K.**, Elected Fellow of the Acoustical Society of America; President, Washington D.C. Chapter, Acoustical Society of America; Technical Committee Member for the Committee on the Status of Women for the ASW.
- O'Grady, W.E.**, Appointed to the General Users Oversight Committee, National Synchrotron Light Source; Appointed to the X-Ray Tenure Review Panel, National Synchrotron Light Source; Appointed to the Editorial Board of the *Frontiers of Electrochemistry* Series, published by VCH Publishers.
- Oran, E.S.**, Vice President-elect of Publications of the American Institute of Aeronautics and Astronautics; Program Chair, 25th International Combustion Symposium; Associate Editor, *Journal of Computational Physics*; Advisory Board, *Computers in Physics*; Received Materials Research Laboratory, Victoria, Australia, Award for Excellence for Best Paper of the Year.
- Ossakow, S.L.**, Fellow, American Physical Society; ONR General Physics Subelement Monitor; Navy Representative, Tri-Service Project Reliance Nuclear Weapons Effects (NWE) Working Group; Navy Representative and Chairman, Tri-Service 6.1 Physics Scientific Planning Group; Official U.S. Representative of the National Academy of Sciences National Research Council to XXIVth URSI General Assembly, Kyoto, Japan; OSD Defense Science Board Task Force on DNA Letter of Commendation for Outstanding Support.
- Ottinger, P.**, Fellow, American Physical Society.
- Pande, C.S.**, Appointed Associate Editor of *Journal of Electronic Materials*.
- Patel, V.L.**, Fellow, American Physical Society; Member, NSF Interagency Committee on Solar-Terrestrial Research; Board Member, Institute for Advanced Physics Studies, La Jolla, California.
- Pellenbarg, R.E.**, Editor, *Applied Organometallic Chemistry*.
- Perkins, J.S.**, Named Fellow of the Acoustical Society of America.
- Piquette, J.C.**, Selected for inclusion in *Who's Who in Science and Engineering*.
- Price, R.R.P.**, Appointed to the Editorial Board of the *Journal of Microencapsulation*; Appointed to the Steering Committee for the International Society of Microencapsulation.
- Priest, R.G.**, Appointed Chairman of the Infrared Information Society Specialty Group on Targets, Backgrounds and Discrimination.
- Prokes, S.M.**, Vice-chair, Publications Committee, Materials Research Society; Subcommittee Chair, MRS Book Committee; Program Committee Member, 26th ISATA Conference New and Alternative Materials for the Automotive Industry; Appointed Fellow by Courtesy, The Johns Hopkins University.
- Qadri, S.B.**, Elected Energy Dispersive Diffraction Special Interest Group Representative to the User's Executive Committee at National Synchrotron Light Source, Brookhaven, New York; included in *Marquis Who's Who in Science and Engineering*, 2nd edition, 1993; invited speaker at VIIth International Workshop on Physics of Semiconductors.
- Rath, B.B.**, Elected to the Engineers Public Policy Council of the American Association of Engineering Societies (AAES); Elected Executive Chairman of the Subgroup on Advanced Materials of the Technical Cooperation Program for the TTCP Countries; Served as Conference Organizer and Chairman of the Materials and Global Environment Conference; Invited Keynote Speaker at the Conference on Mechanics and Mechanisms of Materials Damping; Served on the Guidance and Advisory Board of the DoE Program on Materials Technology; Member, Technical Division Board of the American Society for Materials (ASM).



LCDR Bruce Smith, Assistant Officer-in-Charge, NRL Flight Support Detachment, presents AD1 Glenn Brown with a plaque for his selection as "Supervisor of the Detachment" for the first half of 1993

Reinecke, T.L., Fellow, American Physical Society; Organizing Committee, Workshop on Surface Dynamics, Nashville, October 1993; American Rhodes Scholarship Selection Committee.

Ripin, B.H., Elected Vice-chair, APS Division of Plasma Physics; Appointed Vice-Chair of University of Maryland System Blue Ribbon Committee; Chairman, APS Publication Oversight Committee; Member of Committee on International Freedom of Scientists; Elected Member, APS Council and Executive Board; Appointed to Board of Governors, American Institute of Physics.

Ross, M.M., Elected to Board of Directors of The American Society for Mass Spectrometry.

Rudgers, A.J., Fellow, Acoustical Society of America.

Sartwell, B.D., Editor of the international journal *Surface and Coatings Technology*, published by Elsevier Sequoia; Editor of the Proceedings of the Eighth International Conference on Surface Modification of Metals by Ion Beams; Member of the Bohmische Physical Society.

Schmidt-Nielsen, A., Secretary-treasurer, Division 21 (Applied Experimental and Engineering Psychology) of the American Psychological Association; Representative from

the Technical Committee on Speech Communication to the Acoustical Society of America Committee on Standards.

Schnur, J.M., Awarded the Navy Superior Civilian Service Medal.

Shanabrook, B.V., Member, International Advisory Committee for the Electronic Properties of Two-Dimensional Systems.

Share, G.H., Chair of Nominating Committee, High Energy Astrophysics Division, AAS; Appointed to Committee on Light Pollution, Radio Interference, and Space Debris of the AAS.

Shettle, E.P., Member of the Global Aerosol Model Working Group of the AIAA Atmospheric and Space Environment Committee on Standards; Co-chair SPIE Conference on Passive Infrared Remote Sensing of Clouds and the Atmosphere, 12-16 April 1993, Orlando, Florida; Re-elected Secretary of the National Capital Section of the Optical Society of America.

Siskind, D.E., Appointed Assistant Editor, *Journal of Geophysical Research Space Physics*.

Skelton, E.F., Listed in Marquis *Who's Who in the East* and *Who's Who in Science and Engineering*; invited speaker at the 1993 joint meeting of the International Association for the Advancement of High Pressure Science and Technology and the American Physical Society Topical Group on Shock Compression of Condensed Matter.

Sleger, K., Member, RF Components Subpanel of JDL Reliance Electronic Devices; Navy Deputy Member, Advisory Group on Electron Devices (AGED) Working Group A; Member of Steering Committee, 1993 International Conference on Silicon Carbide and Related Materials.

Sprangle, P.A., Fellow of the American Physical Society; Member, Sigma Xi; Appointed to Editorial Board, *Physics of Fluids B*; Senior Member, Institute of Electrical and Electronics Engineers (IEEE).

Strom, U., Member, Program Committee of International Conference on Millimeter and Submillimeter Waves and Applications.

Tang, C.M., Fellow, American Physical Society.

Ting, R.Y., Fellow, Acoustical Society of America.

Tolstoy, A., Guest editor for Special Issue of *IEEE Journal of Oceanic Acoustics*; Chair of Special Session of ASA; Co-organizer and Co-chair of 6th Bi-annual Matched Field Workshop; Visiting Lecturer for SIAM (invited talks at William and Mary, at NJIT, and at SIAM Conference); Elected to Underwater Acoustics Technical Committee for ASA; Author of monograph: *Match Field Processing for Underwater Acoustics* (World Scientific, 1993).

Trunk, G.V., Chairman, KTP-2, a technical exchange panel on radar data processing under the auspices of subgroup K (radar) with the Technical Cooperation Program (TTCP).

Trzaskoma, P.P., Appointed Member, H.H. Uhlig Award Committee of the Electrochemical Society; listed in *American Men and Women of Science*, 18th edition.

Van Buren, A.L., Fellow, Acoustical Society of America; Member, Committee on Standards, Acoustical Society of America.

Vandermeer, R.A., Appointed Visiting Scientist at Risø National Laboratory Materials Department in Roskilde, Denmark.

Venezky, D.L., Appointed to the American Chemical Society Board-Council Committee on International Activities and elected Vice-Chairman for 1993.

Wang, H.T., Session Chairperson, "Ocean Waves and Energy," 12th International Conference on Offshore Mechanics and Arctic Engineering, Glasgow, Scotland,

June 20-24, 1993; Member, Coordinating Group on Computational Fluid Dynamics, The American Society of Mechanical Engineers.

Wagner, R.J., Member, Program Committee for the 1993 Meeting of IRIS Infrared Materials Specialty Group.

Wagstaff, R.A., Associate Editor, *U.S. Navy Journal of Underwater Acoustics*.

Webb, D.C., Chairman, Intersocietal Liaison Committee, IEEE-Microwave Theory and Techniques Administrative Committee; Member, Technical Program Committee, 1993 IEEE-Microwave Theory and Techniques International Symposium; Chairman, Technical Committee, ARPA Ferrite Development Consortium.

Wieting, T.J., Chairman, OSD HPM System Effects Assessment Team; Member, OSD Microwave Effects Technical Working Group; Navy Member, NATO AC/243 (Panel 1) Research Study Group 1; Chairman, Program Committee, and Member of Steering Committee, 7th High-Power Microwave Technology Conference; U.S. Coordinator, EUROEM 94 Conference, Bordeaux, France, Member, OSD HPM Foreign Asset Assessment Team.

Wilhelm P., Received 1993 Stellar Award from the Rotary National Award for Space Achievement.

Wilsey, N.D., Member of the Editorial Board, *Journal of Materials Science: Materials in Electronics*.

Wurmser, D., Sigma Xi.

Alan Berman Research Publication and Edison Patent Awards

The Annual Research Publications Awards Program was established in 1968 to recognize the authors of the best NRL publications each year. These awards not only honor individuals for superior scientific accomplishments in the field of naval research, but also seek to promote continued excellence in research and in its documentation. In 1982, the name of this award was changed to the Alan Berman Research Publications Award in honor of its founder.

There were 376 separate publications submitted to the divisions in 1993 to be considered for recognition. Of those considered, 35 were selected. These selected publications represent 138 authors, each of whom received a publication awards certificate, a bronze paperweight, and a booklet listing the publications that received special recognition. In addition, NRL authors share in their respective division's monetary award.

The winning papers and their respective authors are listed below by their research units. Non-Laboratory coauthors are indicated by an asterisk.

NRL also recognizes patents as part of its annual publication awards program. The NRL Edison Patent Award was established in January 1991 to recognize NRL employees for outstanding patents issued to NRL by the U.S. Patent and Trademark Office during the preceding calendar year. The award recognizes significant NRL contributions to science and engineering as demonstrated by the patent process that are perceived to have the greatest potential benefit to the country. Of the 79 patents considered for 1993, two were selected and an additional one was selected for a special award, representing 11 inventors. They are listed under the NRL Edison Patent Awards.

Office of Strategic Planning

Vibrational-Internal Rotation Coupling in Trifluoronitromethane
William M. Tolles

Radar Division

*Characteristic of High-Frequency Signals, Noise, Availability and Duration of
Bandwidths Based on ROTHRA Amchitka Spectrum Measurements*
George D. McNeal

Ionospheric Scintillation-Induced Integration Losses for Space-Based Radar
Eric L. Mokole and Dennis L. Knepp*

Information Technology Division

*Northern Exposure 92: An Investigation of Transauroral
HF Radio Skywave Propagation*

Leonard S. Wagner, Joseph A. Goldstein,
Michael A. Rupar, and Edward J. Kennedy

Using Genetic Algorithms for Concept Learning

Kenneth A. DeJong, William M. Spears, and Diana Gordon

Optical Sciences Division

*High-Power, Near-Diffraction-Limited Large-Area
Traveling-Wave Semiconductor Amplifiers*

Lew Goldberg, Marc R. Surette, David Mehuys,*
and Douglas C. Hall*

Fiber-Optic Prism True Time-Delay Antenna Feed

Ronald D. Esman, Michael Y. Frankel, James L. Dexter, Lew Goldberg,
Mark G. Parent, P. Denzil Stilwell, and David G. Cooper*

Tactical Electronic Warfare Division

Hierarchical Wavelet Representations of Ship Radar Returns

Sheldon Wolk and John S. Baras*

Frequency Shift for ECM Applications

James L. Dexter, Keith J. Williams, Ronald D. Esman,
and Michael J. Monsma

Underwater Sound Reference Detachment

*An Analytical Evaluation of Turbulence-Induced Flexural Noise
in Planar Arrays of Extended Sensors*

Robert E. Montgomery and Bertrand Dubus*

Chemistry Division

*Analysis of Phencyclidine and Cocaine in Human Hair
by Tandem Mass Spectrometry*

David A. Kidwell

Cyclocarbon Coalescence: Mechanisms for Tailor-Made Fullerene Formation

Stephen W. McElvany, M. Mark Ross, Nancy S. Goroff,* and Francois Diederich*

Materials Science and Technology Division

*Influence of Intralayer Quantum-Well States on the
Giant Magnetoresistance in Magnetic Multilayers*

A. C. Ehrlich

A Theory of Condensation Model Reduction

Luther D. Flippin, Jr.

Laboratory for Computational Physics and Fluid Dynamics

*The Effect of Shape in the Three-Dimensional Ablative Rayleigh-Taylor
Instability I: Single Mode Perturbations*

Jill P. Dahlburg, John H. Gardner, Gary D. Doolen,*
and Steven W. Haan*

Condensed Matter and Radiation Sciences Division

Electronic Structure of $\text{HgBa}_2\text{Ca}_2\text{Cu}_3\text{O}_8$: The Role of Mercury

David J. Singh

*Electron Cyclotron Resonance Reactive Ion Etching of Fine Features
in $\text{Hg}_x\text{Cd}_{1-x}\text{Te}$ Using CH_4/H_2 Plasmas*

Charles R. Eddy, Jr., Elizabeth A. Dobisz, Jerry R. Meyer,
and Craig A. Hoffman

Plasma Physics Division

*Current Neutralization of Intense MeV Proton Beams
Transported in Low-Pressure Gas*

Frank C. Young, Richard F. Hubbard, Martin Lampe, Jesse M. Neri,
Paul F. Ottinger, Steven P. Slinker, Stavros J. Stephanakis,
David Hinshelwood,* David V. Rose,* Craig L. Olson,* and Dale W. Welch*

New Results and Applications for the Quasioptical Gyrotron

Arne W. Fliflet, Richard P. Fischer, and Wallace M. Manheimer

Electronics Science and Technology Division

Fabrication of Silicon Nanostructures with a Scanning Tunneling Microscope

E. S. Snow, P. M. Campbell, and P. J. McMarr*

*Linear and Nonlinear Theory of Gyroharmonic Radiation into Modes of a
Cylindrical Waveguide from Spatiotemporally Modulated Electron Beams*

A. K. Ganguly and J. L. Hirshfield*

Center for Bio/Molecular Sciences and Engineering

*X-ray Diffuse Scattering Study of Static Undulations in Multilayer
Films of a Liquid-Crystalline Polymer*

Robert E. Geer, Robert Shashidhar, Angela F. Thibodeaux,* and Randolph S. Duran*

*Projection X-ray Lithography with Ultrathin Imaging Layers
and Selective Electroless Metallization*

Jeffrey M. Calvert, Walter J. Dressick, Charles S. Dulcey, Timothy S. Koloski, Martin C. Peckerar,
Franco Cerrina,* James W. Taylor,* Doowon Suh,* Obert R. Wood, II,*
Raisa D'Souza,* and Alastair A. MacDowell*

Acoustics Division

A Split-Step Padé Solution for the Parabolic Equation Method
Michael D. Collins

Broadband Source Signature Extraction Using a Vertical Array
Steven Finette, Peter C. Mignerey, James F. Smith III, and Christ D. Richmond*

Remote Sensing Division

*SSM/I Observations of ERICA IOP 4 Marine Cyclone:
A Comparison with In Situ Observations and Model Simulation*
Simon W. Chang, Randall J. Alliss,* Sethu Raman,* and Jainn-Jong Shi*

Polarimetric SAR Image Signatures of the Ocean and Gulf Stream Features
Dale L. Schuler, Jong-Sen Lee, and Karl W. Hoppel

Oceanography Division

Sulfur Isotope Fractionation by Sulfate-Reducing Bacteria in Corrosion Products
Brenda Little, Patricia Wagner, and Joanne Jones-Meehan*

Marine Geosciences Division

*Fine Structure of Methane Hydrate-Bearing Sediments on the Blake Outer
Ridge as Determined from Deep-Tow Multichannel Seismic Data*
Mary M. Rowe and Joseph F. Gettrust

Marine Meteorology Division

The Forcing and Balance of Zonally Symmetric Modes in a Global Model
Ronald Gelaro and Ronald M. Errico*

Detection of Oil Fire Smoke over Water in the Persian Gulf Region
Kim A. Richardson and Nahid Khazenie*

Space Science Division

The 5 January 1992 Flare at 13.3 UT: Observations from Yokoh

George A. Doschek, Charles M. Brown, John T. Mariska, Keith T. Strong,* Loren W. Acton,* Marilyn E. Bruner,* Robert D. Bentley,* J. Leonard Culhane,* Andrzej Fludra,* Eijiro Hiei,* Tetsuya Watanabe,* Tadashi Hirayama,* Takeo Kosugi,* James Lang,* Kenneth J. Phillips,* C. David Pike,* Alphonse C. Sterling,* Saku Tsuneta,* Eric Rolli,* Masata Yoshimori,* Hugh Hudson,* Thomas R. Metcalf,* Jean-Pierre Wuelser,* Yutaka Uchida,* and Yoshiaki Ogawara*

The Oriented Scintillation Spectrometer Experiment: Instrument Description

W. Neil Johnson, Robert L. Kinzer, James D. Kurfess,
Mark S. Strickman, William R. Purcell,* David A. Grabelsky,* Melville P. Ulmer,*
Donald A. Hillis,* Gregory V. Jung,* and Robert A. Cameron*

Space Systems Development Department

Thin-Phase Screen Estimates of TID Effects on Midlatitude Transionospheric Radio Paths

Michael H. Reilly

Along Track Formationkeeping for Satellites With Low Eccentricity

Jay W. Middour

NRL Edison Patent Awards

Detection of Explosive and Narcotics by Low Power, Large Sample Volume Nuclear Quadrupole Resonance (NQR)

Allen N. Garroway, Joel B. Miller, and Michael L. Buess*

CHEMISTRY DIVISION

Barry Edelberg

OFFICE OF COUNSEL

Flow Immunosensor Method and Apparatus

Frances S. Ligler, Bruce P. Gaber, Anne W. Kusterbeck, and Gregory A. Wemhoff*

CENTER FOR BIO/MOLECULAR SCIENCE AND ENGINEERING

Barry Edelberg

OFFICE OF COUNSEL

Special Award

Hard Magnetic Alloy: of a Transition Metal and Lanthanide

Norman C. Koon

MATERIALS SCIENCE AND TECHNOLOGY DIVISION

Thomas E. McDonald

OFFICE OF COUNSEL

Awards for *NRL Review* Articles

Awards for *NRL Review* articles were established in 1990 to recognize authors who submit outstanding research articles for this scientific publication. The articles are judged on the relevance of the work to the Navy and DoD, readability to the college-graduate level, and the use of graphics that are interesting and informative. The following awards were presented for articles that appeared in the 1993 *NRL Review*.

FEATURED RESEARCH ARTICLE

Ultrathin Magnetic Film Research at NRL

James J. Krebs

MATERIALS SCIENCE AND TECHNOLOGY DIVISION

DIRECTORATE AWARDS FOR SCIENTIFIC ARTICLES

Warfare Systems and Sensors Research Directorate

Nanochannel Glass Technology

Ronald J. Tonucci and Anthony J. Campillo

OPTICAL SCIENCES DIVISION

Materials Science and Component Technology Directorate

A Plasma Mirror for Microwaves

Anthony E. Robson, Wallace A. Manheimer, and Robert A. Meger

PLASMA PHYSICS DIVISION

Ocean and Atmospheric Science and Technology Directorate

Numerical Modeling of the Atmosphere and Ocean

Richard M. Hodur

MARINE METEOROLOGY DIVISION

Naval Center for Space Technology

The High Temperature Superconductivity Space Experiment (HTSSE)

Amey R. Peltzer, Christopher L. Lichtenberg, and George E. Price

SPACE SYSTEMS DEVELOPMENT DEPARTMENT



Dr. Bhakta Rath (r), Associate Director of Research for the Materials Science and Component Technology Directorate, presents the featured research article award to Dr. Krebs



Drs. Tonucci and Campillo (l to r) receive their award for the 5000 Directorate



Mr. Price, Ms. Peltzer, and Mr. Lichtenberg (l to r) receive their award for the 8000 Directorate

PROFESSIONAL DEVELOPMENT

- 269 Programs for NRL Employees—University education and scholarships, continuing education, professional development, and other activities
- 275 Programs for Non-NRL Employees—Fellowships, exchange programs, and cooperative employment

Programs for NRL Employees

During 1993, under the auspices of the Employee Development Branch, NRL employees participated in about 5500 individual training events. Many of these were presented as either videotaped or on-site instructed courses on diverse technical subjects, management techniques, and enhancement of such personal skills as efficient use of time, speed reading, memory improvement, and interpersonal communications. Courses are also available by means of computer-based training (CBT) and live television courses for monitoring nationwide.

One common study procedure is for employees to work full time at the Laboratory while taking job-related scientific courses at universities and schools in the Washington area. The training ranges from a single course to full graduate and postgraduate programs. Tuition for training is paid by NRL. The formal programs offered by NRL are described here.

GRADUATE PROGRAMS

- **The Advanced Graduate Research Program** (formerly the Sabbatical Study Program, which began in 1964) enables selected professional employees to devote full time to research or pursue work in their own or a related field for one year at an institution or research facility of their choice without the loss of regular salary, leave, or fringe benefits. NRL pays all educational costs, travel, and moving expenses for the employee and dependents. Criteria for eligibility include professional stature consistent with the applicant's opportunities and experience, a satisfactory program of study, and acceptance by the facility selected by the applicant. The program is open to paraprofessional (and above) employees who have completed 6 years of Federal Service, 4 of which are required at NRL.



Dr. Ellen Livingston of the Acoustics Division recently participated in the Advanced Graduate Research Program. She spent the 1992-1993 academic year at the Massachusetts Institute of Technology and the summer of 1993 at the New Jersey Institute of Technology.

- **The Edison Memorial Graduate Training Program** enables employees to pursue advanced studies in their fields at local universities. Participants in this program work 24 hours each workweek and pursue their studies during the other 16 hours. The criteria for eligibility include a minimum of 1 year of service at NRL, a bachelor's or master's degree in an appropriate field, and professional standing in keeping with the candidate's opportunities and experience.

- To be eligible for the **Select Graduate Training Program**, employees must have a college degree in an appropriate field and must have demonstrated ability and aptitude for advanced training. Students accepted in this program devote a full academic year to graduate study. While attending school, they receive one half of their salary; and NRL pays for tuition, books, and laboratory expenses.



Alfredo J. Alvendia of the Oceanography Division participates in the Edison Memorial Graduate Training Program. He is pursuing a master of science degree in electrical engineering at the University of New Orleans.

- The Naval Postgraduate School (NPS), located in Monterey, California, provides graduate programs to enhance the technical preparation of Naval officers and civilian employees who serve the Navy in the fields of science, engineering, operations analysis, and management. It awards a master of arts degree in national security affairs and a master of science degree in many technical disciplines. In addition, a doctor of philosophy degree may be earned in select fields of science and engineering.

NRL employees desiring to pursue graduate studies at NPS may apply for a maximum of six quarters away from NRL, with thesis work accomplished at NRL. Specific programs are described in the NPS catalog. Participants will continue to receive full pay and benefits during the period of study.

- In addition to NRL and university offerings, application may be made to a number of noteworthy programs and fellowships. Examples of such opportunities are the **Alfred P. Sloan Fellows Program**, **Brookings Institute Advanced Study Program**, **The Fellowship in Congressional Operations**, and the **Women's Executive Leadership Program**. These and other programs are announced from time to time as schedules are published.

- Research conducted at NRL may be used as **thesis material for an advanced degree**.

This original research is supervised by a qualified employee of NRL who is approved by the graduate school. The candidate should have completed the required course work and should have satisfied the language, residence, and other requirements of the graduate school from which the degree is sought. NRL provides space, research facilities, and supervision but leaves decisions on academic policy to the cooperating schools.

CONTINUING EDUCATION

- Local colleges and universities offer **undergraduate and graduate courses** at NRL for employees interested in improving their skills and keeping abreast of current developments in their field. These courses are also available at many other DoD installations in the Washington, DC area.

- The Employee Development Branch at NRL offers to all employees **short courses** in a number of fields of interest including technical subjects, computer operation, supervisory and management techniques, and clerical/secretarial skills. Laboratory employees may attend these courses at nongovernment facilities as well. Interagency courses in management, personnel, finance, supervisory development, and clerical skills are also available.

For further information on any of the above programs, contact the Employee Development Branch (Code 1840) at (202) 767-2956.

TECHNOLOGY TRANSFER

- The **Office of Research and Technology Applications Program (ORTA)** ensures the full use of the results of the Nation's federal investment in research and development by transferring federally owned or originated technology to state and local governments and the private sector.

- The **Navy Science Assistance Program (NSAP)** establishes an information loop between the Fleet and the R&D shore establishments to expedite technology transfer to the user. The

program addresses operational problems, focuses resources to solve specific technical problems, and develops a nucleus of senior scientific personnel familiar with the impact of current research and system performance on military operations.

- **The Scientist-to-Sea Program (STSP)** provides increased opportunities for Navy R&D laboratory/center personnel to go to sea to gain first-hand insight into operational factors affecting system design, performance, and operations on a variety of ships.

Inquiries concerning NRL's programs should be made to Dr. Richard Rein (Code 1003.1) at (202) 767-3744. Inquiries concerning NSAP or STSP programs should be made to Dr. George Abraham (Code 1003.1) at (202) 767-3521.

PROFESSIONAL DEVELOPMENT

NRL has several programs, professional society chapters, and informal clubs that enhance the professional growth of employees. Some of these are listed below.

- **The Counseling Referral Service (C/RS)** helps employees to achieve optimal job performance through counseling and resolution of problems such as family, stress and anxiety, behavioral, emotional, and alcohol- or drug-related problems that may adversely impact job performance.

C/RS provides confidential assessments and short-term counseling, as well as training workshops and referrals to additional resources in the community. (Contact Robert Power at (202) 767-6857.)

- A chartered chapter of **Women in Science and Engineering (WISE)** was established at NRL in 1983. Informal monthly luncheons and seminars are scheduled to inform scientists and engineers of women's research at NRL and to provide an informal environment for members to practice their presentations. WISE also sponsors a colloquium series to feature outstanding women scientists. (Contact Dr. Wendy Fuller-Mora at (202) 767-2793, Dr. Debra Rolison at (202) 767-3617, or Dr. Cha-Mei Tang at (202) 767-4148.)



Anne Kusterbeck from the Center for Bio/Molecular Science and Engineering participated this past summer in NRL's Scientist-to-Sea Program. To assist in her work with the Environmentally Sound Ships program, she spent one week on board the USS *Fahrion* learning about present Navy efforts in shipboard recycling and environmental quality.

- **Sigma Xi**, the Scientific Research Society, encourages and acknowledges original investigation in pure and applied science. As an honor society for research scientists, individuals who have demonstrated the ability to perform original research are elected to membership in local chapters. The NRL chapter, comprised of approximately 600 members, recognizes original research by presenting awards annually in pure and applied science to outstanding NRL staff members. The chapter also sponsors lectures at NRL on a wide range of scientific topics for the entire NRL community. These lectures are delivered by scientists from all over the nation and the world. The highlight of the Sigma Xi lecture series is the Edison Memorial Lecture, traditionally featuring a Nobel laureate. (Contact

Dr. Robert Pellenbarg at (202) 767-2479 or 2002.)

- **The NRL Mentor Program Pilot Project** for NRL scientists and engineers was established to explore the feasibility of instituting a laboratory wide mentoring program. The Pilot Project is managed by a steering committee formed by the NRL Women's Science and Technology Network. The program offers a personal approach to career development and personal training. NRL mentors are identified as successful, experienced scientists and engineers. Mentorees, who are colleagues with less developed technical and/or managerial skills, are paired with selected mentors. The program's focus is on imparting knowledge and expertise necessary for the professional and career growth and development of the mentorees. NRL NOTICE 12400 established the Pilot Project and provides the policy and procedures for the program. (Contact Zakya Kafafi at (202) 767-9529 or Kay Howell at (202) 767-3353.)

- The Charlotte Moore-Sitterly Chapter of **Federally Employed Women, Inc. (FEW)** was

chartered at NRL in 1993. FEW is an international organization of federally employed women and men whose purpose is to eliminate sex discrimination and sexual harassment and enhance career opportunities for women in government. FEW works closely with other Federal agencies and organizations, including the Office of Personnel Management, Equal Employment Opportunity Commission, and Federal Women's Program subcommittees. (Contact Chris Thorowgood at (202) 767-3121.)

- Employees interested in developing effective self expression, listening, thinking, and leadership potential are invited to join either of two NRL chapters of **Toastmasters International**. Members of these clubs, who possess diverse career backgrounds and talents, meet three times a month in an effort to learn to communicate not by rules but by practice in an atmosphere of understanding and helpful fellowship. NRL's Commanding Officer and the Director of Research endorses Toastmasters, and the Employee Development Branch pays for membership and educational materials for those employees whose supervisors see a need for their active



Volunteers from NRL's Thomas Edison Chapter of Toastmasters International provided Youth Leadership training to students from Patterson Elementary School under the NRL Community Outreach Program. Youth leadership graduates flanked by (left) Ms. Kathleen Parrish, Technical Information Division (TID); Ms. Bessie Wells, Principal; Ms. Vivian Gibson, Counselor; (right) Ms. Leona Jackson, TID; and Ms. Leslie Chaplin, Acoustics Division.

training in public speaking or communication skills. (Contact Kathleen Parrish at (202) 767-2782.)

EQUAL EMPLOYMENT OPPORTUNITY (EEO) PROGRAMS

Equal employment opportunity is a fundamental NRL policy for all persons, regardless of race, color, sex, religion, national origin, age, or physical/mental handicap. The EEO office's major functions include affirmative action in employment, discrimination complaint process, EEO training, advice and guidance to management on EEO policy, and the following special emphasis programs:

- **The Federal Women's Program (FWP)** supports and enhances employment and advancement opportunities for women and addresses issues that affect women in the workplace. It provides counseling and referral services and sponsors a chapter of Women in Science and Engineering to recognize outstanding female scientists and engineers. Distinguished women scientists are guest lecturers at quarterly presentations.

- **The Hispanic Employment Program (HEP)** focuses on working with supervisors, managers, and subcommittees to recruit and place qualified Hispanics. The program is involved with Hispanic community organizations and local schools and provides activities specifically designed to offer employment opportunities to Hispanics. "El Ingeniero" (The Engineer), which encourages Hispanic youth to pursue a career in engineering, is one such program.

The Black Employment Program (BEP) concentrates on recruiting, placing, developing, and advancing African American employees throughout NRL. It also encourages them to achieve their maximum potential.

- **The Individuals with Disabilities Program (IDP)** assists management to improve employment and advancement opportunities for qualified handicapped and disabled veteran employees. It also advises on accommodations

necessary for handicapped persons. It recruits handicapped summer students from colleges and universities for technical positions in engineering and science and paraprofessional positions in accounting and administration; it also seeks Cooperative Education Program (Co-op) candidates who are pursuing degrees in engineering, computer sciences, or the physical sciences.

- **The Asian-American/Pacific Islander Program (API)** identifies areas of concern regarding the recruitment, selection, advancement, retention, and utilization of API employees throughout NRL. The program interacts with API professional/community organizations to address employment concerns.

- **The American Indian/Alaskan Native Employment Program (AI/ANEP)** focuses on the employment concerns of AI/ANEP employees. The program provides counseling and referral services on recruitment, hiring, placement, promotion, retention, and other areas of employee interest.

- **The Federal Employment Opportunity Recruitment Program (FEORP)** is designed to establish, maintain, and update targeted recruitment programs to reduce the conspicuous absence or manifest imbalance categories of NRL employment through innovative internal and external recruitment. In addition, it fosters relationships with minority and women's institutions and organizations.

Special programs are held during the year to promote an awareness of the contributions and capabilities of women and minorities. (Contact the EEO office at (202) 767-2486 for all EEO programs.)

OTHER ACTIVITIES

- **The Community Outreach Program** traditionally has used its extensive resources to foster programs that provide benefits to students and other community citizens. Volunteer employees assist with and judge science fairs, give lectures, tutor, mentor, coach, and serve as classroom resource teachers. The program also sponsors Black History Month art and essay



Buddy Brownstein of the Space Science Division stands among the students he tutors at Leckie Elementary School. Mr. Brownstein received a special award from Leckie for his outstanding support as a volunteer through NRL's Community Outreach Program.

contests for local schools, student tours of NRL, a student Toastmasters Youth Leadership Program, an annual Christmas party for neighborhood children, and an annual collection for Children's Hospital. Through this program NRL has active partnerships with four District of Columbia public schools. (Contact the Public Affairs Office at 767-2541.)

• Other programs that enhance the development of NRL employees include four computer user groups (IBM PC, Mac, NeXT, and Sun), the Microcomputer Software Support Center, and the Amateur Radio Club. The Recreation Club accommodates the varied interests of NRL's employees with its numerous facilities, such as a refurbished 25-yard, 6-lane indoor swimming pool; basketball and volleyball courts; a weight room and exercise area; table tennis; meeting room; softball and basketball leagues; jacuzzi whirlpool; saunas; classes in five different types of martial arts; aerobics exercise; swimming and water walking; and specialized sports clubs (running, skiing, biking, and golfing). The Showboaters, a nonprofit drama group that presents live theater for the enjoyment of NRL and the community, performs two major productions each year in addition to occasional performances at Laboratory functions and benefits for local charities. The most recent productions were "The Murder Room" and "Pajama Game." Though based at NRL, membership in Showboaters is not limited to NRL employees.



Shown are the NRL Showboaters' cast and crew members of their fall production of "The Murder Room"

Programs for Non-NRL Employees

Several programs have been established for non-NRL professionals. These programs encourage and support the participation of visiting scientists and engineers in research of interest to the Laboratory. Some of the programs may serve as stepping-stones to federal careers in science and technology. Their objective is to enhance the quality of the Laboratory's research activities through working associations and interchanges with highly capable scientists and engineers and to provide opportunities for outside scientists and engineers to work in the Navy laboratory environment. Along with enhancing the Laboratory's research, these programs acquaint participants with Navy capabilities and concerns.

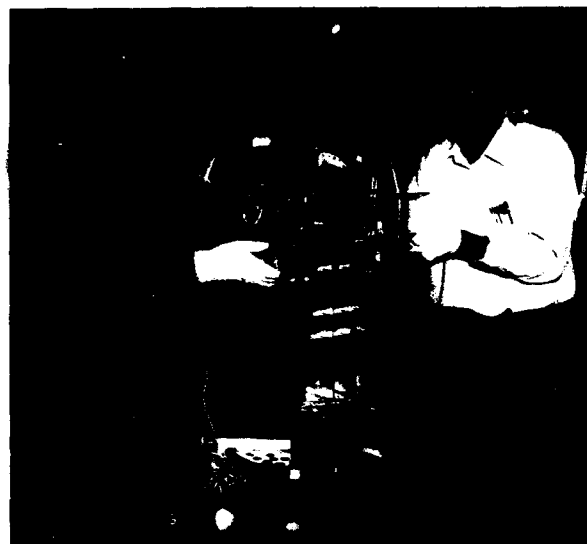
RECENT Ph.D., FACULTY MEMBER, AND COLLEGE GRADUATE PROGRAMS

- The National Research Council (NRC)/NRL Cooperative Research Associateship Program selects associates who conduct research at NRL in their chosen fields in collaboration with NRL scientists and engineers. The tenure period is 2 years. The Office of Naval Research offers the associate post-tenure research grants tenable at an academic institution.

- The American Society for Engineering Education (ASEE) administers the Office of Naval Research (ONR) Postdoctoral Fellowship Program that aims to increase the involvement of highly trained scientists and engineers in disciplines necessary to meet the evolving needs of naval technology. Appointments are for 1 year (renewable for a second and sometimes a third year). These competitive appointments are made jointly by ONR and ASEE.

- The American Society for Engineering Education also administers the Navy/ASEE Summer Faculty Research Program for university faculty members to work for 10 weeks with professional peers in participating Navy laboratories on research of mutual interest.

- The NRL/United States Naval Academy (USNA) Cooperative Program for Scientific Interchange allows faculty members of the U.S. Naval Academy to participate in NRL research. This collaboration benefits the Academy by providing the opportunity for USNA faculty members to work on research of a more practical or applied nature. In turn, NRL's research program is strengthened by the available scientific and engineering expertise of the USNA faculty.



Dr. George Carruthers of the Space Science Division (right) and Garland Dixon work on the final assembly of the lunar camera back-up model prior to its placement in the National Air and Space Museum, Washington, DC. Mr. Dixon, an aerospace engineering student from the University of Maryland, is now working as an NRL student appointee.

- **The Office of Naval Research Graduate Fellowship Program** helps U.S. citizens obtain advanced training in disciplines of science and engineering critical to the U.S. Navy. The 3-year program awards fellowships to recent outstanding graduates to support their study and research leading to doctoral degrees in specified disciplines such as electrical engineering, computer sciences, material sciences, applied physics, and ocean engineering. Award recipients are encouraged to continue their study and research in a Navy laboratory during the summer.

For further information about the above five programs, please contact Mrs. Jessica Hileman at (202) 767-3865.

- **The United States Naval Academy Ensign Program** assigns Naval Academy graduates to NRL to work in areas of their own choosing commensurate with their academic qualifications. These graduates provide a fruitful summer of research assistance, while gaining valuable experience in the Navy's R&D program. (Contact the Military Administrative Office at (202) 767-2103.)

PROFESSIONAL APPOINTMENTS

- **Faculty Member Appointments** use the special skills and abilities of faculty members

for short periods to fill positions of a scientific, engineering, professional, or analytical nature.

- **Consultants and experts** are employed because they are outstanding in their fields of specialization, or because they possess ability of a rare nature and could not normally be employed as regular civil servants.

- **Intergovernmental Personnel Act Appointments** temporarily assign personnel from the state or local government or educational institution to the federal government (or vice versa) to improve public services rendered by all levels of government.

UNDERGRADUATE COLLEGE STUDENT PROGRAMS

Several programs are tailored to the undergraduate that provide employment and work experience in naval research. These are designed to attract applicants for student and full professional employment in the Laboratory's shortage category positions, such as engineers, physicists, mathematicians, and computer scientists. The student employment programs build an understanding of NRL job opportunities among students and educational personnel, so that educators can provide students who will



NRL 1040-hour appointee Mitch Crowder from Ballou High School explains science projects that he and his fellow students developed for exhibition at the National Air and Space Museum

meet NRL's occupational needs. The employment programs for college students include the following:

- **The Cooperative Education Program** alternates periods of work and study for students pursuing bachelor degrees in engineering, computer science, or the physical sciences. Several universities participate in this program.

- **The Clerical Cooperative Education Program** employs students interested in pursuing careers in the clerical occupation. Students work part time during the school year and full time during school breaks.

- **The Federal Junior Fellowship Program** hires needy students entering college to be assistants to scientific, professional, or technical employees.

- **The Summer Employment Program** employs students for the summer in paraprofessional and technician positions in engineering, physical sciences, and computer sciences.

- **The Student Volunteer Program** helps students gain valuable experience by allowing them to voluntarily perform educationally related work at NRL.

- **The 1040-Hour Appointment** employs students on a half-time basis to assist in scientific work related to their academic program.

For additional information, contact Cindy Stiles at (202) 767-3030.



Ms. Lea Potts, a SEAP student, stands next to her project, which she presented at the European Community Young Scientists Contest in Berlin, Germany

HIGH SCHOOL PROGRAMS

- **The DoD Science & Engineering Apprenticeship Program (SEAP)** employs high school juniors and seniors to serve for 8 weeks as junior research associates. Under the direction of a mentor, students gain a better understanding of research, its challenges, and its opportunities through participation in scientific programs. Criteria for eligibility are based on science and mathematics courses completed and grades achieved; scientific motivation, curiosity, and capacity for sustained hard work; a desire for a technical career; teacher recommendations; and achievement test scores. The NRL program is the lead program and the largest in DoD.

For additional information on these programs, please contact the Employee Development Branch (Code 1840) at (202) 767-2956.

GENERAL INFORMATION

Technical Output

The Navy continues to be a pioneer in initiating new developments and a leader in applying these advancements to military requirements. The primary means of informing the scientific and engineering community of the advances made at NRL is through the Laboratory's technical output—reports, articles in scientific journals, contributions to books, papers presented to scientific societies and topical conferences, patents, and inventions.

The figures for Calendar Year 1993 presented below represent the output of NRL facilities in Washington, DC; Orlando, Florida; Bay St. Louis, Mississippi; and Monterey, California.

In addition to the output listed, NRL scientists made more than 1,300 oral presentations during 1993.

A complete listing of the publications by NRL authors appears in the *Bibliography of NRL Publications*, a separate annual publication.

Type of Contribution	Unclass.	Class.	Total
Articles in periodicals, chapters in books, and papers in published proceedings	1,056	0	1,056*
NRL Formal Reports	53	32	85
NRL Memorandum Reports	134	23	157
Other NRL Reports and NRL Publications	39		39
Books	2		2
Patents granted			81
Statutory Invention Registrations (SIRs)			7

*This is a provisional total based on information available to the Ruth H. Hooker Research Library and Technical Information Center on January 31, 1994. Additional publications carrying a 1993 publication date are anticipated.

Key Personnel

		Direct-in-Dialing (202)76 & (202)40; Autovon 29-	
Code	Office		Extension
EXECUTIVE DIRECTORATE			
1000	Commanding Officer	CAPT R.M. Cassidy, USN	73403
1001	Director of Research	Dr. T. Coffey	73301
1000.1	Scientific Staff Assistant	Mr. K.W. Lackie	72880
1002	Chief Staff Officer/Inspector General	CAPT J.R. Love, USN*	73621
1003	Associate Director of Research for Strategic Planning	Dr. W.M. Tolles	73584
1004	Head, Technology Transfer	Dr. R. Rein	73744
1005	Head, Office of Management and Administration	Ms. M. Oliver	73086
1010	Deputy for Space Systems	Dr. R. LeFande*	73324
1200	Head, Command Support Division	CAPT J.R. Love, USN	73621
1220	Head, Security	Mr. J.C. Payne	73048
1230	Public Affairs Officer	Mr. J. Gately, Jr.*	72541
1240	Head, Safety Branch	Mr. K.J. King*	72232
1280	Officer in Charge, Pax River Flight Support Detachment	CDR S.S. Smith, USN	301-863-3751
1800	Director, Human Resources Office	Ms. B. Duffield	73421
1803	Deputy EEO Officer	Ms. D. Erwin*	72486
3008	Legal Counsel	Ms. H. Halper*	72244
BUSINESS OPERATIONS DIRECTORATE			
3000	Associate Director of Research	Mr. R.E. Doak	72371
3030	Head, Management Information Systems Staff	Mr. R.L. Guest	72030
3200	Head, Contracting Division	Mr. J.C. Ely	75227
3300	Comptroller, Financial Management Division	Mr. D.T. Green	73405
3400	Supply Officer, Supply Division	Ms. Cindy Hartman	73446
3500	Director, Research and Development Services Division	Mr. D.K. Woodington	73371
GENERAL SCIENCE AND TECHNOLOGY DIRECTORATE			
4000	Associate Director of Research	Dr. R.A. LeFande	73324
4003	Consultant for Critical Technology Assessment	Mr. L.M. Winslow	72887
4040	Technology Base Manager/BMDO-POC	Dr. S. Sacks	73666
4050	Signature Technology Office	Dr. D.W. Forester	73116
WARFARE SYSTEMS AND SENSORS RESEARCH DIRECTORATE			
5000	Associate Director of Research	Mr. R.R. Rojas	73294
5200	Head, Technical Information Division	Mr. P.H. Imhof	73388
5300	Superintendent, Radar Division	Dr. M.I. Skolnik	72936
5500	Superintendent, Information Technology Division	Dr. R.F. Shumaker	72903
5600	Superintendent, Optical Sciences Division	Dr. T.G. Giallorenzi	73171
5700	Superintendent, Tactical Electronic Warfare Division	Dr. J.A. Montgomery	76278
5900	Superintendent, Underwater Sound Reference Detachment	Dr. J.E. Blue	407-857-5230
MATERIALS SCIENCE AND COMPONENT TECHNOLOGY DIRECTORATE			
6000	Associate Director of Research	Dr. B.B. Rath	73566
6030	Head, Laboratory for Structure of Matter	Dr. J. Karle	72665
6100	Superintendent, Chemistry Division	Dr. J.S. Murday	73026
6300	Superintendent, Materials Science & Technology Division	Dr. D.U. Gubser	72926
6400	Director, Lab. for Computational Physics and Fluid Dynamics	Dr. J.P. Boris	73055
6600	Superintendent, Condensed Matter & Radiation Sciences Division	Dr. D.J. Nagel	72931
6700	Superintendent, Plasma Physics Division	Dr. S. Ossakow	72723
6800	Superintendent, Electronics Science & Technology Division	Dr. G.M. Borsuk	73525
6900	Center for Bio/Molecular Sciences and Engineering	Dr. J. Schnur	73344
OCEAN AND ATMOSPHERIC SCIENCE AND TECHNOLOGY DIRECTORATE			
7000	Associate Director of Research	Dr. E.O. Hartwig	48690
7030	Head, Systems Support and Requirements	Dr. R.M. Root	601-688-4010
7100	Superintendent, Acoustics Division	Dr. E.R. Franchi (Acting)	73482
7200	Superintendent, Remote Sensing Division	Dr. P. Schwartz (Acting)	72351
7300	Superintendent, Oceanography Division	Dr. W.B. Moseley	601-688-4670
7400	Superintendent, Marine Geosciences Division	Dr. H.C. Eppert, Jr.	601-688-4650
7500	Superintendent, Marine Meteorology Division	Dr. J.B. Hovermale	408-656-4721
7600	Superintendent, Space Science Division	Dr. H. Gursky	76343
NAVAL CENTER FOR SPACE TECHNOLOGY			
8000	Director	Mr. P.G. Wilhelm	76547
8100	Superintendent, Space Systems Development Department	Mr. R.E. Eisenhauer	70410
8200	Superintendent, Spacecraft Engineering Department	Mr. H.E. Senasack, Jr. (Acting)	76407

*Additional Duty

ORGANIZATIONAL CHART EXECUTIVE DIRECTORATE



COMMANDING OFFICER
Code 1000
CAPT R.M. Cassidy, USN



DIRECTOR OF RESEARCH
Code 1001
Dr. T. Coffey

ASSOCIATE DIRECTORS OF RESEARCH



**OFFICE FOR
STRATEGIC PLANNING**
Code 1003
Dr. W.M. Tolles



**BUSINESS
OPERATIONS
DIRECTORATE**
Code 3000
R.E. Doak



**GENERAL
SCIENCE AND
TECHNOLOGY
DIRECTORATE**
Code 4000
Dr. R.A. LeFande



**WARFARE
SYSTEMS
AND SENSORS
RESEARCH
DIRECTORATE**
Code 5000
R.R. Rojas



**MATERIALS
SCIENCE AND
COMPONENT
TECHNOLOGY
DIRECTORATE**
Code 6000
Dr. B.B. Rath

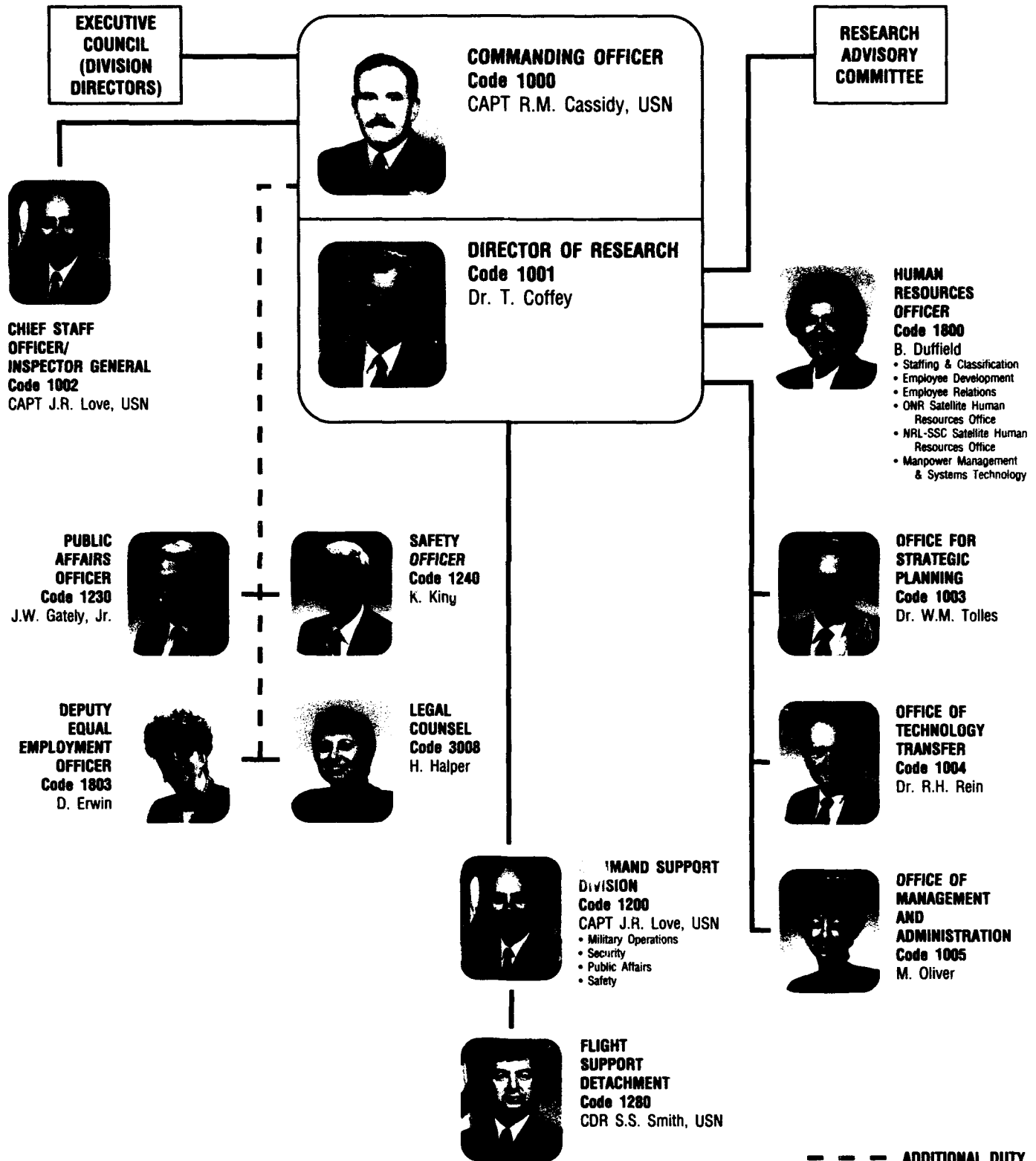


**OCEAN AND
ATMOSPHERIC
SCIENCE AND
TECHNOLOGY
DIRECTORATE**
Code 7000
Dr. E.O. Hartwig



**NAVAL CENTER
FOR SPACE
TECHNOLOGY**
Code 8000
P.G. Wilhelm

ORGANIZATIONAL CHART (Continued) EXECUTIVE DIRECTORATE





**BUSINESS
OPERATIONS
DIRECTORATE**
Code 3000
R.E. Doak



**CONTRACTING
DIVISION**
Code 3200
J. Ely
• Policy & Analysis
• Contract Negotiations
• Acquisition Strategies/Training
• Advance Acquisition Planning
• Contractual Execution
• Contract Administration
• Acquisition Policy Interpretations
• Implementation



**FINANCIAL
MANAGEMENT
DIVISION**
Code 3300
D.T. Green
• Budget
• Systems Operations
• Accounting
• Financial
• Disbursing



**SUPPLY
DIVISION**
Code 3400
C. Hartman
• Purchasing
• Technical
• Customer Liaison
• Credit Card
• Material Control
• Supply Stores
• Delivery & Storage



**RESEARCH AND
DEVELOPMENT SERVICES
DIVISION**
Code 3500
D.K. Woodington
• Project Management
• Chesapeake Bay Detachment
• Operations
• Services
• Administrative
• Engineering



**GENERAL SCIENCE AND
TECHNOLOGY DIRECTORATE/
DEPUTY FOR SPACE SYSTEMS**
Code 4000/1010
Dr. R.A. LeFande



**CRITICAL
TECHNOLOGY
ASSESSMENT**
Code 4003
L.M. Winslow



TECH BASE/BMDO-POC
Code 4040
Dr. S. Sacks



**SIGNATURE
TECHNOLOGY
OFFICE**
Code 4050
Dr. D.W. Forester



**WARFARE SYSTEM
AND SENSORS
RESEARCH
DIRECTORATE**
Code 5000
R.R. Rojas



**TECHNIC/
DIVISION**
Code 520
P. Imhof
• Technical
• Publication
• Graphic D
• Systems/I



**RADAR C
Code 530**
Dr. M.J.
• Radar An
• Advanced
• Search Ra
• Target Ch
• Identificat
• Airborne I



**INFORMA
Code 550**
Dr. R.P.
• Navy Cent
• in Artifi
• Commun
• Human-Co
• Center for
• Assuran



**OPTICAL
Code 560**
Dr. T.G.
• Advanced
• Applied O
• Laser Phy
• Electro-op
• Optical Te



**TACTICAL
Code 570**
Dr. J.A.
• On-Board
• EW Supp
• Airborne
• Ships EW
• Integrated



**UNDERW
DETACH
Code 590**
Dr. J.E.
• Acoustical
• Acoustical
• Technical
• Measurem

11

ORGANIZATIONAL CHART (Continued)



WARFARE SYSTEMS AND SENSORS RESEARCH DIRECTORATE Code 5000 R.R. Rojas



**TECHNICAL INFORMATION
DIVISION**
Code 5200
P. Imhof
• Technical Library/Software Support
• Publications
• Graphic Design Services
• Systems/Photographic



RADAR DIVISION
Code 5300
Dr. M.I. Skolnik
• Radar Analysis
• Advanced Radar Systems
• Search Radar
• Target Characteristics
• Identification Systems
• Airborne Radar



INFORMATION TECHNOLOGY DIVISION
Code 5500
Dr. R.P. Shumaker
• Navy Center for Applied Research
in Artificial Intelligence
• Communication Systems
• Human-Computer Interaction
• Center for Computer High
Assurance Systems
• Transmission Technology
• Advanced Information
Technology
• Center for Computational
Science



OPTICAL SCIENCES DIVISION
Code 5600
Dr. T.G. Giallorenzi
• Advanced Concepts
• Applied Optics
• Laser Physics
• Electro-optical Technology
• Optical Techniques



TACTICAL ELECTRONIC WARFARE DIVISION
Code 5700
Dr. J.A. Montgomery
• Off-Board Countermeasures
• EW Support Measures
• Airborne EW Systems
• Ships EW Systems
• Integrated EW Simulation



**UNDERWATER SOUND REFERENCE
DETACHMENT**
Code 5900/NRL-ORL
Dr. J.E. Blue
• Acoustical Materials & Transduction
• Acoustical Systems
• Technical Services
• Measurements



MATERIALS SCIENCE AND COMPONENT TECHNOLOGY DIRECTORATE Code 6000 Dr. B.B. Rath



**LABORATORY FOR THE
STRUCTURE OF MATTER**
Code 6030
Dr. J. Karle



**CHEMISTRY
DIVISION**
Code 6100
Dr. J.S. Murday
• Chemical Dynamics & Diagnostics
• Materials Chemistry
• Surface Chemistry
• Navy Technology Center for Safety & Survivability



**MATERIALS SCIENCE AND
TECHNOLOGY DIVISION**
Code 6300
Dr. D.U. Gubser
• Physical Metallurgy
• Materials Physics
• Composites & Ceramics
• Mechanics of Materials



**LABORATORY FOR COMPUTATIONAL
PHYSICS AND FLUID DYNAMICS**
Code 6400
Dr. J.P. Boris
• Center for Reactive Flow & Dynamical Systems
• Center for Computational Physics Developments
• Reactive Flow Physics



**CONDENSED MATTER AND
RADIATION SCIENCES DIVISION**
Code 6600
Dr. D.J. Nagel
• Radiation Effects
• Directed Energy Effects
• Surface Modification
• Dynamics of Solids
• Complex Systems Theory



PLASMA PHYSICS DIVISION
Code 6700
Dr. S. Ossakow
• Radiation Hydrodynamics
• Laser Plasma
• Charged Particle Physics
• Pulsed Power Physics
• Space Plasma
• Beam Physics



**ELECTRONICS SCIENCE
AND TECHNOLOGY DIVISION**
Code 6800
Dr. G.M. Borsuk
• Nanoelectronics
• Solid State Devices
• Vacuum Electronics
• Microwave Technology
• Surface & Interface Sciences
• Electronic Materials



**CENTER FOR BIO/MOLECULAR
SCIENCE AND ENGINEERING**
Code 6900
Dr. J. Schnur
• Molecular Architectures
• Biomaterials
• Biological & Environmental Systems
• Advanced Programs

ued)

SCIENCE CENT

**LABORATORY FOR THE
STRUCTURE OF MATTER**
Code 6830
J. Karle

**CHEMISTRY
DIVISION**
Code 6100
J.S. Murday
• Chemical Dynamics & Diagnostics
• Plasma Chemistry
• Surface Chemistry
• Technology Center for Safety & Survivability

**MATERIALS SCIENCE AND
TECHNOLOGY DIVISION**
Code 6300
D.U. Gubser
• Physical Metallurgy
• Materials Physics
• Composites & Ceramics
• Mechanics of Materials

**LABORATORY FOR COMPUTATIONAL
PHYSICS AND FLUID DYNAMICS**
Code 6400
J.P. Boris
• Center for Reactive Flow & Dynamical Systems
• Center for Computational Physics Developments
• Active Flow Physics

**CONDENSED MATTER AND
NATION SCIENCES DIVISION**
Code 6600
D.J. Nagel
• Radiation Effects
• Selected Energy Effects
• Surface Modification
• Dynamics of Solids
• Complex Systems Theory

PLASMA PHYSICS DIVISION
Code 6700
S. Ossakow
• Radiation Hydrodynamics
• Laser Plasma
• Charged Particle Physics
• Pulsed Power Physics
• Space Plasma
• Beam Physics

**ELECTRONICS SCIENCE
AND TECHNOLOGY DIVISION**
Code 6800
G.M. Borsuk
• Microelectronics
• Solid State Devices
• Vacuum Electronics
• Microwave Technology
• Surface & Interface Sciences
• Electronic Materials

**CENTER FOR BIO/MOLECULAR
SCIENCE AND ENGINEERING**
Code 6900
J. Schnur
• Molecular Architectures
• Materials
• Biological & Environmental Systems
• Advanced Programs



**OCEAN AND
ATMOSPHERIC SCIENCE
AND TECHNOLOGY
DIRECTORATE**
Code 7000
Dr. E.O. Hartwig



SYSTEMS SUPPORT AND REQUIREMENTS
Code 7030/NRL-SSC
Dr. R.M. Root



ACOUSTICS DIVISION
Code 7100
Dr. E.R. Franchi (Acting)
• Center for Environmental Acoustics
• Acoustic Signal Processing
• Physical Acoustics

- Acoustic Systems
- Ocean Acoustics
- Acoustic Simulation
& Tactics



REMOTE SENSING DIVISION
Code 7200
Dr. P. Schwartz (Acting)
• Special Projects Office
• Radio/IR/Optical Sensors
• Remote Sensing Physics
• Imaging Systems & Research

- Remote Sensing Applications
- Remote Sensing
Hydrodynamics



OCEANOGRAPHY DIVISION
Code 7300/NRL-SSC
Dr. W.B. Moseley
• Ocean Dynamics & Prediction
• Ocean Sciences
• Ocean Technology



MARINE GEOSCIENCES DIVISION
Code 7400/NRL-SSC
Dr. H.C. Eppert, Jr.
• Tactical Oceanography Warfare Support
• Marine Physics
• Seafloor Sciences
• Mapping, Charting, and Geodesy



MARINE METEOROLOGY DIVISION
Code 7500/NRL-MRY
Dr. J.B. Hovermale
• Prediction Systems
• Forecast Support



SPACE SCIENCE DIVISION
Code 7600
Dr. H. Gursky
• Office of Strategic Phenomena
• Engineering Management
• Ultraviolet Measurements
• X-Ray Astronomy
• Upper Atmosphere Physics

- Gamma & Cosmic Ray
Astrophysics
- Solar Physics
- Solar Terrestrial Relationships
- E.O. Hulburt Center for
Space Research



**NAVAL CENTER FOR
SPACE TECHNOLOGY**
Code 8000
P.G. Wilhelm



**SPACE SYSTEMS DEV
DEPARTMENT**
Code 8100
R.E. Eisenhauer
• SDI Office
• Mission Development
• Advanced Systems Technol.
• Space Electronic Systems I
• Command, Control, Comm.,
Computers, & Intelligence
• Space Applications



**SPACECRAFT
ENGINEERING
DEPARTMENT**
Code 8200
H.E. Senasack, Jr. (Ac)
• Design, Test, & Processing
• Systems Analysis
• Control Systems



**NAVAL CENTER FOR
SPACE TECHNOLOGY**
Code 8000
P.G. Wilhelm



**SPACE SYSTEMS DEVELOPMENT
DEPARTMENT**
Code 8100
R.E. Eisenhower
• SDI Office
• Mission Development
• Advanced Systems Technology
• Space Electronic Systems Development
• Command, Control, Communications,
Computers, & Intelligence
• Space Applications



**SPACECRAFT
ENGINEERING
DEPARTMENT**
Code 8200
H.E. Senasack, Jr. (Acting)
• Design, Test, & Processing
• Systems Analysis
• Control Systems

AND REQUIREMENTS

ng)
Acoustics
• Acoustic Systems
• Ocean Acoustics
• Acoustic Simulation
& Tactics

VISION

ng)
• Remote Sensing Applications
• Remote Sensing
Hydrodynamics

SION

ES DIVISION

are Support

adesy

GY DIVISION

SION

na
• Gamma & Cosmic Ray
Astrophysics
• Solar Physics
• Solar Terrestrial Relationships
E.O. Hulburt Center for
Space Research

(4)

Contributions by Divisions, Laboratories, and Departments

Command Support Division (1200)

- 9 A Career That Matters
Bower Award Recognizes Pioneering
Contributions of Dr. Isabella Karle
David K. van Keuren

Radar Division (Code 5300)

- 153 Missile Hit-Points on the DDG-53
Dale A. Zolnick and Harold L. Toothman
213 High-Frequency Approximations to
Physical Optics
William B. Gordon

Information Technology Division (Code 5500)

- 105 High-Resolution Underwater Acoustic Imaging
Behzad Kamgar-Parsi
167 Secure Information Through Replicated
Architecture (SINTRA) Database System
Judith N. Froscher and John P. McDermott

Optical Sciences Division (Code 5600)

- 127 Fiber-Optic Sensor for Detection of Trace
Levels of Mercury in Water
*Kenneth J. Ewing, Ishwar D. Aggarwal,
Gregory M. Nau, and Thomas Bilodeau*
137 Multispectral Infrared Visualization and
Processing for Dim Target Detection
*Dean A. Scribner, Michael P. Satyshur, and
Melvin R. Kruer*
215 Broadband Thermal Optical Limiter
*Brian L. Justus, Alan L. Huston, and
Anthony J. Campillo*
217 High-Speed, Low-Loss Transmission Line on
Silicon Membrane
Michael Y. Frankel

Tactical Electronic Warfare Division (Code 5700)

- 139 Flying Radar Target (FLYRT) Testing and
Final Demonstration
*Christopher S. Bovais, Ciaran J. Murphy,
and Peggy L. Toot*

- 141 The Microwave Monolithic Integrated Circuit/
Electronic Warfare Receiver
Leo W. Lemley
168 Embedded Training Methods for Command and
Control Systems
Gene E. Layman

Underwater Sound Reference Detachment (Code 5900)

- 108 Cylindrical Wavenumber Calibration Array
Little D. Luker and Arnie L. Van Buren
111 Direct Measurement of Edge Diffraction from
Acoustic Panels of Decoupling Materials
Jean C. Piquette

The Laboratory for the Structure of Matter (Code 6030)

- 130 Observing the Growth of Protein Crystals
*John H. Konnert, Peter D'Antonio, and
Keith B. Ward*

Chemistry Division (Code 6100)

- 61 Diamond Surface Chemistry
*Pehr E. Pehrsson, John N. Russell, Jr.,
Brian D. Thoms, James E. Butler,
Michael Marchywka, and Jeffrey M. Calvert*
132 Global Warming Potential of Potential CFC
Replacements
*Nancy L. Garland, Herbert H. Nelson, and
Laura J. Medhurst*

Materials Science and Technology Division (Code 6300)

- 73 Computational Materials Science
*Larry L. Boyer, Michael J. Mehl, Dimitrios
A. Papaconstantopoulos, Warren E. Pickett,
and David J. Singh*
177 Simulation and Visualization of Ultrasonic
Waves in Solids by Using Parallel Processing
*Richard S. Schechter, Henry H. Chaskelis,
Richard B. Mignogna, and P.P. Delsanto*

- 181 Ultimate Strength of Ultrafine Polycrystalline Materials
Chandra S. Pande and Robert A. Masumura
- 182 Element-Specific Magnetometry
Yves U. Idzerda and Gary A. Prinz
- 184 Origins of Magnetic Anisotropy in Magneto-optical Storage Materials
William T. Elam, Vincent G. Harris, and Norman C. Koon

Laboratory for Computational Physics and Fluid Dynamics (Code 6400)

- 189 Reactive Flows in Ram Accelerators
Chiping Li, Kazhikathra Kailasanath, Elaine S. Oran, and Jay P. Boris

Condensed Matter and Radiation Sciences Division (Code 6600)

- 154 Capillary Optics for X-ray Lithography
Charles M. Dozier, Michael I. Bell, and Dan Newman
- 184 Origins of Magnetic Anisotropy in Magneto-optical Storage Materials
William T. Elam, Vincent G. Harris, and Norman C. Koon

Plasma Physics Division (Code 6700)

- 144 The Ionospheric Focussed Heating (IFH) Experiment
Paul A. Bernhardt
- 156 Ultra Intense Laser Physics Research at NRL
Phillip A. Sprangle, Antonio C. Ting, Eric H. Esarey, and Jacob Grun

Electronics Science and Technology Division (Code 6800)

- 146 Control of Interface Properties of GaSb/InAs Superlattices
Robert J. Wagner, Brian R. Bennett, Benjamin V. Shanabrook, John L. Davis, James R. Waterman, and Mark E. Twigg
- 220 Paramagnetic Resonance and Optical Studies of GaN
William E. Carlos, Evan R. Glaser, Thomas Kennedy, and Jaime A. Freitas, Jr.

Center for Bio/Molecular Science and Engineering (Code 6900)

- 61 Diamond Surface Chemistry
Pehr E. Pehrsson, John N. Russell, Jr., Brian D. Thoms, James E. Butler, Michael Marchywka, and Jeffrey M. Calvert

- 83 Self-assembled Molecular Templates: Microtubule-based Controlled Release for Biofouling Control and Medical Applications
Ronald R. Price, Alan S. Rudolph, Jonathan V. Selinger, and Joel M. Schnur

Acoustics Division (Code 7100)

- 114 Structural Acoustics of Nearly Periodic Structures
Douglas M. Photiadis
- 118 Acoustic Reverberation at Selected Sites in the Mid-Atlantic Ridge Region
Jerald W. Caruthers, J. Robert Fricke, and Ralph A. Stephen
- 122 Overcoming Chaos
Michael D. Collins and William A. Kuperman

Remote Sensing Division (Code 7200)

- 199 Sea Surface Temperature Retrievals from Satellite
Douglas A. May
- 222 Interferometric "Seeing" Measurements on Mt. Wilson: Power Spectra and Outer Scales
David Mozurkewich and David F. Buscher
- 227 Hubble Space Telescope Image Reconstruction on the NRL Connection Machine
Paul L. Hertz and Michael L. Cobb

Oceanography Division (Code 7300)

- 190 Numerical Ocean Models
NRL Global Modeling Team
- 200 Events Leading to the 1991-92 El Niño
John C. Kindle and Patricia A. Phoebus

Marine Geosciences Division (Code 7400)

- 91 Monitoring Whales and Earthquakes by Using SOSUS
Clyde E. Nishimura
- 203 Field Tests of the DOLPHIN—A Remotely Operated Survey Vehicle
Maria T. Kalcic and Edit J. Kaminsky

Marine Meteorology Division (Code 7500)

- 200 Events Leading to the 1991-92 El Niño
John C. Kindle and Patricia A. Phoebus
- 206 Impacts of Weather Model Forecasts on Tactical Environmental Decision Aids
Gary G. Love and John Cook

Space Science Division (Code 7600)

- 61 Diamond Surface Chemistry
Pehr E. Pehrsson, John N. Russell, Jr., Brian D. Thoms, James E. Butler, Michael Marchywka, and Jeffrey M. Calvert

- 159 HRTS Ultraviolet Observations of a Solar Active Region

Kenneth P. Dere, Clarence M. Korendyke, and Guenter E. Brueckner

- 227 Hubble Space Telescope Image Reconstruction on the NRL Connection Machine

Paul L. Hertz and Michael L. Cobb

**Space Systems Development Department
(Code 8100)**

- 171 Historical Perspective on the NAVSTAR Global Positioning System

Ronald L. Beard

- 162 LIDAR Backscatter from a Rocket Plume

G. Charmaine Gilbreath, Amey R. Peltzer, and Anne E. Clement

- 229 Impedance Model Study for the Common Pressure Vessel Battery

Daniel J. Shortt, William E. Baker, Jr., James C. Garner, and George Barnard

**Spacecraft Engineering Department
(Code 8200)**

- 231 Advanced Release Technologies Program

William E. Purdy

- 233 Vibration Excitation Test of the LACE Satellite as Observed by a Ground-based Laser Radar

Shalom Fisher, K.I. Schultz, and L.W. Taylor, Jr.

Employment Opportunities for Entry-Level and Experienced Personnel

The *NRL Review* illustrates some of the exciting science and engineering carried out at NRL as well as the potential for new personnel.

The Naval Research Laboratory offers a wide variety of challenging positions that involve the full range of work from basic and applied research to equipment development. The nature of the research and development conducted at NRL requires professionals with experience. Typically, there is a continuing need for electronics, mechanical, aerospace, ceramic, and materials engineers; metallurgists and oceanographers with bachelor's and/or advanced degrees; and physical and computer scientists with Ph.D. degrees. Opportunities exist in the areas described below.

Ceramic Engineers and Materials Scientists/Engineers. These employees are recruited to work on materials, microstructure characterization, electronic ceramics, solid-state physics, fiber optics, electro-optics, microelectronics, fracture mechanics, vacuum science, laser physics technology, and radio frequency/microwave/millimeter wave/infrared technology.

Electronics Engineers and Computer Scientists. These employees may work in the areas of communications systems, electromagnetic scattering, electronics instrumentation, electronic warfare systems, radio frequency/microwave/millimeter wave/infrared technology, radar systems, laser physics technology, radio-wave propagation, electron device technology, spacecraft design, artificial intelligence, information processing, signal processing, plasma physics, vacuum science, microelectronics, electro-optics, fiber optics, solid state, software engineering, computer design/architecture, ocean acoustics, stress analysis, and expert systems.

Mechanical Engineers. These employees may be assigned to spacecraft design, remote sensing, propulsion, experimental fluid mechanics, experimental structural mechanics, solid mechanics, elastic/plastic fracture mechanics, materials, finite-element methods, nondestructive evaluation, characterization of fracture resistance of structural alloys, combustion, and CAD/CAM.

Chemists. Chemists are recruited to work in the areas of combustion, polymer science, bio-engineering and molecular engineering, surface science, materials, fiber optics, electro-optics, microelectronics, electron device technology, and laser physics.

Physicists. Physics graduates may concentrate on such fields as materials, solid-state physics, fiber optics, electro-optics, microelectronics, vacuum science, plasma physics, fluid mechanics, signal processing, ocean acoustics, information processing, artificial intelligence, electron device technology, radiowave propagation, laser physics, ultraviolet/X-ray/gamma ray technology, electronic warfare, electromagnetic interaction, communications systems, radio frequency/microwave/millimeter wave/infrared technology, and computational physics.

Oceanographers, Meteorologists, and Marine Geophysicists. These employees work in the areas of ocean dynamics, air-sea interaction, upper ocean dynamics, oceanographic bio-optical modeling, ocean and atmosphere numerical modeling and prediction, artificial intelligence applications for satellite analysis, benthic processes, aerogeophysics, marine sedimentary processes, and advanced mapping techniques. Oceanographers and marine geophysicists are located in Washington, DC, and the Stennis Space Center, Bay St. Louis, Mississippi.

Meteorologists are located in Washington, DC, and Monterey, California.

FOR FOREIGN NATIONALS

U.S. citizenship is required for employment with NRL.

APPLICATION AND INFORMATION

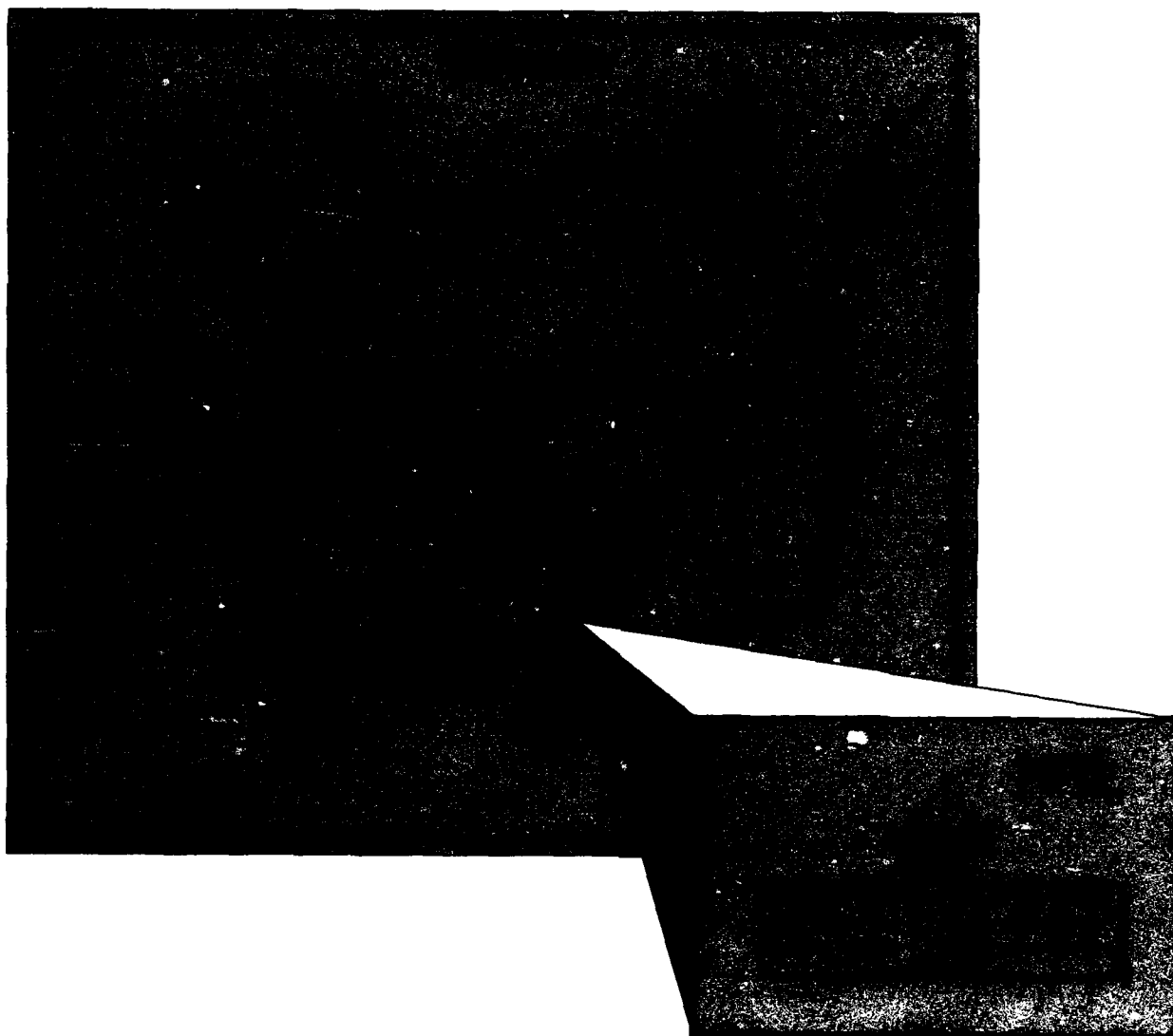
Interested applicants should submit an Application for Federal Employment (SF-171), which

can be obtained from local offices of the Office of Personnel Management and personnel offices of Federal agencies, to the address below.

Direct inquiries to:

Naval Research Laboratory
Human Resources Office, Code 1813 RV 94
Washington, DC 20375-5324
(202) 767-3030

Location of NRL in the Capital Area



Subject Index

- Acoustic, 108
- Acoustic lens, 105
- Acoustics, 32, 91
- Active decoy, 139
- Active experiments, 144
- Advanced Graduate Research Program, 269
- Air-sea interaction, 200
- Alan Berman Research Publication and Edison Patent Awards, 259
- Alfred P. Sloan Fellows Program, 270
- Amateur Radio Club, 274
- American Indian/Alaskan Native Employment Program, 273
- Anisotropy, 184
- Asian-American/Pacific Islander Program, 273
- Atmospheric seeing, 222
- Atomic clocks, 171
- Atomic Force Microscopy, 130
- Attenuation, 217
- Author Index, 294
- Bathymetry, 203
- Battery impedance, 229
- Battery model, 229
- Bio/Molecular Science and Engineering, 32, 42
- Black Employment Program, 273
- Brookings Institute Advanced Study Program, 270
- Calibration, 108
- Capillary optics, 154
- Center for Computational Science, 37
- Chaos, 122
- Chemical vapor deposition, 61
- Chemistry, 29
- Chesapeake Bay Detachment, 38
- Clerical Cooperative Education Program, 277
- Color Presentation, 55
- Community Outreach Program, 273
- Computer user groups, 274
- Concurrency control, 167
- Condensed Matter and Radiation Sciences, 30
- Connection machine, 227
- Consultant and expert appointments, 276
- Contributions by Divisions, Laboratories, and Departments, 287
- Controlled release, 83
- Cooperative Education Program, 277
- Counseling Referral Service, 271
- Database, 167
- Detonation, 189
- Diamond, 61
- Differential GPS (DGPS), 203
- Diffraction, 111
- Dislocations, 181
- Dispersion, 217
- DoD Science & Engineering Apprentice Program, 277
- DOLPHIN, 203
- Edge diffraction, 111
- Edison Memorial Graduate Training Program, 269
- Eigenray, 122
- Elastic wave propagation, 177
- Electromagnetic propagation, 206
- Electromagnetic scatter, 213
- Electronic properties, 73
- Electronics, 154
- Electronics Science and Technology, 32, 42, 44
- Electronic Warfare, 28, 141
- Electron spin resonance, 220
- Electro-optic, 217
- El Niño, 190, 200
- Embedded training, 168
- Employment Opportunities, 290
- Equal Employment Opportunity (EEO) Programs, 273
- Evanescent, 108
- Faculty member appointments, 276
- Federal Employment Opportunity Recruitment Program, 273
- Federal Junior Fellowship Program, 277
- Federally Employed Women, Inc., 272
- Federal Women's Program, 273
- Fellowship in Congressional Operations, 270
- Fiber-optic chemical sensor, 127
- Flight Support Detachment, 38, 43
- Flying radar target, 139
- GaN, 220
- GaSb/InAs interfaces, 146
- Global Warming Potential, 132
- Highlights of NRL Research in 1993, 45
- High-power radio waves, 144
- Hispanic Employment Program, 273
- Hubble Space Telescope, 227
- Hydrofluorocarbons, 132
- Hydrographic survey, 203
- Image processing, 137
- Image reconstruction, 227
- Individual Honors, 247
- Individuals with Disabilities Program, 273
- Information Technology, 27, 43
- Infrared, 137
- Infrared detector materials, 146
- Intergovernmental Personnel Act appointments, 276
- Iron, 184
- Kelvin waves, 200
- Key Personnel, 282
- Laboratory for Computational Physics and Fluid Dynamics, 29
- Laser ordnance, 231
- Laser radar, 233
- LIDAR, 162
- Location of NRL in the Capital Area, 291
- Long-Line Hydrophone Calibrator Facility, 41
- Magnetic materials, 182
- Magnetometry, 182

Magneto-optic, 184
 Marine Corrosion Test Facility, 39
 Marine Geosciences, 34
 Marine Meteorology, 35
 Materials, 29
 Materials Science and Technology, 43
 Meet the Researchers, 52
 Mercury, 127
 Midway Research Center, 40
 Missile hit-points, 153
 MMIC, 141
 Multibeam, 203
 Multilevel secure, 167
 Multispectral, 137
 Nanoscience, 182
 National Research Council/NRL Cooperative Research Associateship, 275
 Naval Postgraduate School, 270
 Navigation technology, 171
 NAVSTAR GPS, 171
 Navy Science Assistance Program, 270
 Near periodic, 114
 New materials, 73
 Nonlinear, 122
 Nonlinear interactions, 156
 NRL Mentor Program Pilot Project, 272
 NRL-Monterey, 40
 NRL Review Award Articles, 264
 NRL Review Staff, Inside Back Cover
 NRL-Stennis Space Center, 39
 NRL/United States Naval Academy Cooperative Program for Scientific Interchange, 275
 Numerical weather prediction, 206
 Ocean Acoustics Research Laboratory, 42
 Ocean models, 190
 Oceanography, 34
 Ocean prediction, 190
 ODMR, 220
 Office of Naval Research Graduate Fellowship Program, 276
 Office of Naval Research Postdoctoral Fellowship Program, 275
 On-orbit data, 233
 Optical interferometry, 222
 Optical limiting, 215
 Optical Sciences, 27, 41
 Organizational Charts, 283
 Panel measurements, 111
 Parallel processing, 177
 Phospholipids, 83
 Photoluminescence, 220
 Physical Optics, 213
 Picosecond, 217
 Plasma Physics, 31, 42, 43
 Protein crystals, 130
 Radar, 26, 41, 43
 Radar cross section calculation, 213
 Radar signature, 153
 Ram accelerator, 189
 Receiver, 141
 Receiver-on-a-chip, 141
 Recreation Club, 274
 Refrigerants, 132
 Release mechanisms, 231
 Remotely operated vehicle (ROV), 203
 Remote Sensing, 33, 199
 Replica control, 167
 Research Platforms, 40
 Reverberation, 118
 RF, 141
 Rocket plume, 162
 Scattering, 118
 Scientist-to-Sea Program, 271
 Sea surface temperature, 199
 Secondary experiment, 233
 Select Graduate Training Program, 269
 Self-assembly, 83
 Semiconductor superlattices, 146
 Sensor protection, 215
 Separation devices, 231
 Shock, 189
 Showboaters, 274
 Sigma Xi, 271
 Solar Physics, 159
 SOSUS, 91
 Spacecraft, 231
 Space plasma physics, 144
 Space Science, 35
 Space Technology, 36
 Special Awards and Recognition, 239
 Strength, 181
 Structural acoustics, 114
 Structural dynamics, 233
 Structure of Matter, 29
 Student Volunteer Program, 277
 Subject Index, 292
 Summer Employment Program, 277
 Summer Faculty Research Program, 275
 Superheterodyne, 141
 Surface chemistry, 61
 Table-top-terawatt laser, 156
 Target detection, 137
 Technical Information Services, 37
 Technical Output, 281
 1040-Hour Appointment, 277
 Terahertz, 217
 Terbium, 184
 Theory of materials, 73
 Thermal defocusing, 215
 Thin film, 184
 3-D sonar imaging, 105
 Toastmasters International, 272
 T-phases, 91
 Transaction management, 167
 Transmission line, 217
 Ultrafine grains, 181
 Ultra intense, 156
 Ultrasonic waves, 177
 Undergraduate college student programs, 276
 Underwater acoustic imaging, 105
 Underwater Sound Reference Detachment, 38
 United States Naval Academy Ensign Program, 276
 Vacuum Ultraviolet Space Instrument, 42
 Vibration characteristics, 233
 Visible absorption, 127
 Westerly wind bursts, 200
 Whales, 91
 Women in Science and Engineering, 271
 Women's Executive Leadership Program Office of Research and Technology Applications Program, 270
 X-ray, 154
 X-ray lithography, 154

Author Index

- | | | |
|-------------------------|-----------------------|-------------------------------|
| Aggarwal, I.D., 127 | Gilbreath, G.C., 162 | NRL Global Modeling Team, 190 |
| Baker, Jr., W.E., 229 | Glaser, E.R., 220 | Oran, E.S., 189 |
| Barnard, G., 229 | Gordon, W.B., 213 | Pande, C.S., 181 |
| Beard, R.L., 171 | Grun, J., 156 | Papaconstantopoulos, D.A., 73 |
| Bell, M.I., 154 | Harris, V.G., 184 | Pehrsson, P.E., 61 |
| Bennett, B.R., 146 | Hertz, P.L., 227 | Peltzer, A.R., 162 |
| Bernhardt, P.A., 144 | Huston, A.L., 215 | Phoebus, P.A., 200 |
| Bilodeau, T., 127 | Idzerda, Y.U., 182 | Photiadis, D.M., 114 |
| Boris, J.P., 189 | Justus, B.L., 215 | Pickett, W.E., 73 |
| Bovais, C.S., 139 | Kailasanath, K., 189 | Piquette, J.C., 111 |
| Boyer, L.L., 73 | Kalcic, M.T., 203 | Price, R.R., 83 |
| Brueckner, G.E., 159 | Kamgar-Parsi, B., 105 | Prinz, G.A., 182 |
| Buscher, D.F., 222 | Kaminsky, E.J., 203 | Purdy, W.E., 231 |
| Butler, J.E., 61 | Kennedy, T.A., 220 | Rudolph, A.S., 83 |
| Calvert, J.M., 61 | Kindle, J.C., 200 | Russell, Jr., J.N., 61 |
| Campillo, A.J., 215 | Konnert, J.H., 130 | Satyshur, M.P., 137 |
| Carlos, W.E., 220 | Koon, N.C., 184 | Schechter, R.S., 177 |
| Caruthers, J.W., 118 | Korendyke, C.M., 159 | Schnur, J.M., 83 |
| Chaskelis, H.H., 177 | Kruer, M.R., 137 | Schultz, K.I., 233 |
| Clement, A.E., 162 | Kuperman, W.A., 122 | Scribner, D.A., 137 |
| Cobb, M.L., 227 | Layman, G.E., 168 | Selinger, J.V., 83 |
| Collins, M.D., 122 | Lemley, L.W., 141 | Shanabrook, B.V., 146 |
| Cook, J., 206 | Li, C., 189 | Shortt, D.J., 229 |
| D'Antonio, P., 130 | Love, G.G., 206 | Singh, D.J., 73 |
| Davis, J.L., 146 | Luker, L.D., 108 | Sprangle, P.A., 156 |
| Delsanto, P.P., 177 | Marchywka, M., 61 | Stephen, R.A., 118 |
| Dere, K.P., 159 | Masumura, R.A., 181 | Taylor, Jr., L.W., 233 |
| Dozier, C.M., 154 | May, D.A., 199 | Thoms, B.D., 61 |
| Elam, W.T., 184 | McDermott, J.P., 167 | Ting, A.C., 156 |
| Esarey, E.H., 156 | Medhurst, L.J., 132 | Toot, P.L., 139 |
| Ewing, K.J., 127 | Mehl, M.J., 73 | Toothman, H.L., 153 |
| Fisher, S., 233 | Mignogna, R.B., 177 | Twigg, M.E., 146 |
| Frankel, M.Y., 217 | Mozurkewich, D., 222 | Van Buren, A.L., 108 |
| Freitas, Jr., J.A., 220 | Murphy, C.J., 139 | van Keuren, D.K., 9 |
| Fricke, J.R., 118 | Nau, G.M., 127 | Wagner, R.J., 146 |
| Froscher, J.N., 167 | Nelson, H.H., 132 | Ward, K.B., 130 |
| Garland, N.L., 132 | Newman, D.A., 154 | Waterman, J.R., 146 |
| Garner, J.C., 229 | Nishimura, C.E., 91 | Zolnick, D.A., 153 |

NRL Review Staff

Senior Science Editor: John D. Bultman
Senior TID Editor: Beba Zevgolis
TID Consultants: Kathleen Parris and Timothy Calderwood

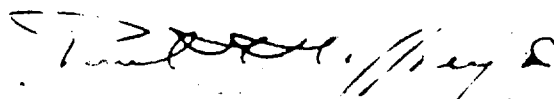
Cover design: Beba Zevgolis
Graphic support: T. Zevell Ruffy, Jan Morrow, and Carol Hambrie
Computerized composition and design production: Donna Gloystein and Dora Wilbanks
Editorial assistance: Maureen Long and David van Keuren
Mission page photograph: Michael Savell
Photographic production: Richard Bussey, Gayle Fullerton, James Marshall,
Chris Morrow, Barbara Padgett, and Michael Savell
Production assistance: Rosie Bankert, Diltricia Montgomery, Leona Sprankel
and Paul Sweeney
Distribution: Joyce Harris and Barbara Jolliffe

Head, Technical Information Division: Peter H. Imhof

Further Information: Information on the research described in the *NRL Review* may be obtained by contacting Dr. Richard Stein, Head, Technology Transfer and Special Programs, Code 1003.1, (202) 767-2744. General information about NRL may be obtained from the Public Affairs Office, Code 1230, (202) 767-2541. The sources of information on the various nonresearch programs at NRL are listed in the *NRL Review* chapter entitled "Programs for Professional Development."

The *NRL Fact Book* gives details about the Laboratory and its operations. It lists major equipment, current fields of research, field sites, and outlying facilities. It also presents information about the responsibilities, organization, key personnel, and funding. A copy may be obtained by contacting the Technical Information Division, Publications Branch, Code 5231, (202) 767-2782.

REVIEWED AND APPROVED
NRL/PU/5200-94 246
March 1994



Paul G. Gaffney II
Captain, USN
Commanding Officer

Approved for public release; distribution is unlimited.

510
6-94